EXPLORING INFLAMMASOME EXPRESSION AND ACTIVATION USING NOVEL REPORTER MICE

James Duc Hung Ong

A thesis submitted for the degree of

Doctor of Philosophy (PhD)

at Monash University in 2019

Monash University, Hudson Institute of Medical Research

Copyright notice

Declaration

This thesis contains no material which has been accepted for the award of any other degree or diploma at any university or equivalent institution and that, to the best of my knowledge and belief, this thesis contains no material previously published or written by another person, except where due reference is made in the text of the thesis.

Print Name: JAMES DUC HUNG ONG

Date: 13/8/2019

The undersigned hereby certify that the above declaration correctly reflects the nature and extent of the student's contribution to this work.

Print Name: A/PROF ASHLEY MANSELL

Date: 13/8/2019

Table of Contents

Table of Contents

Table of Contents

Table of Contents

Table of Contents

List of figures

List of figures

List of figures

List of figures

List of tables

Abstract

The innate immune system maintains homeostasis by restricting the spread of infection to give the adaptive immune system time to be activated, enabling pathogen clearance. One important component of the innate immune system is the NLRP3 inflammasome, a protein complex that matures pro-inflammatory cytokines IL-1β and IL-18 and stimulates pyroptosis, an inflammatory form of cell death. The current dogma of inflammasome biology is that inflammasome components are upregulated by priming signals and assembled into an all-encompassing speck by a second activating signal. The latter premise is built on studies using over-expression and cell-free systems, neither of which simulate the behaviour of inflammasome components under cellular conditions. My project studied the expression and activation of the inflammasome in an endogenous setting using novel reporter mice, where the reporters are placed in their native promoters.

I initially showed that an all-encompassing speck is not formed during inflammasome activation despite reporter cells being able to activate caspase-1, mature IL-1β and stimulate pyroptosis, implying that the formation of an all-encompassing speck is not required. Rather, inflammasome activation is associated with the condensation of ASC into an ASC-enriched area and the unfolding of NLRP3 throughout the whole cell. These might only occur in a subset of LPS-responsive cells which upregulated NLRP3 upon exposure to priming signals. These results challenge our current understanding of inflammasome biology built on overexpression and cell-free systems and establish a new paradigm of inflammasome activation associated with the appearance of numerous small inflammasome complexes in the cytosol.

A hyper-active innate immune system damages tissues and organs, contributing to inflammatory and chronic diseases. The NLRP3 inflammasome is no exception, being linked to the pathophysiology of various diseases. Previous findings in our laboratory have found that the NLRP3 inflammasome is protective in the early stages of influenza A virus (IAV) infection but also promotes hyper-inflammatory responses later on, leading to mortality. My project extend these findings by looking at

Abstract

inflammasome expression and MCC950 uptake at the single-cell level in the lung during IAV infection.

I found that during IAV infection of NLRP3 reporter mice, NLRP3 was upregulated to a greater extent in infiltrating leukocytes such as neutrophils and inflammatory macrophages compared to lung-resident cells such as alveolar macrophages and epithelial cells. Furthermore, following intranasal delivery of MCC950 into IAV-infected WT mice, MCC950 was taken up by myeloid- and non-myeloid-derived cell populations. However, as infection progressed MCC950 uptake into myeloid-derived cells increased, particularly in infiltrating leukocytes such as inflammatory macrophages and neutrophils. These studies not only identified cells that may exhibit latent inflammasome activity during IAV infection but also underline the need to develop therapeutics to modulate inflammasome activity in specific cell populations to control inflammation.

Collectively, my studies not only present a new model of inflammasome activation in an endogenous setting but also underline the need to study associations between infection, inflammasome activity and inhibitor uptake. The use of novel endogenously-expressed reporter mice in these studies provide a proof-of-concept for studying inflammasome expression and activity in a biological context in health and disease.

Acknowledgements

Completing my PhD has been a long and hard journey full of ups and downs. Throughout this journey, there have been a couple of people that have helped me along the way.

I would like to thank my main supervisor A/Prof. Ashley Mansell for guiding me on the research process and what I should be doing next. He has been a sounding board for me throughout my PhD, providing feedback and ideas for my project which have been incorporated into the thesis. I would also like to thank my co-supervisor Dr. Michelle Tate for teaching me how to run *in vivo* experiments as well as analysing flow cytometry data. I was able to bounce a lot of ideas during my conversations with her which has made me think hard about my *in vivo* experiments and results.

I would like to recognise the people that have taught me the techniques that were vital to the completion of my thesis. Firstly, I would like to thank Dr. Jennifer Dowling, a former Mansell group post-doctorate, who taught me how to conduct immunoblotting experiments. Secondly, I would like to thank Louise McLeod, Issac Woodhouse and Jodee Gould for educating and guiding me on the genotyping experiments that were used to maintain homozygous reporter murine colonies. Lastly, I would like to acknowledge the research platform staff that have assisted me throughout my PhD. These include Dr. Sarah Creed from Monash Micro Imaging for teaching me how to use the confocal microscopes required to complete my thesis; Dr. Kirstin Elglass from Monash Micro Imaging for collecting the FLIM-FRET data for my thesis; Dr. Michael Thomson from Flowcore for teaching me how to run the flow cytometer machines; and the staff at Monash Animal Services and Monash Medical Centre Animal Facilities for maintaining the reporter murine colonies.

As well as that, there have been some people in the scientific field that have contributed ideas or reagents for my research. I would first like to recognise Prof. Paul Hertzog for providing the background information on the reporter mice which has been used in discussing the results. I would also like to thank Prof. Matt Cooper and Dr. Avril Robertson from the University of Queensland for

providing the MCC950 small molecule inhibitor required to conduct some experiments. Lastly, this research was supported by an Australian Government Research Training Program (RTP) Scholarship, without which it would have been impossible to complete my PhD.

Last but not least, throughout my PhD I was supported by other people in the Centre for Innate Immunity and Infectious Diseases and beyond. In particular, I would like to thank the students that have worked with me in the Hudson Institute Student Society (HISS) throughout my PhD. Not only did we run some academic and social events for students but they also gave me support and forged friendships that have alleviated some stress from completing a thesis. I would also like to thank my parents for supporting me throughout my PhD.

Publications during enrolment

Ong, J.D., Mansell, A., and Tate, M.D. (2017). Hero turned villain: NLRP3 inflammasome-induced inflammation during influenza A virus infection. J. Leukoc. Biol. *101*, 863-874.

Tate, M.D., **Ong, J.D.**, Dowling, J.K., McAuley, J.L., Robertson, A.B., Latz, E., Drummond, G.R., Cooper, M.A., Hertzog, P.J., and Mansell, A. (2016). Reassessing the role of the NLRP3 inflammasome during pathogenic influenza A virus infection via temporal inhibition. Sci. Rep. *6*, 27912.

Presentations at Meetings and Conferences

2018

Hudson Institute Student Retreat

Oral presentation: Uncovering aspects of inflammasomes using novel reporter mice

Lorne Infection and Immunity

Poster presentation: Unearthing new findings of the NLRP3 inflammasome using novel reporter mice

2017

VIIN Young Investigator Symposium

Oral presentation: Validation of an NLRP3 reporter mouse to study the NLRP3 inflammasome at the single-cell level

Abbreviations

Abbreviation	Full words
AEC	Airway epithelial cell
AIM2	Absent in melanoma 2
ARDS	Acute respiratory distress syndrome
ASC	Apoptosis-associated speck-like protein containing a CARD
ATP	Adenosine triphosphate
BAL	Bronchoalveolar lavage
BRCC3	BRCA1/BRCA2-Containing Complex Subunit 3
BRISC	BRCC36 isopeptidase complex
BSA	Bovine serum albumin
CAPS	Cryopyrin-associated periodic syndrome
CARD	Caspase activation and recruitment domain
Caspase	Cysteine aspartate proteases
CCL2	C-C motif chemokine ligand 2
CD	Cluster of differentiation
cDC	Conventional dendritic cell
COP	Caspase activation and recruitment domain (CARD)-only proteins
CPPD	Calcium pyrophosphate dihydrate
CTL	Cytotoxic T lymphocyte
CXCL8	C-X-C motif chemokine ligand 8
CXCL8	C-X-C motif chemokine ligand 10
DAMP	Damage-associated molecular pattern
DC	Dendritic cell
DIC	Differential interference contrast
DMEM	Dulbecco's Modified Eagle Medium
DR5	Death receptor 5
dsDNA	Double-stranded deoxyribonucleic acid
dsRNA	Double-stranded ribonucleic acid
EDTA	Ethylenediaminetetraacetic acid
EID_{50}	50% Egg Infective Dose
ELISA	Enzyme-linked immunosorbent assay
ESAT	Early secretory antigenic target
ESC	Embryonic stem cell
F3	Flippase 3 site
FCAS	Familial cold autoinflammatory syndrome
FCS	Fetal calf serum
FIIND	Function to find domain
FLIM	fluorescence lifetime imaging microscopy
FLP	Flippase
FRET	Fluorescence resonance energy transfer
FRT	Flippase recognition target
GATA4	GATA binding protein 4
GFP	Green fluorescent protein
GM-CSF	Granulocyte-macrophage colony-stimulating factor
H1N1pdm09	2009 swine-origin H1N1 pandemic strain
H_2O	Water

Abbreviations

HA	Haemagglutinin
HIN-200	Haematopoietic interferon-inducible nuclear proteins with a 200-amino-acid repeat
HIV	Human immunodeficiency virus
HMGB1	High-mobility group box 1 protein
HSC	Haematopoietic stem cell
IAV	Influenza A virus
iBMDM	Immortalised bone marrow-derived macrophage
ICAM-1	Intercellular Adhesion Molecule 1
ICE	Interleukin-1β-converting enzyme
IFN	Interferon
IFNAR	Interferon-α receptor
IFNGR	Interferon γ receptor
IKK	Inhibitor of κB kinase
IL	Interleukin
IL-1R	Interleukin-1 receptor
INCA	Inhibitor of CARD
IRAK1	Interleukin-1 receptor-associated kinase 1
IRF	Interferon regulatory factor
ISG	Interferon-stimulated gene
ISGF3	Interferon-stimulated gene factor 3
IκB	Inhibitor of κB
JAK	Janus kinase
LDH	Lactate dehydrogenase
LF	Lethal factor
LGP2	Laboratory of genetics and physiology 2
LPS	Lipopolysaccharide
LRR	Leucine-rich repeat
M1	Matrix protein 1
M2	Matrix protein 2
Mal	MyD88 adaptor-like molecule
MAPK	Mitogen-activated protein kinase
MARK4	Microtubule-affinity regulating kinase 4
MAVS	Mitochondrial antiviral-signalling protein
mCherry	Monomeric Cherry
mCitrine	Monomeric Citrine
MD	Myeloid differentiation factor
MDA5	Melanoma differentiation associated antigen 5
MHC	Major histocompatibility complex
MONMAN	Monash and Manitoba Universities
mQ	MilliQ
MSU	Monosodium urate
mtDNA	Mitochondrial DNA
mtROS	Mitochondrial reactive oxygen species
MWS	Muckle-Wells Syndrome
MyD88	Myeloid differentiation primary response gene 88
NA	Neuraminidase
NACHT	Domain present in NAIP, CIITA, HET-E, and TP-1
NAD	Domain present in NAIP, CIITA, HET-E, and TP-1 (NACHT)-associated domain

Abbreviations

NADPH	Nicotinamide adenine dinucleotide phosphate
NAIP	NLR family apoptosis inhibitory protein
NBD	Nucleotide-binding domain
NET	Neutrophil extracellular trap
NF-κB	Nuclear factor κB
NK	Natural killer
NLR	NOD-like receptor
NLRC4	NLR family, CARD domain containing member 4
NLRP1b	NLR family, PYD domain containing member 1b
NLRP3	NLR family, PYD domain containing member 3
NOD	Nucleotide-binding oligomerisation domain
NOMID	Neonatal onset multisystem inflammatory disease
NORCOMM	North American Conditional Mouse Mutagenesis
NOS2	Nitric oxide synthase 2
NOX2	Nicotinamide adenine dinucleotide phosphate oxidase 2
NP	Nucleoprotein
NS1	Non-structural protein 1
NS2	Non-structural protein 2
PA	Protective antigen (for anthrax)/Polymerase acidic protein (for influenza)
PAMP	Pathogen-associated molecular pattern
PB1	Polymerase basic protein 1
PB2	Polymerase basic protein 2
PBMC	Peripheral blood mononuclear cell
pBMDC	Primary bone marrow-derived dendritic cells
pBMDM	Primary bone marrow-derived macrophages
PBS	Phosphate-buffered saline
PCR	Polymerase chain reaction
pDC	Plasmacytoid dendritic cell
PEC	Peritoneal exudate cell
PFA	Paraformaldehyde
POP	Pyrin-only protein
PP2A	Protein phosphatase 2A
PR8	A/Puerto Rico/8/34 (H1N1)
PrP	Prion protein
PRR	Pattern recognition receptor
PTEN	Phosphatase and tensin homolog
PYD	Pyrin domain
PYDC3	PYD-containing protein 3
RDC	Respiratory dendritic cell
RIG-I	Retinoic acid-inducible gene-I-like receptor
RIP2	Receptor interacting protein 2
RLR	RIG-I-like receptor
ROS	Reactive oxygen species
SIRT1	Sirtuin 1
SNP	Single nucleotide polymorphism
SPF	Specific pathogen-free
SSC	Side scatter
STAT	Signal transducer and activator of transcription
Strep	Streptavidin

Abbreviations

TBK1	TANK binding kinase 1
TIR	Toll/IL-1 receptor-like domain
TLR	Toll-like receptor
TNFR	Tumour necrosis factor receptor
TNF-α	Tumour necrosis factor α
TRAM	TRIF-related adaptor molecule
T_{reg}	Regulatory T cell
TRIF	TIR-domain-containing adapter-inducing interferon-β
TYK	Tyrosine kinase
USP	Ubiquitin-specific-processing protease
VCAM-1	Vascular cell adhesion protein 1

1 Introduction

1.1 The innate immune system

The innate immune system is designed to impede infection by restricting the replication and spread of pathogens and activating the adaptive immune system (reviewed in Medzhitov and Janeway (2000)). The innate immune system is made up of both cells and proteins (Figure 1.1). The cellular compartment of the innate immune system includes leukocytes or white blood cells such as macrophages, dendritic cells (DCs) and neutrophils. Proteins that are part of the innate immune system include cytokines and chemokines as well as antimicrobial peptides and complement proteins (reviewed in Turvey and Broide (2010)). As such, the cells and proteins in the innate immune system restrict infection and activate the adaptive immune system.

1.1.1 Physical and chemical barriers

Physical and chemical barriers in the body prevent pathogens and foreign agents in the external environment from entering the internal environment of the body (Figure 1.1). Skin is a well-known physical barrier to infection. The skin has two layers: the inner dermis containing stratified epithelial cells connected by tight junctions and the outer epidermis consisting of layers of keratinocytes reinforced by keratin (reviewed in Matsui and Amagai (2015)). Intact skin acts as a physical barrier against pathogens and foreign agents from the external environment. The skin also acts as a chemical barrier by secreting antimicrobial peptides and enzymes such as lysozyme to degrade pathogens colonising the skin (reviewed in Matsui and Amagai (2015)). Mucosal membranes in body cavities such as the respiratory and gastrointestinal tracts are physical barriers that prevent pathogens or foreign agents from entering the internal environment. Similar to skin, mucosal membranes are also chemical barriers, secreting antimicrobial peptides and enzymes as well as mucus to trap and degrade pathogens (Akinbi et al., 2000). The stomach within the gastrointestinal tract has hydrolytic enzymes and an acidic environment to arrest the growth of most bacteria while natural flora in the colon competes against potential pathogens for attachment sites and metabolites (reviewed in Bowdish et al. (2005)).

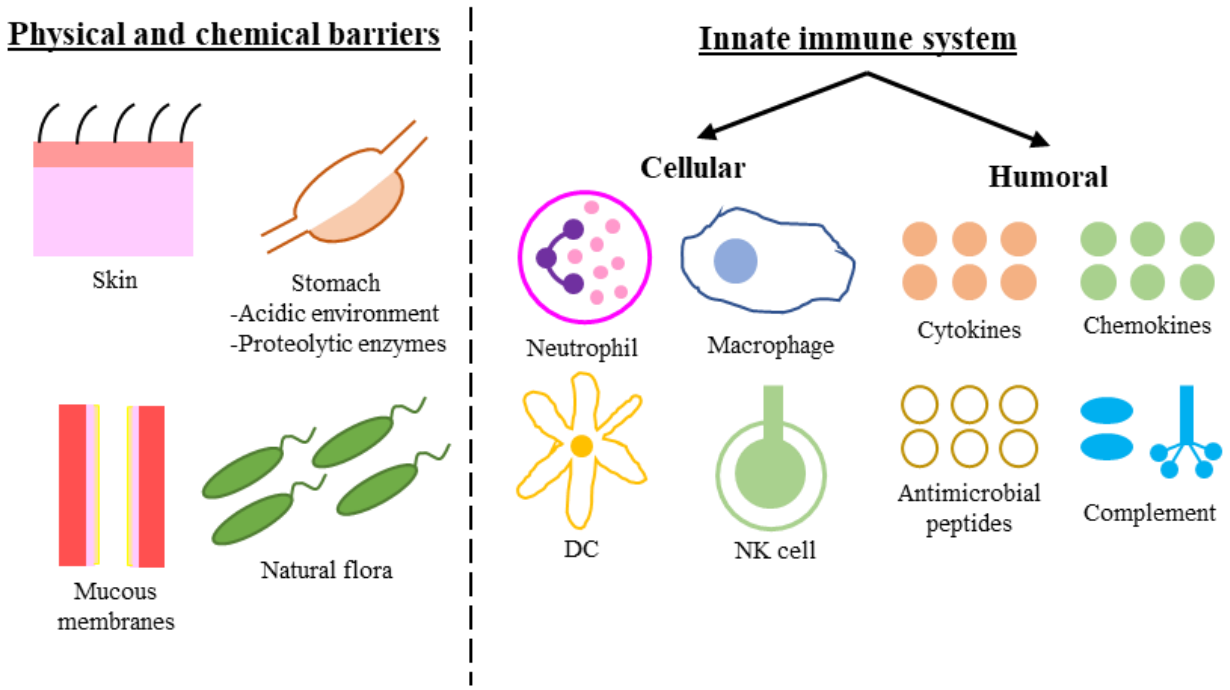

Figure 1.1: Components of physical and chemical barriers and the innate immune system

Physical and chemical barriers and the innate immune system constitute the "first" and "second" lines of defence against pathogens respectively. Physical and chemical barriers prevent pathogens or foreign agents in the external environment from entering the body. Intact skin and mucous membranes prevent pathogens from entering the body via the outside and body cavities respectively. Pathogens are also broken down by the acidic environment and enzymes in the stomach and are outgrown by the natural flora in the colon. Should these barriers be breached, the innate immune system is activated. This is made of two compartments: the cellular compartment containing leukocytes such as neutrophils and macrophages and the humoral compartment consisting of proteins such as cytokines and chemokines. The innate immune system is designed to restrict infection while the adaptive immune response is being activated. DC = dendritic cell.

Physical and chemical barriers; therefore, prevent pathogens from entering and colonising the internal environment to initiate infection. Both the skin and mucosal membranes have immune-associated tissue that sense pathogens and foreign agents in the external environment (reviewed in Riera Romo et al. (2016)). This enables physical barriers to detect pathogens or cellular damage, activating the immune system and inflammation.

1.1.2 Inflammation

Breaching of physical and chemical barriers that separate the internal and external environments stimulates a response to remove foreign contents in the body. Inflammation is the coordinated response against pathogens such as viruses, foreign agents such as silica and tissue injury such as damaged cells (Figure 1.2). Inflammation activates the immune system to remove the pathogen, foreign agent or tissue injury. In the process, inflammation damages tissues to enable leukocytes to more easily access the inflamed site. This produces the cardinal symptoms of redness, warmth, pain, swelling and loss of function.

Inflammation is initiated by danger signals that indicate the presence of pathogen, foreign agent or damaged tissue. While pathogens can be detected via highly-conserved structures called pathogen-associated molecular patterns (PAMPs), tissue injury can be sensed by the release of damage-associated molecular patterns (DAMPs). Both PAMPs and DAMPs are recognized by pattern recognition receptors (PRRs) expressed on myeloid- and non-myeloid-derived cells (reviewed in Bryant et al. (2015)). The engagement of PAMPs or DAMPs with PRRs stimulates various signalling pathways that activate the prototypical inflammatory protein nuclear factor κB (NF-κB), leading to the expression and secretion of mediators, chemokines and cytokines. Mediators such as histamine act on capillaries to induce vasodilation and increase vascular permeability, allowing plasma fluid, proteins and leukocytes to diffuse into the tissue. The release of chemokines and cytokines attracts and activates leukocytes such as macrophages and neutrophils to eliminate the pathogen or foreign agent (reviewed in Okin and Medzhitov (2012)).

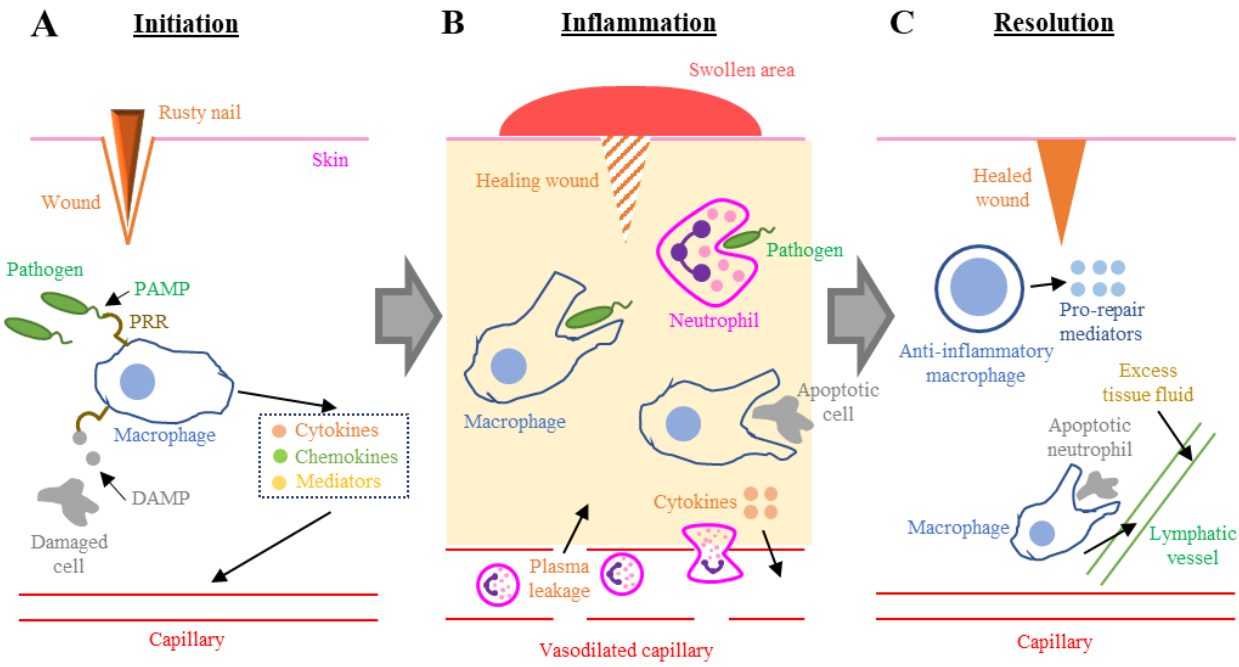

Figure 1.2: The process of inflammation

(A) Inflammation is initiated when pattern recognition receptors (PRRs) on cells such as macrophages sense pathogen-associated molecular patterns (PAMPs) or damage-associated molecular patterns (DAMPs) from pathogens or damaged cells respectively. They release cytokines, chemokines and mediators that act on the capillary, causing vasodilation and increasing permeability that allow cells and plasma to leak into the tissue. (B) Cells such as macrophages and neutrophils phagocytose and degrade pathogens and apoptotic cells while damaging tissue. This produces the cardinal symptoms of inflammation such as swelling and redness in the inflamed area, but tissue damage is necessary for wound healing. Cytokines may also diffuse into plasma, circulating around the body to initiate systemic responses to inflammation such as fever. (C) As soon as pathogens and/or damaged cells are removed, resolution begins. This is where tissue repair is initiated to heal the wound, mediated by the release of pro-repair mediators from anti-inflammatory macrophages such as protectins and resolvins. Macrophages also phagocytose apoptotic neutrophils in the tissue. Along with excess tissue fluid, macrophages drain into the lymphatic system, reducing the swelling in the tissue.

Introduction

Some cytokines such as interleukins (IL)-1α and IL-1β, IL-6 and tumour necrosis factor α (TNF-α) also diffuse into the bloodstream, inducing systemic responses to inflammation such as fever (reviewed in Ashley et al. (2012)). Once the pathogen or foreign agent is removed, the process of resolution dampens inflammation and immune activity and promotes tissue repair. This involves the secretion of anti-inflammatory, pro-repair mediators such as protectins and resolvins and the re-programming of leukocytes such as macrophages towards an anti-inflammatory, pro-repair phenotype (reviewed in Headland and Norling (2015); Netea et al. (2017)).

Acute inflammation describes the above process occurring over a short period of time to remove the pathogen or foreign agent. However, if the pathogen or foreign agent is not removed, inflammatory and immune processes can remain active over the medium- to long-term, leading to chronic inflammation. Chronic inflammation is associated with a range of different diseases, including rheumatoid arthritis (Rosenblum et al., 2015), cancer (Mantovani et al., 2008) and atherosclerosis (Duewell et al., 2010). Inflammation can also be hyper-activated over a short period of time. This process, called hyper-inflammation, damages tissues over eliminating pathogens which may lead to mortality (Xiao et al., 2013b). Hyper-inflammation is closely associated with hyper-cytokinaemia or the ‘cytokine storm’, where a variety of cytokines and chemokines are secreted at high concentrations (Chang et al., 2011). For instance, pathogenic avian influenza viruses such as H5N1 promote hyper-cytokinaemia, causing hyper-inflammation that damages the lung. This leads to reduced gas exchange, multi-organ failure and poorer prognosis of infection (de Jong et al., 2006; To et al., 2001). In summary, inflammation serves a dual purpose in the body. While acute inflammation is initiated to remove the pathogen or foreign agent, chronic inflammation and hyper-inflammation can cause disease and mortality.

1.1.3 Pattern recognition receptors (PRRs)

PRRs are germ-line encoded receptors that sense pathogens via highly-conserved structures called PAMPs (Figure 1.3). These PAMPs are only present in pathogens and are integral for their survival (reviewed in Bryant et al. (2015)). PRRs can also detect danger signals from cell death or tissue injury due to infection or sterile inflammation by sensing DAMPs. Examples of DAMPs include high-mobility group box 1 protein (HMGB1), alarmins, heat shock proteins and urate (reviewed in Bianchi (2007)). PRRs are split into different groups depending on their protein structure and what they sense (Table 1.1).

1.1.3.1 Toll-like receptors (TLRs)

Mammalian TLRs are proteins that are homologous to the drosophila Toll protein (Rock et al., 1998). The Toll protein is a transmembrane protein that was initially described in drosophila development (Hashimoto et al., 1988) but was also found to play a role in the expression of antimicrobial peptides via the NF-κB pathway (Lemaitre et al., 1996). TLRs are homologues of the drosophila Toll protein with an extracellular leucine-rich repeat (LRR) domain and an intracellular Toll/IL-1 receptor-like (TIR) domain (Gay and Keith, 1991). Altogether, there are ten TLRs in humans which recognise different PAMPs and DAMPs. Most TLRs are expressed on the plasma membrane, but some such as TLR3, 7, 8 and 9 that tend to recognise nucleic acids are expressed on the endosomal membrane (reviewed in O'Neill and Bowie (2007)). Inactive TLRs exist as a monomer, but upon ligand binding dimerise. This brings the two intracellular TIR domains in close proximity, recruiting signalling proteins such as Myeloid differentiation primary response gene 88 (MyD88) and TIR-domain-containing adapter-inducing interferon-β (TRIF). In association with adaptor proteins such as MyD88 adaptor-like (Mal) and TRIF-related adaptor molecule (TRAM) and protein kinases such as interleukin-1 receptor-associated kinase 1 (IRAK1), MyD88 and TRIF form the Myddosome (Motshwene et al., 2009) and Triffosome (Sato et al., 2003) complexes respectively.

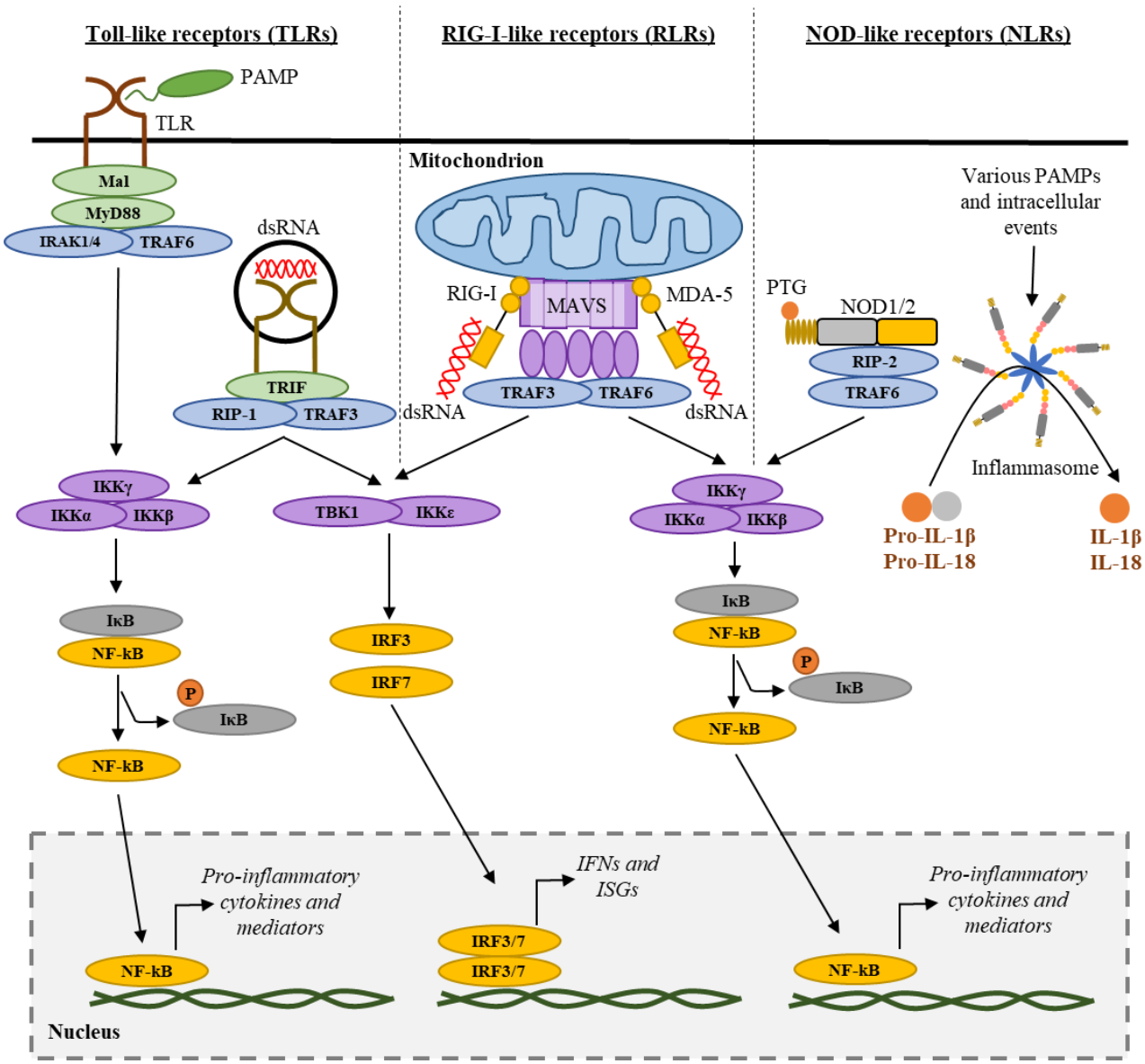

Figure 1.3: Signalling pathways of various pattern recognition receptors (PRRs)

PRRs such as toll-like receptors (TLRs), RIG-I-like receptors (RLRs) and NOD-like receptors (NLRs) recognise various pathogen-associated molecular patterns (PAMPs) such as viral RNA and peptidoglycan (PTG). Once engaged, PRRs recruit various adaptor and intracellular proteins, activating two main signalling pathways. The first signalling pathway involves the activation of NF-κB via phosphorylation and proteasomal degradation of IκB. NF-κB then enters the nucleus to promote the expression of pro-inflammatory cytokines and mediators. The second pathway involves the activation of IRF3 or IRF7. IRF3 or IRF7 enters the nucleus to induce the expression of interferons (IFNs) and interferon-stimulated genes (ISGs).

Table 1.1: List of PRRs and what PAMPs/DAMPs they recognise

PRR class	PRR	PAMP/DAMP sensed
Toll-like receptors (TLRs)	TLR2	Di-acylated lipopeptide (in association with TLR6. E.g., lipoteichoic acid) (Kang et al., 2009) Tri-acylated lipopeptide (in association with TLR6. E.g., Pam_3CSK_4) (Jin et al., 2007)
	TLR3	dsRNA (Alexopoulou et al., 2001)
	TLR4	Lipopolysaccharide (LPS) (Hoshino et al., 1999a)
	TLR5	Flagellin (Hayashi et al., 2001)
	TLR7	Guanosine- and uridine-rich ssRNA (Hemmi et al., 2002). Imidazoquinoline derivatives such as imiquimod and R848 (Colak et al., 2014)
	TLR9	CpG motifs on microbial dsDNA (Haas et al., 2008; Hemmi et al., 2000)
RIG-like receptors (RLRs)	RIG-I	ssRNA (Pichlmair et al., 2006) Small dsRNAs with a 5'-triphosphate or 5'-diphosphate terminii (Goubau et al., 2014; Hornung et al., 2006)
	MDA5	Long dsRNA (Kato et al., 2006)
NOD-like receptors (NLRs)	NOD1	γ-D-glutamyl-meso-diaminopimelic acid (ie-DAP) from bacterial peptidoglycan (Chamaillard et al., 2003) Lipopolysaccharide (LPS) (Girardin et al., 2001)
	NOD2	Muramyl dipeptide from bacterial peptidoglycan (Girardin et al., 2003)

Protein kinases in these complexes activate transcription factors such as NF-κB and interferon regulatory factor (IRF)3 to induce the expression of immune and pro-inflammatory genes (reviewed in Bryant et al. (2015)).

Individual TLRs interact with different PAMPs to activate the immune system in response to various pathogens (Table 1.1). For example, TLR4 is required for responding to lipopolysaccharide (LPS) because TLR4-deficient mice were unresponsive to LPS, rendering them resistant to endotoxic shock (Hoshino et al., 1999a; Poltorak et al., 1998). Other proteins are required for TLR4 to respond to LPS. TLR4 requires cluster of differentiation (CD)14, an LPS-binding receptor that receives LPS from LPS-binding protein (Zanoni et al., 2011) and lowers the threshold for TLR4 activation (Gioannini et al., 2004). Myeloid differentiation factor (MD)-2, which is constitutively associated with TLR4, is also required for responses to LPS (Shimazu et al., 1999). These proteins form the TLR4 complex which enable cells to receive and respond to LPS, activating NF-κB to express and release various pro-inflammatory cytokines.

1.1.3.2 **RIG-I-like receptors (RLRs)**

Retinoic acid-inducible gene-I-like receptor (RIG-I)-like receptors (RLRs) are cytoplasmic RNA sensors. They possess a helicase domain that senses double-stranded RNA (dsRNA) and signalling domains that initiate a signalling cascade to activate transcription factors such as IRFs and NF-κB. There are three members in the family: RIG-I, melanoma differentiation associated antigen 5 (MDA5) and laboratory of genetics and physiology 2 (LGP2) (Goubau et al., 2014). RLRs tend to sense viral dsRNA (Table 1.1). While RIG-I senses ssRNA and short dsRNA fragments (1000 base pairs or below) via 5’-di or triphosphate motifs, MDA5 binds to longer dsRNA molecules (Goubau et al., 2014; Hornung et al., 2006; Kato et al., 2008; Pichlmair et al., 2006). Upon recognition of dsRNA, RLR caspase activation and recruitment domains (CARD) interact with mitochondrial antiviral-signalling protein (MAVS) CARD domains on the mitochondrion (Figure 1.3). This triggers a polymerisation of RLRs and MAVS to form a filament, enabling the recruitment of adaptor proteins

and kinases to activate transcription factors such as IRF3 (Peisley et al., 2014; Peisley et al., 2013). This leads to the expression of pro-inflammatory and anti-viral genes in the cell.

1.1.3.3 NOD-like receptors (NLRs)

Nucleotide-binding oligomerisation domain (NOD)-like receptors (NLRs), derived from plant R proteins responding to bacterial infection (Inohara et al., 2001), sense intracellular PAMPs and DAMPs (Table 1.1). Structurally, they consist of an N-terminal domain, a domain present in NAIP, CIITA, HET-E, and TP-1 (NACHT) nucleotide-binding domain (NBD) and C-terminal LRRs.

Altogether, there are 22 human and 34 murine NLRs, classified according to their N-terminal domain (Ting et al., 2008). For instance, NLRCs and NLRPs are NLRs with the N-terminal CARD and pyrin domains (PYD) respectively. There are two effector pathways of NLR activation (Figure 1.3). NOD1 and NOD2 sense intracellular LPS (Girardin et al., 2001) and peptidoglycan fragments such as muramyl dipeptide (Girardin et al., 2003). Once engaged, these NOD proteins localise to the plasma or endosomal membrane to recruit the receptor interacting protein 2 (RIP2) kinase, leading to NF-κB activation (Barnich et al., 2005; Irving et al., 2014; Kufer et al., 2008). Some activated NLRs form protein complexes called inflammasomes. These complexes stimulate the maturation of pro-inflammatory cytokines such as IL-1β and IL-18 via cleavage of their pro forms (Agostini et al., 2004; Martinon et al., 2002). Additionally, they induce an inflammatory form of cell death called pyroptosis (Fernandes-Alnemri et al., 2007). Hence, NLRs serve a variety of roles depending on the pathway induced.

1.1.3.4 Signalling pathways in the innate immune system

Construction of signalling complexes containing PRRs or cytokine receptors leads to the activation of the NF-κB pathway (Figure 1.3). The presence of the signalling complex activates Inhibitor of κB (IκB) kinase (IKK) α and β. These kinases phosphorylate N-terminal serines of IκB, a protein that sequesters and inactivates NF-κB in the cytosol. Phosphorylated IκB becomes ubiquitinated, directing

it for degradation by the 26S proteasome. This allows NF-κB to translocate to the nucleus and induce the expression of pro-inflammatory genes, leading to inflammation (reviewed in Liu et al. (2017)).

Certain PRRs such as the RLRs also phosphorylate and activate IRF3/IRF7 (Figure 1.3). The construction of a TRIF- or MAVS-containing intracellular complex from TLR and RLR signalling respectively attracts kinases TANK binding kinase 1 (TBK1) and IKKε. These kinases phosphorylate IRF3 and IRF7 which form homodimers or heterodimers. These dimers enter the nucleus to induce the expression of type I IFNs and interferon-stimulated genes (ISGs) (reviewed in Honda et al. (2006).

The immune system, particularly interferons (IFNs), also uses the Janus kinase (JAK)-signal transducer and activator of transcription (STAT) pathway. The association of IFN-α/β with the interferon-α receptor (IFNAR) brings together two tyrosine kinases: JAK1 and tyrosine kinase (TYK)2. These are auto-activated to phosphorylate STAT1 and STAT2. Phosphorylated STAT1 and STAT2 associate with IRF9 to form the ISG factor 3 (ISGF3) complex which enters the nucleus to stimulate the expression of ISGs (reviewed in Stark et al. (1998)). This enables anti-viral responses to be set-up in the cell.

1.1.4 Innate immune cells

Innate immune cells can be split into two sub-populations: polymorphonuclear and mononuclear cells. Polymorphonuclear cells such as neutrophils have a segmented nucleus and protein-containing granules (Rorvig et al., 2013). Neutrophils normally reside in the bone marrow but are rapidly recruited to inflamed tissue due to infection or tissue injury (Martin et al., 2003). Once in the inflamed tissue, they degrade pathogens or foreign agents by a variety of methods. They can phagocytose pathogens and degrade them with granule proteins and reactive oxygen species (ROS) (Pham, 2006; Rada et al., 2004). Neutrophils can also release neutrophil extracellular traps (NETs) containing granule proteins and chromatin to trap and degrade extracellular bacteria (Brinkmann et al., 2004). Neutrophils are short-lived, living for only up to five days (Pillay et al., 2010), and upon apoptosis

are cleared by macrophages (A-Gonzalez et al., 2009). Though neutrophils only survive for a short time, they are rapidly recruited to inflamed sites to contain infection.

Mononuclear phagocytes such as monocytes/macrophages and DCs not only engulf and degrade pathogens but also present antigens to activate adaptive immune responses (reviewed in Beutler (2004)). DCs are the cellular link between innate and adaptive immune systems, activating cell-mediated immune responses by processing and presenting protein antigens to T cells (Nussenzweig et al., 1980; Steinman and Witmer, 1978). DCs can be classified into smaller subsets. Conventional DCs (cDCs) present antigens to T cells. The most well-characterised cDCs are CD8α^+ and CD103$^+$ cDCs which are found in lymphoid and non-lymphoid organs respectively (Bursch et al., 2007; Crowley et al., 1989). These cDCs present antigens to CD4$^+$ T cells via major histocompatibility complex (MHC) class II proteins and CD8$^+$ T cells via MHC class I proteins (Bedoui et al., 2009; del Rio et al., 2007). CD11b$^+$ DCs are the most common cDCs in lymphoid and non-lymphoid organs. Even though they cannot cross-present antigens to CD8$^+$ T cells, they can strongly activate CD4$^+$ T cells due to their efficient MHC class II antigen processing machinery (Dudziak et al., 2007; Lewis et al., 2011). Monocyte-derived DCs are also known as inflammatory DCs. These cells, which express the monocyte marker CD64, are derived from monocytes that have differentiated into DCs under inflammatory conditions (Serbina et al., 2003). Lastly, plasmacytoid DCs (pDCs) are associated with the rapid production of type I IFNs during viral infection due to the endogenous expression of IRF7 (Asselin-Paturel et al., 2001; Sato et al., 1998; Siegal et al., 1999). With these different DC subsets, DCs serve a variety of roles to maintain innate immunity while activating adaptive immune responses.

Most macrophages are derived from bone marrow-derived monocytes that circulate in the bloodstream (Geissmann et al., 2003). Tissue-resident macrophages such as liver Kuppfer and lung alveolar macrophages are derived from foetal macrophages (Yona et al., 2013). They can self-proliferate to maintain tissue macrophage populations independent of bone marrow-derived monocytes (Hashimoto et al., 2013). Macrophages serve a variety of roles depending on their

phenotype. M1 macrophages tend to promote inflammation and anti-microbial activity by secreting pro-inflammatory cytokines such as TNF-α, IL-1β and IL-6 and producing ROS. On the other hand, M2 macrophages promote tissue repair by secreting proteins such as arginase-1 and IL-10 (reviewed in Wynn et al. (2013)). Macrophages play a critical role in clearing bacterial (Shaughnessy and Swanson, 2007) and viral (Hoeve et al., 2012) infections by phagocytosing and eliminating pathogens. However, macrophages also contribute to inflammatory diseases such as atherosclerosis (Swirski and Nahrendorf, 2013), obesity (Kosteli et al., 2010) and asthma (Moreira and Hogaboam, 2011). Hence, macrophages can play both beneficial and detrimental roles in health and disease.

1.1.5 Chemokines/cytokines

Innate immune cells secrete various messenger proteins to coordinate immune responses. Chemokines are small messenger proteins that control leukocyte migration and recruitment to specific parts of the body (reviewed in Moser et al. (2004)). Chemokines are split into different families depending on where the N-terminal cysteine residues are located. CC chemokines have two cysteine residues next to each other while CXC chemokines have a non-cysteine residue between two cysteines (reviewed in Rollins (1997)). Chemokines engage with chemokine receptors expressed on leukocytes (reviewed in Thiele and Rosenkilde (2014)). Specific chemokines and chemokine receptors direct leukocytes to specific tissues in the body. For example, C-X-C motif chemokine ligand 8 (CXCL8) interacts with CXCR1 and CXCR2 on neutrophils to induce their migration and activation (Holmes et al., 1991; Murphy and Tiffany, 1991).

During viral infection, interferons (IFNs) are important for limiting the dissemination of the virus around the body (Dupuis et al., 2003; Johansson et al., 2007). IFNs are split into three subtypes that engage different receptors: type I IFNs consisting of IFN-α, -β, -ε, -κ and -ω; type II IFNs consisting of IFN-γ and type III IFNs consisting of IFN-λ1 (IL-29) and IFN-λ2/3 (IL-28a/b) (reviewed in Ank and Paludan (2009)). Type I IFNs interact with the IFNAR receptor consisting of IFNAR1/2 while type III IFNs interact with the IL-28R consisting of IL-10R2 and IL-28Rα (Kotenko et al., 2003;

Pestka et al., 2004). Both type I and III IFNs activate receptor tyrosine kinases JAK1 and TYK2 which phosphorylate STAT1 and STAT2. Combined with IRF9, they form the ISGF3 complex which induce ISG expression (Dumoutier et al., 2004; Stark et al., 1998). IFN-γ, the lone type II IFN, interacts with interferon γ receptor (IFNGR) to activate the JAK/STAT pathway to coordinate immune responses, particularly in activating macrophages and natural killer (NK) cells, as well as activating antiviral responses (Briscoe et al., 1996; Darnell et al., 1994; Marsters et al., 1995).

Conversely, cytokines are messenger proteins that induce inflammation and specific immune responses such as leukocyte activation, proliferation, differentiation and survival. Cytokines are mostly secreted from leukocytes such as macrophages and neutrophils, but they can also be released from non-myeloid cells such as fibroblasts and hepatocytes (reviewed in Arend et al. (2008)). Engagement of cytokines with their receptors stimulates intracellular pathways that lead to the expression of pro-inflammatory genes. For example, TNF-α acts on the TNF receptor (TNFR)1 receptor to form one of two complexes. Complex I, which is formed on the cell surface, induces pro-inflammatory gene expression, leading to the induction of inflammatory and innate immune responses (Roach et al., 2002). Should complex I fail to form, the TNFR complex is internalised and transformed into complex II which activates the extrinsic pathway of apoptosis (Micheau and Tschopp, 2003).

Initially, cytokines activate innate immune cells such as macrophages and neutrophils and increase permeability on the endothelium, allowing leukocytes to enter tissue (reviewed in Dinarello (2007)). However, at high concentrations, pro-inflammatory cytokines IL-1β, IL-6 and TNF-α diffuse into the plasma, exerting endocrine actions to induce systemic inflammation. These pro-inflammatory cytokines act on the brain to induce fever, the liver to stimulate the production of acute phase proteins and the bone marrow to speed up leukocyte development (reviewed in Kumar et al. (2014)).

1.1.5.1 The IL-1 family of cytokines

The IL-1 family of cytokines are a group of pro- and anti-inflammatory mediators that share a common protein structure of interconnected β-sheets. This family contains seven pro-inflammatory cytokines (IL-1α, IL-1β, IL-18, IL-33, IL-36α, IL-36β and IL-36γ), three receptor antagonists (IL-1Ra, IL-36Ra and IL-38) and an anti-inflammatory cytokine (IL-37). These mediators engage with members of the IL-1 receptor (IL-1R) family that possess three extracellular immunoglobulin-like domains and an intracellular TIR domain (reviewed in Garlanda et al. (2013)). IL-1α and IL-1β engage the IL-1R made of IL-1R1 and IL-1RAcP (Cullinan et al., 1998; Dower et al., 1986) while IL-18 interacts with IL-18R consisting of IL-18Rα and IL-18Rβ (Hoshino et al., 1999b; Torigoe et al., 1997). These interactions bring the TIR domains together to attract MyD88 and activate mitogen-activated protein kinase (MAPK) and NF-κB (Muzio et al., 1998; Muzio et al., 1997). They can be blocked by receptor antagonists such as IL-1Ra (Dripps et al., 1991), providing a tightly-regulated feedback loop for IL-1R signalling. IL-1β and IL-18 are initially expressed in their longer, inactive pro-forms with the N-terminal region inhibiting folding of the cytokine in the C-terminal region (Lomedico et al., 1984; Okamura et al., 1995). These cytokines are only activated in the presence of inflammatory caspases, including caspase-1, cleaving and removing the N-terminal region, allowing the cytokine to fold to its active state (Gu et al., 1997; Thornberry et al., 1992).

IL-1β and IL-18 can play both beneficial and detrimental roles in the body. Both cytokines are required for the mediation of immune responses against pathogens such as *Staphylococcus aureus* (Miller et al., 2007) and *Leishmania* (Lima-Junior et al., 2013; Wei et al., 1999). However, excessive IL-1β and IL-18 concentrations can promote inflammatory disease. Initially, excessive IL-1β concentrations are associated with a group of autoinflammatory diseases called cryopyrin-associated periodic syndromes (CAPS) that promote chronic systemic inflammation, producing symptoms such as fever and skin rash (Feldmann et al., 2002; Hoffman et al., 2001). Since then, IL-1β and IL-18 have been linked to various inflammatory diseases such as type II diabetes (Gao et al., 2014; Larsen

et al., 2007), heart disease (Abbate et al., 2008) and arthritis (Banda et al., 2003). The study of the IL-1 cytokine family; therefore, is important for understanding how they are linked to various diseases. New therapeutics can then be designed which specifically target these cytokines to treat disease.

1.2 Inflammasomes

The inflammasome is a protein complex in the innate immune system that matures pro-inflammatory cytokines IL-1β and IL-18 and stimulates downstream pathways such as pyroptosis. First discovered by Hoffman et al. (2001) in the context of CAPS, the inflammasome requires two to three inflammasome components: a sensor protein, the adaptor protein ASC and an inflammatory caspase (Figure 1.4).

1.2.1 The components of the inflammasome

1.2.1.1 Sensor proteins

Most sensor proteins in inflammasomes are NLRs. All NLRs have a NACHT NBD which binds to nucleoside triphosphates such as adenosine triphosphate (ATP) to change NLR conformation and C-terminal LRRs which sense intracellular PAMPs or DAMPs (Figure 1.4). The N-terminal domain, which varies among different NLR families, binds to other proteins by establishing homo-dimeric associations (Ting et al., 2008). NLR family, CARD domain containing member 4 (NLRC4) is an inflammasome-forming NLR with an N-terminal CARD domain (Poyet et al., 2001). In contrast, NLR family, PYD domain containing members 1b and 3 (NLRP1b and NLRP3 respectively) contain an N-terminal PYD domain. NLRP1b also possesses C-terminal function to find domain (FIIND) and CARD domains (Finger et al., 2012). Absent in melanoma 2 (AIM2), like NLRP1b and NLRP3, has an N-terminal PYD domain, but it also has a C-terminal haematopoietic interferon-inducible nuclear protein with a 200-amino-acid repeat (HIN-200) domain that interacts with dsDNA (Hornung et al., 2009) (Figure 1.4).

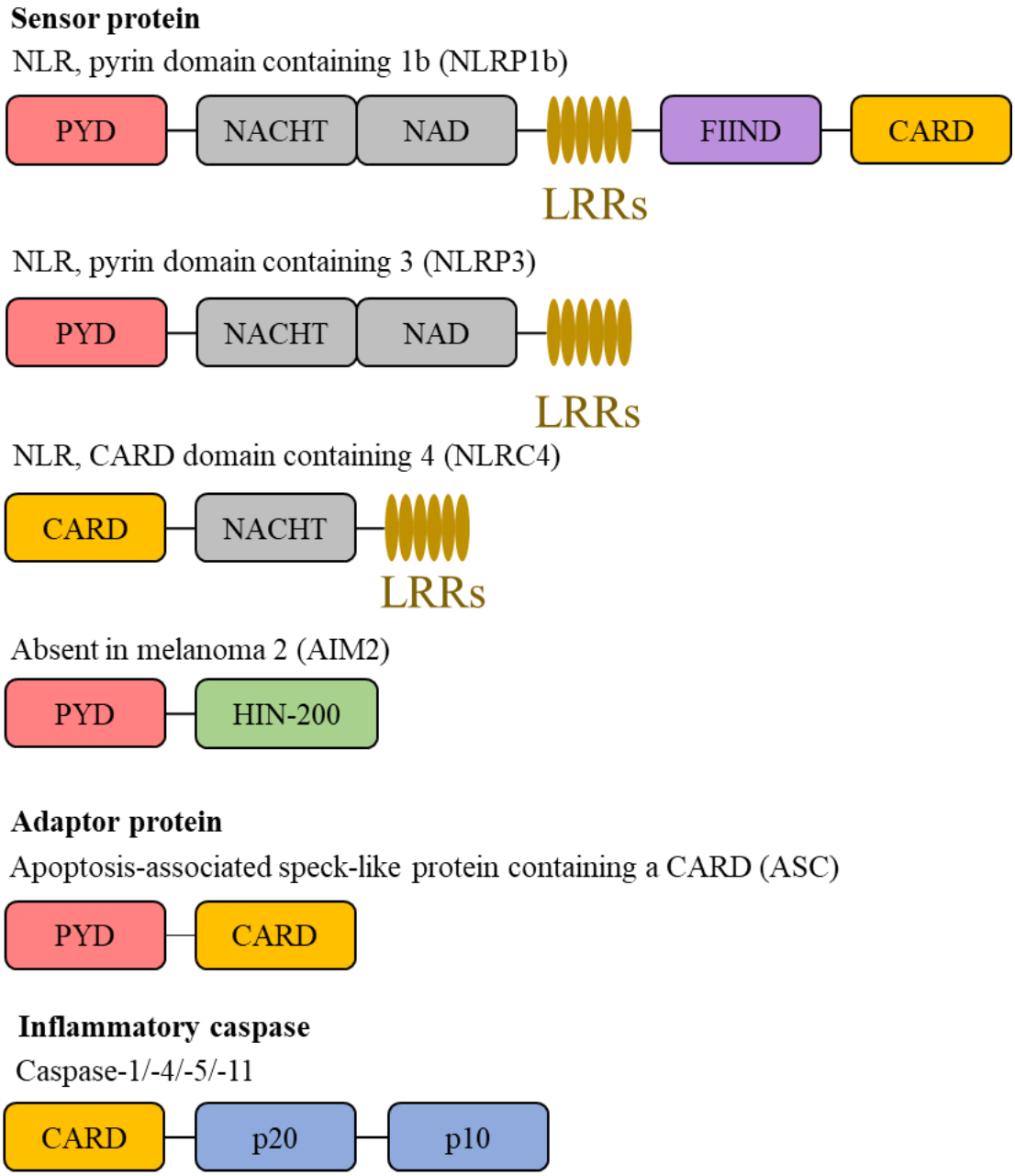

Figure 1.4: Domains of inflammasome components

Inflammasomes are comprised of two to three proteins: a sensor protein, the adaptor protein ASC and an inflammatory caspase. The sensor protein detects intracellular danger signals from pathogens or cell damage to trigger inflammasome assembly. Most sensor proteins are NLR family members such as NLRP1b, NLRP3 and NLRC4, but AIM2 is an atypical sensor protein that uses its HIN-200 domain to bind to dsDNA. Adaptor proteins connect the sensor protein to the inflammatory caspase, amplifying the danger signal to induce effector functions. The inflammatory caspase, when activated, cleaves inactive forms of pro-inflammatory cytokines IL-1β and IL-18. It also initiates an inflammatory form of cell death called pyroptosis by cleaving inactive gasdermin D. PYD = pyrin domain, NACHT = domain present in NAIP, CIITA, HET-E, and TP-1, NAD = NACHT-associated domain, LRRs = leucine-rich repeats, FIIND = function to find domain, CARD = caspase activation and recruitment domain, HIN-200 = haematopoietic interferon-inducible nuclear protein with a 200-amino-acid repeat.

These NLRs have two conformations depending on whether the inflammasome is active. The NLR adopts a closed conformation when the inflammasome is inactive. In NLRC4, the LRRs fold onto their NACHT NBD domain (Hu et al., 2015; Zhang et al., 2015) while in NLRP3, the PYD domain folds onto its own NACHT NBD domain (Hafner-Bratkovic et al., 2018; Martín-Sánchez et al., 2016). Upon inflammasome activation, the NLR unfolds and adopts an open conformation with either the LRRs (Hu et al., 2015; Zhang et al., 2015) or PYD domain (Hafner-Bratkovic et al., 2018; Martín-Sánchez et al., 2016) uncovering the NBD domain, allowing NLR oligomerisation.

Sensor proteins are expressed in a variety of myeloid and non-myeloid cells. For instance, NLRP3 is expressed in a variety of leukocytes such as neutrophils, monocytes, macrophages, cDCs and B and T lymphocytes (Guarda et al., 2011; Kummer et al., 2007; Sutterwala et al., 2006; Tran et al., 2012). NLRP3 is also expressed in non-myeloid cells such as type I airway epithelial cells (AECs), oral and oesophageal epithelial cells, thymic, splenic and hepatic sinusoidal endothelial cells, cortical neurons, cardiac muscle and renal tubular cells (Huang et al., 2014; Kummer et al., 2007; Tran et al., 2012). This enables inflammasomes to be activated in not only leukocytes but also non-myeloid cell populations such as epithelial cells which allow initiation and maintenance of inflammation.

1.2.1.2 **ASC**

Apoptosis-associated speck-like protein containing a CARD (ASC) is a 22kDa protein with 195 amino acids (Masumoto et al., 1999). It has an N-terminal PYD and a C-terminal CARD domain, six-helix bundle motifs with charged surfaces that enable ASC to bind to other proteins via homo-dimeric interactions (Bae and Park, 2011; Jin et al., 2013b) (Figure 1.4). The CARD domain in ASC interacts with the CARD domain of inflammatory caspases such as caspase-1 (Proell et al., 2013) while the PYD domain of ASC binds to the PYD domain in NLRs such as NLRP3 (Richards et al., 2001). Both the PYD and CARD domains have two charged surfaces, allowing ASC to interact with up to four proteins (Liepinsh et al., 2003; Nambayan et al., 2018). The two domains are connected by a flexible linker that not only prevents steric hindrance of the domains but also enables ASC to change

conformation (de Alba, 2009). With these properties, ASC acts as an adaptor protein, linking the sensor protein to the inflammatory caspase to construct the inflammasome (Mariathasan et al., 2004).

Asc mRNA in mice and humans is mostly expressed in leukocytes such as macrophages, DCs and neutrophils (Lattin et al., 2008; Mabbott et al., 2013). ASC is also expressed in non-myeloid-derived cells. In humans, ASC is expressed in glandular cells in the small intestine and colon as well as epidermal cells in the skin (Uhlen et al., 2015). In mice, *Asc* mRNA is expressed in the small intestine and colon as well as the lacrimal gland and cornea in the eye (Lattin et al., 2008).

1.2.1.3 **Inflammatory caspase**

Cysteine **asp**artate prote**ase**s (caspases) are enzymes that cleave peptide bonds joining aspartate to another amino acid. Most caspases are involved in apoptosis with caspase-2, -8, -9 and -10 being initiator caspases and caspase-3, -6 and -7 being effector caspases. Of the remaining caspases, human caspase-1, -4 and -5 as well as murine caspase-1, -11 and -12 are described as inflammatory caspases because they cleave substrates related to inflammation (reviewed in Jimenez Fernandez and Lamkanfi (2015)).

Caspase-1 is an inflammatory caspase that is closely associated with inflammasome function. Caspase-1 was initially termed IL-1β-converting enzyme (ICE) because it is a protease that cleaves pro-IL-1β to IL-1β (Black et al., 1989; Kostura et al., 1989). It is now classified as a cysteine protease (Thornberry et al., 1992), where it uses a cysteine residue (cys284 in mice or cys285 in human) in the active site to cleave peptide bonds between aspartate and a small hydrophobic residue such as glycine or alanine (Howard et al., 1991; Molineaux et al., 1993). Caspase-1 is initially translated as an inactive p45 subunit that is 402 amino acids long and has five domains: the N-terminal CARD domain, the CARD domain linker, the p20 subunit, the interdomain linker and the C-terminal p10 subunit (Boucher et al., 2018; Molineaux et al., 1993) (Figure 1.4). Upon activation, pro-caspase-1 dimerises and undergoes autoproteolysis at the interdomain linker, establishing an active site spanning both the p10 and p20 subunits (Boucher et al., 2018; Molineaux et al., 1993). Arg179 and Gln283 in the

caspase-1 active site recognise aspartate in the substrate while His237 and the cysteine residue (cys284 in mice or cys285 in human) cleave aspartate-linked peptide bonds (Wilson et al., 1994). Caspase-1 is inactivated via cleavage of the CARD domain linker which releases the CARD domain (Boucher et al., 2018).

Caspase-1 is expressed in a variety of leukocytes. Human caspase-1 is expressed in peripheral blood monocytes, pulmonary macrophages, lymphocytes and neutrophils, peripheral T cells and placenta (Cerretti et al., 1992; Uhlen et al., 2015). Similarly, murine caspase-1 is expressed in peritoneal exudate cells (PECs) and macrophage cell lines (Molineaux et al., 1993). To note, humans and mice also express caspase-1 in the gastrointestinal tract, particularly in the small intestine (Lattin et al., 2008; Uhlen et al., 2015).

Murine caspase-11 and human caspase-4/5 are recently-discovered inflammatory caspases. Being 54% homologous with caspase-1 (Wang et al., 1996), caspase-11 acts upstream of caspase-1 to promote IL-1β maturation (Wang et al., 1998), possibly by directly interacting with and activating caspase-1 (Wang et al., 1998) or promoting potassium efflux (Ruhl and Broz, 2015). Caspase-11 is also part of the non-canonical inflammasome, where its CARD domain binds to LPS (Hagar et al., 2013; Kayagaki et al., 2013; Shi et al., 2014). This enables cells to respond to intracellular bacteria and their products such as *Burkholderia thailandensis* and *Salmonella typhimurium* (Meunier et al., 2014). Murine *caspase-11* mRNA is expressed not only in lymphoid organs such as the spleen and thymus but also in non-lymphoid organs such as the heart, lung and kidney (Van de Craen et al., 1997; Wang et al., 1996).

Human caspase-4 and caspase-5 can also respond to cytosolic LPS, activating the NLRP3 inflammasome to induce caspase-1 activation, IL-1β maturation and pyroptosis via the non-canonical inflammasome pathway (Baker et al., 2015; Schmid-Burgk et al., 2015; Vigano et al., 2015). Similar to murine caspase-11, human caspase-4/5 is widely expressed in lymphoid and non-lymphoid organs, including the lung, stomach, small intestine, and kidney (Uhlen et al., 2015). These results show that

caspase-4/5/11 may act as LPS sensors that induce IL-1β maturation and secretion via the non-canonical inflammasome.

1.2.2 Functions of the inflammasome

The main function of the NLRP3 inflammasome is to mature pro-inflammatory cytokines. This process involves caspase-1 cleaving the inactive pro-forms of pro-inflammatory cytokines IL-1β and IL-18 to their bio-active secretory forms (Dowds et al., 2004; Martinon et al., 2004; Masters et al., 2010b). Caspase-1 does this by cleaving peptide bonds between aspartate and a small hydrophobic residue such as glycine or alanine within the substrate (Howard et al., 1991; Molineaux et al., 1993). Caspase-1 also matures the anti-inflammatory cytokine IL-37 by cleaving pro-IL-37 at Asp20 which is required for IL-37 to exhibit anti-inflammatory activity (Bulau et al., 2014).

Besides cytokine maturation, the NLRP3 inflammasome also induces an inflammatory form of cell death called pyroptosis (Brennan and Cookson, 2000; van der Velden et al., 2003). Pyroptosis is mainly associated with the formation of pores on the cell membrane. These pores mediate the swelling and lysing of cells via osmosis. Pores are also where mature IL-1β and IL-18 and cytosolic proteins such as lactate dehydrogenase (LDH) are released (Fink and Cookson, 2006; He et al., 2015). Pyroptosis is mediated by inflammatory caspases such as caspase-1 and caspase-11 cleaving the cytosolic protein gasdermin D (Kayagaki et al., 2015; Shi et al., 2015). The cleavage relieves the autoinhibition on the N-terminal gasdermin D domain which enhances the activities of the canonical and non-canonical inflammasomes (Kayagaki et al., 2015; Shi et al., 2015) and forms pores on the cell surface (Aglietti et al., 2016; Liu et al., 2016b) to induce pyroptosis.

Caspase-1 activation by the NLRP3 inflammasome also has other downstream effects besides cytokine maturation and pyroptosis. NLRP3 inflammasome particles from macrophages can be secreted to activate caspase-1 extracellularly or, when phagocytosed by other cells, intracellularly (Baroja-Mazo et al., 2014; Wang et al., 2011). Besides cytokines and gasdermin D, bioactive caspase-1 also cleaves other proteins, affecting various biochemical reactions. In terms of immune responses,

caspase-1 cleaves the nicotinamide adenine dinucleotide phosphate (NADPH) oxidase NADPH oxidase 2 (NOX2), preventing the enzyme from producing hydroxide ions. This enables the phagosome to acidify to degrade gram-positive bacteria (Sokolovska et al., 2013). Caspase-1 also cleaves pro-apoptotic proteins Bid and caspase-6 in human and murine neurons (Guo et al., 2006; Zhang et al., 2003) and pro-survival protein GATA binding protein 4 (GATA4) in murine cardiomyocytes (Aries et al., 2014) to induce apoptosis. Finally, caspase-1 degrades metabolic enzymes such as glyceraldehyde-3-phosphate to reduce glycolysis (Shao et al., 2007) and sirtuin 1 (SIRT1) to drive obesity and metabolic dysfunction (Chalkiadaki and Guarente, 2012). Hence, in addition to promoting inflammation, the NLRP3 inflammasome via caspase-1 may also affect other biochemical reactions in the cell.

1.2.3 The role of the NLRP3 inflammasome in disease

The NLRP3 inflammasome is an important therapeutic target because it is linked to a variety of diseases. Activation of the NLRP3 inflammasome by PAMPs or DAMPs promotes inflammation which contributes to disease. At the same time, NLRP3 inflammasome activity is important for protection against infection.

1.2.3.1 Autoinflammatory syndromes

The role of the NLRP3 inflammasome in disease was initially identified in a group of autoinflammatory syndromes called CAPS. These diseases, which include familial cold autoinflammatory syndrome (FCAS), Muckle-Wells Syndrome (MWS) and neonatal onset multisystem inflammatory disease (NOMID), are associated with periodic fever, skin rash and systemic inflammation (Feldmann et al., 2002; Hoffman et al., 2001). These diseases are linked to mutations in the NBD domain of NLRP3, enabling NLRP3 to constitutively adopt its active conformation (Aksentijevich et al., 2007). This leads to increased *Nlrp3* mRNA expression in leukocytes (Feldmann et al., 2002), elevated IL-1β protein expression in monocytes and enhanced *Tnfα* and *Il6* mRNA expression in peripheral blood mononuclear cells (Aksentijevich et al., 2002).

The recombinant human IL-1Ra biologic anakinra resolved the symptoms of CAPS (Hawkins et al., 2004; Matsubayashi et al., 2006; Ramos et al., 2005), implying that CAPS is driven via aberrant NLRP3-IL-1β signalling

1.2.3.2 **Particulate diseases**

Activation of the NLRP3 inflammasome by crystals is linked to various diseases. Initially, the NLRP3 inflammasome was associated with arthritic diseases gout and pseudogout. This is because the accumulation of monosodium urate (MSU) and calcium pyrophosphate dihydrate (CPPD) crystals in the joint in gout and pseudogout respectively activated the NLRP3 inflammasome in human and mouse macrophages, leading to IL-1β and IL-18 maturation (Martinon et al., 2006). Silicosis and asbestosis, pulmonary fibrotic diseases, are associated with the phagocytosis of silica and asbestos crystals respectively by alveolar macrophages and mesothelial cells to activate the NLRP3 inflammasome (Cassel et al., 2008; Dostert et al., 2008; Hillegass et al., 2013). These studies imply that accumulation of crystals in tissue may lead to disease via NLRP3 inflammasome activity.

1.2.3.3 **Neurodegenerative diseases**

The NLRP3 inflammasome is also activated by protein aggregates, contributing to the development of neurological diseases such as Alzheimer's disease. Alzheimer's disease patients were more likely to exhibit enhanced NLRP3 inflammasome activity compared to healthy controls (Halle et al., 2008; Heneka et al., 2013). This is due to microglia and astrocytes phagocytosing amyloid-β fibrils which activate the NLRP3 inflammasome (Cho et al., 2014; Couturier et al., 2016; Halle et al., 2008). Other protein aggregates that activate the NLRP3 inflammasome include α-synuclein fibrils from Parkinson's disease (Codolo et al., 2013) and prion protein (PrP) fibrils from prion disease (Hafner-Bratkovič et al., 2012). Activation of the NLRP3 inflammasome in microglia by protein aggregates induces the release of proinflammatory and neurotoxic factors such as IL-1β and nitric oxide (Hafner-Bratkovič et al., 2012; Halle et al., 2008). These factors attract microglia to the site of protein aggregation to amplify neuronal damage (Hafner-Bratkovič et al., 2012; Halle et al., 2008). Hence,

accumulation of protein aggregates in cells may activate the NLRP3 inflammasome to drive neurodegenerative diseases.

1.2.3.4 **Metabolic diseases**

More recently, the NLRP3 inflammasome has been linked to the development of metabolic diseases such as obesity, diabetes and atherosclerosis. Obesity is associated with inflammation in the adipose tissue due to increased macrophage and reduced regulatory T (T_{reg}) cell counts (Esser et al., 2013). Obese subjects, compared to lean individuals, also had increased caspase-1 activity, resulting in enhanced IL-1β maturation in adipose tissue (Esser et al., 2013). These results were similar in mice consuming a high-fat diet, where they exhibited enhanced caspase-1 and IL-1β activities in adipose tissue (Stienstra et al., 2010; Sun et al., 2012). The NLRP3 inflammasome is activated in macrophages in the presence of ceramides (Vandanmagsar et al., 2011) or saturated fatty acids such as palmitate (Wen et al., 2011), suggesting that fatty acid accumulation in adipose tissue may drive obesity-associated inflammation.

NLRP3 inflammasome activity contributes to the pathogenesis of type II diabetes. Patients with type II diabetes had increased protein and mRNA expression of NLRP3 inflammasome components in macrophages compared with healthy controls (Lee et al., 2013). NLRP3 inflammasome activity in the pancreas was induced by the accumulation of human islet amyloid polypeptide oligomers (Masters et al., 2010b), causing islet cell death and fibrosis which reduced insulin production (Youm et al., 2011). Knocking out NLRP3 to remove inflammasome activity re-established insulin secretion to normal levels to restore insulin sensitivity (Youm et al., 2011). Furthermore, it was found that NLRP3 inflammasome activity stimulated by diet- or genetic-induced obesity induces tissue inflammation and influenced adipocytes to become insulin-resistant (Stienstra et al., 2010; Vandanmagsar et al., 2011). Conversely, deficiencies in NLRP3 inflammasome components or inhibiting NLRP3 inflammasome activity reduced adipose tissue inflammation, restoring insulin sensitivity (Stienstra et al., 2010; Stienstra et al., 2011; Vandanmagsar et al., 2011). Type II diabetes

treatments such as metformin (Lee et al., 2013) as well as omega-3 fatty acids such as docosahexaenoic acid (Yan et al., 2013) also inhibited NLRP3 inflammasome activity, blunting tissue inflammation and insulin resistance. These studies identify the NLRP3 inflammasome as a potential therapeutic target for type II diabetes.

Lastly, the NLRP3 inflammasome is linked to atherosclerosis. Human studies found that NLRP3, caspase-1, IL-1β and IL-18 protein and mRNA expression were positively associated with increased severity of coronary artery disease, a form of atherosclerosis (Wang et al., 2014a). The mechanisms linking the NLRP3 inflammasome to atherosclerosis are varied. Macrophages phagocytose cholesterol crystals within plaques in blood vessels to activate the NLRP3 inflammasome (Duewell et al., 2010; Samstad et al., 2014). The uptake of cholesterol crystals by macrophages is enhanced in the presence of ATP (Li et al., 2014). Oxidised low-density lipoprotein within plaque also enhances *Il1β* mRNA and protein expression and maturation (Jiang et al., 2012; Liu et al., 2014). Consequently, IL-1β secreted from macrophages promotes the formation of macrophage foam cells which play an important role in the pathogenesis of atherosclerosis (Liu et al., 2014).

Collectively, these findings and examples suggest that the NLRP3 inflammasome is an important contributor to inflammatory and metabolic diseases.

1.2.3.5 **Infection**

Most studies of the NLRP3 inflammasome in infection have identified a protective role against pathogenic bacteria. The NLRP3 inflammasome is required for immune responses against Gram-positive bacteria such as *Staphylococcus aureus* (Mariathasan et al., 2006) and *Listeria monocytogenes* (Meixenberger et al., 2010; Wu et al., 2010) as well as Gram-negative bacteria such as *Neisseria gonorrhoeae* (Duncan et al., 2009) and *Aeromonas veronii biotype sobria* (McCoy et al., 2010). Although the role of the NLRP3 inflammasome is dispensable for *Salmonella typhimurium* infection (Lara-Tejero et al., 2006; Mariathasan et al., 2006), knocking out both NLRP3 and NLRC4 increased the susceptibility of mice to *S. typhimurium* infection (Broz et al., 2010a). NLRP3 and

NLRC4 inflammasomes are also involved in protection against gastrointestinal *Citrobacter rodentium* (Liu et al., 2012b) and pulmonary *Burkholderia pseudomallei* (Ceballos-Olvera et al., 2011) infections. These studies suggest that different inflammasomes are involved in immune responses against bacteria.

The NLRP3 inflammasome is also involved in immune responses against viral infections. These include Sendai, influenza, rabies, West Nile and Dengue viral infections (Kanneganti et al., 2006b; Lawrence et al., 2013; Ramos et al., 2012; Wu et al., 2013). Human immunodeficiency virus (HIV) promotes IL-1β protein expression and secretion from macrophages (Hernandez et al., 2014) and DCs (Pontillo et al., 2012). Ironically, DCs from HIV-infected patients failed to activate the NLRP3 inflammasome when challenged with HIV (Pontillo et al., 2012), perhaps due to suppressed immune responses from chronic HIV infection. The NLRP3 inflammasome also contributes to viral-mediated immunopathology. For instance, during chronic hepatitis C infection, IL-1β from hepatic Kuppfer cells and blood monocyte-derived macrophages promote chronic hepatic inflammation, damaging the liver (Negash et al., 2013; Shrivastava et al., 2013). Nevertheless, these studies show that inflammasomes are critically required for immune responses against various pathogens.

1.2.4 Inflammasome activation

The notion that inflammasome activation requires two signals was first proposed by Faustin et al. (2007) to describe NLRP1b inflammasome activation (Figure 1.5). Briefly, NOD2 senses muramyl dipeptide from peptidoglycan, activating NF-κB to upregulate inflammasome components and pro-inflammatory cytokines. This is known as the first or priming signal of inflammasome activation. Once inflammasome components and cytokines are upregulated, inflammasome activators such as ATP stimulate intracellular events, leading to inflammasome assembly. This is described as the second or activating signal of inflammasome activation (Faustin et al., 2007).

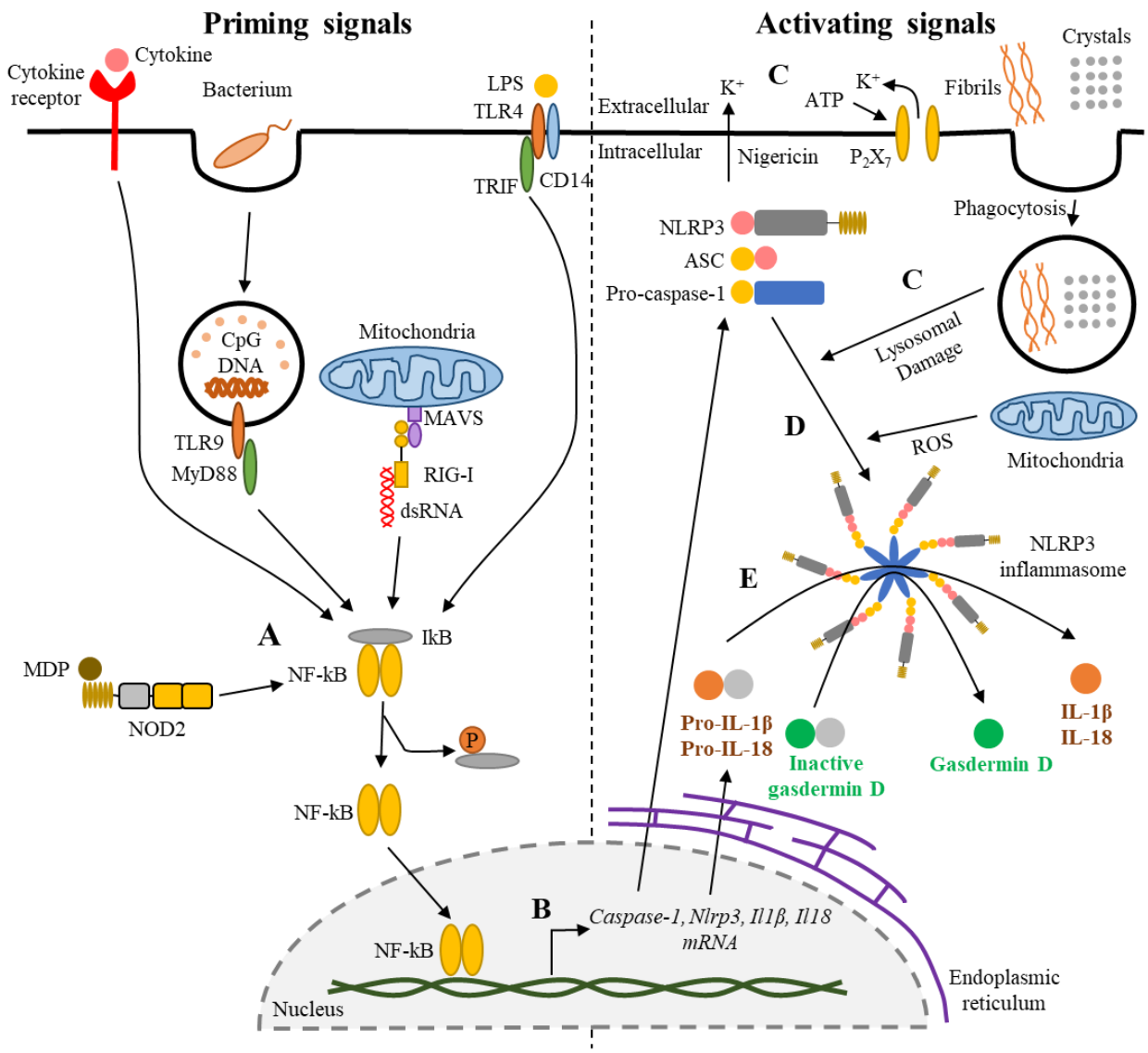

Figure 1.5: Two-signal model of inflammasome activation

Activation of the inflammasome requires two signals. (A) Priming signals are associated with NF-κB activation in response to PRR or cytokine receptor activation. (B) Activated NF-κB migrates to the nucleus, interacting with promoters to stimulate the expression of inflammasome components and pro forms of pro-inflammatory cytokines. (C) Activating signals are associated with the presence of soluble, particulate or aggregated inflammasome activators such as nigericin, crystals and fibrils respectively. They induce various intracellular events such as potassium (K+) efflux, lysosomal damage and ROS production. (D) These events lead to inflammasome assembly, where caspase-1 is activated. (E) Active caspase-1 matures pro-inflammatory cytokines IL-1β and IL-18 and cleaves gasdermin D to induce pyroptosis, an inflammatory form of cell death.

1.2.4.1 Priming signals

Priming signals of inflammasome activation upregulate inflammasome components and pro-inflammatory cytokines via NF-κB activity (Figure 1.5). NF-κB activity is triggered by signalling from TLRs, particularly the LPS receptor TLR4 (Bauernfeind et al., 2009), and cytokine receptors such as the TNF-α receptor TNFRI/II (Bauernfeind et al., 2009; Franchi et al., 2009). NF-κB activity leads to increased mRNA and protein expression of pro-IL-1β and pro-IL-18 as well as inflammasome components NLRP3 and pro-caspase-1 (Bauernfeind et al., 2009; Sutterwala et al., 2006). In the presence of priming signals, *Nlrp3* mRNA and protein are upregulated in leukocytes such as primary bone marrow-derived macrophages (pBMDMs) (Bauernfeind et al., 2009), neutrophils (Cho et al., 2012; Karmakar et al., 2015) and T cells (Eleftheriadis et al., 2015; Martin et al., 2016) as well as non-myeloid-derived cells such as AECs (Sebag et al., 2017; Tran et al., 2012). To note, priming signals do not upregulate ASC protein in PECs and pBMDMs (Franklin et al., 2014; Yamamoto et al., 2004). Nevertheless, priming signals lead to cells expressing inflammasome components and cytokine pro-forms, enabling them to activate the inflammasome in the presence of inflammasome activators.

1.2.4.2 Activating signals of the NLRP3 inflammasome

Priming signals are necessary but insufficient for inflammasome activation. It also requires an additional activating signal from an inflammasome activator (Figure 1.5). Inflammasome activators are endogenous or exogenous compounds from pathogens, damaged cells or the external environment that stimulate inflammasome assembly by initiating intracellular events such as potassium efflux, lysosomal damage and mitochondrial dysfunction (Table 1.2).

Table 1.2: List of inflammasome activators

Inflammasome	Inflammasome activator
AIM2	• dsDNA (Bürckstümmer et al., 2009; Fernandes-Alnemri et al., 2009; Hornung et al., 2009) • poly(dA:dT) (Hornung et al., 2009; Roberts et al., 2009)
NLRC4	• *Salmonella typhimurium* flagellin (via murine NAIP5) (Kofoed and Vance, 2011; Miao et al., 2006; Yang et al., 2014; Zhao et al., 2011) • Type III secretion system rod proteins such as *Salmonella* PrgJ and *Burkholderia* BsaK (via murine NAIP2) (Kofoed and Vance, 2011; Zhao et al., 2011) (Lightfield et al., 2011) • Type III secretion system needle protein Cprl from *Chromobacterium violaceum* (via human NAIP) (Zhao et al., 2011)
NLRP1b	• Anthrax lethal toxin (Boyden and Dietrich, 2006; Moayeri et al., 2010; Terra et al., 2010)

NLRP3	• Soluble activators:
	  o Nigericin (Mariathasan et al., 2006; Muñoz-Planillo et al., 2013)
	  o ATP (Mariathasan et al., 2006; Muñoz-Planillo et al., 2013)
	• Particulate activators:
	  o Monosodium urate crystals (Martinon et al., 2006)
	  o Calcium pyrophosphate dihydrate crystals (Martinon et al., 2006)
	  o Asbestos (Cassel et al., 2008; Dostert et al., 2008)
	  o Silica (Cassel et al., 2008; Dostert et al., 2008)
	  o Cholesterol crystals (Duewell et al., 2010)
	  o Alum (Franchi and Núñez, 2008)
	• Protein aggregate activators:
	  o Amyloid-β fibrils (Cho et al., 2014; Halle et al., 2008)
	  o α-synuclein aggregates (Codolo et al., 2013)
	  o Prion protein fibrils (Hafner-Bratkovič et al., 2012)
	  o Human islet amyloid polypeptide oligomers (Masters et al., 2010b)
	  o Hyaluronan (Yamasaki et al., 2009)
	  o IAV PB1-F2 fibrils (McAuley et al., 2013; Pinar et al., 2017)
	• Pathogen-derived activators:
	  o Bacterial RNA (Kanneganti et al., 2006a; Sha et al., 2014)
	  o Viral RNA (Chen et al., 2014; Kanneganti et al., 2006b)
	  o IAV RNA (Ren et al., 2017; Thomas et al., 2009)
	  o Muramyl dipeptide from peptidoglycan (Marina-García et al., 2008; Martinon et al., 2004)
	  o Pneumolysin from *Streptococcus pneumoniae* (Hoegen et al., 2011; Witzenrath et al., 2011)
	  o β-haemolysin from *Streptococcus agalactiae* (Costa et al., 2012; Gupta et al., 2014)
	  o α-, β- and γ-haemolysins from *Staphylococcus aureus* (Muñoz-Planillo et al., 2009)
	  o Listeriolysin O from *Listeria monocytogenes* (Meixenberger et al., 2010)
	  o Viroporin 2B proteins from viruses (Ito et al., 2012; Triantafilou et al., 2013b)
	  o M2 channel protein (Ichinohe et al., 2010)

Introduction

The NLRP3 inflammasome is assembled under a variety of exogenous and endogenous inflammasome activators signifying infection or tissue damage (Table 1.2). Soluble chemicals such as nigericin, a bacterial toxin from *Streptomyces hygroscopicus,* and ATP, an energy transfer molecule, were initially identified as NLRP3 inflammasome activators (Hogquist et al., 1991; Perregaux et al., 1992). These chemicals induce IL-1β maturation via the NLRP3 inflammasome in macrophages within 30 minutes of administration (Kahlenberg and Dubyak, 2004; Perregaux and Gabel, 1994). Crystalline compounds such as MSU from gout (Martinon et al., 2006), silica from silicosis (Cassel et al., 2008; Dostert et al., 2008) and cholesterol from atherosclerosis (Duewell et al., 2010) also activate the NLRP3 inflammasome. To note, these crystals can also present priming signals to promote the expression of pro-IL-1β and NLRP3 in cells (Hillegass et al., 2013; Zheng et al., 2015), providing a positive feedback loop to amplify NLRP3 inflammasome activity. Protein aggregates formed in neurodegenerative diseases such as amyloid-β fibrils in Alzheimer's disease (Cho et al., 2014; Halle et al., 2008) as well as other inflammatory diseases such as human islet amyloid polypeptide oligomers from type II diabetes (Masters et al., 2010b) are also NLRP3 inflammasome activators. Lastly, pathogen components such as bacterial (Kanneganti et al., 2006a; Sha et al., 2014) and viral RNA (Chen et al., 2014; Kanneganti et al., 2006b) and muramyl dipeptide (Marina-García et al., 2008; Martinon et al., 2004) can act as NLRP3 inflammasome activators. Alternatively, bacterial pore-forming proteins such as pneumolysin from *S. pneumoniae* (Hoegen et al., 2011; Witzenrath et al., 2011) and early secretory antigenic target (ESAT)6 from *Mycobacterium tuberculosis* (Mishra et al., 2010) that enable the migration of ligands and ions from the pathogen to the host cell can activate the inflammasome. Collectively, given the variety of different endogenous and exogenous compounds that can activate the NLRP3 inflammasome, the NLRP3 inflammasome is a central element in responses against infection and the pathogenesis of inflammatory diseases.

The presence of inflammasome activators stimulates a variety of intracellular pathways that lead to the assembly and activation of the NLRP3 inflammasome. Potassium efflux from the intracellular to extracellular environment is a well-known pathway for inflammasome activation (Petrilli et al., 2007;

Walev et al., 1995). Soluble NLRP3 inflammasome activators typically use this intracellular event to activate the NLRP3 inflammasome. Nigericin as a bacterial toxin is an ionophore, able to transport intracellular potassium ions out of the cell (Mariathasan et al., 2006). In contrast, extracellular ATP induces potassium efflux by binding to P_2X_7, a purinergic receptor (Riteau et al., 2012; Riteau et al., 2010), to open the channel, allowing potassium efflux. Potassium efflux is also a central mechanism in which pore-forming toxins such as α-, β- and γ-hemolysins from *S. aureus* (Muñoz-Planillo et al., 2009) and listeriolysin O from *L. monocytogenes* (Meixenberger et al., 2010) activate the NLRP3 inflammasome.

Lysosomal damage is another potential pathway of NLRP3 inflammasome activation, particularly for crystalline activators such as silica and alum (Duewell et al., 2010; Hornung et al., 2008) and protein aggregates such as amyloid-β fibrils (Codolo et al., 2013; Hafner-Bratkovič et al., 2012; Halle et al., 2008). Activation of the NLRP3 inflammasome by lysosomal damage involves three events: phagocytosis, lysosomal acidification and lysosome membrane permeabilization. Blocking phagocytosis with chemical inhibitors such as cytochalasin D prevented IL-1β secretion in LPS-primed human peripheral blood mononuclear cells (PBMCs) treated with MSU or silica crystals (Hornung et al., 2008). Lysosomal acidification is also required for inflammasome activation because inhibition of H^+-ATPase activity by bafilomycin A prevented silica from inducing IL-1β secretion in pBMDMs (Jessop et al., 2017). Phagocytosis and lysosomal acidification swell lysosomes which damages and ruptures the lysosomal membrane (Hornung et al., 2008; Katsnelson et al., 2016), releasing lysosomal proteases called cathepsins that are intermediaries of NLRP3 inflammasome activation (Orlowski et al., 2015). Chemically inhibiting cathepsin B, a cathepsin, with Ca-074-Me blocked NLRP3 inflammasome activation in pBMDMs (Jessop et al., 2017; Orlowski et al., 2015) as well as endothelial cells (Chen et al., 2015). Hence, phagocytosis of particulate and protein aggregate activators can damage lysosomes, leading to NLRP3 inflammasome activation.

Damaged or dysfunctional mitochondria can produce by-products that activate the NLRP3 inflammasome. A common by-product of damaged mitochondria is mitochondrial ROS (mtROS) which are released when oxidative phosphorylation is inhibited (Zhou et al., 2011), when intracellular calcium accumulates in the mitochondria (Triantafilou et al., 2013a; Yaron et al., 2015) or when inflammasome activators are present (Heid et al., 2013; Pinar et al., 2017). mtROS targets a variety of proteins to activate the NLRP3 inflammasome. For instance, mtROS inactivates the inhibitor phosphatase and tensin homolog (PTEN) to activate the PI3K/Akt pathway, stimulating the expression of oxidative stress genes and activation of the NLRP3 inflammasome (Cruz et al., 2007). Besides mtROS, other mitochondrial by-products such as mitochondrial DNA (mtDNA) (Nakahira et al., 2011; Shimada et al., 2012) and the mitochondrial lipid cardiolipin (Iyer et al., 2013) can act as co-activators of caspase-1, further promoting its activity. Active caspase-1 in turn can cleave Parkin, a pro-mitophagy protein, to produce more damaged mitochondria to amplify NLRP3 inflammasome activity (Yu et al., 2014). Dysfunctional mitochondria; hence, can stimulate NLRP3 inflammasome activity in a positive-feedback loop.

1.2.4.3 **Activating signals of other inflammasomes**

Different inflammasomes besides NLRP3 can be assembled depending on the inflammasome activator (Table 1.2). The NLRP1b inflammasome is assembled in the presence of anthrax lethal toxin. Anthrax lethal toxin has two components: the protective antigen (PA) which transports the toxin to the intracellular environment and lethal factor (LF) which cleaves kinases to block the MAPK pathway, impeding immune responses and cell survival (Agrawal and Pulendran, 2004). Variations in the NLRP1b gene determine whether murine macrophages are responsive to anthrax lethal toxin which determine survival against *Bacillus anthracis* infection (Boyden and Dietrich, 2006). Inbred murine strains such as BALB/c mice that had the anthrax-responsive NLRP1b allele resisted infection. Conversely, murine strains such as DBA/2J mice that had the non-responsive NLRP1b succumbed to infection (Moayeri et al., 2010; Terra et al., 2010). Survival of *Bacillus anthracis*

infection; therefore, is dependent on responses towards anthrax lethal toxin by the NLRP1b inflammasome.

Bacterial ligands activate the NLRC4 inflammasome by directly binding to NLR family apoptosis inhibitory protein (NAIP). NAIP5 binds to cytoplasmic bacterial flagellin from pathogenic bacteria such as *S. typhimurium* (Kofoed and Vance, 2011; Miao et al., 2006; Yang et al., 2014; Zhao et al., 2011) while NAIP2 directly binds to type III secretion system rod proteins such as *Salmonella* PrgJ and *Burkholderia* BsaK (Kofoed and Vance, 2011; Lightfield et al., 2011; Zhao et al., 2011). NAIP2 and NAIP5 are only expressed in mice, but human NAIP can bind to the type III secretion system needle protein Cprl from *Chromobacterium violaceum* (Zhao et al., 2011). Binding of bacterial ligands to NAIP proteins allows them to induce conformation changes on NLRC4, leading to the formation of an NLRC4 oligomer which initiates inflammasome assembly (Halff et al., 2012; Hu et al., 2015).

The activator of the AIM2 inflammasome is double-stranded DNA (dsDNA) from the host or pathogen (Bürckstümmer et al., 2009; Fernandes-Alnemri et al., 2009). The artificial dsDNA analogue poly(dA:dT) also activates the AIM2 inflammasome (Hornung et al., 2009; Roberts et al., 2009). Both dsDNA and poly(dA:dT) directly bind to the dsDNA-binding HIN-200 domain of AIM2 (Fernandes-Alnemri et al., 2009). This binding leads to ASC recruitment, caspase-1 and -3 cleavage and NF-κB activation to induce IL-1β maturation (Bürckstümmer et al., 2009; Hornung et al., 2009; Roberts et al., 2009). Hence, inflammatory responses can be raised against DNA via the AIM2 inflammasome.

1.2.4.4 **Assembly of the inflammasome**

Priming signals induce the expression of pro-IL-1β, pro-IL-18 and inflammasome components while activating signals enable NLRP3 inflammasome assembly (Figure 1.5). NLRP3 inflammasome assembly most likely follows the unified polymerisation model, where ASC and pro-caspase-1 are added to a growing inflammasome complex from the NLRP3 oligomer (Lu et al., 2014) (Figure 1.6).

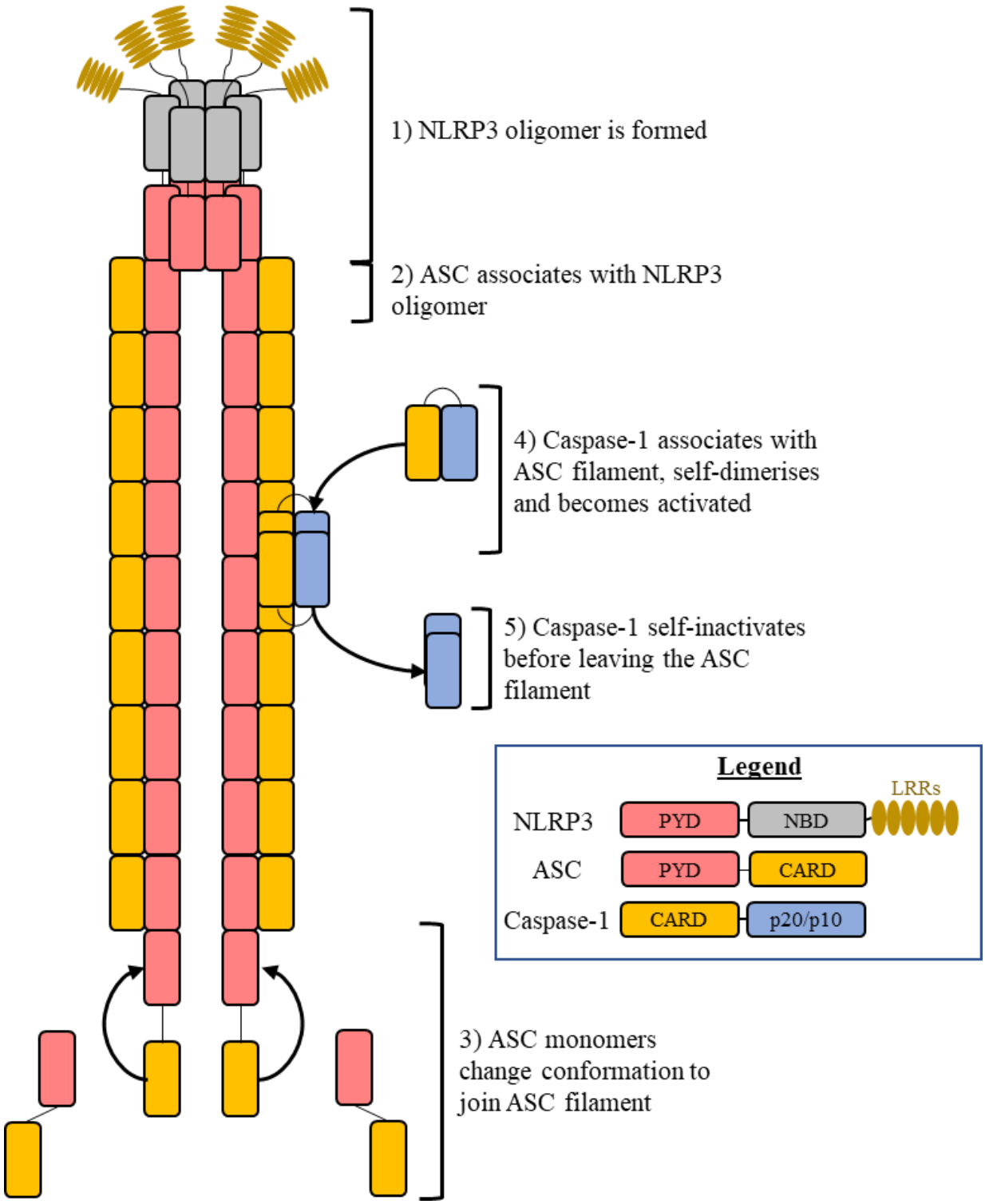

Figure 1.6: Process of inflammasome assembly

In the presence of cytosolic PAMPs or DAMPs, an NLRP3 oligomer is formed (step 1). Monomeric ASC bind to the NLRP3 oligomer via PYD interactions (step 2). This initiates ASC polymerisation, where monomeric ASC change conformation to join onto the end of the ASC filament (step 3). The establishment of an ASC filament allows caspase-1 to dimerise and become activated (step 4). Later, dimerised caspase-1 is cleaved further to its inactive state, where it leaves the inflammasome complex and is secreted (step 5).

Initially, NLRP3 is lowly expressed in resting cells, ubiquitinated (Palazon-Riquelme et al., 2018; Py et al., 2013) and kept in a folded conformation with the PYD domain folding onto its own NBD domain (Hafner-Bratkovic et al., 2018; Martín-Sánchez et al., 2016). After upregulation by priming signals and upon exposure to inflammasome activators, NLRP3 undergoes post-translational modifications to transition to its active unfolded form. First, the BRCA1/BRCA2-containing complex subunit 3 (BRCC3)-containing BRCC36 isopeptidase complex (BRISC) deubiquitinates NLRP3 LRRs (Juliana et al., 2012; Py et al., 2013). Deubiquitinases ubiquitin-specific-processing protease (USP)7 and USP47 also deubiquitinate NLRP3 which is a required event for NLRP3 inflammasome activation (Palazon-Riquelme et al., 2018). Second, protein phosphatase 2A (PP2A) dephosphorylates a serine residue in the NLRP3 PYD domain (Ser3 in mice or Ser5 in human), enabling NLRP3 PYD to interact with ASC PYD (Stutz et al., 2017). Lastly, ATP binds to the Walker A motif of the NLRP3 NBD domain (Duncan et al., 2007).

These post-translational modifications on NLRP3 lead to a conformational change from an inactive closed structure to an active open form which exposes the NBD domain (Hafner-Bratkovic et al., 2018; Martín-Sánchez et al., 2016). The open NLRP3 is transported by microtubule-affinity regulating kinase 4 (MARK4) to the microtubule-organising centre where NLRP3 proteins interact with each other (Li et al., 2017). This enables NLRP3 to nucleate into an oligomer (Duncan et al., 2007; Subramanian et al., 2013). However, only a small amount of NLRP3 is required to form an NLRP3 oligomer, leaving most cytosolic NLRP3 free (Yu et al., 2006).

The PYD domains of NLRP3 recruit ASC via PYD-PYD homodimeric interactions, establishing a small NLRP3 inflammasome complex (Liepinsh et al., 2003; Oroz et al., 2016). ASC accumulates around the small NLRP3 inflammasome complex, establishing supercritical concentrations of ASC. In this state, ASC at the tip of the fibril exhibits prion-like behaviour, inducing a conformational change in free ASC (Gambin et al., 2018). This increases the affinity of free ASC, allowing it to associate with the ASC fibril (Cheng et al., 2010; Gambin et al., 2018). ASC continually polymerises

with the NLRP3 inflammasome to establish an ASC filament stretching from the NLRP3 oligomer (Lu et al., 2014; Schmidt et al., 2016). Within the ASC filament, the CARD and PYD domains of ASC are packed tightly, where the core of the filament contains PYD domains and the outer surface is lined with CARD domains (Gambin et al., 2018; Sborgi et al., 2015; Schmidt et al., 2016). CARD domains on the outer edge of adjacent ASC filaments can interact with each other. This establishes cross-links among separate ASC filaments, bringing them together to form a high molecular-weight complex called an ASC speck (Dick et al., 2016; Kuri et al., 2017; Schmidt et al., 2016).

The ASC filaments on the NLRP3 inflammasome recruits caspase-1 via CARD-CARD homodimeric interactions between ASC and caspase-1 (Boucher et al., 2018). These interactions allow caspase-1 filaments to be established that stretch from ASC filaments (Lu et al., 2014). Alternatively, caspase-1 can homodimerise on the ASC filament to form the p46 subunit. Cleavage of the interdomain linker in dimerised caspase-1 generates a transient p33/p10 species that efficiently matures pro-IL-1β and pro-IL-18 to their active forms (Boucher et al., 2018). Caspase-1 is cleaved again at the CARD domain linker, forming the inactive p20/p10 species which is dissociated from the inflammasome and secreted (Boucher et al., 2018).

With NLRP3 oligomerisation and ASC polymerisation, the NLRP3 inflammasome amplifies the danger signal from the PAMP or DAMP. This enables multiple caspase-1 dimers to bind to the NLRP3 inflammasome, inducing IL-1β and IL-18 maturation and other downstream pathways. Most studies on inflammasome assembly have used cell-free systems where recombinant proteins form inflammasome complexes in solution. These studies; though, are limited in that recombinant proteins are often truncated and complexes are formed under non-physiological conditions such as acidic pH. Further studies on the formation of inflammasome complexes under cellular conditions using full-length inflammasome components are needed to confirm or clarify results of cell-free experiments.

1.2.4.5 Role of ASC specks in inflammasome activity

ASC speck formation is a quintessential feature of models of inflammasome assembly (reviewed in (Broz and Dixit, 2016; Elliott and Sutterwala, 2015)) as this cellular event is required for downstream effects of inflammasome activation. ASC specks act as a platform where intracellular caspase-1 is auto-activated to mature IL-1β and IL-18 (Broz et al., 2010b) and induce pyroptosis (Fernandes-Alnemri et al., 2007; Fink and Cookson, 2006). ASC deficiency and mutants in macrophages prevent caspase-1 activation which blunts IL-1β and IL-18 maturation (Mariathasan et al., 2004; Yamamoto et al., 2004) and pyroptosis (Fernandes-Alnemri et al., 2007), implying that functional ASC and subsequently ASC specks are required for inflammasome-induced cytokine maturation and pyroptosis. ASC specks can also be formed in apoptotic cells (Masumoto et al., 1999), where it acts as a platform to attract and activate caspase-8 to trigger apoptosis as an alternative death pathway to pyroptosis (Pierini et al., 2012; Vajjhala et al., 2015). In addition, ASC specks can be secreted into the interstitial space. Secreted ASC specks can activate extracellular caspase-1 to mature IL-1β and IL-18 outside cells or be phagocytosed by macrophages, where they damage lysosomes to promote further ASC polymerisation and subsequent IL-1β and IL-18 maturation (Baroja-Mazo et al., 2014; Franklin et al., 2014). Collectively, these studies highlight the importance of ASC specks in mediating the downstream events of inflammasome activity.

1.2.5 Measuring NLRP3 inflammasome activation

Biochemically measuring NLRP3 inflammasome activation is an important part of studying this protein complex. NLRP3 inflammasome activation is commonly measured by the secretion and maturation of IL-1β (Groß, 2012). The secretion of IL-1β can be measured by an IL-1β enzyme-linked immunosorbent assay (ELISA) of supernatant samples. However, current commercial ELISA kits cannot distinguish the longer pro-IL-1β protein from cleaved, active IL-1β. To differentiate these two forms of IL-1β, an IL-1β immunoblot of supernatant samples is commonly conducted. Here, active IL-1β, which has a molecular mass of 17kDa, can be distinguished from its longer pro-form at

34kDa (Kostura et al., 1989; Lomedico et al., 1984). An IL-1β immunoblot can also be conducted on lysate samples to measure intracellular IL-1β protein expression, particularly in the presence of priming signals.

NLRP3 inflammasome activation is also associated with the secretion of cleaved caspase-1. This can be detected by a caspase-1 immunoblot. Depending on the caspase-1 antibody, cleaved caspase-1 is associated with the presence of a p20 or p10 band at 20kDa and 10kDa respectively (Miller et al., 1993). A caspase-1 immunoblot can also be conducted on lysate samples to measure intracellular pro-caspase-1 protein expression at 45kDa (Miller et al., 1993). Hence, by using ELISA and immunoblotting, we can biochemically measure the activation of the NLRP3 inflammasome as well as intracellular protein expression of inflammasome components and cytokine pro-forms.

1.2.5.1 **Reporter models of inflammasome activation**

There are existing *in vitro*- and *in vivo*-based models of the NLRP3 inflammasome. *In vitro*-based models of the NLRP3 inflammasome are commonly used to screen for potential inflammasome activators. The most commonly used *in vitro*-based models use fluorescently-tagged ASC reporters which are transduced onto primary or immortalised cells. A well-known example of these cells is the ASC-Cerulean immortalised bone marrow-derived macrophages (iBMDMs) (Beilharz et al., 2016; Stutz et al., 2013). Attaching the Cerulean fluorescent protein to ASC enables the distribution of intracellular ASC to be measured. In a resting cell, ASC is normally diffuse throughout the cytosol. However, upon inflammasome activation, all cytosolic ASC condenses into one large structure called an ASC speck with a typical size of 1-3µm (Beilharz et al., 2016; Stutz et al., 2013; Tzeng et al., 2016). The formation of an ASC speck is a common indicator of inflammasome activation and can be measured in bio-imaging (Beilharz et al., 2016; Stutz et al., 2013) and flow cytometric (Sester et al., 2015) experiments. The limitation of ASC-Cerulean iBMDMs is that the ASC-Cerulean reporter is overexpressed. This may overestimate the size of the ASC specks and the extent of inflammasome activation exerted by a potential inflammasome activator.

Introduction

Recently, *in vivo* models of NLRP3 inflammasome activation have been developed. For example, an ASC-mKate2 reporter was knocked into zebrafish eggs (Kuri et al., 2017). Using the resultant zebrafish larvae, the authors found ASC protein expression in mucosal surfaces such as the intestine and ASC specks upon exposure to the stress signal copper sulfate. Besides zebrafish, murine models of inflammasome activation have also been generated. This was initially done by transducing the ASC-green fluorescent protein (GFP) reporter into *Rag2*$^{-/-}$ haematopoietic stem cells (HSCs). The resultant cells were then mixed with WT or caspase-1-deficient HSCs and reconstituted into irradiated WT mice (Sagoo et al., 2016). This technique was used to visualise and track ASC speck formation in draining lymph node macrophages during modified vaccinia Ankara viral infection *in vivo.* In their model, the authors discovered that inflammasome activation led to cell death and ASC speck release as well as inflammatory and T cell infiltration into the draining lymph nodes. The limitation of this model; though, is that ASC speck formation is restricted to myeloid cell populations. Therefore, it was not possible to study inflammasome expression and activation in non-myeloid-derived cell populations such as epithelial cells.

The problem was rectified in ASC-monomeric Citrine (mCitrine) mice generated by Tzeng et al. (2016). Here, the ASC-mCitrine reporter was knocked into murine embryonic stem cells (ESCs), enabling ASC to be expressed in myeloid- and non-myeloid-derived cells. Using these mice, they could identify and count ASC specks in cells *in vitro* as well as in influenza-infected lung tissue and *Streptococcus*-infected splenic tissue *ex vivo*. The limitation of this study; however, is that the ASC-mCitrine reporter was placed under the Rosa26 promoter. The Rosa26 promoter is known to overexpress the reporter in all cells and tissues of the mouse (Friedrich and Soriano, 1991). Similar to ASC-Cerulean iBMDMs; therefore, results from ASC-mCitrine mice may not accurately reflect what happens in an endogenous setting because the model may exaggerate the size of the ASC specks or the extent of inflammasome activation. Also, previous models of the inflammasome have only used ASC. To my knowledge, there is no characterisation of an NLRP3 reporter cell or mouse.

Therefore, it is important that new *in vitro*- and *in vivo*-based inflammasome models are generated that more accurately replicate the biological environment of the NLRP3 inflammasome.

1.2.5.2 **Inflammasome inhibitors and MCC950**

Endogenous and exogenous inhibitors can regulate inflammasome activity. Endogenous inhibitors include PYD-only proteins (POPs) and CARD-only proteins (COPs) that bind to PYD and CARD domains to inhibit elongation of ASC (Dorfleutner et al., 2007; Ratsimandresy et al., 2017) and caspase-1 (Humke et al., 2000; Lee et al., 2001) complexes respectively. Although most POPs and COPs have been found in human cells, a recent study discovered the murine POP orthologue Pydc3 which is able to inhibit IL-1β secretion from pBMDMs, suggesting inflammasome inhibitory activities (Vijay et al., 2017). Exogenous compounds such as auranofin (Isakov et al., 2014), glyburide (Lamkanfi et al., 2009) and parthenolide (Juliana et al., 2010) can also inhibit NLRP3 inflammasome expression and/or activity.

MCC950, previously called CRID3, is a small molecule inhibitor of the NLRP3 inflammasome. MCC950 is a diarylsulfonylurea, derived from the sulfonylurea glyburide with two aromatic groups. It was first found that glyburide and two diarylsulfonylurea derivatives could dose-dependently inhibit IL-1β maturation and secretion from LPS and ATP-treated human monocytes *in vitro* as well as LPS and ATP-challenged mice *in vivo* (Perregaux et al., 2001). MCC950 was first discovered as CRID3 by Laliberte et al. (2003) and was later resynthesised and tested by Coll et al. (2015). MCC950 could inhibit nigericin- and MSU-induced NLRP3 inflammasome activation and blunted caspase-1 activation and IL-1β maturation without affecting pro-caspase-1 or pro-cytokine protein expression. MCC950 blocked increases in sera IL-1β and IL-6 concentrations in an intraperitoneal LPS challenge and delayed the onset and severity of a mouse model of multiple sclerosis (Coll et al., 2015). Pharmacokinetically, MCC950 has a half-life of 3.27 hours. The mechanism behind the inhibitory actions of MCC950 have not currently been published, although studies have found that MCC950

does not block potassium efflux (Laliberte et al., 2003) or bind to proteins such as glutathione S-transferase omega 1-1 (Primiano et al., 2016).

Nevertheless, MCC950 is used to discover novel aspects of the NLRP3 inflammasome and its role in disease. In terms of the former, MCC950 was used to discover that the NLRP3 inflammasome is the downstream protein complex of caspase-4 and -5-induced IL-1β maturation (Baker et al., 2015) and that the NLRP3 inflammasome is activated in microglia phagocytosing amyloid-β (Dempsey et al., 2017). In terms of the latter, MCC950 is used to link the NLRP3 inflammasome to kidney disease (Krishnan et al., 2016), head and neck squamous cell carcinoma (Chen, 2018), diabetic encephalopathy (Zhai et al., 2018), traumatic brain injury (Ismael et al., 2018), cardiovascular disease (Pavillard et al., 2017) and intracerebral haemorrhage (Ren et al., 2018). Hence, MCC950 is a widely-used chemical inflammasome inhibitor that can be applied to various studies. Inhibitory targeting of the NLRP3 inflammasome with MCC950 also opens the possibility of targeting the inflammasome to treat various diseases. One potential disease linked to the NLRP3 inflammasome that might be amenable to targeting is influenza.

1.3 Influenza

1.3.1 Influenza biology

Influenza A virus (IAV) is an enveloped RNA virus in the *Orthomyxoviridae* family, infecting warm-blooded animals such as humans, birds and pigs (Hause et al., 2014; Shaw and Palese, 2013) (Figure 1.7). IAV infects and replicates well in epithelial cells in the upper and lower respiratory tracts (Kebaabetswe et al., 2013; Matrosovich et al., 2004; Tate et al., 2011d). IAV can also infect immune cells such as macrophages (Campbell et al., 2015; Rodgers and Mims, 1982b), DCs (Hargadon et al., 2011; VanoOsten Anderson et al., 2010) and neutrophils (Wang et al., 2008), though it is non-productive and leads to apoptosis (Cassidy et al., 1988; Hofmann et al., 1997).

The IAV genome has eight segments of negative-sense, single-stranded RNA expressing eleven proteins (Kash and Taubenberger, 2015). While matrix protein 1 (M1) forms a protein layer underneath the viral envelope, three IAV proteins are embedded in the envelope: haemagglutinin (HA) which binds to N-acetyl neuraminic acid (sialic acid) on host membrane glycoproteins to allow virion entry into host cells; neuraminidase (NA) which cleaves the bond between HA in budding IAV virions and sialic acid on host membrane glycoproteins to release IAV virions; and matrix protein 2 (M2) which transports protons across the viral envelope, acidifying the interior of virions in endosomes to assist in the unpacking of its contents (reviewed in Pielak and Chou (2011)). HA and NA are used to subtype IAV strains. IAVs that infect humans are commonly H1N2 and H3N2 subtypes. Avian IAV strains have H5N1, H7N9 and H9N2 as the most frequent subtypes while swine IAV strains commonly express H1N1, H1N2 and H3N2 (World Health Organisation, 2018).

Inside the M1 capsule, polymerase basic proteins 1 and 2 (PB1 and PB2) and polymerase acidic protein (PA) form the RNA-dependent RNA polymerase which associate with RNA and nucleoprotein (NP) to form ribonucleoproteins.

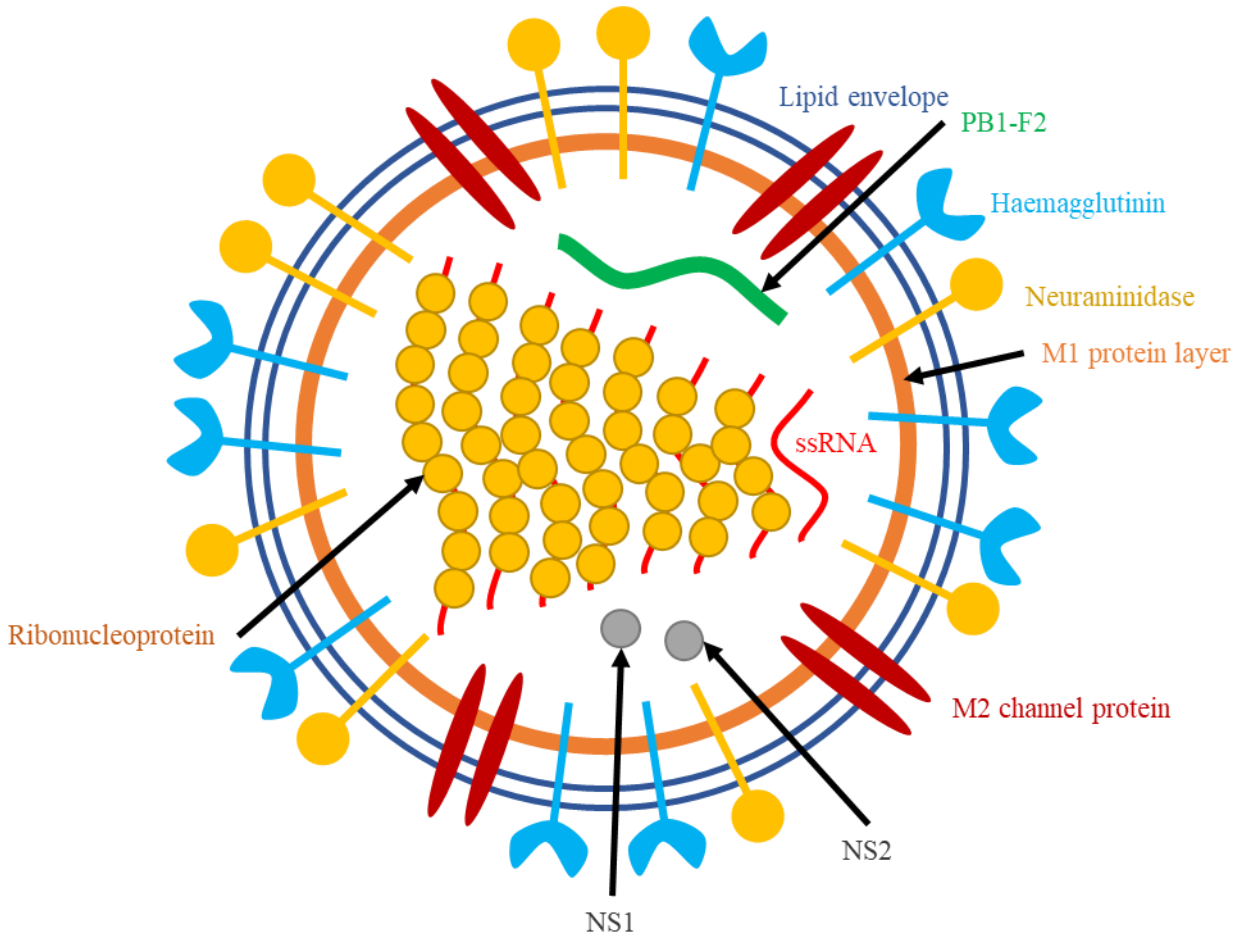

Figure 1.7: Diagram of the influenza A virus (IAV) virion

IAV is an enveloped virus containing eight ssRNA segments. Embedded in the lipid envelope are the surface proteins haemagglutinin, neuraminidase and M2 channel protein. Underneath the lipid envelope is the M1 protein layer. Within the virion, ssRNA is encapsulated by nucleoprotein and polymerase basic and acidic proteins to form ribonucleoproteins. There are some non-structural proteins that are neither expressed on the surface nor are part of ribonucleoproteins. These include non-structural proteins 1 and 2 (NS1 and NS2 respectively) and PB1-F2.

IAVs also express non-structural proteins 1 and 2 (NS1 and NS2) which inhibit interferon responses and export ribonucleoproteins respectively (Shimizu et al., 2011; Wang et al., 2000) and PB1-F2 (a polypeptide produced from the second open reading frame of PB1) which induces the intrinsic pathway of apoptosis in host cells (Zamarin et al., 2005).

1.3.2 Clinical aspects of influenza

IAV infection is a persistent public health problem associated with not only seasonal influenza epidemics but also pandemics and zoonotic infections. Influenza pandemics are linked to severe infection and mortality with the 1918 Spanish influenza pandemic causing an estimated 50 to 100 million deaths (Johnson and Mueller, 2002). Zoonotic IAV infections from swine and avian IAV subtypes such as H5N1 and H7N9 are also associated with severe illness and death with mortality rates of around 40-50% (Chotpitayasunondh et al., 2005; Hien et al., 2004; World Health Organisation, 2018). Zoonotic IAV infections have the mutagenic potential to become human-transmissible, possibly causing an influenza pandemic with increased rates of infection, hospitalisations and deaths.

Most people show no or mild symptoms of IAV infection such as cough, fever, sputum production and myalgia (Yu et al., 2008). However, IAV infection of the lower respiratory tract, particularly those from pathogenic strains from birds such as A/Anhui/1/2013 (H7N9), causes rapid, disordered breathing which may worsen to acute respiratory distress syndrome (ARDS), where plasma leaks into the alveoli through the damaged epithelial-endothelial layer (Short et al., 2014). This reduces gas exchange and consequently blood oxygen concentrations, leading to respiratory failure, organ dysfunction and death (Pabst et al., 2011).

Current treatments against IAV infection may not be sufficient to contain a potential influenza pandemic. Influenza vaccines are effective in reducing the incidence of IAV infection (Demicheli et al., 2018a; Demicheli et al., 2018b; Jefferson et al., 2018). However, vaccines may not be readily available in the early stages of an influenza pandemic due to the time taken to characterise the IAV

strain and manufacture the vaccine (reviewed in Houser and Subbarao (2015); Robertson et al. (2011); Sullivan et al. (2017)). Antivirals such as adamantanes and neuraminidase inhibitors can potentially treat IAV-infected patients. However, they are limited because they are only efficacious within forty-eight hours of symptom onset (Aoki et al., 2003; Fry et al., 2014) and are ineffective against antiviral-resistant IAV strains (Baranovich et al., 2015; Ciancio et al., 2009; Dharan et al., 2009; Dong et al., 2015). In addition, there are no treatments for patients that are hospitalised with late-stage pathogenic IAV infection. Hence, there is an urgent need to develop novel therapies for IAV infection.

1.3.3 The immune response to influenza

1.3.3.1 Sensing of IAV infection by PRRs

Various PRRs such as TLRs and RLRs sense IAV components to activate innate and adaptive immune responses. Within the TLR family, TLR3 and TLR7 sense endosomal IAV RNA. While TLR3 is required for NF-κB activation and cytokine production against IAV infection (Guillot et al., 2005; Le Goffic et al., 2007), TLR7 not only drives pro-inflammatory cytokine and interferon responses (Lund et al., 2004; Pang et al., 2013b) but also promotes Th1 (Jeisy-Scott et al., 2011; Madera and Libraty, 2013) and antibody responses (Jeisy-Scott et al., 2012; Sundararajan et al., 2012) against IAV.

RLRs also sense IAV RNA. RIG-I, which senses IAV ssRNA and dsRNA, is required for inducing IFN-β secretion from human epithelial cell lines such as A549 (Sirén et al., 2006; Wu et al., 2015) during IAV infection. IFN-β in turn can promote RIG-I expression in a positive feedback loop, amplifying antiviral responses (Pothlichet et al., 2013). Although the role of MDA5 in IAV infection is unclear (Benitez et al., 2015; Kato et al., 2006), MAVS, which acts downstream of the RLRs, is required for inducing cytokine and interferon secretion and inflammatory cell infiltration during IAV infection (Chakrabarti et al., 2015; Le Goffic et al., 2006; Teijaro et al., 2014). Hence, PRRs play an integral role in stimulating immune responses against IAV.

1.3.3.2 Soluble mediators

IAV infection activates interferon (IFN) responses to restrict viral replication in neighbouring cells. IAV infection induces the secretion of type I and III IFNs from murine tracheal epithelial cells (Crotta et al., 2013), murine primary bone marrow-derived dendritic cell (pBMDCs) (Jewell et al., 2010), human AECs (Ioannidis et al., 2013) and human primary monocyte-derived macrophages and pDCs (Ank et al., 2006; Coccia et al., 2004). Type I IFNs such as IFN-α and IFN-β restrict IAV replication in leukocytes such as primary human macrophages (Osterlund et al., 2010) and cDCs (Phipps-Yonas et al., 2008) as well as human bronchial epithelial cells (Thomas et al., 2014). Similarly, type III IFNs such as IFN-λ reduce IAV replication in human immortalised (Svetlikova et al., 2010) and primary epithelial cells (Davidson et al., 2016; Mordstein et al., 2008; Wang et al., 2009). Functional IFN signalling is required for immunity against IAV infection because deficiencies in both IFNAR1 and IL-28Rα, receptors for both type I and III IFNs respectively, enhanced the susceptibility of mice to NS1-deficient IAV strains (Mordstein et al., 2008) and PR8 (Crotta et al., 2013). Hence, IFN responses are important in immunity against IAV.

Individual cytokines and chemokines also play specific roles in mediating immunity against IAV. For instance, TNF-α is a pro-inflammatory cytokine that regulates $CD8^+$ T cell responses. While TNF-α enhances $CD8^+$ T cell responses to HKx31 (H3N2) (Wortzman et al., 2013) and PR8 (H1N1) (Kuwano et al., 1993) infections, it also limits $CD8^+$ T cell activity to prevent lung injury (De Berge et al., 2014). C-C motif chemokine ligand 2 (CCL2) secreted from infected epithelial cells interacts with the receptor CCR2 to induce monocyte migration to the infected lung to limit lung damage and viral replication (Herold et al., 2006; Narasaraju et al., 2010). Collectively, cytokines and chemokines are required to coordinate immune responses against IAV infection without causing lung injury.

1.3.3.3 Non-myeloid derived cells

Epithelial and endothelial cells express and secrete a variety of cytokines and chemokines during IAV infection. Pro-inflammatory cytokines such as TNF-α and IL-6 and chemokines such as CCL2 and

C-X-C motif chemokine ligand 10 (CXCL10) are secreted from primary murine alveolar epithelial cells during PR8 (H1N1) infection (Herold et al., 2006; Kebaabetswe et al., 2013; Tate et al., 2011d) and primary human respiratory epithelial cells during A/Vietnam/1194/04 (H5N1) infection (Chan et al., 2009; Chan et al., 2005b). Epithelial-derived cytokines and chemokines initiate the inflammatory response against IAV by attracting and activating leukocytes in the infected lung. Cytokines and chemokines are also released from infected primary human (Chan et al., 2005a; Ocaña-Macchi et al., 2009; Short et al., 2014) and murine endothelial cells (Teijaro et al., 2011). Additionally, endothelial cells upregulate adhesion molecules E- and P-selectin (Colden-Stanfield et al., 1993; Ocaña-Macchi et al., 2009), intercellular adhesion molecule 1 (ICAM-1) and vascular adhesion molecule 1 (VCAM-1) (Zeng et al., 2012), allowing inflammatory cells such as neutrophils to migrate and adhere onto the pulmonary endothelium to enter the lung.

1.3.3.4 **Resident immune cells**

Lung-resident macrophages and DCs restrict IAV infection while presenting antigens to activate the adaptive immune response. Alveolar macrophages in the pulmonary airways phagocytose and degrade IAV virions and IAV-infected apoptotic cells (Fujisawa et al., 1987; Hashimoto et al., 2007). They play an important role in promoting immune responses against and clearance of IAV because chemical (Murphy et al., 2011; Tate et al., 2010; Tumpey et al., 2005) and genetic (Purnama et al., 2014; Schneider et al., 2014) depletion of alveolar macrophages increased the susceptibility and severity of mice to IAV infection. Interstitial macrophages are present within the lung parenchyma, where they have similar surface marker and TLR expression to alveolar macrophages (reviewed in Schyns et al. (2018)). Unlike alveolar macrophages, interstitial macrophages show a more immunoregulatory role, secreting more immunoregulatory cytokines such as IL-10 and IL-1ra than pro-inflammatory cytokines such as IL-1β and TNF-α (Hoppstadter et al., 2010; Sabatel et al., 2017). Although the number of interstitial macrophages in the lung increases during IAV infection (LeMessurier et al., 2016), the role of interstitial macrophages in IAV infection is unknown.

Respiratory DCs (RDCs) also phagocytose IAV virions and IAV-infected cells and are required for activating adaptive immune responses. Upon IAV infection, $CD103^+$ and $CD11b^+$ RDCs migrate to the draining lymph nodes to present IAV antigens to naïve $CD4^+$ T cells (GeurtsvanKessel et al., 2008; Kim and Braciale, 2009; Kim et al., 2010). Activated $CD4^+$ T cells assist in the development of humoral immune responses against IAV virions (Ekiert et al., 2009; Ekiert et al., 2011). $CD103^+$ RDCs additionally cross-present IAV antigens to $CD8^+$ T cells, stimulating its proliferation and differentiation to cytotoxic T lymphocytes (CTLs) (Kim and Lee, 2014; Kim and Braciale, 2009). CTLs then migrate to the infected lung, killing IAV-infected cells via the induction of the extrinsic pathway of apoptosis and the release of perforin and granzymes to degrade cells (Topham et al., 1997). Hence, respiratory immune cells restrict IAV infection while activating the adaptive immune response.

1.3.3.5 **Infiltrating immune cells**

Blood-derived immune cells migrate to the infected lung to phagocytose IAV virions and kill IAV-infected cells. Neutrophils are recruited to the respiratory tract in the early stages of IAV infection and are required for protection against IAV infection (Tate et al., 2008; Tate et al., 2009). They restrict pulmonary IAV infection by phagocytosing IAV virions and producing ROS (Daigneault et al., 1992; Fujisawa, 2008; Tate et al., 2008; Tate et al., 2009). Neutrophils may also augment cell-mediated immune responses by presenting IAV antigens to $CD8^+$ T cells (Hufford et al., 2012; Tate et al., 2012).

Inflammatory macrophages, associated with murine Ly6C or human CD14 expression, originate from blood-derived monocytes that have differentiated in infected or inflamed sites (Wynn et al., 2013). IAV infection is associated with the infiltration of inflammatory macrophages into the airways and the lung (Lin et al., 2008) and are required for limiting viral replication and maintaining airway epithelium integrity and regeneration (Narasaraju et al., 2010). Inflammatory macrophages do this by

secreting a variety of pro-inflammatory cytokines such as TNF-α and TGF-β (Lin et al., 2008; van Riel et al., 2011) and priming $CD4^+$ T cells to activate adaptive immune responses (Diao et al., 2014).

Lastly, NK cells infiltrate the lung to lyse IAV-infected cells. Pulmonary NK cells are activated during IAV infection upon human NKp46 or murine NCR1 recognising IAV HA on the surface of the infected cell (Achdout et al., 2010; Glasner et al., 2012). Activated NK cells lyse IAV-infected cells via granzyme and perforin, limiting PR8 (H1N1) (Glasner et al., 2012) and A/Vietnam/1203/04 (H5N1) replication (Achdout et al., 2010) *in vitro* and *in vivo*.

1.3.4 **Pathophysiology**

Pathogenic IAV infection is associated with lung damage and injury, reducing respiratory function which can cause organ dysfunction and death (Pabst et al., 2011). There are three aspects of the pathophysiology of pathogenic IAV infection: primary viral pneumonia, secondary bacterial pneumonia and hyper-inflammation (Figure 1.8). IAV infection of epithelial cells, leukocytes and endothelial cells produces primary viral pneumonia (Armstrong et al., 2012; Shieh et al., 2010; Takiyama et al., 2010). IAV infection of epithelial cells stimulates apoptosis (Lam et al., 2008; Tripathi et al., 2013) which is associated with reduced lung compliance and respiratory function (Hofer et al., 2015; Sanders et al., 2013). The resultant damage to the respiratory epithelium may allow respiratory bacteria such as *Staphylococcus aureus* and *Streptococcus pneumoniae* to infect the lung, causing secondary bacterial pneumonia which enhances lung injury (Hussell and Cavanagh, 2009; Morens et al., 2008). Infection and apoptosis of endothelial cells also degrades the epithelial-endothelial barrier, allowing plasma to leak into the lung to produce ARDS (Armstrong et al., 2012; Ocaña-Macchi et al., 2009). IAV virions and bacteria may also travel through the damaged epithelial-endothelial barrier to circulate in the bloodstream, causing septicaemia (Jain et al., 2012; Yang et al., 2015) and extra-pulmonary infection in organs such as the brain and heart (Mori et al., 1995).

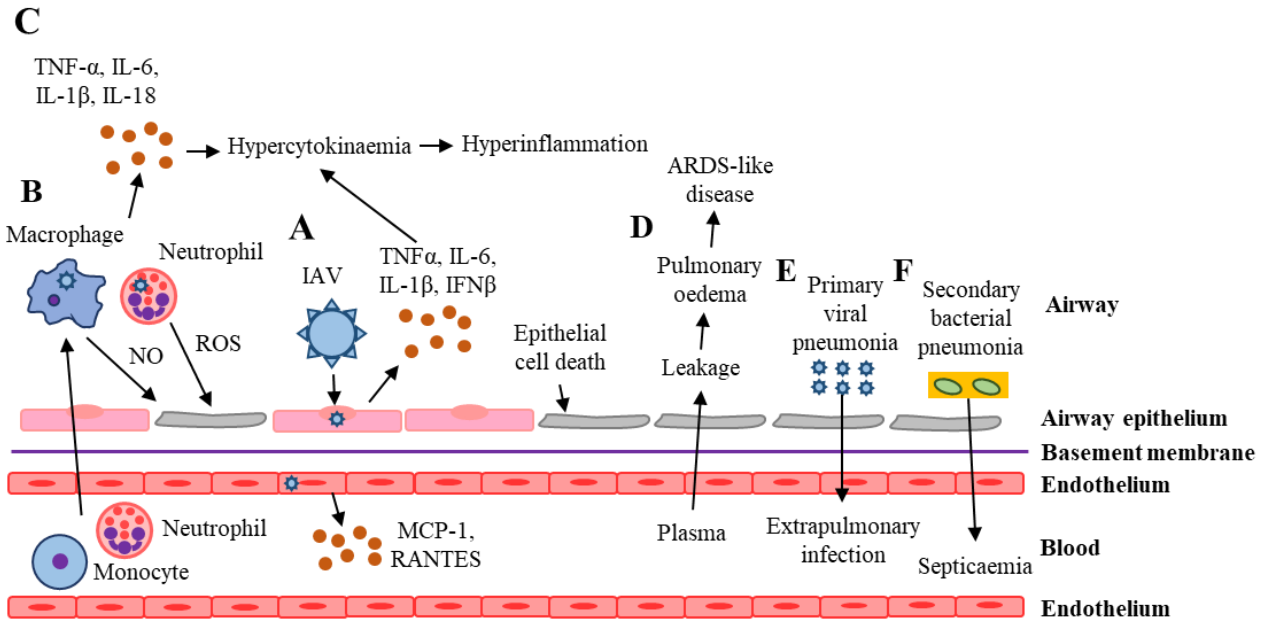

Figure 1.8: Pathophysiology of IAV infection

(A) Influenza A virus (IAV) initially infects respiratory epithelial and endothelial cells. (B) This causes cytokines and chemokines to be released which attracts and activates leukocytes such as macrophages and neutrophils. (C) Active macrophages and neutrophils release various pro-inflammatory cytokines and mediators such as nitric oxide (NO) and reactive oxygen species (ROS). This promotes inflammation to restrict IAV infection, but it can also lead to tissue damage and cell death due to hyper-cytokinaemia-induced hyper-inflammation. (D) The death of epithelial and endothelial cells leads to the leakage of plasma into the lung, causing pulmonary oedema which leads to acute respiratory distress syndrome (ARDS)-like disease. The degradation of the epithelial-endothelial barrier may also lead to (E) extrapulmonary infection and (F) septicaemia due to IAV and bacteria in the lung leaking into the plasma respectively.

Besides primary viral and secondary bacterial pneumonia, pulmonary hyper-inflammation can enhance lung injury which can contribute to reduced respiratory function and death.

1.3.4.1 Hyper-inflammation in IAV infection

Hyper-inflammation, where immune, inflammatory and cell death pathways are hyper-activated (Kash et al., 2006a; Xiao et al., 2013a), is an important contributor to the pathophysiology of pathogenic IAV infection. The presence of hyper-inflammation is associated with increased risk of hospitalisation from 2009 swine-origin H1N1 pandemic strain (H1N1pdm09) infection (Bermejo-Martin et al., 2009; Lee et al., 2011b) as well as enhanced severity and mortality from H7N9 (Chi et al., 2013; Guo et al., 2015a), H5N1 (de Jong et al., 2006; To et al., 2001) and H1N1pdm09 (To et al., 2010) infections. The magnitude of hyper-inflammation is positively associated with pulmonary H5N1 (de Jong et al., 2006) and H1N1pdm09 viral loads (Gao et al., 2013), indicating that primary viral pneumonia is required to initiate and enhance hyper-inflammation. Hyper-inflammation also enhances pulmonary damage initiated by primary viral and secondary bacterial pneumonia, reducing pulmonary function (Lee et al., 2011b).

Hyper-inflammation has two cardinal features. One feature is hyper-cytokinaemia which is present in mice infected with pandemic IAV strains such as reconstructed 1918 influenza virus (Kash et al., 2006b; Kobasa et al., 2007) and A/Hong Kong/483/97 (H5N1) (Szretter et al., 2007). In hyper-cytokinaemia, various cytokines and protein mediators are secreted. These can be pro-inflammatory mediators such as IL-1β, TNF-α and IL-6; anti-inflammatory proteins such as IL-1Ra and IL-10; adaptive immune cytokines such as IFN-γ and IL-17; type I IFNs such as IFN-α and chemokines such as CCL2, CXCL10 and CXCL8 (Arankalle et al., 2010; Chang et al., 2011). The secretion of various cytokines and protein mediators not only produces uncontrolled inflammation that damages the lung but also downregulates adaptive immunity that allows IAV to persist longer (Bermejo-Martin et al., 2010). Certain cytokines can promote hyper-cytokinaemia or drive pathological responses against IAV. For instance, IL-1β can promote hyper-cytokinaemia by upregulating pro-inflammatory

cytokine mRNA expression in human pulmonary microvascular endothelial cells infected with A/California/7/2009 (H1N1pdm09) (Kim et al., 2015). Conversely, type I IFNs can drive pathological responses against IAV by promoting pro-inflammatory cytokine secretion and upregulating death-associated receptors such as death receptor 5 (DR5) in the lung (Davidson et al., 2014). As well as that, the chemokine MIP-2 was found to mediate severity against PR8 (H1N1) infection (Sakai et al., 2000). These results surmise that cytokines and chemokines can promote immune and hyper-inflammatory responses against IAV infection.

Hyper-inflammation is also associated with the infiltration of inflammatory cells such as inflammatory macrophages, neutrophils and NK cells into the lung and airways. Inflammatory macrophages contribute to hyper-inflammation by secreting pro-inflammatory cytokines such as TNF-α to strengthen hyper-cytokinaemia (van Riel et al., 2011) and inducing alveolar epithelial cell apoptosis (Herold et al., 2008). Consequently, reducing inflammatory macrophage infiltration decreased alveolar epithelial cell apoptosis and lung injury, resulting in less severe IAV infection (Coates et al., 2018; Dawson et al., 2000; Lin et al., 2008; Wareing et al., 2007). Neutrophils also contribute to pathogenic responses against IAV by secreting NETs, a mixture of DNA, chromatin proteins and enzymes, that enhances epithelial-endothelial barrier damage (Narasaraju et al., 2011). Additionally, NK cells contribute to the pathology of IAV infection because its depletion reduced the susceptibility of mice to lethal PR8 infection by decreasing inflammatory cell infiltration and pro-inflammatory cytokine secretion (Abdul-Careem et al., 2012; Zhou et al., 2013). These studies highlight the role of infiltrating inflammatory cells in promoting the immunopathology of IAV infection and how their depletion might be used to develop cell-specific therapeutics that reduce disease severity.

1.3.5 The mouse model of IAV infection

A variety of animals such as mice, ferrets and guinea pigs are used to model IAV infection. Mice are the most commonly used animal model to study IAV infection because they are cheap to house and maintain, can be genetically modified to study specific host proteins and can be measured using widely-available mouse-specific reagents (reviewed in Bouvier and Lowen (2010)). Grossly, the severity of IAV infection in mice can be measured by weight loss and mortality as well as viral titres, pathology scores and lung weights (Sidwell et al., 1998). Histologically, mice exhibit primary viral pneumonia with lung lesions, pulmonary oedema and inflammatory cell infiltration (Kobasa et al., 2004; Perrone et al., 2008). IAV strains, particularly avian H5 and H7 subtypes, can also infect extra-pulmonary organs such as the brain, spleen and liver (Belser et al., 2009; Lu et al., 1999).

The murine strain affects the severity of IAV infection. Some murine strains such as DBA/2J exhibit more severe PR8 (Srivastava et al., 2009) and HKx31 (Trammell et al., 2012) infection compared to others such as C57BL6/J and BALB/c. This might be due to enhanced hyper-inflammatory responses in DBA/2J mice because they had higher lung (Trammell et al., 2012) and bronchoalveolar lavage (BAL) (Srivastava et al., 2009) pro-inflammatory cytokine concentrations and stronger upregulation of cytokine and chemokine genes (Alberts et al., 2010) compared to other murine strains such as C57BL6/J. Hence, the murine background is a factor to consider when designing an IAV infection study.

The IAV strain used in an experiment also affects the severity of infection. Some pathogenic IAV strains such as A/California/04/2009 (H1N1pdm09) (Itoh et al., 2009), A/Hong Kong/483/1997 (H5N1) (Lu et al., 1999) and A/Anhui/1/2013 (H7N9) (Belser et al., 2013) can cause severe infection in mice without prior adaptation. However, most studies use IAV strains such as PR8 (H1N1) and WSN (H1N1) that have been adapted to infect mice via serial passages in murine lungs (Brown, 1990; Ilyushina et al., 2010; Taylor, 1941). These strains have acquired mutations that allow them to

replicate in murine lungs more efficiently while suppressing and evading the immune response (Narasaraju et al., 2009; Tate et al., 2011a; Xu et al., 2011).

PR8 is a commonly-used murine-adapted IAV strain derived from A/Puerto Rico/8/1934 (H1N1). The dose of PR8 can be adjusted to induce sub-lethal IAV infection associated with epithelial shedding, bronchiolitis and alveolitis (Buchweitz et al., 2007) or lethal IAV infection linked to lung injury and diffuse alveolar damage (Fukushi et al., 2011; Tate et al., 2011d). The limitation of PR8; though, is that it is unable to infect murine macrophages because its HA cannot interact with sialic acid residues on murine macrophages (Tate et al., 2011d). This is an important aspect of IAV infection research because seasonal (Ramírez-Martínez et al., 2013; Rodgers and Mims, 1982a) and pandemic (Cheung et al., 2002; Perrone et al., 2008; Zhao et al., 2016) IAV strains can infect human macrophages during infection. To overcome this limitation, re-assorted PR8 viruses were generated that can infect both epithelial cells and macrophages. These viruses are HKx31 and BJx109, where the HA and NA of PR8 are replaced by those from A/Aichi/2/1968 (H3N2) and A/Beijing/353/1989 (H3N2) respectively. Even though these viruses infect both epithelial cells and macrophages, they tend to cause milder IAV infection compared to PR8 (Sanders et al., 2013; Tate et al., 2011d). Nevertheless, similar to PR8, the dose of HKx31 can be adjusted to cause sub-lethal or lethal IAV infection (Tate et al., 2016; Tate et al., 2011d). Hence, HKx31 may more realistically simulate IAV infection in mice where both epithelial cells and macrophages need to be infected.

1.4 The role of the inflammasome in IAV infection

1.4.1 Human studies of inflammasome in influenza

Hyper-cytokinaemia is a driver of the hyper-inflammatory state in severe IAV infection that can cause lung injury, organ failure and death. Indeed, the downstream products of the inflammasome IL-18 and IL-1β have been linked to the severity of IAV infection. Plasma IL-18 concentrations were positively associated with the severity of H1N1 (Lee et al., 2011a) and H7N9 (Guo et al., 2015b) IAV infections. Most of the studies; though, have focused on the association between IL-1β and IAV

infection severity in humans. Plasma IL-1β concentrations were found to be increased in severe cases of H1N1 infection (Chiaretti et al., 2013; Wang et al., 2014b) and IAV-induced brain damage (Sun et al., 2015) compared to patients with no or mild IAV infection. Airway IL-1β concentrations were also elevated in fatal cases of H7N9 IAV infection (Wang et al., 2014c). Moreover, single nucleotide polymorphisms (SNPs) in the human *Il1β* gene are associated with increased susceptibility to H1N1pdm09 infection (Garcia-Ramirez et al., 2015; Liu et al., 2013; Morales-García et al., 2012). The mechanisms behind these SNPs influencing IL-1β expression or function; though, are not precisely known due to the SNPs being found in the promoter or intronic regions of the *Il1β* gene. Nevertheless, these studies reveal the indirect influence of the inflammasome on the severity of IAV infection via the downstream cytokines IL-1β and IL-18.

1.4.2 *In vitro* studies of inflammasome in influenza

IAV infection is associated with the expression and activation of the NLRP3 inflammasome. PR8 infection led to increased mRNA expression of inflammasome components *Nlrp3, Asc, caspase-1* and *Il1β* in the murine lung three days post-infection (Allen et al., 2009). Inflammasome activation in the form of IL-1β secretion and maturation and caspase-1 cleavage can be identified in both immune cells such as murine pBMDMs (Ichinohe et al., 2009) and non-immune cells such as primary human bronchial epithelial cells (Pothlichet et al., 2013). This is dependent on lysosomal damage and ROS production inducing and maintaining NLRP3 inflammasome activity (Allen et al., 2009; Pinar et al., 2017). NLRP3 inflammasome activity in primary human bronchial epithelial cells is also dependent on RIG-I and IFN-β activity because inhibition of type I IFN responses suppressed IL-1β secretion and inflammasome component mRNA expression (Pothlichet et al., 2013). NS1, which blunt interferon responses, also suppresses NLRP3 inflammasome responses by directly binding to NLRP3 to inhibit NLRP3 inflammasome assembly (Moriyama et al., 2016; Pothlichet et al., 2013). Collectively, these *in vitro* studies show how the NLRP3 inflammasome is responsive to IAV, contributing to immune and inflammatory responses against IAV infection.

1.4.3 *In vivo* studies of inflammasome in influenza

Initial *in vivo* studies have identified a protective role of the NLRP3 inflammasome in IAV infection. *Caspase1*$^{-/-}$, *Asc*$^{-/-}$ and *Nlrp3*$^{-/-}$ mice were more susceptible to lethal PR8 infection compared to WT mice with reduced survival and increased lung viral titres from 7 days post-infection (Allen et al., 2009; Ichinohe et al., 2009; Thomas et al., 2009). *Caspase1*$^{-/-}$, *Asc*$^{-/-}$ and *Nlrp3*$^{-/-}$ mice had less extensive airway inflammation as shown by decreased inflammatory cell infiltration and BAL and serum pro-inflammatory cytokine concentrations (Allen et al., 2009; Thomas et al., 2009). *Caspase1*$^{-/-}$ and *Nlrp3*$^{-/-}$ mice also showed enhanced epithelial cell necrosis with more extensive airway obstruction which contributed to reduced respiratory function (Thomas et al., 2009). These studies indicate that the NLRP3 inflammasome provides a functional level of inflammation and immunity against IAV to limit primary viral pneumonia.

Whether the NLRP3 inflammasome contributes to adaptive immune responses against IAV; though, is conflicting. While Thomas et al. (2009) failed to find differences in PR8-specific adaptive immune responses among WT, *Nlrp3*$^{-/-}$ and *caspase-1*$^{-/-}$ mice, Ichinohe et al. (2009) found that *caspase-1*$^{-/-}$ and *Asc*$^{-/-}$ but not *Nlrp3*$^{-/-}$ mice exhibited impaired humoral- and cell-mediated responses against PR8. The differences between these two studies might be due to the dose of PR8. While Thomas et al. (2009) administered a lethal amount of PR8 (4000 50% Egg Infective Dose (EID_{50})) in failing to find a difference in adaptive immune responses, Ichinohe et al. (2009) used a sublethal PR8 dose (10 PFU) to highlight an impairment in humoral- and cell-mediated immune responses among inflammasome-deficient mice. These differences show that the viral load of IAV may influence whether the NLRP3 inflammasome contributes to adaptive immune responses against IAV.

The NLRP3 inflammasome can also stimulate hyper-inflammatory responses against IAV. Ren et al. (2017) found that c*aspase1*$^{-/-}$, *Asc*$^{-/-}$ and *Nlrp3*$^{-/-}$ mice were less susceptible to A/Shanghai/4664T/2013 (H7N9) infection with reduced mortality and morbidity and weaker pulmonary inflammation compared with WT mice. These changes did not affect pulmonary viral

titres, indicating that the NLRP3 inflammasome only contributes to hyper-inflammatory responses against IAV. In another study, four-week old 129S mice were more susceptible to lethal WSN infection with more severe pulmonary damage compared with eight to ten-week old mice. The younger mice exhibited more substantial hyper-inflammation during IAV infection, including increases in NLRP3 and ASC protein expression as well as IL-18 secretion and caspase-1 activation compared to the older mice (Coates et al., 2018). The NLRP3 inflammasome may also contribute to the development of secondary bacterial pneumonia because inhibition of the NLRP3 inflammasome with *Asc*$^{-/-}$ mice or MCC950 treatment enhanced *S. aureus* clearance from the lung during PR8 (H1N1) infection (Robinson et al., 2018). Collectively, differences among studies that have shown a protective or pathological role of the NLRP3 inflammasome in IAV infection might be due to the different IAV strains being used. While initial studies have exclusively used PR8, later studies utilised a wider variety of IAV strains and subtypes. Hence, the IAV strain may influence whether the NLRP3 inflammasome has a protective or pathological role in IAV infection.

1.4.4 IAV proteins that are inflammasome activators

Engagement of IAV components with PRRs leads to the activation of NF-κB that induces the expression of inflammasome components and pro forms of pro-inflammatory cytokines (Figure 1.9A-C). Specific components of IAV have also been identified as NLRP3 inflammasome activators to promote protective or hyper-inflammatory responses (Figure 1.9D-E). Two IAV components: viral RNA (Ren et al., 2017; Thomas et al., 2009) and the M2 channel protein (Ichinohe et al., 2010), were initially identified as potential NLRP3 inflammasome activators, triggering IL-1β secretion from BMDCs. The mechanisms behind IAV RNA activating the NLRP3 inflammasome to induce IL-1β secretion is unknown (Ren et al., 2017; Thomas et al., 2009). On the other hand, placing pBMDMs and pBMDCs in potassium chloride solution blocked M2-induced IL-1β production, suggesting that M2 activates the NLRP3 inflammasome via ionic fluxes. This could be induced in the cell via the localisation of M2 to the acidified Golgi apparatus (Ichinohe et al., 2010).

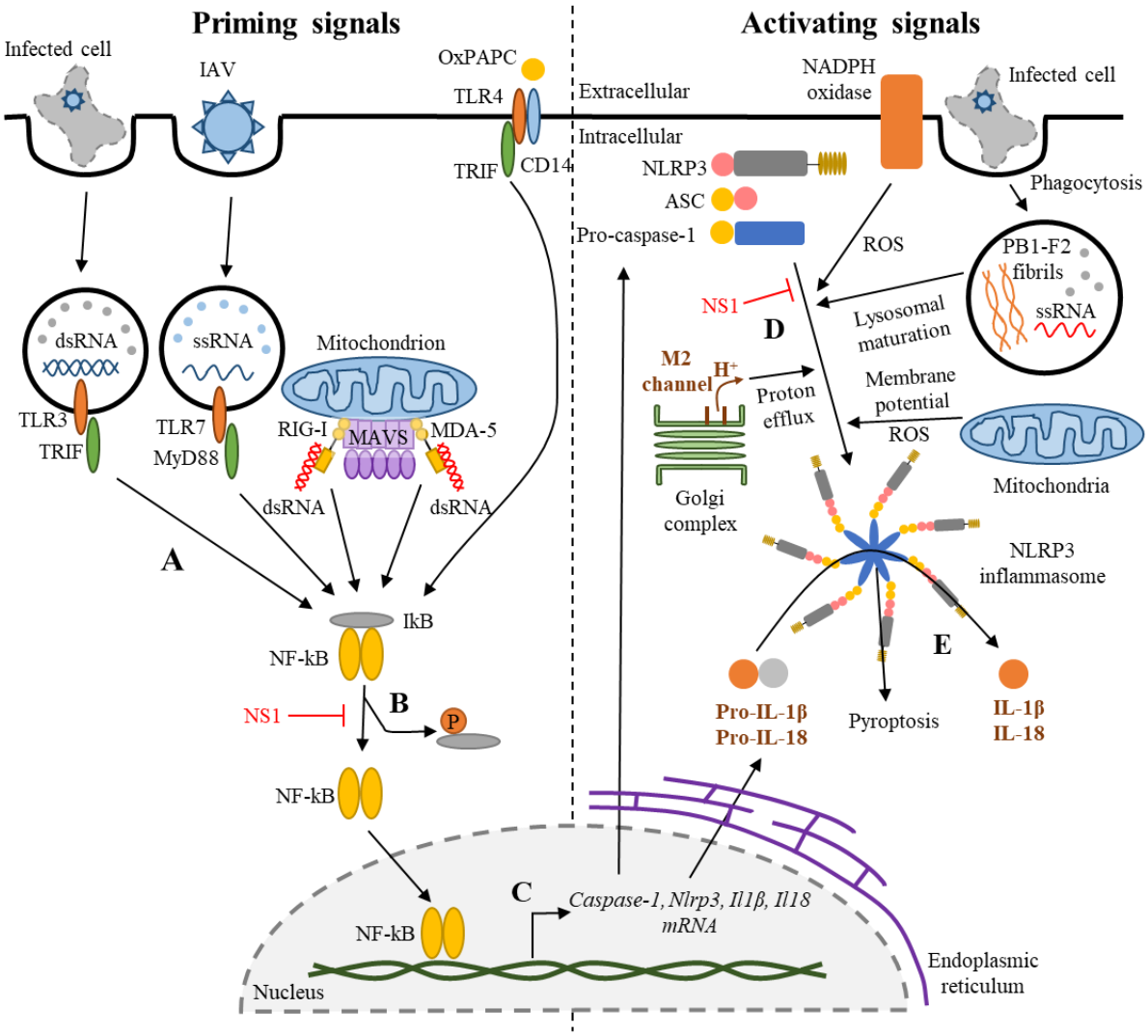

Figure 1.9: Sensing of IAV by PRRs and inflammasome activation

(A) Various components of IAV such as viral RNA are sensed by TLRs and RLRs. (B) These induce the phosphorylation, ubiquitination and degradation of IκB, enabling NF-κB to be activated. (C) Active NF-κB enters the nucleus to induce the expression of inflammasome components and pro forms of pro-inflammatory cytokines. (D) The inflammasome is only assembled in the presence of activating signals. This is again provided by various components of IAV such as PB1-F2 and M2 protein which stimulate various intracellular events to induce inflammasome assembly. (E) Active NLRP3 inflammasome matures IL-1β and IL-18 to promote inflammation during IAV infection as well as stimulate pyroptosis.

Given that viral RNA and the M2 channel protein are present in all seasonal and pandemic IAV strains, these NLRP3 inflammasome activators may contribute to protective responses against IAV infection.

More recently, an IAV component was found to induce hyper-inflammatory responses in the NLRP3 inflammasome. PB1-F2 is an 87-amino acid IAV polypeptide encoded by an alternative reading frame of the *Pb1* gene that induces the intrinsic pathway of apoptosis (Chen et al., 2010) and forms amyloid fibrils in infected cells (Chevalier et al., 2010). Importantly, the length of PB1-F2 varies among different IAV strains. While the *Pb1-f2* gene is truncated in H1N1pdm09 subtypes associated with relatively mild disease, pandemic strains associated with severe infection such as the reconstructed 1918 pandemic strain and avian subtypes such as H5N1 and H7N9 express the full-length *Pb1-f2* gene (McAuley et al., 2010; Trifonov et al., 2009). McAuley et al. (2013) found that full-length PB1-F2 activates the NLRP3 inflammasome. It was found that aggregated, but not monomeric, PB1-F2 stimulated IL-1β secretion from LPS-primed pBMDMs *in vitro* via the NLRP3 inflammasome. PB1-F2 was also found to promote IAV-induced inflammation *in vivo* because administering PR8 PB1-F2 intranasally induced inflammatory cell infiltration and IL-1β production in the airways (McAuley et al., 2013). These results were further supported by Pinar et al. (2017) using H7N9 PB1-F2, where it promoted NLRP3 inflammasome activation via phagocytosis and ROS production. Collectively, PB1-F2 is identified as an NLRP3 inflammasome activator that promotes pulmonary hyper-inflammation. Given that the length of the *Pb1-f2* gene differentiates mild and pathogenic IAV strains, this polypeptide may contribute to more severe infection and poorer prognosis from pathogenic IAV strains compared with seasonal IAV strains.

From these results, we have hypothesised that while some IAV components such as viral RNA and the M2 channel protein temporarily activate the NLRP3 inflammasome to clear infection, other IAV proteins such as PB1-F2 expressed by pathogenic IAV strains may strongly and constitutively activate the NLRP3 inflammasome.

This may produce hyper-inflammatory responses that may lead to mortality. How the NLRP3 inflammasome temporally contributes to the survival or mortality of IAV infection was further studied in our laboratory.

1.4.5 Temporal role of NLRP3 inflammasome during IAV infection

Studies using knockout mice have highlighted the role of the NLRP3 inflammasome in innate immune responses against IAV. However, small molecule inhibitors offer the possibility of antagonising NLRP3 inflammasome activity at specific points of infection. Using MCC950, previous studies in our laboratory have revealed a dual role of the NLRP3 inflammasome in mediating the immunity and hyper-inflammation of IAV infection (Tate et al., 2016). Mice infected with an intranasal dose of HKx31 (H3N2) or PR8 (H1N1) and temporally treated with MCC950 displayed disparate roles of the NLRP3 inflammasome during infection.

Mice given MCC950 one day after IAV infection had reduced survival compared with control mice. However, delaying MCC950 administration until three days post-infection prolonged survival. Furthermore, these mice had decreased inflammatory cell infiltration into the airways and reduced pro-inflammatory cytokine and chemokine concentrations in BAL and serum. These changes did not affect pulmonary viral titres, implying that MCC950 reduces pulmonary inflammation without affecting IAV replication. These results were supported by Coates et al. (2017), where MCC950 administration into juvenile WSN-infected mice once per day from three days post-infection reduced mortality, lung injury and pulmonary inflammation. This occurred via reductions in NLRP3 protein expression in the lung and NLRP3 inflammasome activity in alveolar macrophages without affecting WSN titres. These results indicate that temporal inhibition of the NLRP3 inflammasome may present a novel way of treating IAV infection by blocking activity at a point when hyper-inflammation starts to emerge.

1.4.6 Roles of IL-1β and IL-18 in IAV infection

IL-1β and IL-18 can play both protective and pathological roles in IAV infection (Figure 1.10). On the one hand, IL-1β and IL-18 can regulate the secretion of pro-inflammatory cytokines and activate adaptive immune responses. On the other hand, IL-1β and IL-18 can participate in IAV-induced hyper-cytokinaemia to contribute to hyper-inflammation, causing lung injury.

IL-1β can signal via IL-1R to protect mice against IAV infection. *Il1r1*$^{-/-}$ mice were more susceptible to mortality, morbidity and increased pulmonary viral loads from infection with PR8 (Guo et al., 2017; Ichinohe et al., 2009; Schmitz et al., 2005), avian H5N1 subtypes (Szretter et al., 2007) or reconstructed 1918 H1N1 pandemic strains (Belisle et al., 2010). The mechanism behind this is that IL-1β activates adaptive immune responses against IAV via IL-1R (Guo et al., 2017).

IL-1R-mediated signalling is required for RDCs to migrate to the draining lymph nodes to activate CD4^{+} and CD8^{+} T cells (Ichinohe et al., 2009; Pang et al., 2013a). This leads to the induction of humoral-mediated immune responses as indicated by the presence of serum IAV-specific antibodies (Ichinohe et al., 2009; Schmitz et al., 2005). At the same time, the presence of IL-1R also limits pulmonary inflammation. *Il1r1*$^{-/-}$ mice exhibited increases in the expression of pro-inflammatory cytokines such as TNF-α, IFN-β and IFN-γ and earlier upregulation of genes relating to cellular movement and integrins. This enabled inflammatory cells to infiltrate the airways earlier to induce more severe pulmonary inflammation (Belisle et al., 2010). In addition, recently it has been found that IL-1β along with TNF-α engages lung alveolar stem cells to induce their growth, proliferation and differentiation into alveolar epithelial cells, leading to alveoli repair (Katsura et al., 2019). Collectively, IL-1β can act on a variety of cells to direct immune responses towards viral clearance and tissue repair.

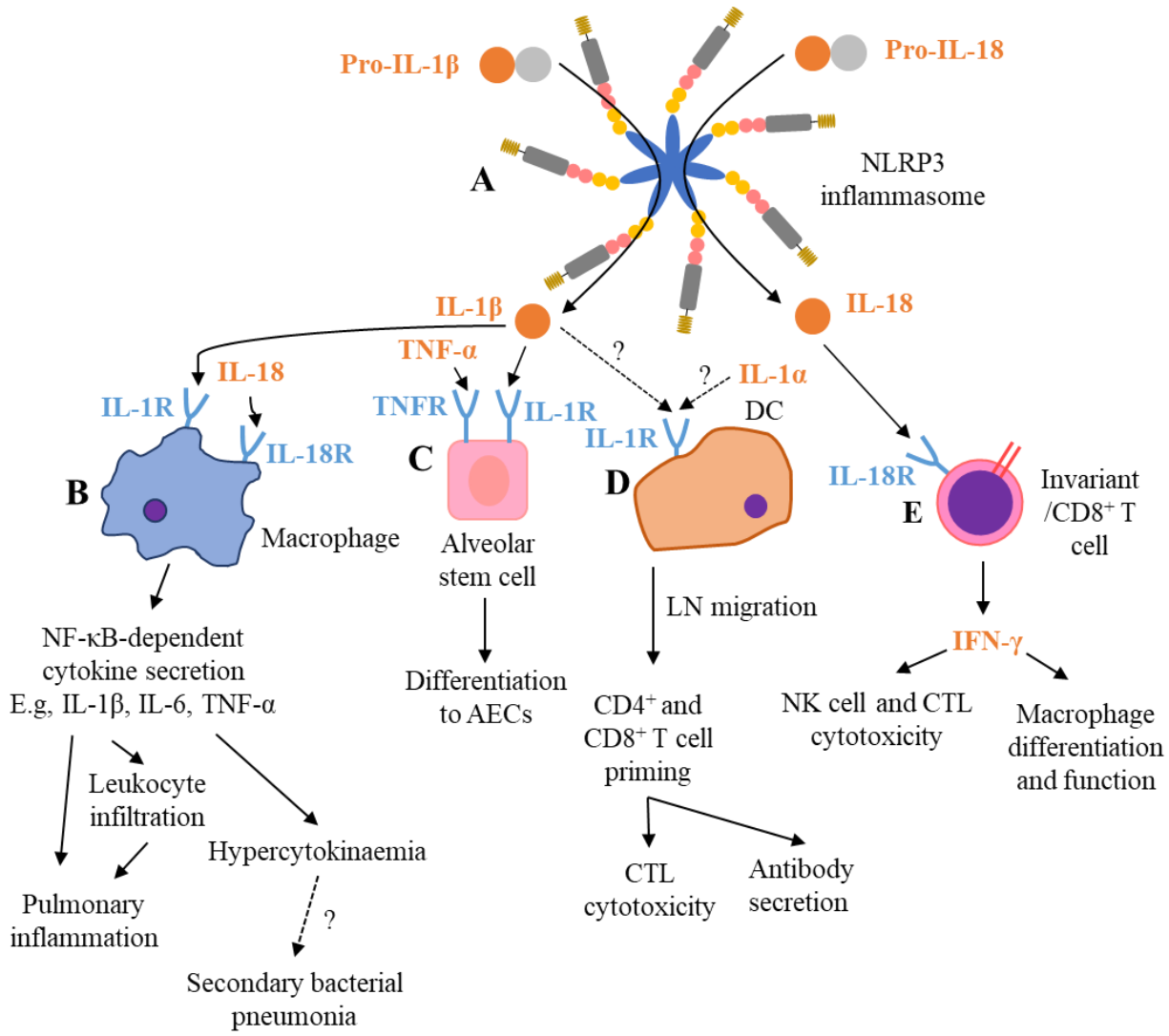

Figure 1.10: Roles of IL-1β and IL-18 in IAV infection

(A) IL-1β and IL-18 are initially produced in their inactive pro forms. However, they are cleaved and activated in the presence of the NLRP3 inflammasome. IL-1β and IL-18 act on various immune cells to promote innate immune responses and immunopathology. (B) IL-1β and IL-18 can act on macrophages to induce cytokine secretion. This promotes the migration and activation of leukocytes in the lung, leading to pulmonary inflammation. However, excessive cytokine secretion can lead to hyper-cytokinaemia which may exacerbate the pathology of IAV infection. (C) Along with TNF-α, IL-1β promotes the growth, division and differentiation of alveolar stem cells to alveolar epithelial cells (AECs). (D) IL-1β can also act on DCs to induce their migration to the draining lymph nodes. Here, they prime $CD4^+$ and $CD8^+$ T cells to activate adaptive immune responses. (E) Lastly, IL-18 acts on invariant and $CD8^+$ T cells to stimulate the secretion of IFN-γ. This leads to increased NK cell and cytotoxic T lymphocyte (CTL) cytotoxicity as well as promoting macrophage differentiation and function.

Nevertheless, IL-1β may promote a hyper-inflammatory state in the lung. Intravenous administration of recombinant IL-1R antagonist (IL-1Ra) into mice from two to six days post-PR8 infection reduced mortality and morbidity compared to phosphate-buffered saline (PBS) controls (Shirey et al., 2016). Mechanistically, IL-1β released from IAV-infected cells could stimulate the mRNA expression and secretion of pro-inflammatory cytokines such as *Il1β, Il6, Cxcl8* and *Tnfα* in primary human microvascular endothelial cells, human A549 alveolar epithelial cell line and human peritoneal macrophages as well as *Cox2* in MRC-5 human fibroblast cell line (Barsness et al., 2004; Indalao et al., 2017; Kim et al., 2015). These studies suggest, in addition to its protective functions, that IL-1β could promote hyper-inflammation by stimulating the expression and secretion of pro-inflammatory cytokines and mediators,

The role of IL-18 in IAV infection is unclear with some protective and pathological roles proposed. On the one hand, IL-18 mediates protection against IAV by inducing IFN-γ production from IAV-specific $CD8^+$ T cells (Denton et al., 2007) as well as mucosal-associated invariant T cells (Loh et al., 2016; van Wilgenburg et al., 2016). IFN-γ secreted from these cells increases the cytotoxic activities of NK cells and $CD8^+$ T cells (Liu et al., 2004; Zhang et al., 2001). This acts to limit viral replication in the lungs because *Il18*$^{-/-}$ mice had increased pulmonary viral titres compared to WT mice during PR8 (Liu et al., 2004) and HKx31 infection (Denton et al., 2007). Conversely, IL-18 may impair clearance of IAV because *Il18*$^{-/-}$ mice had lower pulmonary PR8 titres than WT mice (Van Der Sluijs et al., 2005). Closer investigation indicated that IL-18 induced inflammatory cell infiltration and proinflammatory cytokine production such as TNF-α and CCL2 in the lungs while inhibiting $CD4^+$ T cell activity by downregulating the activation marker CD69 (Van Der Sluijs et al., 2005). It is interesting to note that pulmonary IFN-γ concentrations in IL-18$^{-/-}$ mice were similar to WT mice from four days post-infection (Van Der Sluijs et al., 2005) while another study showed reduced pulmonary IFN-γ concentrations in IL-18$^{-/-}$ mice compared to WT mice in the first three days of infection (Liu et al., 2004). It is also noteworthy that IL-18 promoted cytotoxic activities in NK and $CD8^+$ T cells (Liu et al., 2004; Zhang et al., 2001) but is immunosuppressive towards $CD4^+$ T

cells (Van Der Sluijs et al., 2005). These studies imply that IL-18 may promote cytotoxic activities to clear virions and infected cells but may also induce hyper-inflammation and immunosuppression.

1.5 Concluding remarks

The innate immune system is an integral part of the protection of organisms against pathogens. Comprised of various cellular and humoral components, they not only restrict infection and pathogen spread but also stimulate adaptive immune responses to clear the pathogen. The NLRP3 inflammasome is a central player in the innate immune system, maturing pro-inflammatory cytokines IL-1β and IL-18 and stimulating pyroptosis. Priming and activating signals induce the expression and assembly of inflammasome components with the end-result being an all-encompassing speck residing in the cell. The assembly of an all-encompassing speck; however, is built on the results of overexpression and cell-free studies that may not reflect how inflammasome components behave in cellular conditions. In my project, I aimed to characterise the endogenous expression and activation of the NLRP3 inflammasome using novel inflammasome reporter mice with the reporters placed under their native promoters. This restricts the expression of the reporters and by extension inflammasome components to levels encountered in an endogenous setting, simulating cellular conditions. Results generated from these mice will change our understanding of inflammasome biology which will establish a new paradigm of how the inflammasome works in an endogenous setting.

Just as the innate immune system plays a role in restricting and clearing infection, excessive activity can lead to inflammatory and chronic diseases. The NLRP3 inflammasome, while being a critical player in the protection against infection, is also linked to a variety of infectious and inflammatory diseases. Work in our laboratory using the inhibitor MCC950 has previously demonstrated that the NLRP3 inflammasome can play protective or pathological roles at different stages of IAV infection. The mechanisms behind the NLRP3 inflammasome transitioning from a protective to a pathological role in IAV infection are still being discerned. My project also studies this area by measuring NLRP3

protein expression and MCC950 uptake in individual cell populations of the lung during IAV infection. Understanding where NLRP3 is expressed and MCC950 is taken up will further our understanding of where the inflammasome is potentially active in different stages of IAV infection and whether they may play a protective or pathological role. This information may assist in the development of novel therapeutics that will modulate inflammasome activity to limit inflammation, thereby reducing IAV-induced lung injury to improve the outcome of survival. By extension, findings from my studies will provide a proof-of-concept in which the association among inflammasome expression and activity, pathology and inhibitor uptake can be investigated in a variety of diseases.

1.5.1 Hypothesis

The native expression of the NLRP3 inflammasome and the molecular mechanisms of its activation in an endogenous context using novel fluorescently-tagged reporter mice will provide critical insights into the molecular mechanisms and role of the NLRP3 inflammasome in health and disease and how it can be therapeutically targeted

1.5.2 Aims

1. To explore the expression and activation of ASC inflammasomes *in vitro* using a novel ASC reporter mouse;
2. To characterise the expression and activation of the NLRP3 inflammasome *in vitro* using a novel NLRP3 reporter mouse; and
3. To examine the expression of the NLRP3 inflammasome and uptake of MCC950 *in vivo* during IAV infection.

2 General materials and methods

2.1 Mice

NLRP3-CHCI and monomeric Cherry (mCherry)-ASC reporter mice were generated as part of the Monash and Manitoba Universities (MONMAN) collaboration between Monash University (Paul Hertzog and Alexander Drew) and the University of Manitoba (Arzu Ozturk and Geoff Hicks). This collaboration involved generating a series of reporter mice for innate immune pathways using sophisticated high-throughput gene targeting in ESCs via North American Conditional Mouse Mutagenesis (NORCOMM) replacement technology (Collins et al., 2007). In brief, targeting vectors were generated containing sequences of the gene of interest (genomic and/or cDNA) and a fluorescent protein tag as well as selection cassettes and recombination sites capable of targeting a "docking" site in the ESC cell genome. The "docking" site comprised the gene locus of interest with selection cassettes and recombination sites to insert compatible targeting vectors. This first step of targeting generated an intermediate locus that was 'resolved' using flippase (FLP) 0 recombinase to remove all selection and targeting cassettes.

ESC cells of C57BL/6J origin that had incorporated the reporter into the NLRP3 or ASC locus were microinjected into blastocysts. The resultant chimeric mice were back-crossed at least ten times onto C57BL/6J mice to produce homozygous NLRP3-CHCI and mCherry-ASC mice. Six to twelve-week old male and female C57BL/6J, NLRP3-CHCI and mCherry-ASC mice were used in all experiments. C57BL/6J (designated WT mice), NLRP3-CHCI and mCherry-ASC mice were sourced from Monash Animal Services (Clayton, Victoria, Australia) and housed in Monash Medical Centre Animal Facilities (Clayton, Victoria, Australia). Mice received food and water *ad libitum* and were housed under specific pathogen-free (SPF) conditions in a 12:12 light:dark cycle. Ethics approval to conduct animal experiments were received from Monash Medical Centre Animal Ethics Committee A (approval number MMCA/2015/35) and B (approval number MMCB/2016/12) in Clayton, Victoria, Australia.

2.2 DNA extraction and analysis

A small piece of mouse tail was digested in tail digestion buffer (1% (w/v) SDS (Bio-Rad, Gladesville, NSW, Australia), 50mM ethylenediaminetetraacetic acid (EDTA), 100mM NaCl, 100mM Tris (pH 8.0), 100µg/mL proteinase K (Roche Diagnostics GmbH, Mannheim, Germany)) overnight at 55°C. The next day, salts were precipitated with tail salt solution (4.21M NaCl, 0.63M KCl, 100mM Tris (pH 8.0)). The sample was stored for 30 minutes at 4°C and centrifuged at 10,976 x *g* for 30 minutes at 4°C. The supernatant was isolated, mixed with Qiagen PB Binding Buffer (Hilden, Germany) and vacuumed through a Whatman plate (GE Healthcare Life Sciences, Little Chalford, UK) for 10 minutes. The Whatman plate was then washed with Qiagen PE Wash Buffer (Hilden, Germany) for 10 minutes. DNA was eluted from the Whatman plate with warm (75°C) 0.25X TE solution (0.25mM EDTA and 2.5mM Tris (pH 8.0) in mQH_2O) to a 96-well U-bottom plate (Corning Incorporated, Corning, NY) and stored at 4°C.

2.3 PCR and genotyping

For each sample, 100ng DNA was resuspended in a 50µL volume containing autoclaved milliQ (mQ) water (H_2O) and reagents from the GoTaq Flexi DNA Polymerase kit (Promega, Madison, WI) following the manufacturer's instructions. The primers used for the polymerase chain reaction (PCR) are in Table 2.1. The PCR reaction was conducted in a Veriti 96-well Thermal Cycler (Applied Biosystems, Foster City, CA) according to the protocol in Table 2.2. Following the PCR reaction, DNA samples were mixed with DNA loading dye (0.2% (w/v) Bromophenol Blue (Sigma-Aldrich, Castle Hill, NSW, Australia), 10mM EDTA (pH 8.0), 30% (v/v) glycerol (Merck, Darmstadt, Germany) in mQH_2O) and separated on a 1.2-1.5% (w/v) agarose gel mixed with Invitrogen Sybr Safe DNA gel stain (Life Technologies, Carlsbad, CA) at 100V for 30 minutes. Bands were visualised on the Safe Imager transilluminator (Invitrogen, San Diego, CA) and captured using the Vilber Quantum ST4 3000 (Vilber-Lourmat, Collégien, France).

Table 2.1: Primers for PCR reactions

Genotyping	Primer name	Sequence	Length of primer (base pairs)
mCherry-ASC	ASC forward primer	5’ TCCATCCTGGAACCTGACCT 3’	20
	ASC reverse primer	5’ GTTCTACCACTGGGCCACAT 3’	20
NLRP3-CHCI	NLRP3gt forward primer	5’ ACTGCCAGTGTGGACCTAAG 3’	20
	NLRP3 reverse primer 1	5’ GGTGTAGTCCTCGTTGTGGG 3’	20
	NLRP3 reverse primer 2	5’ GCCTTCTCCTCGCCATTGAA 3’	20

Table 2.2: PCR reaction protocol for mCherry-ASC and NLRP3-CHCI genotyping

Step	Temperature (°C)	Time	Note
1	94	5 mins	
2 (denaturing)	94	30 secs	Repeat for 35 cycles
3 (annealing)	60	30 secs	
4 (extending)	72	1 min	
5	72	5 mins	
6	20	∞	

2.4 Gross phenotyping

NLRP3-CHCI or mCherry-ASC mice and age- and gender-matched WT mice were weighed every two to three days from four to twelve weeks of age under SPF facilities at Monash Medical Centre Animal Facilities (Clayton, Victoria, Australia). Percentage weight change for each mouse was calculated from their weight at week four. At the end of the eight-week period, all mice were euthanised. Internal organs were harvested, washed in PBS and weighed on electronic scales.

2.5 Extracting and culturing pBMDMs

Bone marrow was flushed from the femur and tibia with sterile PBS (Life Technologies, Grand Island, NY). After centrifugation at 272 x *g* for five minutes at room temperature, red blood cells within the bone marrow were lysed in red blood cell lysis buffer (155mM NH_4Cl, 12mM $NaHCO_3$ and 0.1nM EDTA in mQH_2O, pH 7.5) for five minutes at room temperature. Red blood cell lysis buffer was neutralised with sterile PBS before cells were filtered through a 70µm Easystrainer cell strainer (Greiner Bio-One, Kremsmünster, Austria). After centrifugation at 272 x *g* for five minutes at room temperature, bone marrow cells were resuspended in complete media (10% (v/v) FCS, 1% (v/v) L-glut and 1% (v/v) Pen/Strep in Dulbecco's Modified Eagle Medium (DMEM) (all from Life Technologies, Grand Island, NY)) plus 0.1% (v/v) gentamycin (Life Technologies, Grand Island, NY) and counted via Trypan Blue exclusion. Bone marrow cells were resuspended at 1 x 10^6 cells/mL in complete media with 0.1% (v/v) gentamycin and 20% (v/v) L929 cell-conditioned media. They were incubated within square petri dishes (Sarstedt, Mawson Lakes, SA, Australia) at 37°C, 5% CO_2 for six days. After six days, pBMDMs were collected in sterile PBS, centrifuged at 272 x *g* for five minutes at room temperature and resuspended in complete media. After cell counting via Trypan Blue exclusion, pBMDMs were resuspended in complete media at 0.5 x 10^5 cells/mL.

2.6 Priming/stimulation protocol

Cells (1 x 10^5 cells/well pBMDMs) were plated in triplicate in a flat-bottom 96-well plate (Corning Incorporated, Corning, NY) 24 hours before the start of the experiment. Cells were primed with 100ng/mL ultrapure B5 serotype LPS (LPS from *E. coli* O55:B5, InVivoGen, San Diego, CA) for three hours. Afterwards, cells were stimulated with nigericin (InVivoGen, San Diego, CA), silica (Thermo Scientific, Vilnius, Lithuania), ATP (Sigma-Aldrich, St. Louis, MO) or poly(dA:dT) (InVivoGen, San Diego, CA) (transfected by Lipofectamine 2000 (Life Technologies, Carlsbad, CA) following the manufacturer's instructions) at specific concentrations for six hours. Afterwards, cell-free supernatants were collected and assayed separately for IL-1β and TNF-α using ELISA kits from BD (San Diego, CA) or R&D Systems (Minneapolis, MN) following the manufacturer's instructions. Cytotoxicity in the form of LDH release was measured using the Cytotox 96 Assay kit (Promega, Madison, WI) following the manufacturer's instructions. For the LDH assay, the mean optical density $(OD)_{485}$ of the culture medium was subtracted from the OD_{485} of the other wells. Percent cytotoxicity was calculated by the formula % cytotoxicity = OD_{485} (sample) / OD_{485} (maximum LDH control) x 100 and normalised to the untreated control.

The above protocol was used for experiments with MCC950 (resuspended in PBS; gift from Matt Cooper and Avril Robertson in University of Queensland). However, MCC950 was added to wells 30 minutes before cells were stimulated with inflammasome activators.

2.7 Immunoblotting

pBMDMs were plated in a 12-well plate at 5 x 10^5 cells/well in triplicate 24 hours before the start of the experiment. pBMDMs were primed and stimulated as previously described in 2.6 Priming/stimulation protocol. Supernatant samples from the triplicate were pooled, vortexed with Strataclean resin (Agilent Technologies, Cedar Creek, TX) for 30 seconds and centrifuged at 134 x *g* for 30 minutes at 4°C. The supernatant was aspirated and the protein-bound Strataclean resin was

resuspended in 5X SDS buffer (250mM Tris pH 6.8, 10% (w/v) SDS, 20% (v/v) glycerol in dH_2O). Lysate samples were collected by scraping cells in 5X SDS buffer and pooled. Lysate and supernatant samples were boiled for 10 minutes at 95°C. Proteins were separated via SDS-PAGE on Bolt 4-12% (w/v) Bis-Tris Plus gel (Life Technologies, Carlsbad, CA) at 165V for 40 to 180 minutes. Following SDS-PAGE, proteins were transferred onto Immobilon FL PVDF membrane (Merck Millipore, Cork, Ireland) at 30V for 45 to 60 minutes.

For caspase-1, NLRP3, ASC, GFP and β-actin blots, the membrane was blocked with 5% (w/v) skim milk powder for one hour at room temperature. The membrane was then incubated with anti-mouse caspase-1 monoclonal antibody (Adipogen Life Sciences, Liestal, Switzerland), anti-mouse NLRP3 monoclonal antibody (AdipoGen Life Sciences, Liestal, Switzerland), rabbit anti-ASC polyclonal antibody (AdipoGen Life Sciences, Liestal, Switzerland), rabbit anti-GFP polyclonal antibody (ThermoFisher Scientific, Rockford, IL) or anti-mouse β-actin monoclonal antibody (Sigma-Aldrich, Castle Hill, NSW, Australia) in 5% (w/v) skim milk powder overnight at 4°C. After washing the membrane three times with 0.05% (w/v) Tween in TBS (TBS-Tween), the membrane was incubated with rabbit anti-mouse IgG-HRP or goat anti-rabbit IgG-HRP polyclonal antibodies (Dako, Glostrup, Denmark) in 5% (w/v) skim milk powder for one hour at room temperature. After washing the membrane three times in TBS-Tween, bands were visualised on CL-X Posure Film (Thermo Scientific, Rockford, IL) via enhanced chemiluminescence using LumiGLO solution (Cell Signalling Technology, Danvers, MA).

For IL-1β and α-tubulin blots, the membrane was blocked with Odyssey PBS blocking buffer (LI-COR, Lincoln, NE) for one hour at room temperature. For the IL-1β blot, the membrane was incubated in goat anti-mouse IL-1β-biotinylated antibody (R&D Systems, Minneapolis, MN) in Odyssey PBS blocking buffer overnight at 4°C. After washing the membrane three times in TBS-Tween, the membrane was incubated with Streptavidin (Strep)-Alexa Fluor 680 (Life Technologies, Eugene, OR) in Odyssey PBS blocking buffer for one hour at room temperature. For α-tubulin blots,

the membrane was incubated in rat anti-α-tubulin monoclonal antibody (Abcam, Cambridge, MA) overnight at 4°C and Dylight 800-conjugated goat anti-rat IgG (H+L) (Rockland, Limerick, PA) for one hour at room temperature, both in Odyssey PBS blocking buffer. After three washes in TBS-Tween, bands were visualised on the Odyssey imager (LI-COR, Lincoln, NE).

2.8 Fixed cell imaging

pBMDMs were plated at 2 x 10^4 cells/well in an Ibidi 8-well µ-slide (Planegg, Germany) or 4 x 10^4 cells/well in a Greiner Bio-One 10-well cellview cell culture slide (Frickenhausen, Germany) 24 hours before the start of the experiment. pBMDMs were primed with 100ng/mL ultrapure B5 serotype LPS (LPS from *E. coli* O55:B5, InVivoGen, San Diego, CA) for 60-270 minutes. In some experiments, in addition to the 180-minute LPS priming period, pBMDMs were also stimulated with 30µM nigericin for 30 minutes or 150µg/mL silica for four hours. Hoechst 33342 (Thermo-Fisher Scientific, Eugene, OR) stain was added at 1:5000 dilution 15 minutes before pBMDMs were fixed in 4% (v/v) paraformaldehyde (PFA) (Electron Microscopy Sciences, Hatfield, PA) for 15-30 minutes at room temperature. After 4% (v/v) PFA was aspirated, pBMDMs were stored in 1% (v/v) sodium azide in PBS at 4°C. Fixed pBMDMs were visualised at 400X magnification using a 40X oil-based objective on the Olympus FV1200 Confocal Laser Scanning Microscope (Tokyo, Japan). Images were generated via deconvolution of z-stacks with maximum intensity projection using Fiji software (Schindelin et al., 2012).

A similar methodology was used for fixed cell imaging experiments that included an intracellular ASC stain, but Hoechst 33342 was not added to pBMDMs before fixation. After fixed cells were washed in PBS, they were permeabilised with permeabilisation buffer (0.1% (w/v) saponin (Sigma-Aldrich, St Louis, MO), 2.5% (v/v) FCS in PBS) for 30 minutes at room temperature. After permeabilisation, cells were incubated with 1:250-diluted rabbit anti-ASC antibody (N15 clone, Santa Cruz Biotechnology, Dallas, TX) in PBS overnight at 4°C. The next day, cells were washed three times with permeabilisation buffer and incubated with 1:500-diluted Alexa Fluor 488-conjugated or

Alexa Fluor 680-conjugated goat anti-rabbit IgG (H+L) antibody (Life Technologies, Eugene, OR) for one hour at room temperature. After washing cells three times with permeabilisation buffer, cells were stained with 1:10000-diluted Hoechst 33342 (Thermo-Fisher Scientific, Eugene, OR) in PBS for 15 minutes. Cells were washed twice with and mounted on PBS. pBMDMs were visualised at 400X magnification using a 40X oil-based objective on the Olympus FV1200 Confocal Laser Scanning Microscope (Tokyo, Japan). Images were generated via deconvolution of z-stacks with maximum intensity projection using Fiji software.

2.9 Live cell imaging

pBMDMs were plated at 2-4 x 10^4 cells on a FluoroDish (World Precision Instruments, Hitchin, UK) 24 hours before the start of the experiment. pBMDMs were primed with 100ng/mL ultrapure B5 serotype LPS (LPS from *E. coli* O55:B5, InVivoGen, San Diego, CA) and incubated at 37°C, 5% CO_2 for three hours. The Olympus FV1200 Confocal Laser Scanning Microscope (Tokyo, Japan) was equilibrated at 37°C, 5% CO_2 for one hour before the Fluorodish was placed. Microscope settings were optimized and a basal image was taken before 10µM nigericin or 150µg/mL silica was added. Live cells were imaged for two hours for nigericin treatment or four hours for silica stimulation. Images and movies were generated via deconvolution of z-stacks with maximum intensity projection on Fiji software.

2.10 Flow cytometry of iBMDMs and pBMDMs

ASC-Cerulean iBMDMs (kind gift of Prof. Eicke Latz, University of Bonn (Hett et al., 2013)) as well as WT, NLRP3-CHCI and mCherry-ASC pBMDMs were resuspended in complete media at 0.5 x 10^6 cells/mL and seeded in 12-well plates at 37°C, 5% CO_2 for 24 hours. Cells were initially treated with 100ng/mL ultrapure B5 serotype LPS (LPS from *E. coli* O55:B5, InVivoGen, San Diego, CA) for three hours. Afterwards, cells were passaged with 5mM EDTA, centrifuged in Eppendorf tubes for five minutes at 500 x *g*, resuspended in serum-free DMEM and stimulated with

30µM nigericin for 30 minutes. After nigericin treatment, cells were centrifuged at 500 x *g* for five minutes and fixed in 4% (v/v) PFA for five minutes at 4°C. Cells were washed with PBS, centrifuged at 500 x *g* for five minutes to remove PFA and resuspended in PBS. Samples were processed on the BD LSRFortessa X20 (San Jose, CA). Data was analysed with FlowJo 10 (Ashland, OR) according to Sester et al. (2016).

For experiments where an intracellular ASC immunostain was included, cells were blocked extracellularly with 1:200-diluted anti-mouse CD16/CD32 antibody (Invitrogen, San Diego, CA), 2% (v/v) fetal calf serum (FCS) and 0.1% (w/v) bovine serum albumin (BSA) in PBS for 30 minutes at room temperature. Cells were then permeabilised with the eBioscience Foxp3/Transcription Factor Staining Buffer Set (ThermoFisher Scientific, San Diego, CA) following the manufacturer's instructions. An intracellular block of 2% (v/v) FCS and 0.1% (w/v) BSA (FACS blocking solution) in PBS was done for 30 minutes at room temperature before cells were incubated with 1:500-diluted rabbit anti-ASC antibody (N15 clone, Santa Cruz Biotechnology, Dallas, TX) in PBS overnight at 4°C. The next day, cells were washed with FACS blocking solution and stained with 1:500-diluted Alexa Fluor 488-conjugated or Alexa Fluor 680-conjugated goat anti-rabbit IgG (H+L) antibody (Life Technologies, Eugene, OR**)** for one hour at room temperature. After washes in FACS blocking solution and PBS, cells were resuspended in PBS and processed on the BD LSRFortessa X20 (San Jose, CA). Data was analysed with FlowJo 10 (Ashland, OR) according to Sester et al. (2016).

2.11 **FLIM-FRET**

pBMDMs were plated at 4 x 10^4 cells on a FluoroDish (World Precision Instruments, Hitchin, UK) 24 hours before the start of the experiment. pBMDMs were primed with 100ng/mL ultrapure B5 serotype LPS (LPS from *E. coli* O55:B5, InVivoGen, San Diego, CA) and incubated at 37°C, 5% CO_2 for three hours. Any inhibitors such as the caspase-1 inhibitor z-YVAD (5µM) or the small molecule inhibitor MCC950 (50µM) were added at least 30 minutes before cells were stimulated with

10µM nigericin for 45 minutes. mCitrine fluorescence lifetime was measured on the PicoQuant PicoHarp 300 FLIM system (Berlin, Germany) attached to an Olympus FV1000 IX81 Confocal Laser Scanning Microscope (Tokyo, Japan) and analysed via SymPhoTime 64 software (PicoQuant, Berlin, Germany).

2.12 Intranasal nigericin challenge model

Nigericin (Adipogen Life Sciences, Liestal, Switzerland) was reconstituted in sterile PBS at 2.5mg/mL (equivalent to 5mg/kg mouse) immediately before the experiment. Mice were anaesthetised with isoflurane and intranasally administered with 125µg nigericin in a 50µL volume of PBS. Mice were euthanised 14 hours after administration via carbon dioxide asphyxiation. BAL samples were collected via three 1mL PBS washes of the lung from the trachea.

2.13 Intranasal LPS challenge model

Ultrapure B5 serotype LPS (LPS from *E. coli* O55:B5, InVivoGen, San Diego, CA) was reconstituted in sterile PBS at 1.5mg/mL (equivalent to 3mg/kg mouse) immediately before the experiment. Mice were anaesthetised with isoflurane and intranasally administered with 75µg LPS in 50µL PBS. Mice were euthanised three hours after administration via carbon dioxide asphyxiation and BAL and lung samples were collected.

2.14 IAV infection

Mice were intranasally infected with 1 x 10^5 PFU HKx31 (H3N2) in 50µL PBS and monitored over a three-day period. Mice were weighed daily and disease severity was scored on a 3-point scale (Table 2.3). Mice were euthanised if weight loss exceeded 20% of their original weight or disease severity score was 3. Otherwise, mice were euthanised three days after infection via carbon dioxide asphyxiation and BAL and lung samples were collected.

Table 2.3: Disease severity score for IAV infection

Disease score	Symptoms
0	no visible signs
1	slight ruffling of fur
2	ruffled fur, reduced mobility
3	ruffled fur, reduced mobility, rapid breathing

2.15 MCC950-rhodamine in vivo experiment

For infection studies, WT mice were infected with 1 x 10^4 PFU HKx31 (H3N2) one or three days before the experiment. On the day of the experiment, mice were anaesthetised with isoflurane and given 100µg MCC950-rhodamine (gift from Matt Cooper and Avril Robertson) in 50µL PBS intranasally. One, three or five hours after administration, mice were euthanised by carbon dioxide asphyxiation and lungs were harvested.

2.16 Flow cytometry of lung and BAL samples

Lungs were digested in 0.1mg/mL DNaseI and 1mg/mL collagenase A in PBS for 40 minutes at 37°C with agitation and processed through a 70µm Easystrainer cell strainer. Lung and BAL samples were centrifuged at 358 x *g* for five minutes at 4°C. BAL supernatant samples were collected to assay IL-1β and IL-6 using the ELISA kits (BD Biosciences, San Diego, CA or R&D Systems, Minneapolis, MN) following the manufacturer's instructions. Meanwhile, red blood cells within lung and BAL samples were lysed in red blood cell lysis buffer for five minutes at room temperature. The lysis buffer was neutralised with PBS and decanted via centrifugation at 358 x *g* for five minutes at 4°C. BAL and lung cells were resuspended in FACS buffer (2% (v/v) FCS in PBS), counted via trypan blue exclusion and plated in a 96-well U-bottom plate (Corning Incorporated, Corning, NY).

After centrifugation at 454 x *g* for five minutes at 4°C to pellet cells and decant supernatant, Fc receptors were blocked with 1:200-diluted anti-mouse CD16/CD32 antibody (Invitrogen, San Diego, CA) in FACS buffer in the dark for 15 minutes at 4°C. After cells were washed and centrifuged to remove the anti-mouse CD16/CD32 antibody, surface markers were stained with fluorescently-tagged antibodies (Appendix IV) in FACS buffer in the dark for 20 minutes at 4°C to identify specific cell populations (Table 2.4). After surface markers were stained, the fluorescently-tagged antibodies were washed off with FACS buffer and cells were resuspended in FACS buffer.

Table 2.4: Cell markers used to identify specific cell populations

Cell	Cell markers
Myeloid-derived cells	$CD45^{+}$
Non-myeloid-derived cells	$CD45^{-}$
Epithelial cells	$CD45^{-}$cytokeratin 18^{+} or $CD45^{-}EpCAM^{+}$
T cells	$CD3^{+}$
B cells	$CD45^{+}B220^{+}$
NK cells	$NK1.1^{+}$
Neutrophils	$Ly6C^{+}Ly6G^{+}$
Inflammatory macrophages	$Ly6C^{+}Ly6G^{-}$
Macrophages	$CD11c^{+}$I-A[b]^{lo} or $CD11c^{+}F4/80^{+}$
DCs	$CD11c^{+}$I-A[b]^{hi}

Propidium iodide (Sigma-Aldrich, Castle Hill, NSW, Australia) was added to BAL cells in the intranasal nigericin challenge model just before they were analysed on the flow cytometry machine.

For epithelial cells that required intracellular cytokeratin 18-FITC staining, lung cells were fixed in formalin for 30 minutes at 4°C. After the formalin was removed via PBS wash and centrifugation, cells were resuspended in perm/wash buffer (BD, San Diego, CA) following the manufacturer's instructions and incubated in the dark for 10 minutes at 4°C. After removal of the perm/wash buffer, cells were stained with anti-cytokeratin 18-FITC in perm/wash buffer in the dark overnight at 4°C. The next day, anti-cytokeratin 18-FITC antibody was washed off via centrifugation and cells were resuspended in 100µL PBS.

All samples were processed via flow cytometry on either the BD FACSCanto II (San Jose, CA) or BD LSRFortessa X20 (San Jose, CA). Analysis was done on FlowJo 10 (Ashland, OR).

2.17 Statistical analysis

In vitro studies were conducted in triplicate in accordance with previous studies (Masters et al., 2010a; Pinar et al., 2017). *In vivo studies* were conducted with 4-10 mice/group which were also similar to previous studies (Huang et al., 2011; Tate et al., 2016). Graphs were generated in Graphpad Prism 7 for Windows (La Jolla, CA). Comparisons between two groups were analysed via unpaired t-test. Comparisons between three or more groups were analysed via one-way ANOVA with Tukey's post-hoc test. Data is represented as mean ± SEM with significance defined as $p < 0.05$.

3 Uncovering novel aspects of ASC inflammasomes using mCherry-ASC mice

3.1 Introduction

The inflammasome is a protein complex in the innate immune system that promotes and maintains inflammation. It does this by cleaving or maturing pro-forms of pro-inflammatory cytokines IL-1β and IL-18 to their bio-active forms (Martinon et al., 2004; Masters et al., 2010b). The inflammasome also cleaves gasdermin D which promotes an inflammatory form of cell death called pyroptosis (Kayagaki et al., 2015; Shi et al., 2015). The inflammasome consists of three components: a sensor protein which is usually an NLR, an inflammatory caspase that cleaves substrates and an adaptor protein connecting the sensor protein and inflammatory caspase. The adaptor protein in most inflammasomes is ASC. ASC is a 22kDa protein with two domains: a N-terminal PYD domain and a C-terminal CARD domain (Jin et al., 2013a) (Figure 1.4**)**. These two domains are connected by a flexible linker that enables ASC to adopt different conformations (de Alba, 2009). ASC is constitutively expressed in leukocytes such as macrophages, DCs and neutrophils (Lattin et al., 2008; Mabbott et al., 2013). ASC is also found in non-myeloid-derived organs such as the small intestine and colon (Lattin et al., 2008; Uhlen et al., 2015).

When the inflammasome is activated, ASC forms a filament originating from the NLRP3 oligomer. The formation of an ASC filament is initiated following nucleation of a sensor protein such as NLRP3. Here, homodimeric interactions between the PYD domains of NLRP3 and ASC binds a small amount of ASC to the NLRP3 oligomer (Oroz et al., 2016). As ASC migrates to the NLRP3 oligomer, a supercritical concentration of ASC is established (Gambin et al., 2018). Under these conditions, the ASC filament is established when free ASC changes conformation to dovetail to the end of the ASC filament via PYD homodimeric interactions (Gambin et al., 2018). The resultant ASC filament contains a PYD core with an outer surface of CARD domains (Sborgi et al., 2015; Schmidt et al., 2016). The outer CARD domains interact with inflammatory caspases such as caspase-1 to form caspase-1 filaments (Lu et al., 2014) or active inflammatory caspase homodimers (Boucher et al., 2018; Sanders et al., 2015). Alternatively, CARD domains on adjacent ASC filaments can interact

with each other. This establishes cross-links among ASC filaments that result in the formation of a large, oligomeric ASC speck (Dick et al., 2016; Kuri et al., 2017; Schmidt et al., 2016). The ASC filament and speck; therefore, is an important scaffold for promoting inflammation activity.

Existing models aimed at imaging ASC inflammasome complexes have attached fluorescent proteins to ASC to track its distribution and oligomeric function. Examples of such models include ASC-Cerulean iBMDMs *in vitro* (Stutz et al., 2013) and ASC-mCitrine mice *in vivo* (Tzeng et al., 2016). The limitation of these reporter models; however, is that the tagged ASC protein relies on overexpression. For instance, the ASC-mCitrine reporter in ASC-mCitrine mice was placed under the Rosa26 promoter which ubiquitously overexpress the reporter in all cells and tissues (Friedrich and Soriano, 1991). As such, results from these models may not accurately reflect how ASC behaves in a biological setting. To overcome this limitation, our laboratory has generated a novel ASC reporter mouse where the expression of the fluorescently-tagged ASC reporter is biologically regulated by its native promoter. The reporter has the gene for the mCherry fluorescent protein attached to the N-terminal *Pycard* cDNA (Figure 3.1A). The *mCherry-Pycard* reporter gene (mCherry-ASC in its protein form) is then placed under its native promoter in the murine genome, enabling the expression of mCherry-ASC and consequently ASC to be regulated and observed in an endogenous- and tissue-specific setting (Figure 3.1A). mCherry-ASC mice; therefore, can be used to observe and determine the expression, distribution and oligomerisation that is more reflective of where ASC is found and how it behaves in a biological setting.

In this chapter, I aimed to confirm the functionality and inflammasome activation of cells from mCherry-ASC mice *in vitro*. Following this, I used cells from mCherry-ASC mice to determine the expression and activation of inflammasomes in an endogenous setting.

3.2 Results

3.2.1 Establishment of an mCherry-ASC murine colony

The mCherry-ASC reporter contains the mCherry fluorescent protein attached to the PYD domain of ASC (Figure 3.1B). To establish a colony of mice expressing the mCherry-ASC reporter *in vivo*, the *mCherry-Pycard* reporter gene was knocked into the murine *Pycard* gene under its native promoter in murine stem cells (Figure 3.1A). The mCherry-ASC mouse was generated under a collaboration between Prof. Paul Hertzog and Dr. Alec Drew from the Hudson Institute of Medical Research and Dr. Arzu Ozturk and Prof. Geoff Hicks from the University of Manitoba. By attaching the mCherry fluorescent protein to ASC and expressing it under its native promoter, the expression and distribution of ASC can be measured under endogenous conditions. To confirm that the colony is homozygous for the *mCherry-ASC* reporter gene, I genotyped pups that were generated from mCherry-ASC breeding pairs. As shown in Figure 3.2, the genotypes of the mCherry-ASC pups matched those of the homozygous mCherry-ASC control. This result shows that mCherry-ASC pups are homozygous for the reporter gene.

I next determined the gross phenotype and growth of mCherry-ASC mice. I did this by monitoring WT and mCherry-ASC mice from four to twelve weeks of age. Homozygous mCherry-ASC mice were generated in Mendelian ratios at three to seven pups/litter which were comparable to WT mice and exhibited no overt gross phenotype or behaviour (data not shown). mCherry-ASC mice also developed at the same rate as WT mice as measured by similar weight gains between both groups (Figure 3.3). To further compare development between mCherry-ASC and WT mice, I also weighed organs. The weights of most organs such as the lung and small intestine in mCherry-ASC mice were comparable to WT mice (Figure 3.4A-I). To note, mCherry-ASC mice had slightly larger stomachs compared to WT mice (Figure 3.4D), but this had no effect on the health of the mice. These results show that mCherry-ASC mice exhibit normal gross phenotype and development when compared to WT mice.

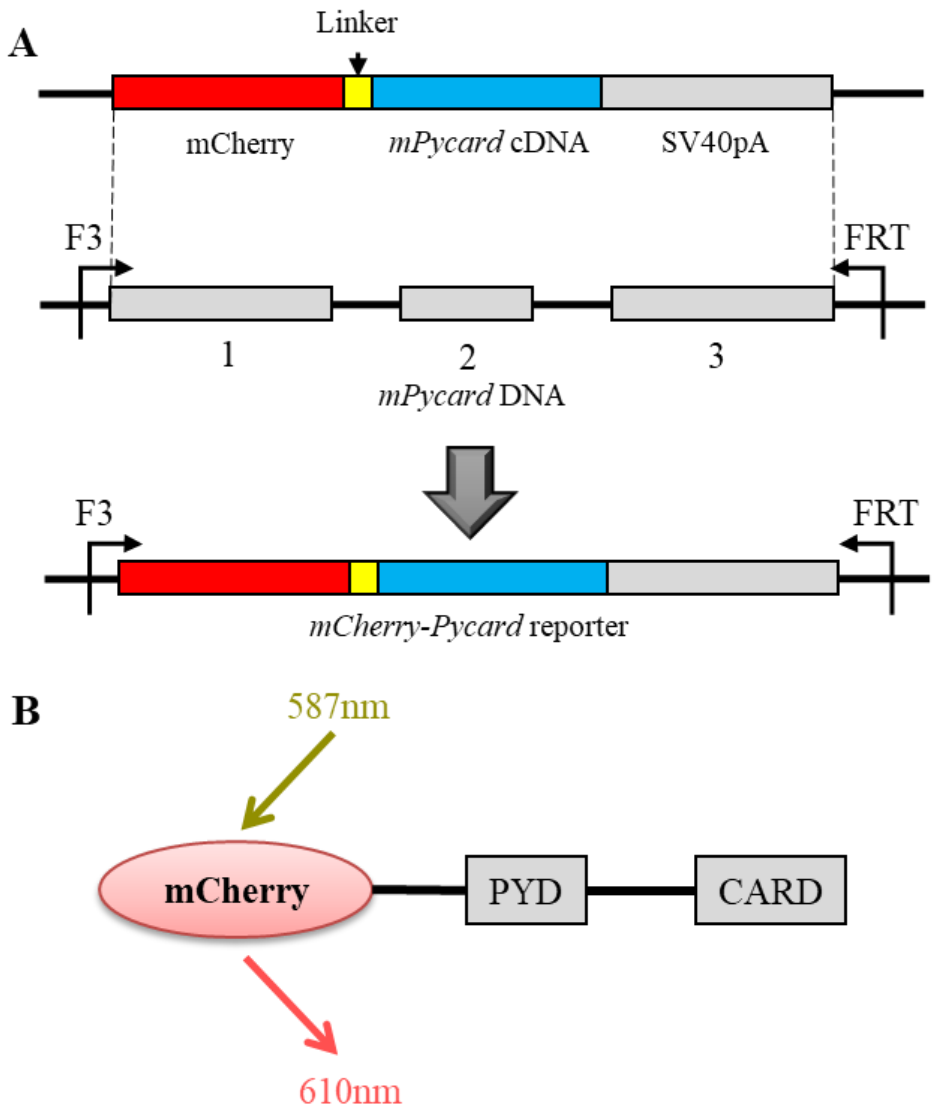

Figure 3.1: Schematics of the mCherry-ASC gene and protein construct

(A) The *mCherry-Pycard* reporter gene was knocked into the whole murine *Pycard* (*mPycard*) gene under its native promoter. Numbers represent exon numbers of the *mPycard* gene. (B) The mCherry fluorescent protein is attached to the pyrin (PYD) domain of ASC. CARD = caspase activation and recruitment domain.

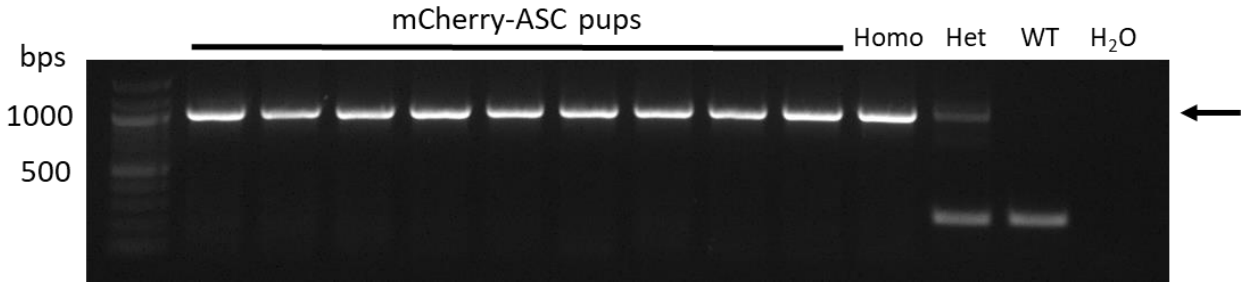

Figure 3.2: mCherry-ASC pups are homozygous for the reporter gene

Pup tails were digested overnight before proteins and SDS were precipitated. After centrifugation, supernatant samples were collected to extract DNA via manifolding. DNA concentration and quality were measured on Nanodrop. Following this, 100ng of each DNA sample as well as wild-type (WT), water (H_2O) and homozygous (Homo) and heterozygous (Het) mCherry-ASC controls were amplified via PCR. The amplified DNA was resolved via gel electrophoresis and visualised via trans-illumination. Arrow indicates the homozygous mCherry-ASC reporter gene. Results are representative of three independent experiments. bps = base pairs

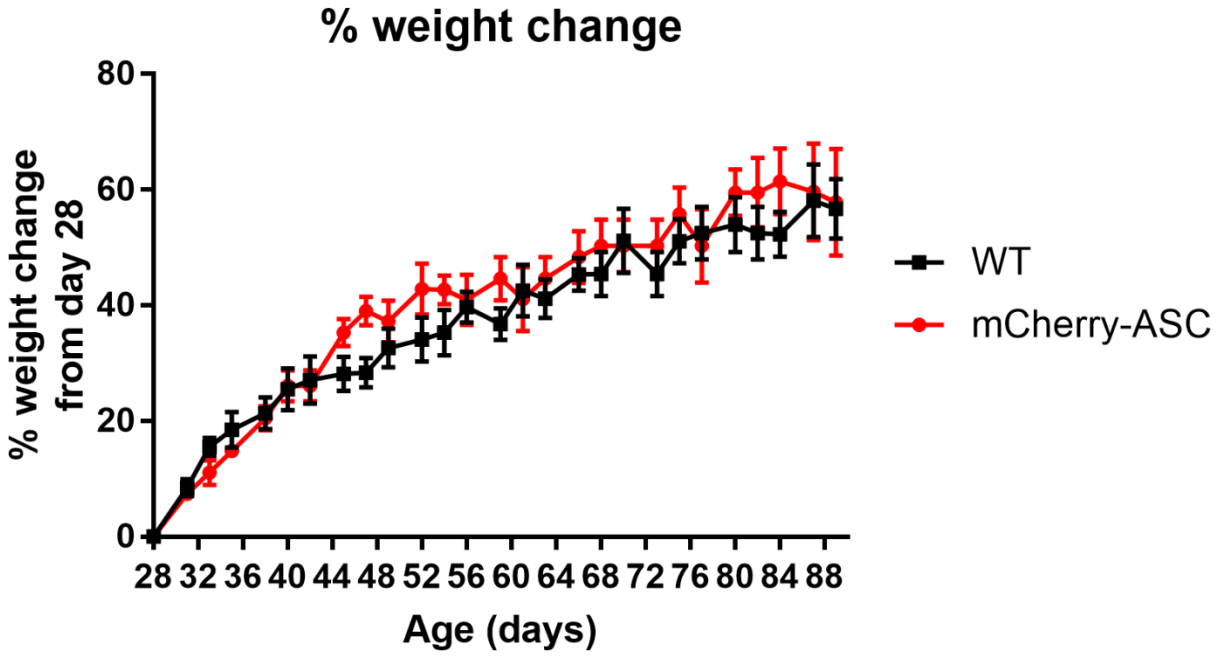

Figure 3.3: mCherry-ASC mice gain weight comparable to WT mice

Female WT and mCherry-ASC mice were weighed every 2-3 days from 4 to 12 weeks of age. For each mouse, percentage (%) weight change was calculated from their respective weight at 28 days of age. Data represented as mean ± SEM with N = 4-5 mice/group.

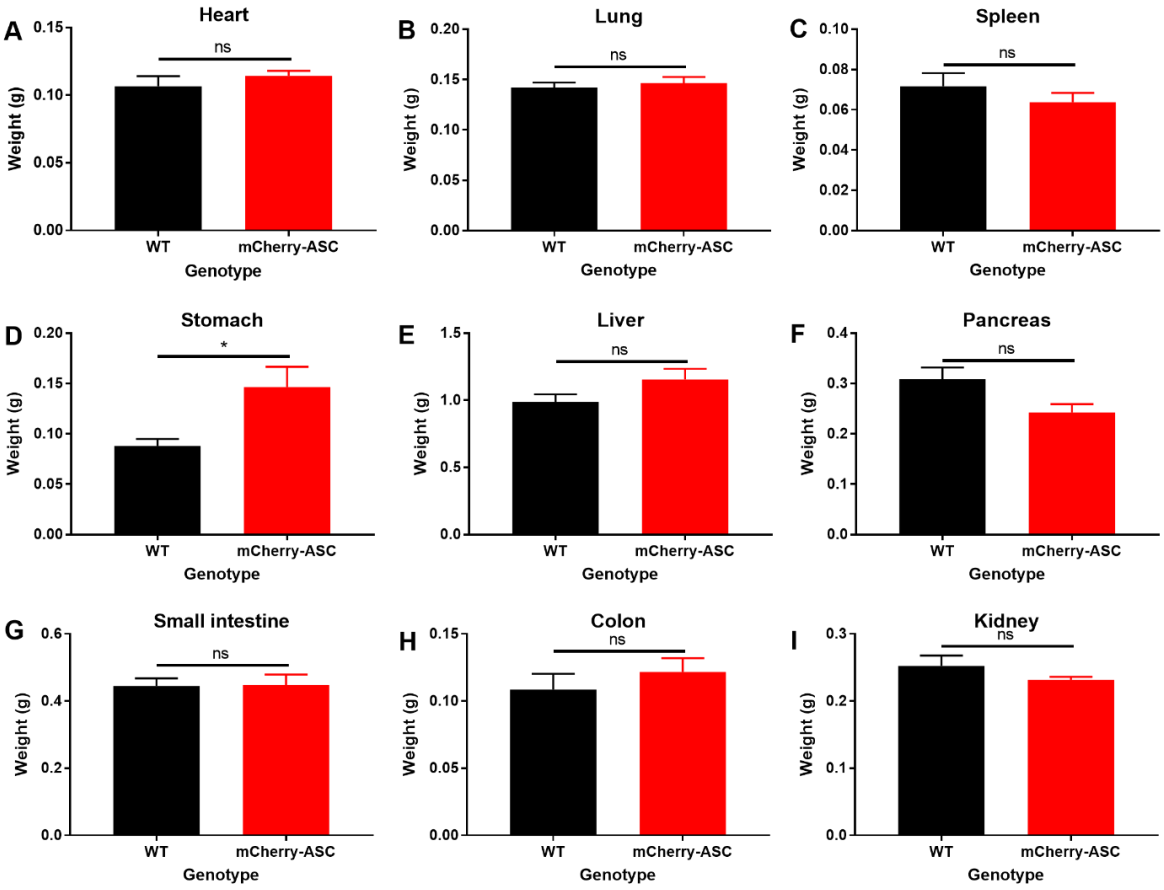

Figure 3.4: Organ weights in mCherry-ASC mice are comparable to WT mice

Organs (A-I) were harvested from 12-week old female WT and mCherry-ASC mice and weighed. Data represented as mean ± SEM with N = 4-5 mice/group. Data analysed via unpaired t-test with significance represented as ns = not significant and *P<0.05.

3.2.2 Expression of ASC in mCherry-ASC reporter cells

I next tested whether cells from mCherry-ASC mice are expressing the functional reporter. Initially, I conducted an ASC immunoblot of WT and mCherry-ASC pBMDM lysate samples to confirm the attachment of mCherry to ASC (Figure 3.5A). The molecular weight of ASC increased from 20kDa in WT pBMDMs (Figure 3.5A, lanes 1-3, top panel) to 50kDa in mCherry-ASC pBMDMs (Figure 3.5A, lanes 4-6, top panel). The difference in molecular weight is approximately 30kDa which is roughly equivalent to the molecular weight of mCherry at 28.8kDa (Duellman et al., 2015), suggesting that mCherry has been successfully attached to ASC in mCherry-ASC pBMDMs. To note, there was a non-specific band at around 28kDa among mCherry-ASC lysates (Figure 3.5A). Importantly, the concentration of ASC appears very similar, if not the same between the WT and mCherry-ASC pBMDMs (Figure 3.5A), implying that ASC in the reporter cells is expressed at commensurate levels as WT cells.

Next, to verify that mCherry is fluorescing in mCherry-ASC pBMDMs, I conducted both flow cytometric (Figure 3.5B) and confocal imaging (Figure 3.5C) experiments on WT and mCherry-ASC pBMDMs. As shown in the flow cytometric results of Figure 3.5B, mCherry-ASC pBMDMs on average had higher mCherry fluorescence intensities compared to the background fluorescence in WT pBMDMs. This was confirmed in confocal imaging of mCherry-ASC pBMDMs which possessed stronger mCherry fluorescence than WT pBMDMs (Figure 3.5C).

Taken together, these results imply that mCherry is fluorescing in mCherry-ASC pBMDMs, suggesting that these cells are successfully expressing the functional ASC reporter.

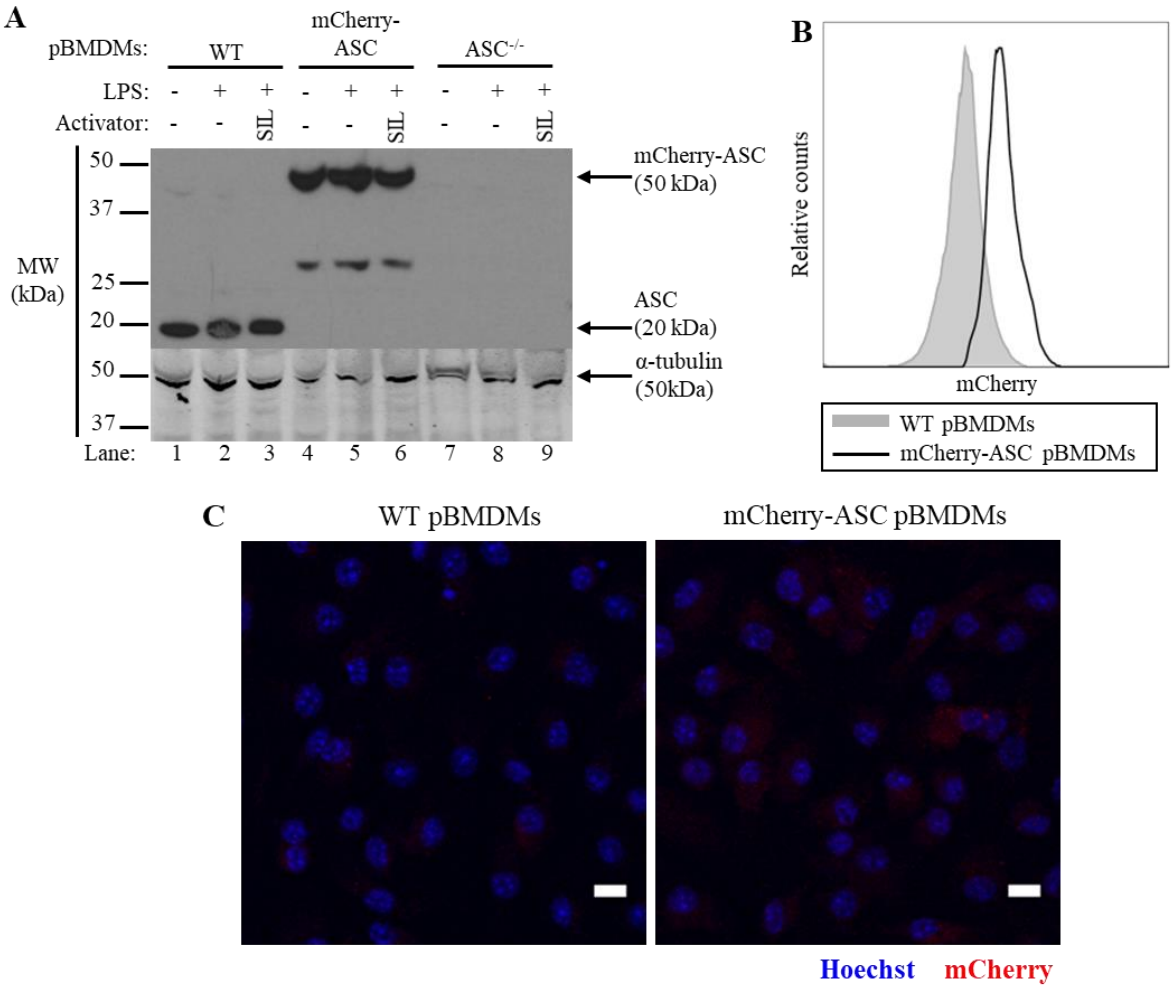

Figure 3.5: mCherry-ASC pBMDMs express the functional fluorescent ASC reporter

(A) WT, mCherry-ASC and ASC$^{-/-}$ pBMDMs were seeded at 5 x 10^5 cells/well in 12-well plates and left to settle for 24 hours. The next day, pBMDMs were treated with 100ng/mL LPS for 3 hours with or without 250µg/mL silica (SIL) stimulation for 6 hours. Cells were lysed with 5X SDS buffer and pooled. Lysate samples were boiled, resolved on 4-12% Bis-Tris gel and transferred onto a PVDF membrane. The membrane was immunoblotted with rabbit anti-ASC polyclonal antibody or rat anti-α-tubulin monoclonal antibody followed by goat anti-rabbit HRP antibody or Dylight 800-conjugated goat anti-rat IgG respectively. Proteins were visualised via enhanced chemiluminescence for the ASC immunoblot and Odyssey for the α-tubulin immunoblot. Results are representative of three independent experiments.

(B) WT and mCherry-ASC pBMDMs were seeded at 5 x 10^5 cells/well in 12-well plates. Twenty-four hours after seeding, pBMDMs were released with 5mM EDTA (in PBS) and fixed in 4% PFA for 30 minutes at 4°C. After washing, cells were resuspended in PBS and processed in the BD LSRFortessa. Result is representative of three independent experiments.

(C) WT and mCherry-ASC pBMDMs were seeded at 4 x 10^4 cells/well in a 10-chamber glass-bottom slide and left to settle for 24 hours. The next day, cells were fixed with 4% PFA for 20 minutes at room temperature, washed with PBS and mounted in 1% sodium azide in PBS. Cells were imaged at 400x magnification (oil-based objective) on the Olympus FV1200 Laser Scanning Microscope and z-stacks were deconvoluted via maximum intensity projection on Fiji software. Scale bar is 10µm. Results are representative of a 3x3 field across three independent experiments.

3.2.3 Biochemical activation of the inflammasome in mCherry-ASC pBMDMs

The attachment of mCherry to ASC in the mCherry-ASC reporter may impede ASC oligomerisation, blocking inflammasome activation. To test whether the presence of mCherry in the mCherry-ASC reporter affects inflammasome activity, I conducted *in vitro* experiments of inflammasome activation in mCherry-ASC pBMDMs.

Initially, I measured cytokine secretion and cell death from WT and mCherry-ASC pBMDMs treated with B5 serotype LPS to prime cells (Gaekwad et al., 2010) and an inflammasome activator such as nigericin (Perregaux and Gabel, 1994), silica (Dostert et al., 2008) and ATP (Mariathasan et al., 2006) for NLRP3 inflammasome activation and poly(dA:dT) (Hornung et al., 2009; Roberts et al., 2009) for AIM2 inflammasome activation. IL-1β (Figure 3.6A-D) and TNF-α (Figure 3.6I-L) secretion were quantified via ELISA while cell death was measured via LDH assay (Figure 3.6E-H). LPS-primed mCherry-ASC pBMDMs exhibited IL-1β secretion in all treatments with an inflammasome activator (Figure 3.6A-D). To note, differences were seen in the capacity of mCherry-ASC pBMDMs, compared to WT pBMDMs, to generate IL-1β to silica and ATP stimulation (Figure 3.6B-C) due to a dose-dependent response. LPS-primed mCherry-ASC pBMDMs also exhibited similar cell death compared to WT cells when exposed to silica or ATP (Figure 3.6F-G) but, intriguingly, not to nigericin or poly(dA:dT) (Figure 3.6E, H). Nevertheless, TNF-α generation was similar between WT and mCherry-ASC pBMDMs regardless of the inflammasome activator (Figure 3.6I-L), highlighting the preservation of responses to priming signals in mCherry-ASC pBMDMs.

These results, taken together, show that mCherry-ASC pBMDMs exhibited IL-1β secretion and cell death during inflammasome activation despite the attachment of mCherry to ASC. This suggests that the fluorescent tag does not sterically hinder inflammasome activation and formation.

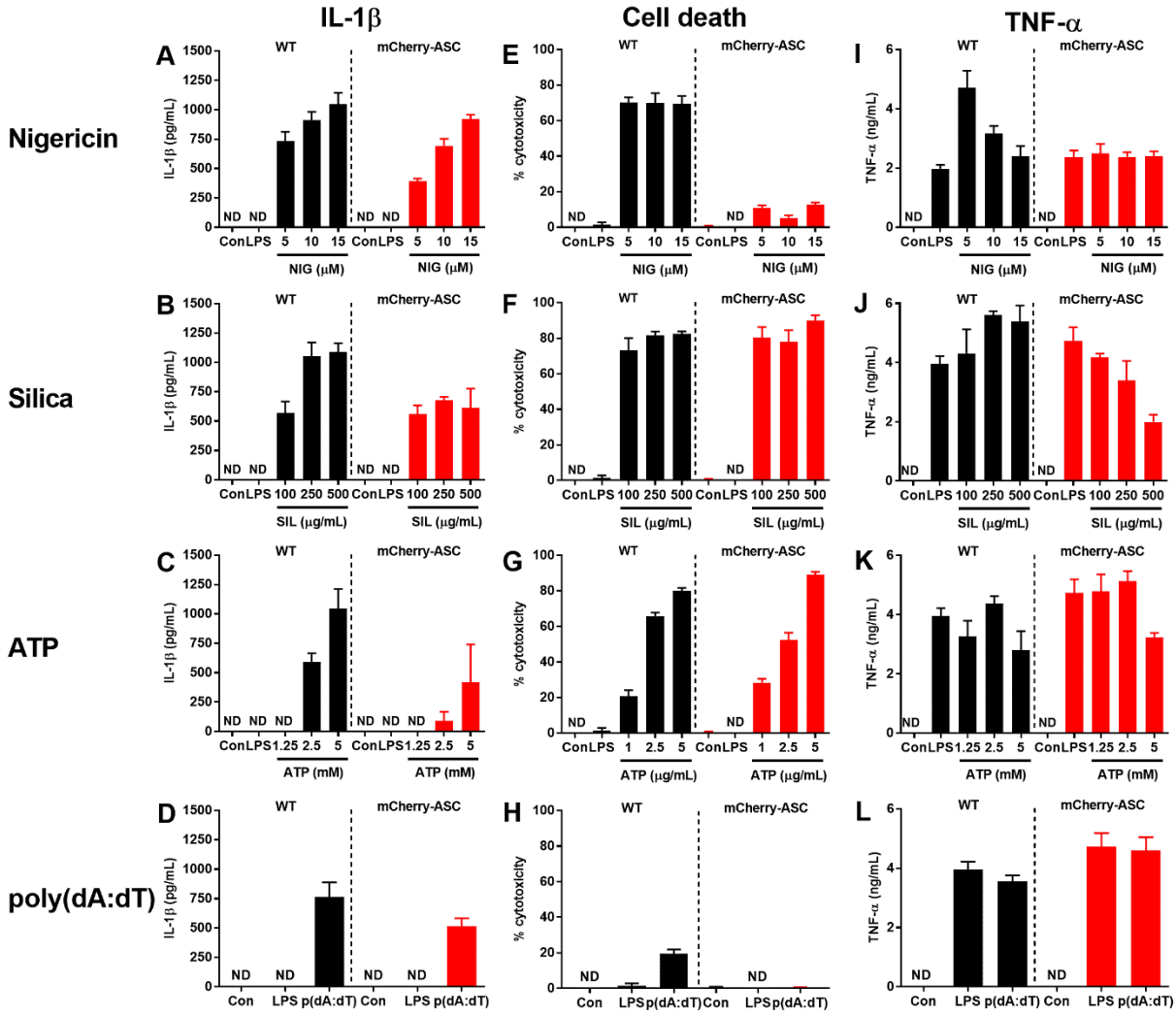

Figure 3.6: IL-1β secretion and cell death in inflammasome-activated mCherry-ASC pBMDMs

WT and mCherry-ASC pBMDMs were plated at 1 x 10^5 cells/well in a 96-well plate 24 hours before being primed with LPS (100ng/mL) for 3 hours. pBMDMs were then stimulated with nigericin (NIG), silica (SIL), ATP or poly(dA:dT) (p(dA:dT), 200ng) in triplicate at the indicated concentrations for 6 hours. Cell-free supernatants were harvested and IL-1β (A-D) and TNF-α (I-L) were assayed via ELISA following the manufacturer's instructions. Percentage (%) cytotoxicity (E-H) was measured via a non-radioactive LDH assay kit following the manufacturer's instructions and normalised to the non-primed, non-stimulated control (Con). Data depicted as mean ± SEM with n = 3/group and are representative of three independent experiments. Con = control pBMDMs without LPS, nigericin, silica, ATP or poly(dA:dT); LPS = pBMDMs treated with LPS only and ND = not detected.

Caspase-1 activation and IL-1β maturation can be measured by immunoblotting cleaved caspase-1 and IL-1β in supernatant samples respectively (Groß, 2012). I used this principle to further assess inflammasome activation in mCherry-ASC pBMDMs by immunoblotting for IL-1β and caspase-1 in supernatant and lysate samples from WT and mCherry-ASC pBMDMs. As expected, LPS treatment of mCherry-ASC pBMDMs increased caspase-1 and IL-1β protein expression in lysate samples commensurate to WT pBMDMs (Figure 3.7, lanes 7-8 in caspase-1 p20 and IL-1β lysate panels), confirming the preservation of inflammasome priming when the mCherry-ASC reporter is present. Importantly, LPS-primed mCherry-ASC pBMDMs challenged with silica or poly(dA:dT) secreted cleaved caspase-1 and IL-1β into the supernatant (Figure 3.7, lanes 10 and 12 in caspase-1 p20 and IL-1β supernatant panels). Interestingly, LPS-primed mCherry-ASC pBMDMs challenged with nigericin secreted mature IL-1β but not cleaved caspase-1 (Figure 3.7, lane 9 in caspase-1 p20 and IL-1β supernatant panels) while neither cleaved IL-1β nor caspase-1 were present in supernatant samples from mCherry-ASC pBMDMs stimulated with LPS and ATP (Figure 3.7, lane 11 in caspase-1 p20 and IL-1β supernatant panels).

These results indicate that although the mCherry-ASC reporter does not impede inflammasome priming, different inflammasome activators had mixed effects on caspase-1 activation and IL-1β maturation in mCherry-ASC pBMDMs.

3.2.4 Effect of MCC950 on inflammasome function in mCherry-ASC pBMDMs

MCC950 is a specific small molecule inhibitor of the NLRP3 inflammasome associated with reducing inflammasome activity (Coll et al., 2015). The presence of mCherry in the mCherry-ASC reporter may prevent MCC950 from inhibiting inflammasome activity. To test this possibility, I pre-treated LPS-primed WT and mCherry-ASC pBMDMs with MCC950 before they were stimulated with nigericin or silica. MCC950 impeded IL-1β secretion in LPS-primed mCherry-ASC pBMDMs stimulated with nigericin (Figure 3.8A) or silica (Figure 3.8B) commensurate to LPS-treated WT pBMDMs.

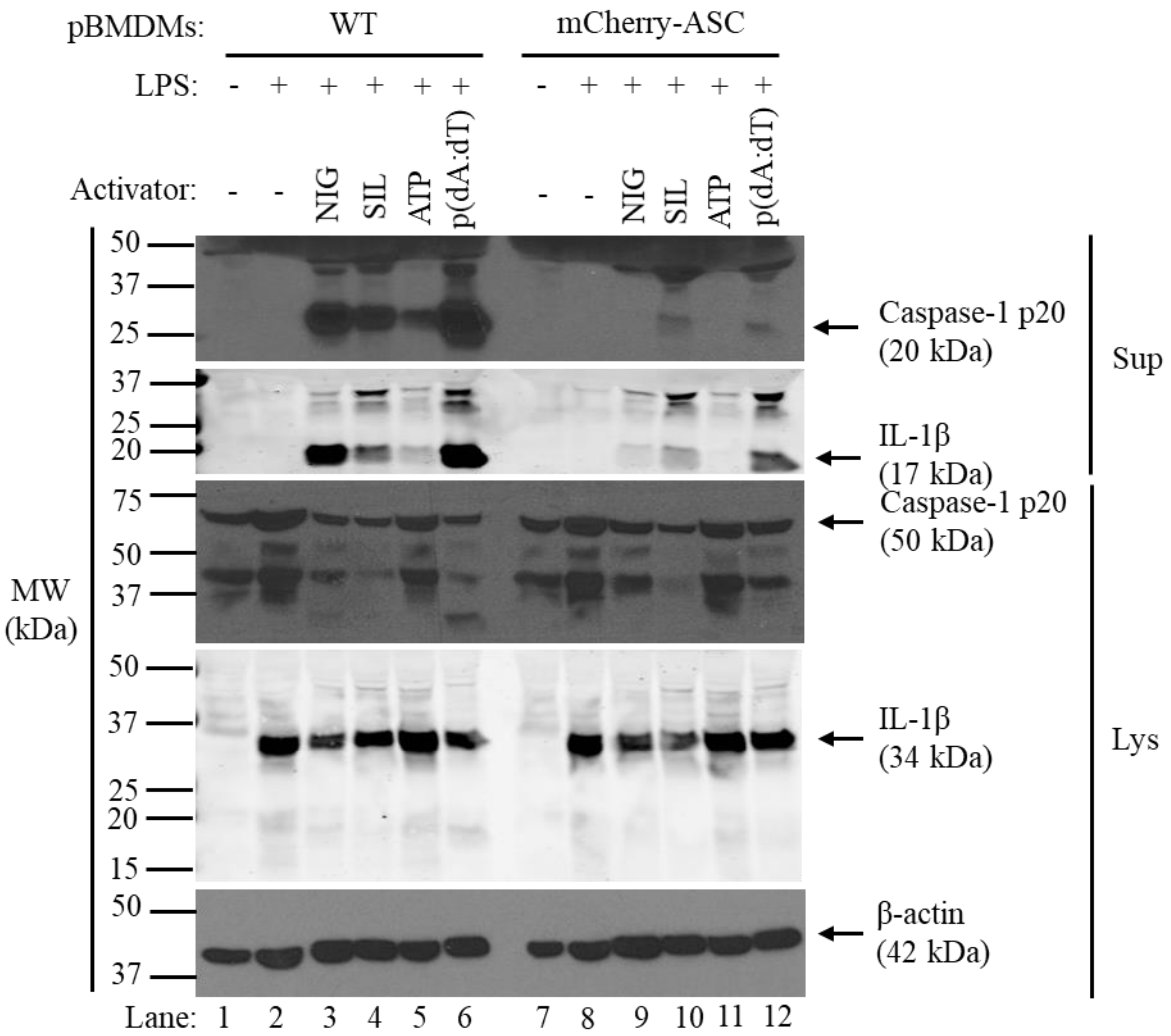

Figure 3.7: Caspase-1 activation and IL-1β maturation in mCherry-ASC pBMDMs

WT and mCherry-ASC pBMDMs were seeded at 5 x 10^5 cells/well in 12-well plates 24 hours before being primed with LPS (100ng/mL) for 3 hours. WT and mCherry-ASC pBMDMs were then stimulated with nigericin (NIG; 10µM), silica (SIL; 250µg/mL), ATP (5mM) or poly(dA:dT) (p(dA:dT), 500ng) in triplicate for six hours. Supernatant (sup) proteins were pooled, concentrated on Strataclean resin and resuspended in 5X SDS buffer. Lysate samples (lys) were prepared by lysing cells in 5X SDS buffer and pooling them. All samples were boiled before proteins were resolved on 4-12% bis-tris gel, transferred onto a PVDF membrane and immunoblotted independently with the indicated antibodies overnight (anti-mouse caspase-1 monoclonal antibody, goat anti-mouse IL-1β-biotinylated antibody or anti-mouse β-actin monoclonal antibody). The caspase-1 and β-actin immunoblots were produced via enhanced chemiluminescence using the rabbit anti-mouse IgG-HRP secondary antibody while the IL-1β blots were generated via Odyssey with strep-Alexa Fluor 680. Immunoblot results are representative of three independent experiments. Arrows in each immunoblot indicate the band of interest. MW = molecular weight.

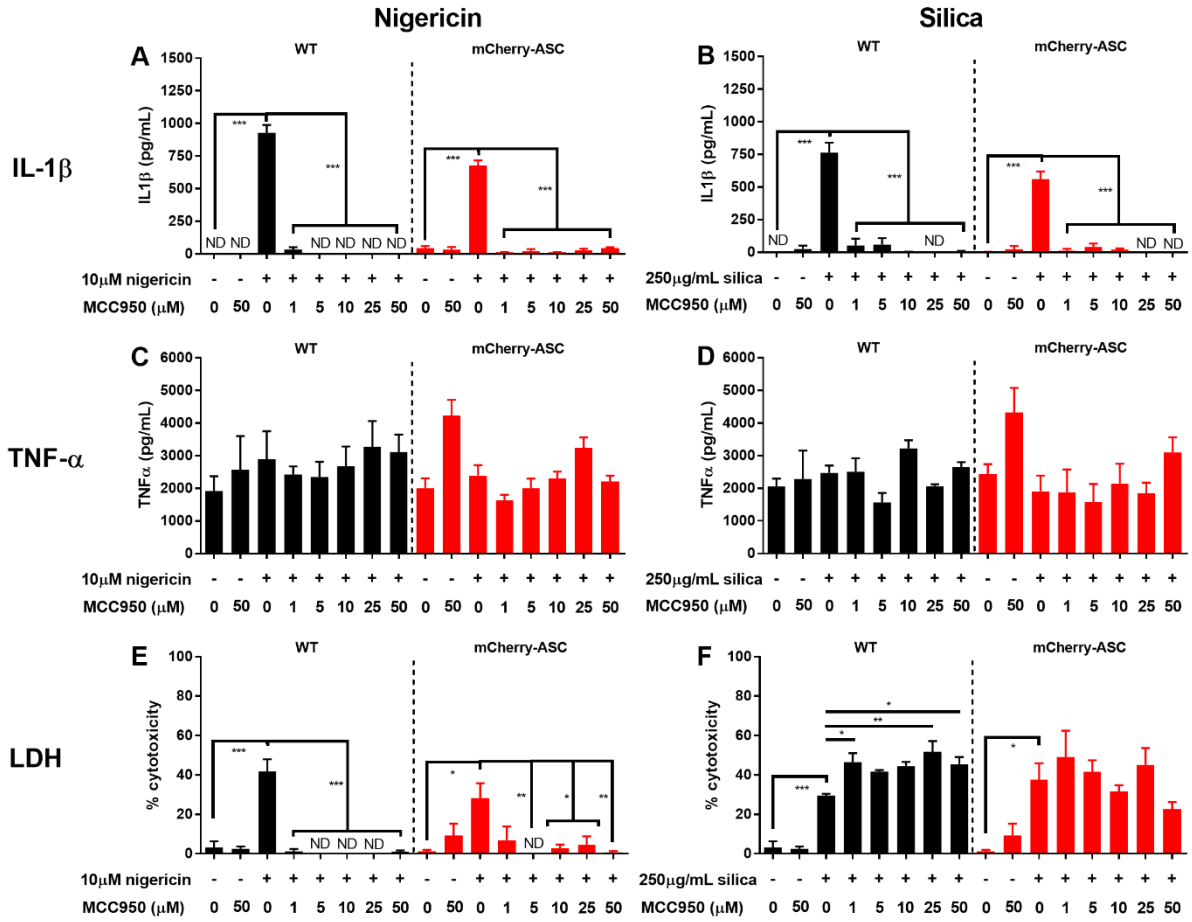

Figure 3.8: The mCherry-ASC reporter still enables MCC950 to inhibit inflammasome activity

WT and mCherry-ASC pBMDMs were plated at 1 x 10^5 cells/well in a 96 well-plate 24 hours before being primed with LPS (100ng/mL) for 3 hours. MCC950 was added to wells at the indicated concentrations 30 minutes before pBMDMs were stimulated with nigericin (NIG; 10µM) or silica (SIL; 250µg/mL) in triplicate for 6 hours. Cell-free supernatants were harvested and assayed for IL-1β (A-B) and TNF-α (C-D) via ELISA. Percent (%) cytotoxicity (E-F) was calculated by measuring LDH using a non-radioactive kit and normalised to the non-MCC950, non-stimulated control. Data were compared via one-way ANOVA with Tukey's post-hoc test and significance represented as *p<0.05, **p<0.01 and ***p<0.001. ND = not detected. Results are representative of three independent experiments.

TNF-α secretion was similar in both WT and mCherry-ASC pBMDMs across all MCC950 concentrations (Figure 3.8C-D), indicating that decreases in IL-1β secretion by MCC950 are due to inhibition of NLRP3 inflammasome activity. MCC950 also impeded cell death in WT and mCherry-ASC pBMDMs treated with LPS and nigericin but not silica (Figure 3.8E-F).

To further investigate the role of MCC950 in inhibiting inflammasome activity in mCherry-ASC pBMDMs, I also measured the capacity of MCC950 to inhibit the secretion of cleaved caspase-1 and IL-1β in supernatant samples via immunoblotting. As shown in Figure 3.9, both LPS-primed WT and mCherry-ASC pBMDMs secreted cleaved caspase-1 and IL-1β when challenged with silica or ATP (Figure 3.9, lanes 2, 4, 7 and 9 in caspase-1 p20 and IL-1β supernatant panels). These proteins were absent in the supernatant when cells were pre-treated with MCC950 before stimulation with silica or ATP (Figure 3.9, lane 3, 5, 8 and 10 in caspase-1 p20 and IL-1β supernatant panels).

These results indicate that the mCherry-ASC reporter does not prevent MCC950 from inhibiting inflammasome activation, supporting the use of mCherry-ASC pBMDMs for screening novel inflammasome inhibitors.

3.2.5 Effect of LPS on ASC protein expression

I next examined the application of mCherry-ASC reporter cells for investigating novel aspects of inflammasome biology. Initially, I used mCherry-ASC reporter cells to measure ASC protein expression and how it might be affected by LPS treatment as reported for NLRP3 expression (Bauernfeind et al., 2009; Sutterwala et al., 2006). I initially investigated this by doing confocal imaging of mCherry-ASC pBMDMs treated with PBS or LPS over a 180 minute time period (Figure 3.10). Although ASC is expressed in untreated mCherry-ASC pBMDMs (Figure 3.10A), PBS or LPS treatment did not increase mCherry fluorescence intensity over all timepoints (Figure 3.10B). This is confirmed by mCherry mean fluorescence intensity (MFI) measurements of the images, where neither PBS nor LPS treatment increased mCherry MFI (Figure 3.10C).

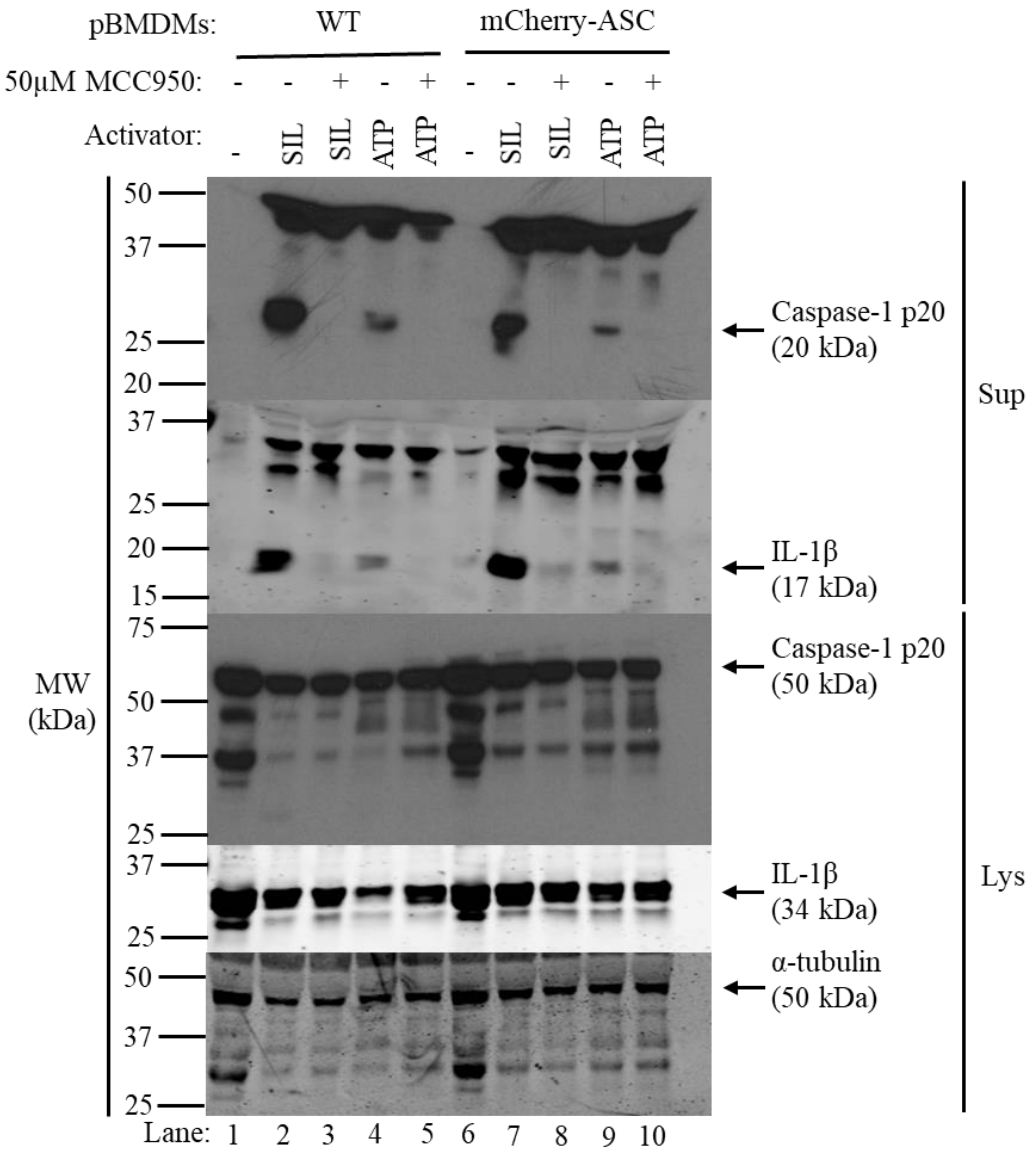

Figure 3.9: MCC950 can inhibit caspase-1 activation and IL-1β maturation in mCherry-ASC pBMDMs

WT and mCherry-ASC pBMDMs were plated at 5 x 10^5 cells/well in 12-well plates 24 hours before being primed with LPS (100ng/mL) for 3 hours. MCC950 (50μM) was added 30 minutes prior to stimulation with silica (SIL; 250μg/mL) or ATP (2.5mM) for 6 hours. Supernatant samples (sup) were collected with proteins concentrated onto Strataclean resin and resuspended in 5X SDS buffer. Cells were lysed in 5X SDS buffer and pooled to generate lysate samples (lys). Both sets of samples were boiled and proteins were resolved on 4-12% Bis-Tris gel, transferred onto a PVDF membrane and immunoblotted independently for the indicated proteins overnight (anti-mouse caspase-1 monoclonal antibody, goat anti-mouse IL-1β-biotinylated antibody or rat anti-α-tubulin monoclonal antibody). The caspase-1 immunoblots were generated via enhanced chemiluminescence using the rabbit anti-mouse IgG-HRP secondary antibody while the IL-1β and α-tubulin immunoblots were produced via Odyssey with strep-Alexa Fluor 680 for IL-1β or Dylight 800-conjugated goat anti-rat IgG for α-tubulin. Arrows indicate the band of interest for each immunoblot. Results are representative of three independent experiments. MW = molecular weight.

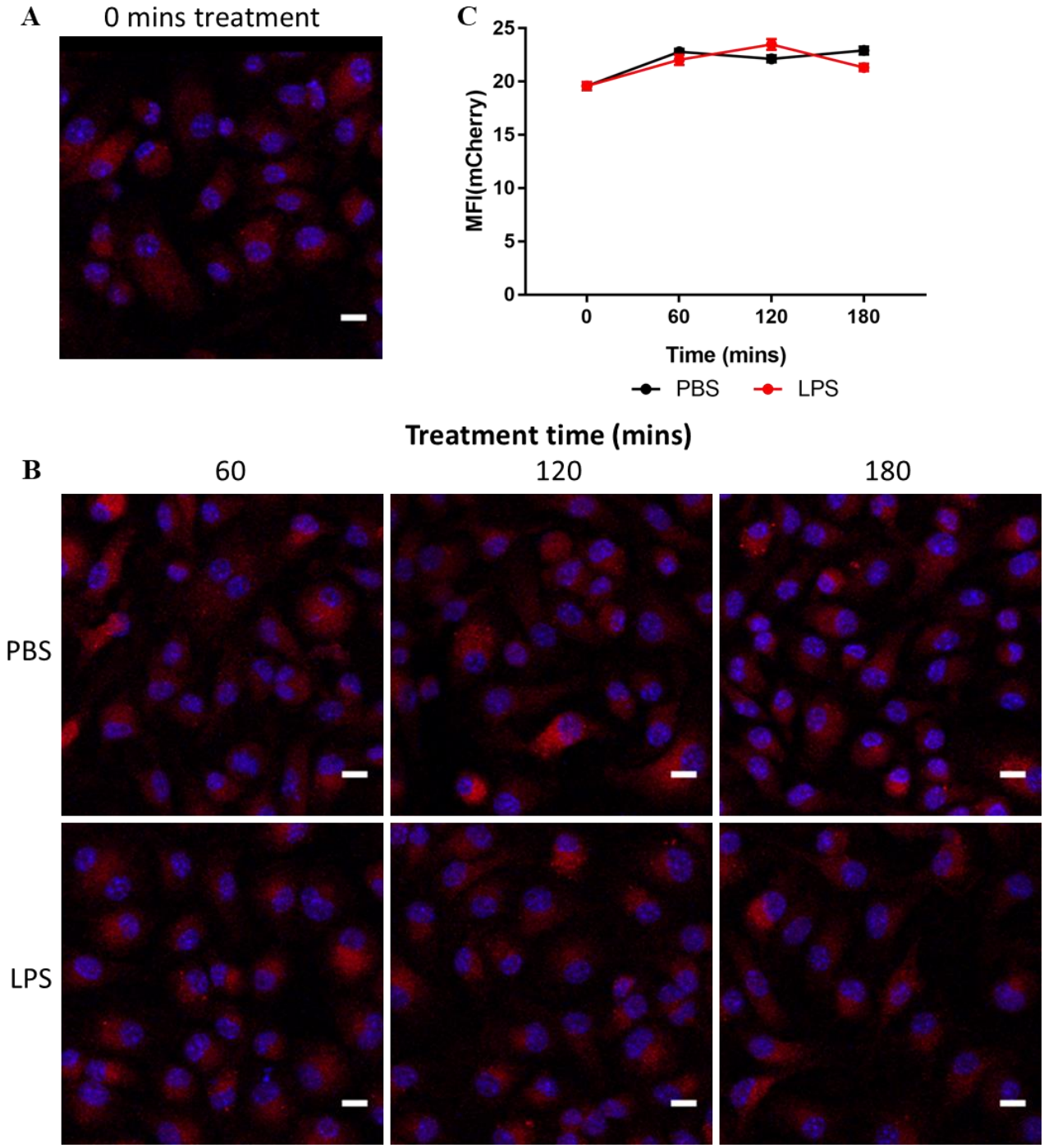

Figure 3.10: Effect of LPS on ASC expression in mCherry-ASC pBMDMs

mCherry-ASC pBMDMs were seeded at 4 x 10^4 cells/well in a 10-chamber slide twenty-four hours before the experiment. pBMDMs were either left untreated (A) or treated with PBS or 100ng/mL LPS for the indicated times (B). After treatment, cells were stained with Hoechst (blue on images) 15 minutes before they were fixed in 4% PFA for 30 minutes. They were washed in PBS before being mounted in 1% sodium azide in PBS. Fluorescent images were taken at 400x magnification (oil-based objective) on the Olympus FV1200 Laser Scanning Microscope. Representative images were generated via deconvolution of z-stacks with maximum intensity projection on Fiji software. Scale bar is 10µm. (C) Mean fluorescence intensities (MFIs) of mCherry were measured over nine fields for each treatment group. Data represented as mean ± SEM. Results are representative of three independent experiments.

To support the confocal imaging results, I used flow cytometry to measure ASC protein expression at the single-cell level. Similar to Figure 3.5B, untreated mCherry-ASC pBMDMs on average had higher mCherry fluorescence intensities compared to WT pBMDMs (Figure 3.11A, B). This result suggests that resting cells express a basal amount of ASC. LPS treatment; however, did not increase the mCherry fluorescence intensities (Figure 3.11A) or MFIs (Figure 3.11B) in mCherry-ASC pBMDMs. Overall, these results demonstrate that although ASC is basally expressed in resting pBMDMs, it is not upregulated by LPS, consistent with previous reports (Franklin et al., 2014; Yamamoto et al., 2004).

3.2.6 Detecting inflammasome activation via confocal imaging

It is previously described that inflammasome activation can be identified in cells by the condensation of all cellular ASC into a large molecular weight, oligomeric ASC speck (Beilharz et al., 2016; Sagoo et al., 2016; Tzeng et al., 2016). However, these studies predominantly use overexpression systems of ASC that may exaggerate the size of ASC specks (Beilharz et al., 2016; Sagoo et al., 2016; Tzeng et al., 2016). I next investigated whether ASC specks could be seen under endogenous conditions. Initially, I conducted confocal imaging of mCherry-ASC pBMDMs treated with nigericin (Figure 3.12). In the mCherry channel, I was unable to identify ASC speck formation within mCherry-ASC pBMDMs (Figure 3.12, *mCherry* column). To confirm the absence of ASC specks within nigericin-stimulated mCherry-ASC pBMDMs, I conducted an ASC counterstain with Alexa Fluor 488-conjugated goat anti-rabbit IgG that targeted the rabbit anti-ASC polyclonal antibody. Within the ASC counterstain, I was also unable to identify ASC specks within mCherry-ASC pBMDMs (Figure 3.12, *Alexa Fluor 488* column). These studies indicate that in an endogenous setting, ASC specks do not form when cells are treated with nigericin.

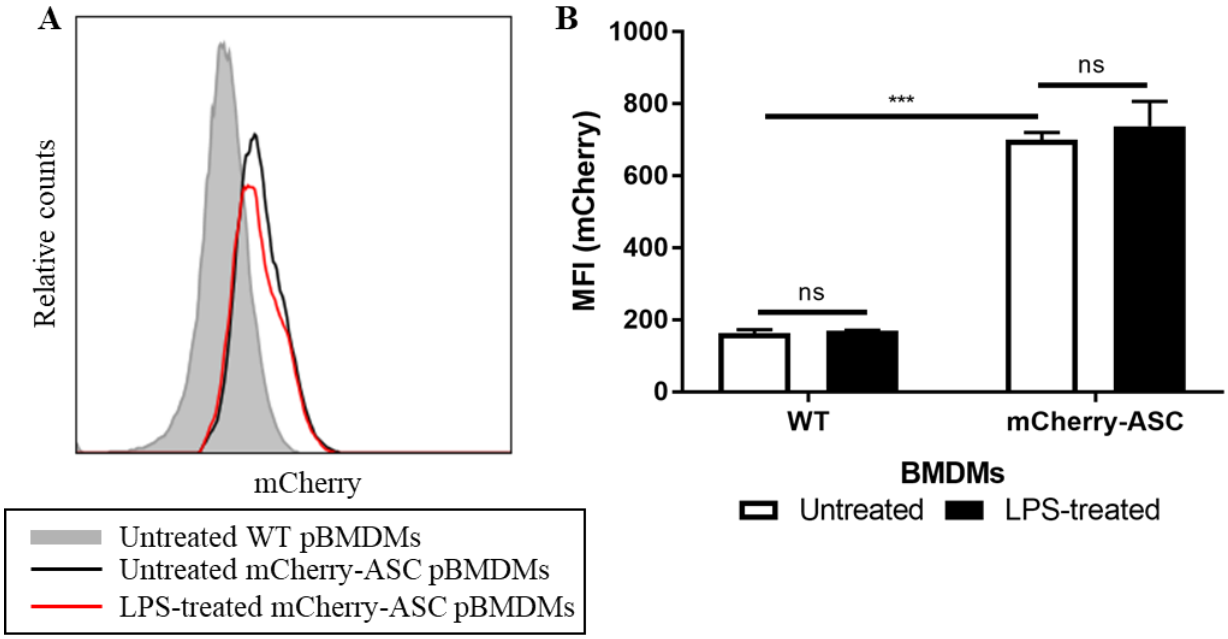

Figure 3.11: Effect of LPS on ASC protein expression at the single-cell level

WT and mCherry-ASC pBMDMs were seeded at 5 x 10^5 cells/well in 12-well plates 24 hours before being primed with LPS (100ng/mL) for 3 hours. pBMDMs were released from wells with 5mM EDTA (in PBS) and fixed in 4% PFA for 30 minutes at 4°C. After washing, cells were resuspended in PBS and processed on the BD LSRFortessa. (A) Overlay mCherry histogram comparing WT pBMDMs and untreated and LPS-treated mCherry-ASC pBMDMs. (B) mCherry MFIs of different pBMDM groups. MFI data presented as mean ± SEM in triplicate. Comparisons made via one-way ANOVA with Tukey's post-hoc test and significance represented as ns = not significant and ***P<0.001. Results are representative of three independent experiments.

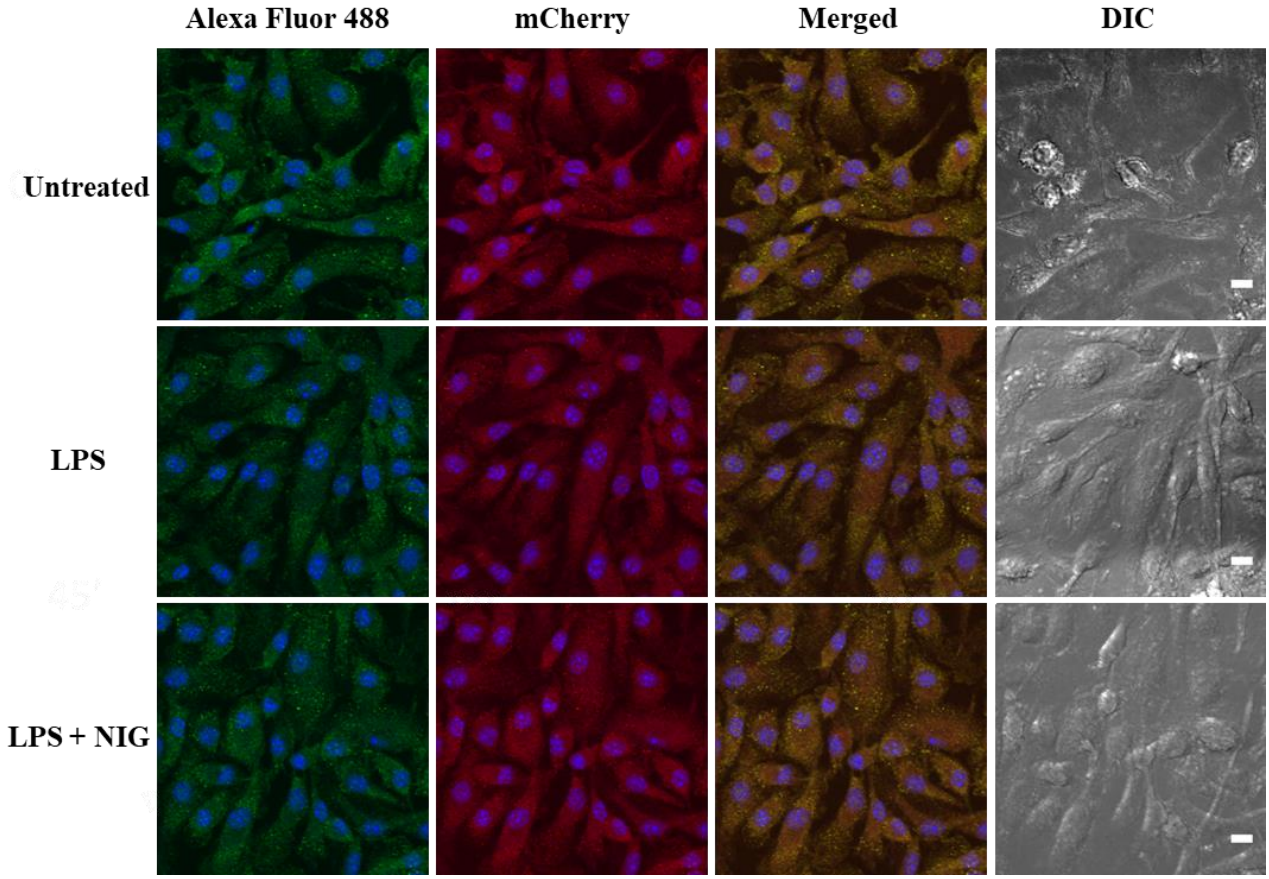

Figure 3.12: Detection of ASC specks in fixed mCherry-ASC pBMDMs stimulated with nigericin

mCherry-ASC pBMDMs were seeded at 4 x 10^4 cells/well in a 10-chamber glass-bottom slide 24 hours before being primed with 100ng/mL LPS for 3 hours. pBMDMs were then stimulated with 10µM nigericin (NIG) for 30 minutes. Cells were fixed in 4% PFA at room temperature for 15 minutes, permeabilised at room temperature for one hour and incubated with rabbit anti-ASC polyclonal antibody at 4°C overnight. The next day, cells were stained with Alexa Fluor 488 goat anti-rabbit IgG at room temperature for one hour and Hoechst for 15 minutes before being mounted in PBS. z-stacks of fluorescent and differential interference contrast (DIC) images were taken at 400X magnification (oil-based objective) on the Olympus FV1200 Laser Scanning Microscope. Representative images were generated via deconvolution of z-stacks with maximum intensity projection on Fiji software. Scale bar is 10µm. Results are representative of a 3x3 field across three independent experiments.

Uncovering novel aspects of ASC inflammasomes using mCherry-ASC mice

To confirm the fixed cell confocal imaging results, I analysed live mCherry-ASC pBMDMs that were treated with nigericin over a 90 minute period (Figure 3.13, Video 3.1). During this period of time, some cells exhibited areas of bright mCherry fluorescence where ASC tended to accumulate (Figure 3.13, Video 3.1). These areas of ASC enrichment were seen in cells that were activating the inflammasome before undergoing cell death (Figure 3.13, Video 3.1). These results may explain the absence of ASC specks in fixed cell images; ASC accumulates in ASC-enriched areas to represent inflammasome activation before cell death.

I also looked at inflammasome activation in fixed mCherry-ASC pBMDMs treated with the particulate NLRP3 inflammasome activator silica (Figure 3.14). Compared to untreated and LPS-treated mCherry-ASC pBMDMs, cells that were additionally treated with silica exhibited small ASC specks in both the *Alexa Fluor 488* and *mCherry* channels (Figure 3.14, bottom row). These ASC specks were around 1.3 to 6.5 µm in diameter and found in approximately 3.4% of cells. To confirm the presence of ASC specks in live mCherry-ASC pBMDMs, I looked at live mCherry-ASC pBMDMs stimulated with silica (Figure 3.15, Video 3.2). Among live mCherry-ASC pBMDMs, some cells displayed the condensation of ASC into an ASC-enriched area from 45 to 135 minutes after the administration of silica before dying by 180 minutes (Figure 3.15, Video 3.2). This ASC-enriched area was not all-encompassing; though, because some cellular ASC was still diffusely distributed (Figure 3.15, Video 3.2).

These results suggest that ASC complexes are formed within ASC-enriched areas of the cell during inflammasome activation that do not involve all cellular ASC.

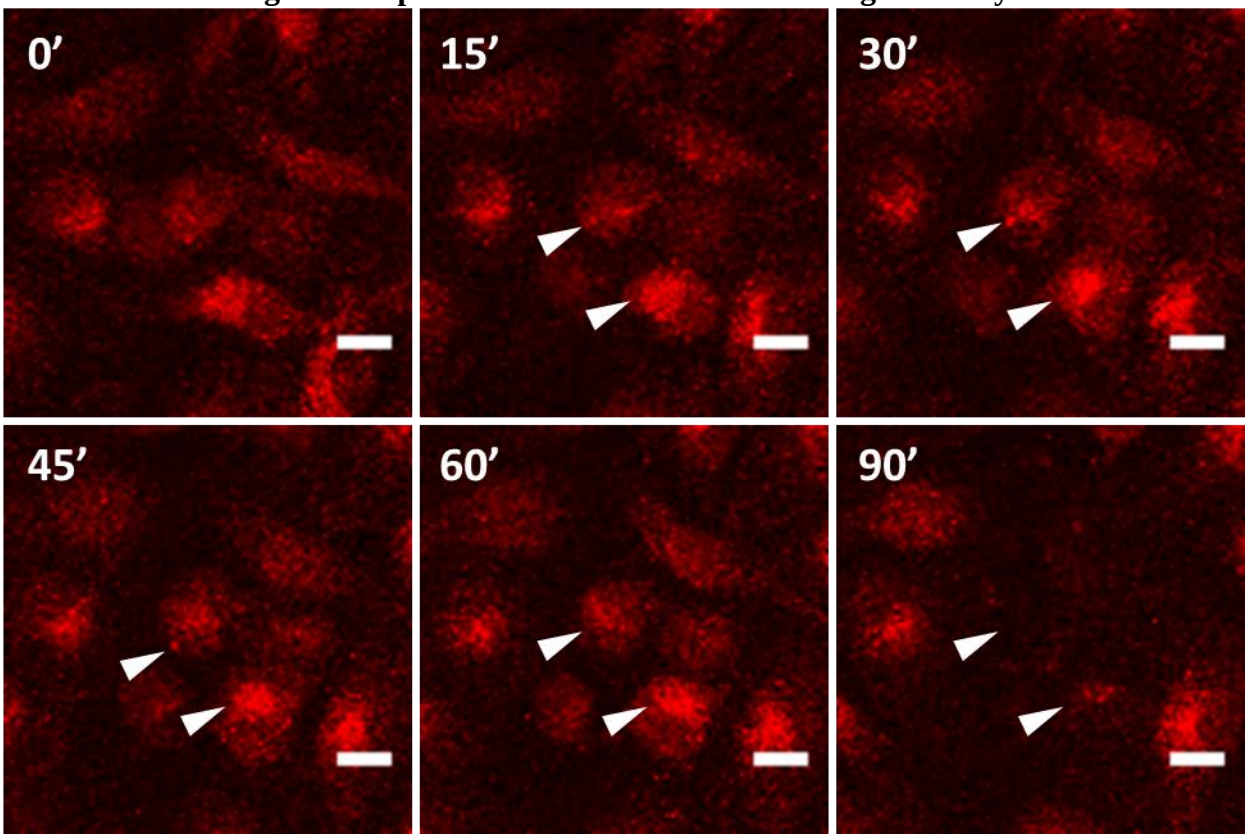

Figure 3.13: Detection of ASC enrichment in mCherry-ASC pBMDMs treated with nigericin

mCherry-ASC pBMDMs were placed on a Fluorodish at 2 x 10^4 cells 24 hours before being primed with 100ng/mL LPS for 3 hours. pBMDMs were then stimulated with 10µM nigericin and imaged every 5 minutes for 90 minutes on the Olympus FV1200 Laser Scanning Microscope. Representative deconvoluted images of mCherry-ASC pBMDMs at specific timepoints are shown with scale bar representing 10µm and arrows pointing to ASC enrichment on image. Results are representative of a 3x3 field across three independent experiments.

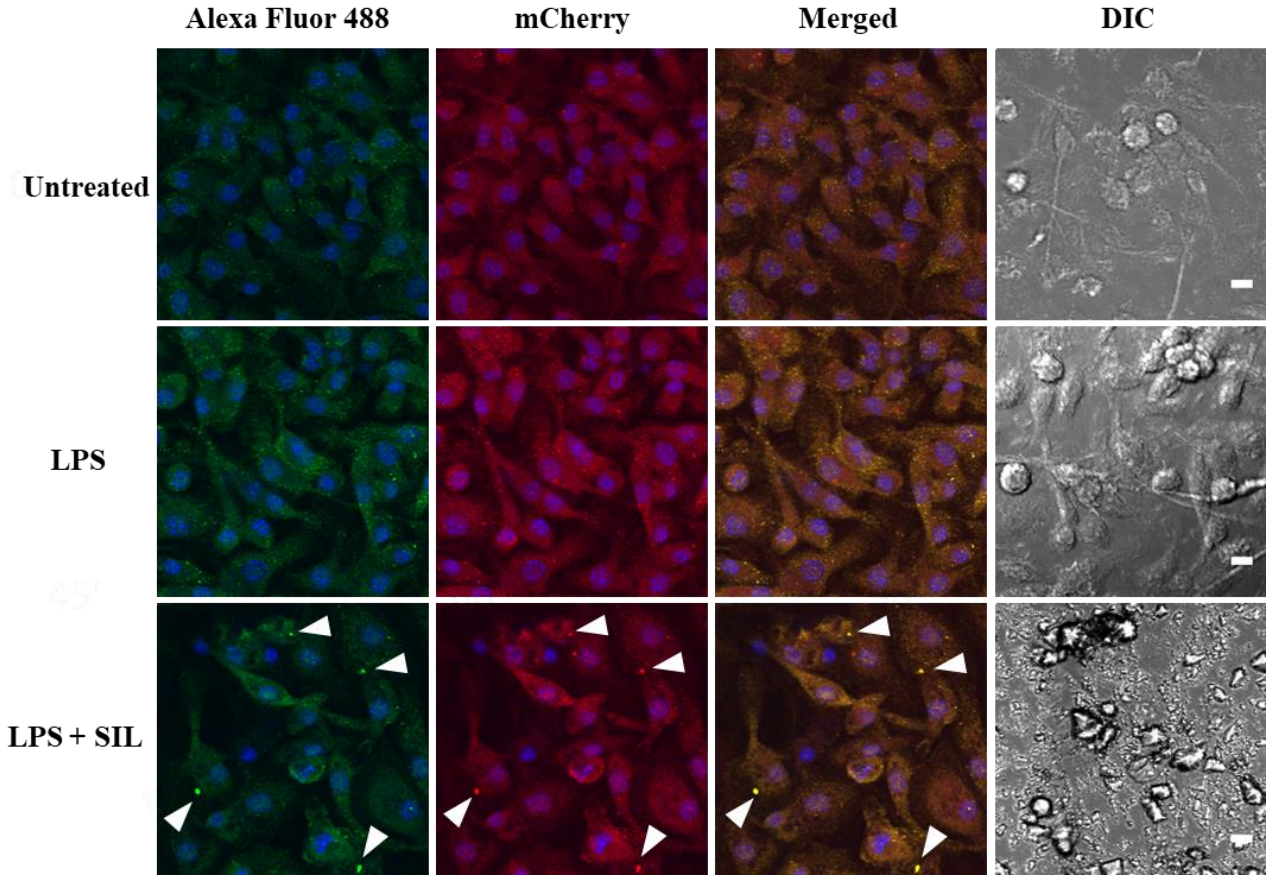

Figure 3.14: Detection of ASC specks in fixed mCherry-ASC pBMDMs stimulated with silica

mCherry-ASC pBMDMs were seeded at 4 x 10^4 cells/well in a 10-chamber glass-bottom slide 24 hours before being primed with 100ng/mL LPS for 3 hours. pBMDMs were then stimulated with 150µg/mL silica (SIL) for 4 hours. Cells were fixed in 4% PFA at room temperature for 15 minutes, permeabilised at room temperature for 30 minutes and incubated with rabbit anti-ASC polyclonal antibody at 4°C overnight. The next day, cells were stained with Alexa Fluor 488 goat anti-rabbit IgG at room temperature for one hour and Hoechst for 15 minutes before being mounted in PBS. z-stacks of fluorescent and differential interference contrast (DIC) images were taken at 400X magnification (oil-based objective) on the Olympus FV1200 Laser Scanning Microscope. Representative images were generated via deconvolution of z-stacks with maximum intensity projection on Fiji software. Scale bar is 10µm and arrows indicate ASC specks. Results are representative of a 3x3 field in three independent experiments.

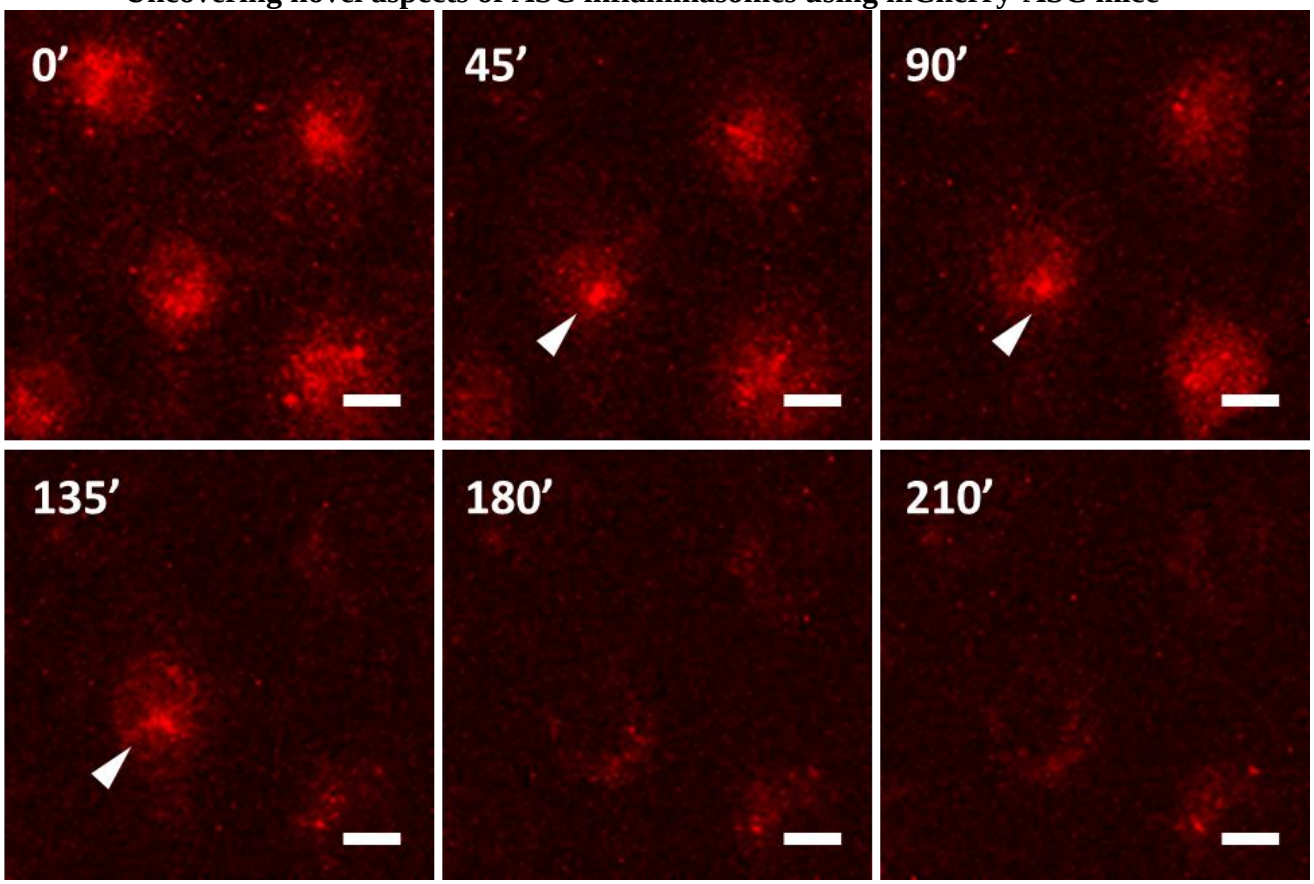

Figure 3.15: Formation of ASC enrichment in live silica-stimulated mCherry-ASC pBMDMs

mCherry-ASC pBMDMs were placed on a Fluorodish at 4 x 10^4 cells 24 hours before being primed with 100ng/mL LPS for 3 hours. pBMDMs were then stimulated with 150µg/mL silica and imaged every 7.5 minutes for 210 minutes on the Olympus FV1200 Laser Scanning Microscope. Representative deconvoluted images of mCherry-ASC pBMDMs at specific timepoints shown with scale bar representing 10µm and arrow pointing to ASC enrichment on image. Results are representative of a 3x3 field in three independent experiments.

3.2.7 Detecting inflammasome activation via flow cytometry

To further support the observation of ASC enrichment in inflammasome-activated mCherry-ASC pBMDMs at the single-cell level, I used the flow cytometry method previously described by Sester et al. (2015) to identify speck formation in cells (Figure 3.16A). Flow cytometry involves the production of a signal peak for each cell as it passes through the laser. The signal peak tracks the fluorescence intensity of each part of the cell as it passes through the laser. The height and area under the curve of each signal peak are measured and mapped on a scatter plot. These measurements vary depending on how ASC is distributed in the cell. A diffuse ASC distribution is associated with a low, wide signal peak, resulting in a low signal height-to-area ratio (Figure 3.16A, *diffuse* label). However, during inflammasome activation, as ASC condenses, the signal peak becomes high and narrow, increasing the signal height-to-area ratio (Figure 3.16A, *speck* label). This produces an ASC speck-positive cell population representing active inflammasomes that is plotted above the inflammasome-inactive population (Figure 3.16A).

To optimise the identification and quantification of ASC speck-positive populations via flow cytometry, I used ASC-Cerulean iBMDMs because they spontaneously form ASC specks upon exposure to inflammasome activators (Stutz et al., 2013). Compared to untreated ASC-Cerulean iBMDMs (Figure 3.16B, left panel), nigericin-treated ASC-Cerulean iBMDMs showed a notable increase in the size of the ASC speck-positive population from 0.99 ± 0.14% in untreated ASC-Cerulean iBMDMs to 20.71 ± 0.96% in nigericin-treated ASC-Cerulean iBMDMs ($p < 0.001$) (Figure 3.16B, right panel). This result confirms flow cytometry as a viable technique to detect ASC speck-positive cells in an overexpression setting.

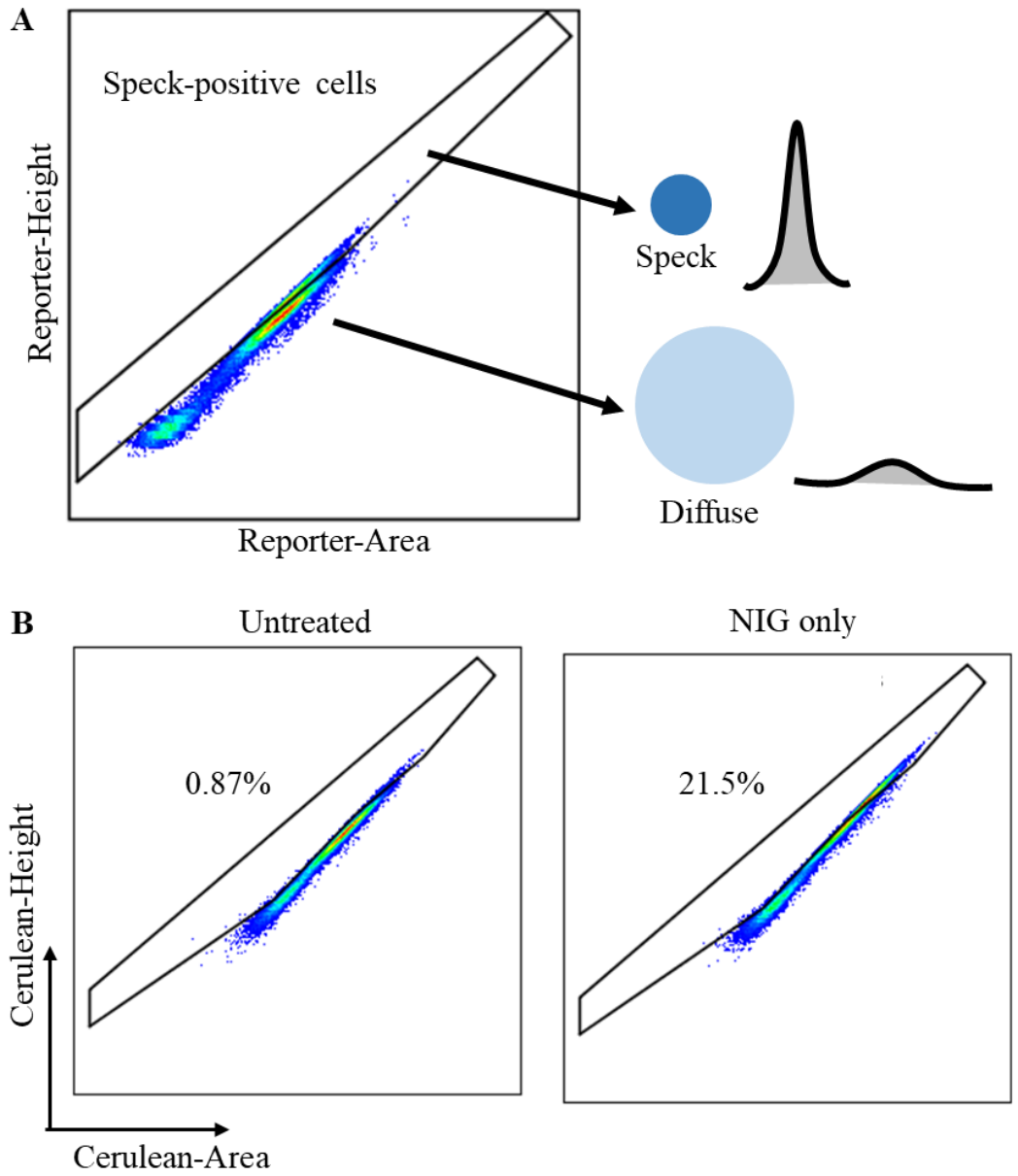

Figure 3.16: Detecting an ASC speck-positive population via flow cytometry in ASC-Cerulean iBMDMs

(A) Schematic of detecting specks via flow cytometry. Speck-positive cells can be detected in flow cytometry by measuring the height and area under the curve of the signal peak of the reporter. The height and width of the signal peaks are dependent on how the reporter is distributed. When the reporter is diffuse, the signal peak is low and wide. This results in a low height-to-area ratio which establishes the main cell population. When the reporter condenses into a speck, a high, narrow signal peak is produced. This increases the height of the peak, raising the height-to-area ratio. This produces a speck-positive cell population representing cells with active inflammasomes that is plotted above the main non-speck-positive cell population.

(B) 2.5 x 10^5 ASC-Cerulean iBMDMs/sample were either left untreated or stimulated with nigericin (NIG, 30µM) in triplicate for 30 minutes. Cells were fixed in 4% PFA for 5 minutes at 4°C before being washed and resuspended in PBS. Cells were processed on the BD LSRFortessa and plotted on the height and area of the reporter to detect a speck-positive population. Results are representative of three independent experiments.

I therefore applied flow cytometry to mCherry-ASC pBMDMs to determine if I could detect ASC specks when the tagged ASC is endogenously expressed. Compared to untreated and LPS-treated mCherry-ASC pBMDMs, adding nigericin to LPS-primed mCherry-ASC pBMDMs resulted in a very small increase in the size of the ASC speck-positive population in the mCherry channel (from 0.20 ± 0.01% and 0.17 ± 0.06% in untreated and LPS-treated mCherry-ASC pBMDMs respectively to 0.37 ± 0.01% in LPS and nigericin-treated mCherry-ASC pBMDMs, both comparisons $p < 0.01$) (Figure 3.17A). However, compared to the ASC-Cerulean iBMDMs, mCherry-pBMDMs did not produce a distinct ASC speck-positive population when treated with LPS and nigericin (Figure 3.17A).

To confirm that I could detect ASC specks at the endogenous level via flow cytometry, I counterstained WT and mCherry-ASC pBMDMs that underwent different treatments with rabbit anti-ASC polyclonal antibody and Alexa Fluor 488 goat anti-rabbit IgG as previously described by Sester et al. (2015). As shown in Figure 3.17B, both WT and mCherry-ASC pBMDMs exhibited increases in the percentage of ASC speck-positive cells when treated with LPS and nigericin compared to the LPS control (from 0.09 ± 0.003% to 0.62 ± 0.09% in WT pBMDMs and from 0.07 ± 0.03% to 0.87 ± 0.12% in mCherry-ASC pBMDMs, both comparisons $p < 0.001$). Importantly, the increase in ASC speck-positive cells is small compared to the treatment of ASC-Cerulean iBMDMs with nigericin (from 0.99 ± 0.14% to 20.71 ± 0.96%, $p < 0.001$) (Figure 3.17B). These results show that a distinct ASC speck-positive population is not formed in endogenously-expressed ASC of both WT and mCherry-ASC pBMDMs, confirming the absence of ASC speck formation during inflammasome activation. These increases; however, were insignificant compared to the increase in ASC speck-positive cell populations among ASC-Cerulean iBMDMs when treated with nigericin (Figure 3.17B).

These results indicate that only a small percentage of cells exhibit inflammasome activation and that the ASC specks formed are too small to be detected by flow cytometry.

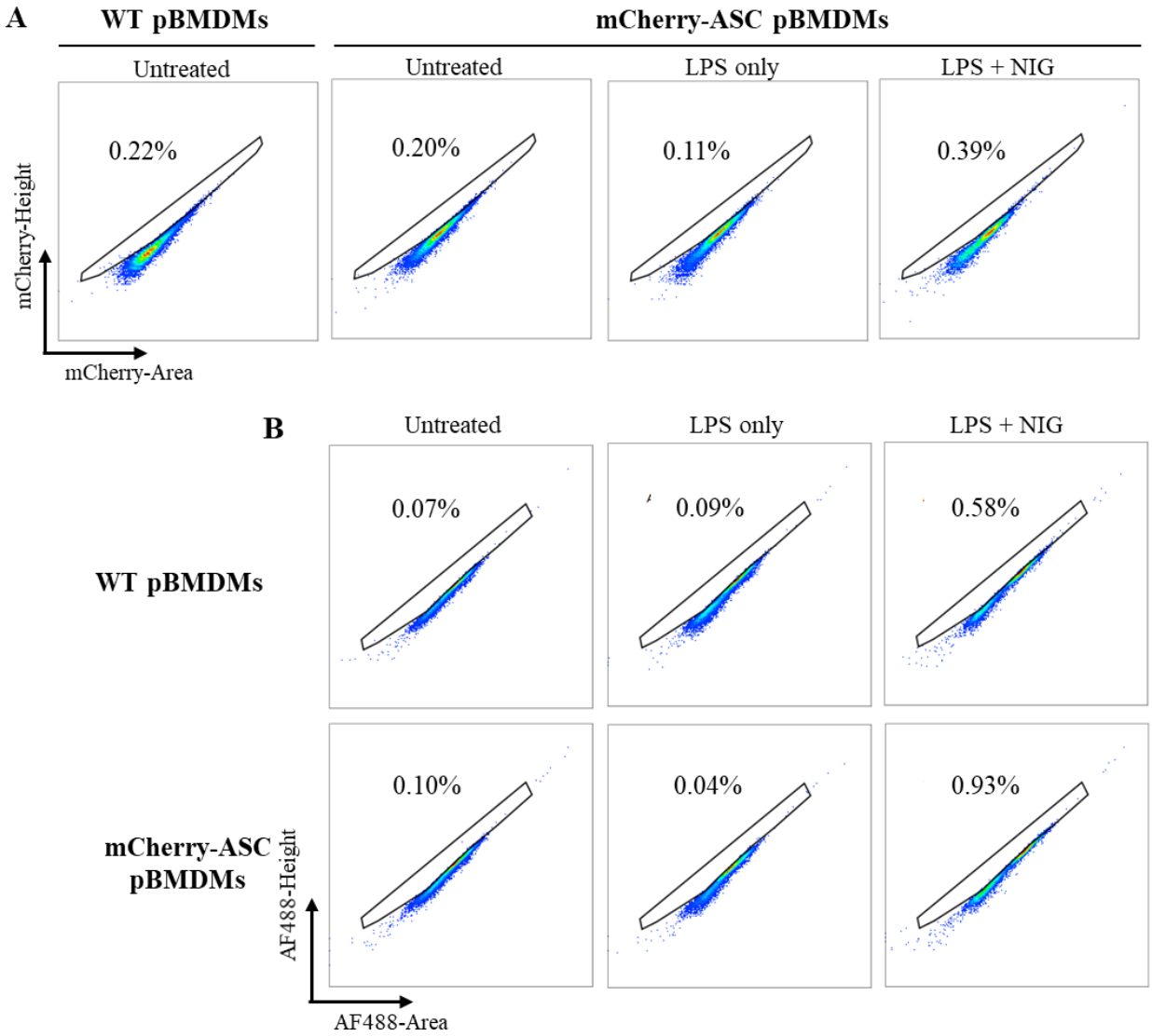

Figure 3.17: Detecting an ASC speck-positive population via flow cytometry in mCherry-ASC pBMDMs

WT and mCherry-ASC pBMDMs were seeded at 3 x 10^5 cells/well in 24-well plates 24 hours before being primed with LPS (100ng/mL) for 3 hours. pBMDMs were released from wells with 5mM EDTA (in PBS) and stimulated with nigericin (NIG, 30µM) for 30 minutes. Cells were fixed in 4% PFA for 5 minutes at 4°C before they were permeabilised and blocked. Cells were incubated with rabbit anti-ASC polyclonal antibody at 4°C overnight before being stained with Alexa Fluor 488 (AF488)-goat anti-rabbit IgG for one hour. pBMDMs were processed on the BD LSRFortessa and plotted on the height and area of mCherry (A) and Alexa Fluor 488 (B) to detect a speck-positive population. Results are representative of two independent experiments.

3.3 Discussion

Previous studies of the inflammasome have used ASC reporter systems, where a fluorescent protein is attached to ASC. These include ASC-Cerulean iBMDMs to assay inflammasome activation *in vitro* (Stutz et al., 2013) and ASC-mCitrine mice to examine the role of the inflammasome in disease *in vivo* (Tzeng et al., 2016). The limitation of these systems; however, is that they overexpress the ASC reporter. This means that the reporter and by extension, ASC are constitutively overexpressed in all cells and tissues beyond what is encountered in an endogenous environment. Consequently, results from these reporter systems may not fully describe how ASC functions in a biological context. In my study, we have generated a reporter mouse where the fluorescent protein mCherry is attached to ASC on the N-terminus, creating the mCherry-ASC reporter (Figure 3.1B). Importantly, this reporter is placed under its native promoter, limiting the expression of ASC in cells and tissues to levels encountered in an endogenous environment (Figure 3.5A). This enables results from mCherry-ASC cells or mice to better reflect how ASC behaves in biologically relevant conditions. The expression of the functional mCherry-ASC reporter in cells of the reporter mouse (Figure 3.5B-C) allows us to measure the expression and distribution of ASC in an endogenous setting by quantifying mCherry fluorescence intensity. There was also a non-specific band in mCherry-ASC pBMDM lysates at around 28kDa (Figure 3.5A). Future studies may investigate the identity of the band and the possibility of it appearing in a small percentage of mCherry-ASC cells.

Gross phenotyping of mCherry-ASC mice indicated that they developed at the same rate as WT mice as measured by their similar growth curves (Figure 3.3) and organ weights (Figure 3.4). It was noted; though, that mCherry-ASC mice had larger stomachs (0.15 ± 0.02g) compared to WT mice (0.09 ± 0.01g) (Figure 3.4D). Nevertheless, the difference in stomach mass between WT and mCherry-ASC mice is small compared to the substantial increases seen in murine models of gastric cancer (from 0.18g in healthy stomachs to 1g in gastric cancer stomachs) (Tye et al., 2012). Hence, it would appear that the slightly larger stomachs in mCherry-ASC mice had no adverse effect on their health.

Uncovering novel aspects of ASC inflammasomes using mCherry-ASC mice

Inflammasome activation is associated with IL-1β maturation, caspase-1 activation and cell death in the presence of inflammasome activators (Groß, 2012). Due to the possibility that mCherry in the mCherry-ASC reporter may sterically hinder inflammasome activation, I measured inflammasome activation in mCherry-ASC pBMDMs. mCherry-ASC pBMDMs exhibited IL-1β secretion when exposed to LPS and nigericin, silica, ATP or poly(dA:dT) (Figure 3.6A-D). This process was inhibited in the presence of the small molecule inhibitor MCC950 (Figure 3.8A-B). MCC950 could also impede caspase-1 activation and IL-1β maturation in mCherry-ASC pBMDMs with similar efficacy as WT pBMDMs (Figure 3.9, lanes 7-10). Given that MCC950 specifically inhibits the NLRP3 inflammasome and not other ASC-dependent inflammasomes such as NLRC4 (Coll et al., 2015), these results suggest that MCC950 does not act on ASC monomers or complexes to block inflammasome activation. Crucially, these results also imply that mCherry in the mCherry-ASC reporter is not sterically preventing MCC950 from inhibiting inflammasome activation.

There were differences; however, in the immunoblots of the stimulation and MCC950 experiments of mCherry-ASC pBMDMs. Both experiments showed caspase-1 activation and IL-1β maturation when mCherry-ASC pBMDMs were exposed to LPS and silica (Figure 3.7, lane 10 and Figure 3.9, lane 7). However, while ATP treatment did not induce IL-1β and caspase-1 maturation in mCherry-ASC pBMDMs of the stimulation experiment (Figure 3.7, lane 11), they were present in the MCC950 experiment (Figure 3.9, lane 9). The reason behind this might be due to the different ATP concentrations used in both experiments. For the stimulation experiment, 5.0mM ATP was used which was reduced to 2.5mM for the MCC950 experiment. It has been described that higher ATP concentrations are associated with reduced signs of inflammasome activation due to the rapid induction of cell death (Hirano et al., 2017). Variations in the stimulation conditions of mCherry-ASC pBMDMs as well as individual mCherry-ASC mice may have affected the biochemical activation of the inflammasome, leading to different results. Importantly; however, I observed consistent activation and maturation of the inflammasome/IL-1β complex from mCherry-ASC cells.

Uncovering novel aspects of ASC inflammasomes using mCherry-ASC mice

The positioning of the mCherry-ASC reporter under its native promoter allows us to study the structure, function and expression of ASC under endogenous *in vitro* and *in vivo* conditions. Priming signals such as TLR ligands and TNF-α activate NF-κB which induce the expression of NLRs, pro-caspase-1, pro-IL-1β and pro-IL-18 (Bauernfeind et al., 2009; Sutterwala et al., 2006). My experiments found that ASC is basally expressed in unstimulated cells (Figure 3.11A-B) but is not upregulated by LPS (Figure 3.10B-C, Figure 3.11A-B). The latter is consistent with previous biochemical studies which found that ASC protein expression as measured by immunoblots does not increase during LPS treatment of murine PECs (Yamamoto et al., 2004) and human THP-1 macrophage cell lines (Franklin et al., 2014). This implies that ASC is constitutively expressed at detectable levels in unstimulated cells and that its expression is differentially regulated from other inflammasome components such as caspase-1 and IL-1β whose upregulation is dependent on NF-κB activity. The constitutive expression of ASC in resting cells may contribute to its inflammasome-dependent and -independent functions. By expressing an abundant amount of ASC in resting conditions, cells are primed to rapidly form ASC filaments upon inflammasome activation (Gambin et al., 2018), contributing to the rapid kinetics and robustness of inflammasome activation when exposed to agonists such as nigericin and ATP (Kahlenberg and Dubyak, 2004; Perregaux and Gabel, 1994). Alternatively, constitutive ASC expression may also be related to its inflammasome-independent functions. For instance, ASC, expressed in the small intestine and colon (Lattin et al., 2008; Uhlen et al., 2015), was identified as a tumour suppressor gene because its expression is suppressed in colorectal cancer (Ohtsuka et al., 2006) and melanoma (Guan et al., 2003). Mechanistically, ASC expression suppresses Src-induced Tyr^{380} phosphorylation in caspase-8 which is associated with increased cell migration in B16 murine melanoma cell lines (Okada et al., 2016) and induces apoptosis in human HT1080 fibrosarcoma (Kitazawa et al., 2017) and human COLO205 colon adenocarcinoma cell lines (Motani et al., 2010). Moreover, activation of ASC was associated with suppressed gastric tumour growth and metastasis *in vivo* (Motani et al., 2010). These two contrasting functions of ASC may explain why it is expressed in both resting and inflammasome-

activated cells. It would be interesting; therefore, to further study the inflammasome-independent functions of ASC.

Previous studies have stated that all ASC in a cell is condensed into an ASC speck upon inflammasome activation (Beilharz et al., 2016; Sagoo et al., 2016; Tzeng et al., 2016). These studies have relied on overexpression of ASC reporter systems that may not reflect how endogenous ASC may behave in a biological context. Biochemical studies in a cell-free system have also described the ASC speck as the cross-linking of separate ASC filaments (Dick et al., 2016; Lu et al., 2014). However, generally speaking, these studies express truncated constructs of ASC that form specific complexes without the presence of other domains that may constrain or alter tertiary structure function. In contrast, the mCherry-ASC reporter is expressed in its full length and placed under its native promoter, limiting the expression of natural ASC to endogenous levels. Therefore, I used mCherry-ASC cells to investigate whether ASC specks form in an endogenous setting.

Interestingly, different inflammasome activators led to contrasting results in the fixed cell images of mCherry-ASC pBMDMs. While nigericin stimulation did not produce discernible ASC specks in mCherry-ASC pBMDMs (Figure 3.12), silica treatment resulted in the appearance of ASC specks in mCherry-ASC pBMDMs (Figure 3.14). Nevertheless, the imaging of live LPS-primed mCherry-ASC pBMDMs stimulated with nigericin (Figure 3.13) or silica (Figure 3.15) showed the localisation of ASC into an ASC-enriched area during inflammasome activation. Critically, I observed that mCherry-ASC pBMDMs do not form an all-encompassing ASC speck as suggested in previous studies (Beilharz et al., 2016; Stutz et al., 2013; Tzeng et al., 2016).

I further investigated the potential to identify ASC specks to form at the single-cell level by using flow cytometry from a method by Sester et al. (2015). Initially applying the method to stably-expressed ASC-Cerulean iBMDMs which spontaneously form ASC specks (Stutz et al., 2013), I found a notable increase in the size of the ASC speck-positive population when treated with nigericin (Figure 3.16B). This is concordant with the Sester et al. (2015) study which found ASC speck

formation in LPS-primed stably-expressed ASC-EGFP iBMDMs treated with nigericin. However, in contrast to previous studies (Sester et al., 2015; Sester et al., 2016), my studies could not find a detectable ASC speck-positive population during nigericin treatment of WT and mCherry-ASC pBMDMs in both mCherry fluorescent protein and Alexa Fluor 488 counterstaining channels (Figure 3.17A-B). Given the basis of analysis for this method is the condensation of all ASC into a speck with limited to no ASC in the surrounding cytosol, the smaller, less defined enrichment of ASC could not be detected or assessed by this flow cytometry method (Figure 3.18).

Even though Sester's studies used the same antibody to identify ASC (rabbit anti-ASC (N(15)-R clone), Santa-Cruz), there were differences in how the cells were treated. The previous experiments from Sester et al. (2015) and Sester et al. (2016) primed cells with 10ng/mL LPS from *Salmonella enterica serovar Minnesota* for four hours and activated the inflammasome with 10µM nigericin for 30 minutes. On the other hand, my studies have treated cells with 100ng/mL LPS from *Escherichia coli* O55:B5 for three hours and 30µM nigericin for 30 minutes. LPS from two different bacteria stimulate varying magnitudes of cellular responses. Compared to LPS from *Escherichia coli* O55:B5, LPS from *Salmonella enterica serovar Minnesota* induced more cell death in murine J774.1 macrophage cell lines (Amano and Akamatsu, 1991) and IL-1β secretion from human monocytes (Newton, 1986). This implies that LPS from *Salmonella enterica serovar Minnesota* may contribute to stronger inflammasome responses and toxicity in cells compared to LPS from *Escherichia coli* O55:B5.

Nevertheless, the results still conform to the principles of detecting ASC specks via flow cytometry. ASC-Cerulean iBMDMs either have all ASC dispersed or condensed into a speck depending on whether the cells are exposed to inflammasome activators (Figure 3.18A-B). Consequently, inflammasome-activated ASC-Cerulean iBMDMs can display a distinct ASC speck-positive population via flow cytometry (Figure 3.18B).

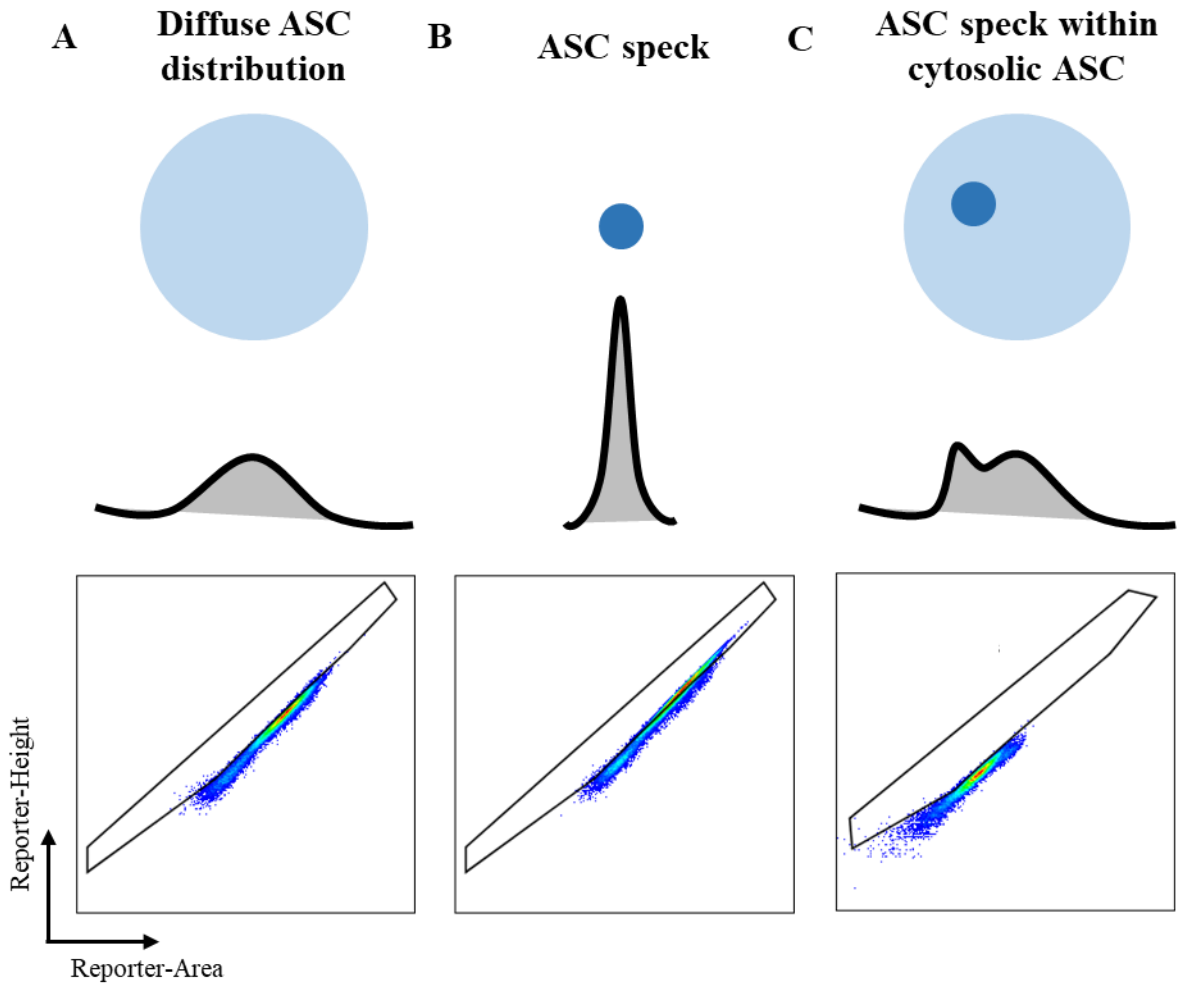

Figure 3.18: Schematic of the effect of cellular ASC distribution on how cells are plotted in flow cytometry

Reporter cells are plotted depending on the height and area under the curve of their signal peaks. These in turn are affected by the distribution of ASC. (A) In inactive cells, ASC is diffuse across the cytosol. This produces a low, wide signal peak, resulting in a cell population that falls below the ASC speck-positive gate. (B) However, when all the ASC condenses into a speck in the case of ASC-Cerulean iBMDMs, it produces a high, narrow signal peak. This results in ASC speck-positive cells forming a separate cell population that is above the ASC speck-negative cells. (C) In the context of mCherry-ASC pBMDMs, an ASC-enriched area is formed that does not involve all cellular ASC. This ASC-enriched area resides within cytosolic ASC which is represented by a blip within the signal peak. The height of the signal peak of these cells does not increase, so consequently an ASC speck-positive population is not detected when inflammasome-activated mCherry-ASC pBMDMs are processed via flow cytometry.

However, live cell confocal imaging of endogenously-expressed mCherry-ASC pBMDMs identified a small, enriched ASC area in inflammasome-activated cells that do not involve all cellular ASC (Figure 3.13, Figure 3.15). As a result, the small, enriched ASC area residing within dispersed cytosolic ASC may produce a small "blip" in the mCherry signal peak that may not raise the mCherry signal peak height enough to increase the mCherry signal height-to-area ratio and establish a distinct ASC enrichment-positive population (Figure 3.18C). Critically, given that ASC is not upregulated by priming signals, the condensation of ASC into one small area suggests an enrichment or super-concentration of ASC as described by Gambin et al. (2018) where ASC filaments are elongated. Endogenous expression of ASC in mCherry-ASC cells may limit the amount and length of ASC filaments formed, reducing the number of cross-links among ASC filaments to produce a loosely-packed ASC-enriched area.

It is also possible that an endogenous protein caps the ends of ASC filaments to limit their length. POPs are a group of regulatory proteins that bind to PYD domains in ASC to restrict the size of ASC complexes (de Almeida et al., 2015; Dorfleutner et al., 2007; Ratsimandresy et al., 2017). Past studies have found that POPs are only expressed in humans, but recently a murine POP orthologue called PYD-containing protein 3 (PYDC3) was found in murine pBMDMs to inhibit inflammasome activity (Vijay et al., 2017). These proteins would have more of an effect in an endogenous system than in an overexpression system because the formation and elongation of ASC filaments in the latter system may outstrip the capping effects of that protein. The prion capacity of ASC and the excessive concentrations of ASC in ASC overexpression systems may eschew the formation of a much larger, all-encompassing speck that previous studies have described.

The formation of small, enriched ASC areas within an inflammasome-activated cell is relevant to the discussion of the biological role of ASC. Previous studies have used overexpressed ASC reporter models that exaggerate the size of the single ASC speck so that it is visible under confocal microscopy and flow cytometry. Conversely, the placement of the mCherry-ASC reporter under its native

promoter restricts the expression of ASC to endogenous levels. Given that ASC is neither overexpressed nor upregulated in the mCherry-ASC mouse, the ASC-enriched area might be detectable under confocal microscopy but not flow cytometry. These results; therefore, imply that flow cytometry may not be the best method to detect inflammasome activation via ASC speck formation in cells that endogenously express ASC.

The limitation of the mCherry-ASC reporter is that mCherry is attached to the PYD end of ASC. Given that the PYD domains of ASC associate to form a PYD core during ASC filament assembly (Sborgi et al., 2015), attaching mCherry to the PYD domain may disrupt the formation of ASC filaments, impeding inflammasome activation. Nevertheless, I did see that mCherry-ASC cells exhibited significant inflammasome activation, implying that the attachment of mCherry to the PYD end of ASC did not completely abolish inflammasome activity. In the future, it may be advantageous to generate an ASC reporter mouse where the fluorescent protein is attached to the CARD domain of ASC which has more space to interact with other proteins such as caspase-1 (Lu et al., 2014; Sborgi et al., 2015). This may restore some inflammasome activity on mCherry-ASC cells, although attachment of the fluorescent tag did not diminish biological activity.

In summary, mCherry-ASC pBMDMs were used to study the inflammasome in an endogenous context. Cells from mCherry-ASC mice express the functional reporter and respond to inflammasome activators and MCC950 commensurate to WT cells. The presence of a fluorescent reporter enables the expression and distribution of ASC to be measured in an endogenous system. mCherry-ASC pBMDMs were used to confirm that ASC is constitutively expressed in resting cells and that it is not upregulated by LPS as described in previous studies. On the other hand, mCherry-ASC pBMDMs form areas of ASC enrichment that are different from the large ASC specks seen in overexpressed ASC reporter systems. Nevertheless, it is biologically relevant given the limited amount of ASC available in cells and the potential capping of ASC filaments. Importantly; however, our accepted dogma that all ASC within a challenged cell oligomerises into one, large, all-encompassing speck is

challenged by our studies that use a fluorescently-tagged ASC expressed under its native promoter. It would appear that upon activation, ASC becomes enriched in the sub-cellular environment to form a loosely-packed, filamentous structure that can enzymatically process caspase-1 and IL-1β/IL-18. This complex may be more in line with other PRR signalling platforms such as the myddosome for TLR signalling which appear to enrich in one small area, form multimeric signalling platforms and potentiate signalling capacity and kinetics (Motshwene et al., 2009). These findings have; therefore, generated new knowledge of how ASC behaves in an endogenous system and will lead to more biologically-relevant discoveries of how the inflammasome functions in an endogenous, *in vivo* context.

The attachment of mCherry to ASC allowed us to measure the expression and distribution of ASC when cells are exposed to priming and activating signals. Similar to the mCherry-ASC reporter, attachment of fluorescent proteins to NLRP3 enables the measurement of the expression and distribution of NLRP3 to be measured in an endogenous setting. The next chapter will explore the use of the NLRP3-CHCI reporter to fulfil this aim.

4 Discovering new aspects of NLRP3 inflammasomes using NLRP3-CHCI mice

4.1 Introduction

The NLR family, PYD domain containing member 3 (NLRP3) inflammasome is a protein complex in the innate immune system that matures pro-inflammatory cytokines IL-1β and IL-18 (Martinon et al., 2004). The NLRP3 inflammasome also induces pyroptosis, an inflammatory form of cell death, by cleaving gasdermin D which form pores on the cell surface to induce lysis (Kayagaki et al., 2015; Liu et al., 2016b). The NLRP3 inflammasome is important to human health because it is linked to various inflammatory diseases (reviewed in Abderrazak et al. (2015)). Initially, mutations in NLRP3 led to constitutive IL-1β maturation in a group of autoinflammatory syndromes called CAPS (Feldmann et al., 2002; Hoffman et al., 2001). Numerous studies have now identified stimuli inducing NLRP3 inflammasome assembly and activation, establishing new connections between the NLRP3 inflammasome and various diseases. These include arthritic diseases such as gout (Martinon et al., 2006), respiratory diseases such as asbestosis (Dostert et al., 2008), neurological diseases such as Alzheimer's disease (Heneka et al., 2013) and metabolic diseases such as diabetes (Lee et al., 2013). Hence, the NLRP3 inflammasome is an important area of study in inflammatory diseases and is a potential target for novel therapeutics.

One of the three components of the NLRP3 inflammasome is the sensor protein NLRP3. NLRP3 is an NLR consisting of an N-terminal PYD domain, a central NBD domain and C-terminal LRRs (Ting et al., 2008) (Figure 1.4). NLRP3 is expressed not only in leukocytes such as macrophages, neutrophils and DCs (Guarda et al., 2011; Sutterwala et al., 2006) but also in non-myeloid cells such as type I AECs and endothelial cells (Huang et al., 2014; Tran et al., 2012). Most of these studies were conducted using real-time polymerase chain reaction (RT-PCR) (Huang et al., 2014; Sutterwala et al., 2006) or immunohistochemistry (Huang et al., 2014; Tran et al., 2012) that may not distinguish NLRP3 protein expression at the single-cell level.

The NLRP3 inflammasome is activated via a two-signal model. The first signal, provided by cytokine receptors such as TNFR and PRRs such as toll-like receptor (TLR) recognising cytokines and agonists

such as TNF-α and LPS respectively, increases *Nlrp3* mRNA and protein expression (Bauernfeind et al., 2009). NLRP3 is initially expressed in its inactive form with the PYD domain folding onto its own NBD domain(Hafner-Bratkovic et al., 2018; Martín-Sánchez et al., 2016). Signal 1 also upregulates substrates of the inflammasome complex such as pro-IL-1β and pro-IL-18 (Bauernfeind et al., 2009; Sutterwala et al., 2006), priming the response mechanism to induce inflammation. The second signal is provided by inflammasome activators such as nigericin, silica or ATP that stimulate various intracellular events such as potassium efflux. These cellular events induce post-translational modifications on NLRP3 (Song et al., 2017), unfolding NLRP3 to expose its NBD domain, enabling NLRP3 oligomerisation (Hafner-Bratkovic et al., 2018). The formation of an NLRP3 oligomer initiates the assembly and activation of the NLRP3 inflammasome.

NLRP3 inflammasome activation; however, is an area that needs to be further studied. Previous studies of the NLRP3 inflammasome have used reporter models of ectopically expressed ASC attached to a fluorescent protein such as Cerulean or mCitrine (Beilharz et al., 2016; McAuley et al., 2013; Pinar et al., 2017; Stutz et al., 2013; Tzeng et al., 2016). This enables detection of ASC speck formation representing inflammasome activation. These models have also been used to extrapolate the oligomerisation and 'speck' formation kinetics and structural viability of NLRP3 inflammasome complexes. These models; however, may not reflect NLRP3 inflammasome function under biological conditions and do not primarily focus on the NLRP3 inflammasome. These limitations are further compounded by a lack of *in vitro* and *in vivo* NLRP3 reporter models which would specifically focus on the NLRP3 inflammasome. Due to these limitations, the expression, mechanisms and kinetics of NLRP3 inflammasome activation and how they can be measured is unclear. To respond to these gaps, we have developed an NLRP3 reporter mouse. These mice have two fluorescent proteins: mCitrine and mCherry, attached to opposite ends of NLRP3 (the NLRP3-CHCI reporter) (Figure 4.1A). The NLRP3-CHCI reporter is placed under an endogenous promoter, meaning these mice can demonstrate basal (endogenous cellular/tissue) and induced expression (signal 1) and activation of NLRP3 under naïve and challenged conditions.

Discovering new aspects of NLRP3 inflammasomes using NLRP3-CHCI mice

The incorporation of dual fluorescent tags in the NLRP3-CHCI reporter (Figure 4.1) enables determination of the conformation of NLRP3 by measuring the energy transfer from mCitrine, the donor fluorophore, to mCherry, the acceptor (Figure 4.1B). This is assessed via a technique called fluorescence lifetime imaging microscopy (FLIM) – fluorescence resonance energy transfer (FRET). FLIM-FRET measures the mCitrine fluorescence lifetime which describes the time taken for emission energy from mCitrine to be quenched (reviewed in De Los Santos et al. (2015)). mCitrine fluorescence lifetime varies on the proximity of mCitrine to mCherry. When NLRP3 adopts a closed conformation, mCitrine and mCherry are proximal to one another. Some of the mCitrine emission energy excites the mCherry, reducing the mCitrine fluorescence lifetime. Conversely, when the inflammasome is activated, NLRP3 is unfolded. mCitrine and mCherry become more distant from one another, reducing energy transfer between the two fluorescent proteins. This increases the mCitrine fluorescence lifetime because the mCitrine emission energy is not used to excite the mCherry. Hence, the NLRP3-CHCI reporter, by measuring the mCitrine fluorescence lifetime, can be used to detect the conformation and activation state of NLRP3 in an endogenous system.

In this chapter, I hypothesised that novel aspects of NLRP3 inflammasome expression and activation can be discovered by using NLRP3-CHCI reporter mice. Having generated the mice, I initially tested the capacity of the reporter to express and activate the NLRP3 inflammasome. Following this, I then used the NLRP3-CHCI mice to investigate how NLRP3 is upregulated and activated.

4.2 Results

4.2.1 Establishing a homozygous NLRP3-CHCI colony

The *Nlrp3-Chci* reporter gene has two fluorescent proteins: mCitrine and mCherry, attached to a cDNA copy of human *Nlrp3* (Figure 4.1A). This gene was knocked into exons two to five of the mouse *Nlrp3* gene under its endogenous promoter (Figure 4.1A). The resultant NLRP3-CHCI colony (Figure 4.1B) was generated in a collaboration between Prof. Paul Hertzog and Dr. Alec Drew from the Hudson Institute of Medical Research and Dr. Arzu Ozturk and Prof. Geoff Hicks from the University of Manitoba. To verify that the NLRP3-CHCI colony is homozygous for the reporter gene, I analysed the genotype of NLRP3-CHCI pups. As shown in Figure 4.2, the NLRP3-CHCI pups (Figure 4.2, lanes 1-7) only had DNA corresponding to that of the homozygous NLRP3-CHCI control (Figure 4.2, lane 8), confirming the homozygosity of the *Nlrp3-Chci* gene within the colony. The maintenance of this homozygosity is confirmed from genotyping experiments of the first litter of each new NLRP3-CHCI breeding pair.

I next compared the development of NLRP3-CHCI and WT mice. Initially, I monitored NLRP3-CHCI mice from four to twelve weeks of age. Grossly, NLRP3-CHCI mice exhibited no overt phenotype and behaviour compared to WT mice and littered in Mendelian ratios at five to eight pups/litter (data not shown). NLRP3-CHCI mice also developed at the same rate as WT mice as shown by similar increases in weight from four to twelve weeks of age (Figure 4.3). To further examine murine development, I weighed organs from adult (twelve-week-old) WT and NLRP3-CHCI mice. As seen in Figure 4.4, organ weights such as the heart and spleen in NLRP3-CHCI mice were similar to WT mice (Figure 4.4A-H). Interestingly, NLRP3-CHCI kidneys were slightly underweight compared to their WT counterparts (Figure 4.4I), but this decrease in kidney weight did not appear to affect the overall health of the NLRP3-CHCI mice. Collectively, these results confirm the homozygosity and normal development of the NLRP3-CHCI murine colony.

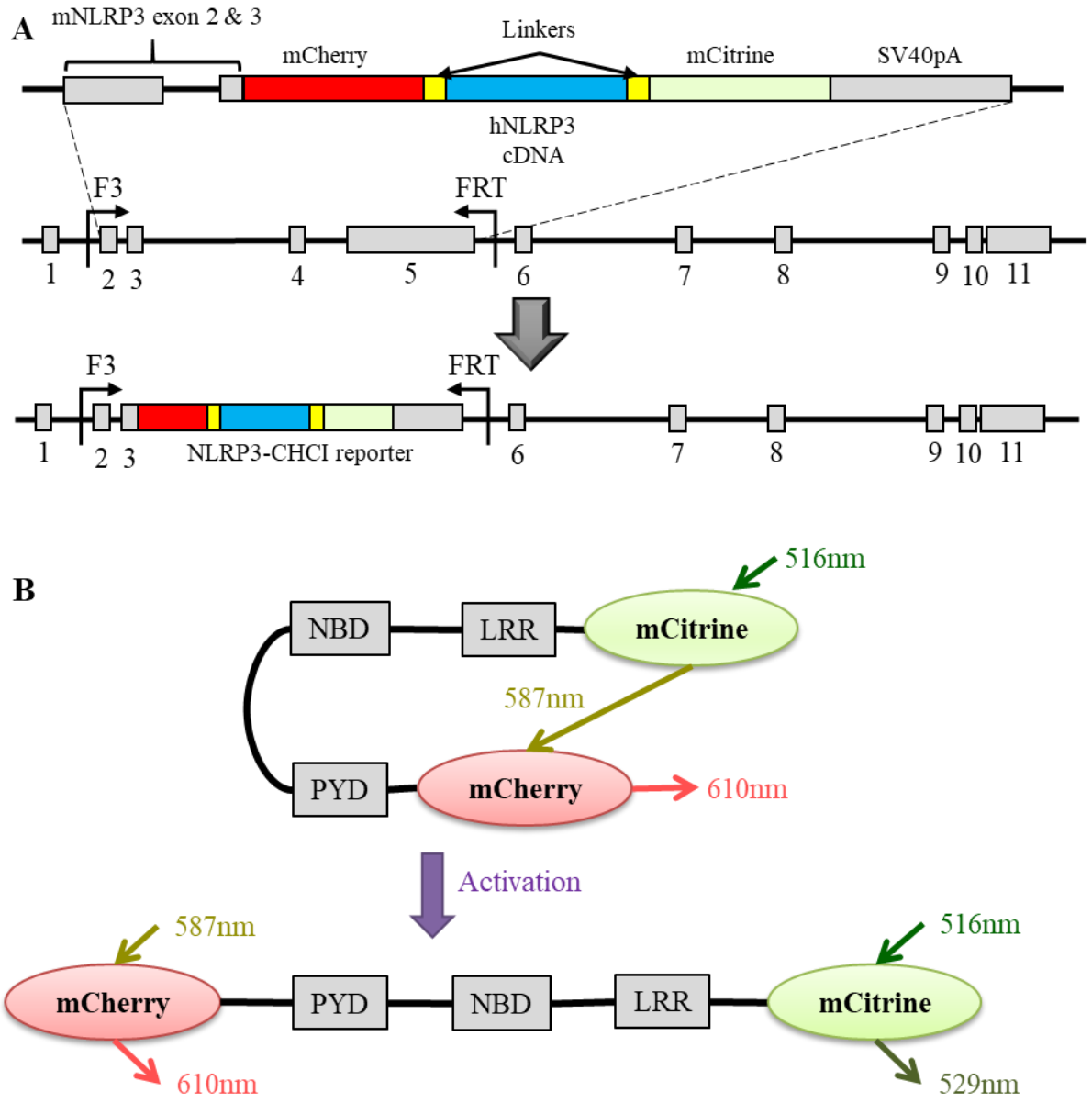

Figure 4.1: Schematic representation of the NLRP3-CHCI reporter gene vector and protein

(A) The Nlrp3-Chci reporter gene is knocked into exons two to five of the murine Nlrp3 gene residing between two recombination sites: FRT and F3. Numbers represent exon numbers of the murine Nlrp3 gene. (B) The NLRP3-CHCI reporter has two fluorescent proteins attached to opposite ends of NLRP3, allowing the NLRP3 conformation to be determined. Inactive NLRP3 is folded onto itself. This brings mCitrine and mCherry close together to enable energy transfer. Unfolding of NLRP3 during inflammasome activation; however, is associated with mCitrine becoming more distant from mCherry. This reduces energy transfer between the two fluorescent proteins. F3 = flippase 3 site, FRT = flippase recognition target, NBD = nucleotide-binding domain, LRR = leucine-rich repeats, PYD = pyrin domain.

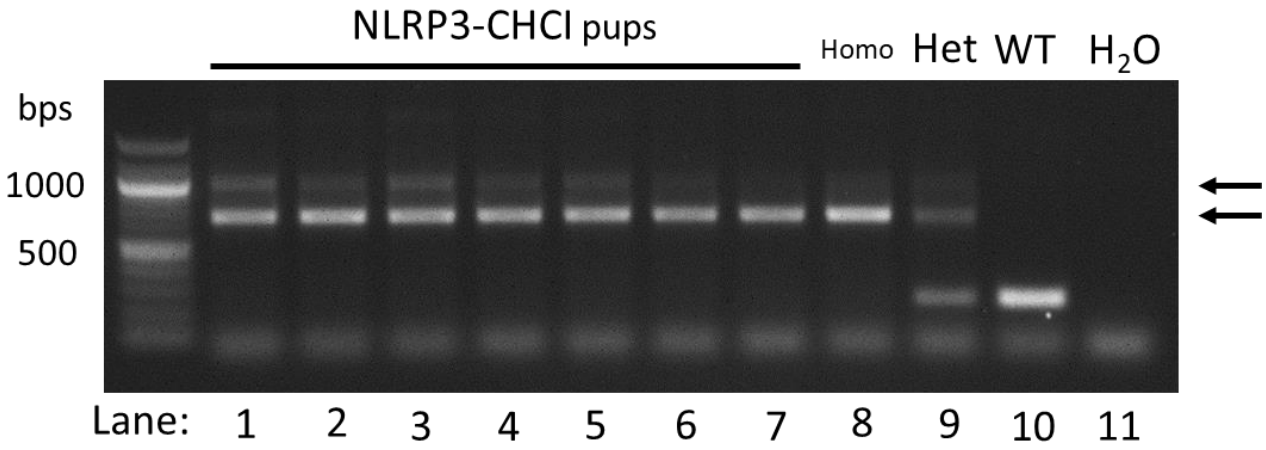

Figure 4.2: NLRP3-CHCI pups are homozygous for the *Nlrp3-Chci* reporter gene

Tails from pups were digested overnight. Proteins and SDS were precipitated by tail salts the next day and supernatant was collected after centrifugation. DNA was extracted via manifolding before its concentration and quality were measured by Nanodrop. 100ng of DNA from each sample and control was amplified via PCR and separated on agarose gel via electrophoresis. Bands were visualised via transillumination. Arrows indicate bands for the *Nlrp3-Chci* reporter gene. Results are representative of three independent experiments. bps = base pairs, Homo = homozygous NLRP3-CHCI control, Het = heterozygous NLRP3-CHCI control, WT = WT control and H_2O = water control.

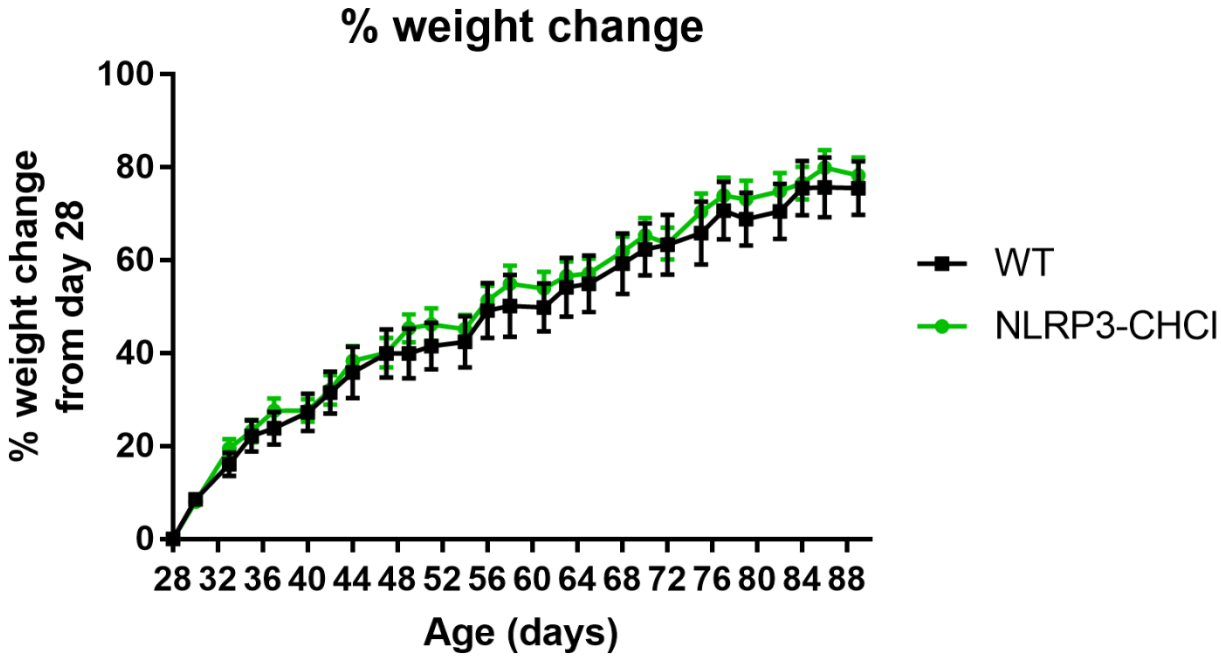

Figure 4.3: NLRP3-CHCI mice develop at the same rate as WT mice

Male WT and NLRP3-CHCI mice were weighed every 2-3 days from 4 to 12 weeks of age. For each mouse, percentage (%) weight change was calculated from the weight at 28 days of age. Data represented as mean ± SEM with N = 7 mice/group.

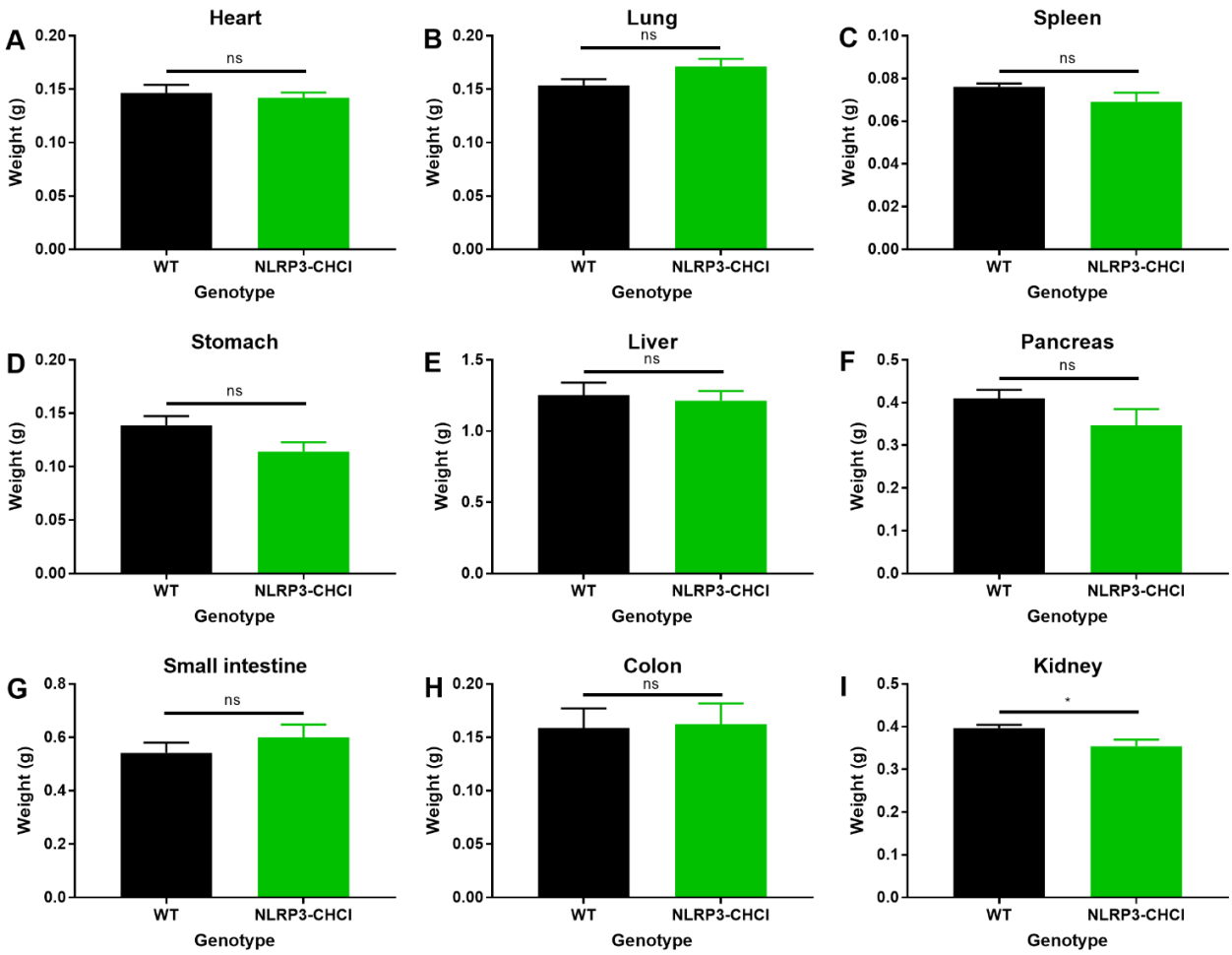

Figure 4.4: Organ weights in NLRP3-CHCI mice are similar to WT mice

Organs (A-I) were harvested from 12-week old male WT and NLRP3-CHCI mice and weighed. Data represented as mean ± SEM with N = 7 mice/group. Data analysed via unpaired t-test with significance represented as ns = not significant and *P<0.05.

4.2.2 NLRP3-CHCI cells express dual fluorescently-tagged proteins

To confirm that NLRP3-CHCI cells express dual fluorescently-tagged NLRP3, I initially examined NLRP3 and mCitrine via immunoblotting of NLRP3-CHCI pBMDM lysates. Anti-GFP antibody was used to detect mCitrine because GFP is a homologue of mCitrine (Ormo et al., 1996). As shown in Figure 4.5A, the molecular weight of NLRP3 in WT pBMDMs (lanes 1-3) is 118kDa. Immunoblotting NLRP3-CHCI pBMDM lysates (lanes 4-6) with anti-NLRP3 antibody identified a protein at approximately 174kDa. The molecular weight difference of 56kDa is equivalent to the sum of the molecular weights of mCitrine (28kDa) and mCherry (28kDa) (Duellman et al., 2015; Hink et al., 2000). The NLRP3 protein in LPS-primed NLRP3-CHCI pBMDMs (Figure 4.5A, lane 5, top panel) also corresponded to the GFP protein in the same lane (Figure 4.5A, lane 5, middle panel). To confirm mCitrine and mCherry fluorescence within NLRP3-CHCI pBMDMs, I conducted flow cytometry (Figure 4.5B) and confocal imaging (Figure 4.5C) of WT and NLRP3-CHCI pBMDMs. In both experiments, NLRP3-CHCI pBMDMs had higher mCitrine and mCherry fluorescence intensities compared to WT pBMDMs (Figure 4.5B-C). Collectively, these experiments show that NLRP3-CHCI cells are successfully expressing the dual fluorescently-tagged NLRP3.

4.2.3 NLRP3-CHCI cells are functionally active

The NLRP3-CHCI reporter has two fluorescent proteins attached to NLRP3 which may sterically impede NLRP3 oligomerisation, blocking NLRP3 inflammasome activation. To examine whether the presence of fluorescent proteins affects inflammasome activity, NLRP3-CHCI pBMDMs were treated with LPS for three hours and challenged with various NLRP3 inflammasome activators such as nigericin (Muñoz-Planillo et al., 2013), silica (Dostert et al., 2008) and ATP (Mariathasan et al., 2006) for six hours. Cells were also treated with LPS and poly(dA:dT) as a positive control that activates the AIM2 inflammasome (Hornung et al., 2009; Roberts et al., 2009). Cultured supernatants were assayed for IL-1β and tumour necrosis factor-α (TNF-α) via ELISA and cell death via LDH assay (Figure 4.6).

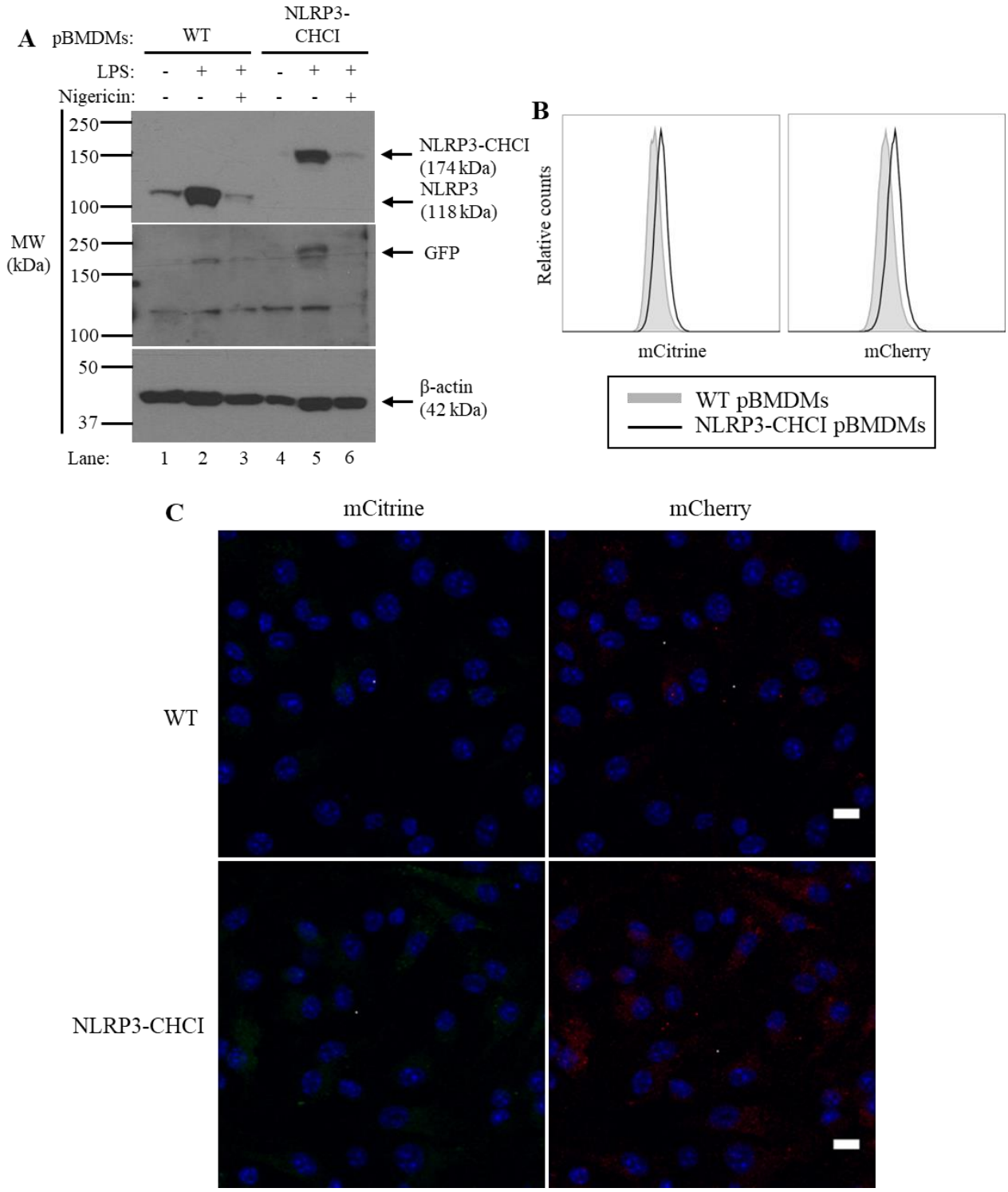

Figure 4.5: NLRP3-CHCI pBMDMs express a dual fluorescently-tagged protein

(A) WT and NLRP3-CHCI pBMDMs were seeded at 5 x 10^5 cells/well in triplicate in 12-well plates and left to settle for 24 hours. pBMDMs were then treated with LPS (100ng/mL) for 3 hours and/or nigericin (10µM) for six hours. Cells were lysed in 5X SDS buffer and boiled for 10 minutes. Lysate proteins were resolved on 4-12% bis-tris gel via SDS-PAGE, transferred onto PVDF membrane and immunoblotted with the indicated antibodies overnight (anti-mouse NLRP3 monoclonal antibody, rabbit anti-GFP polyclonal antibody or anti-mouse β-actin monoclonal antibody). All immunoblots were visualised via enhanced chemiluminescence with either the rabbit anti-mouse IgG-HRP or goat

anti-rabbit IgG-HRP polyclonal antibody. Immunoblot results are representative of three independent experiments. MW = molecular weight.

(B) WT and NLRP3-CHCI pBMDMs were seeded at 5 x 10^5 cells/well in triplicate in 12-well plates and left to settle overnight. pBMDMs were removed with 5mM EDTA and resuspended in 2% FCS in PBS. Cells were processed on the BD LSRFortessa to measure mCitrine and mCherry fluorescence intensities. Histograms are representative samples from a triplicate and replicated across three independent experiments.

(C) WT and NLRP3-CHCI pBMDMs were seeded at 4 x 10^4 cells/well in a 10-chamber slide overnight. The next day, cells were stained with Hoechst (blue) before they were fixed with 4% PFA at room temperature. Cells were washed with PBS, mounted in 1% sodium azide in PBS and imaged at 400x magnification (oil-based objective) on the Olympus FV1200 Laser Scanning Microscope. z-stacks of images were deconvoluted via maximum intensity projection in Fiji software. Scale bar is 10µm. Results are representative of three independent experiments.

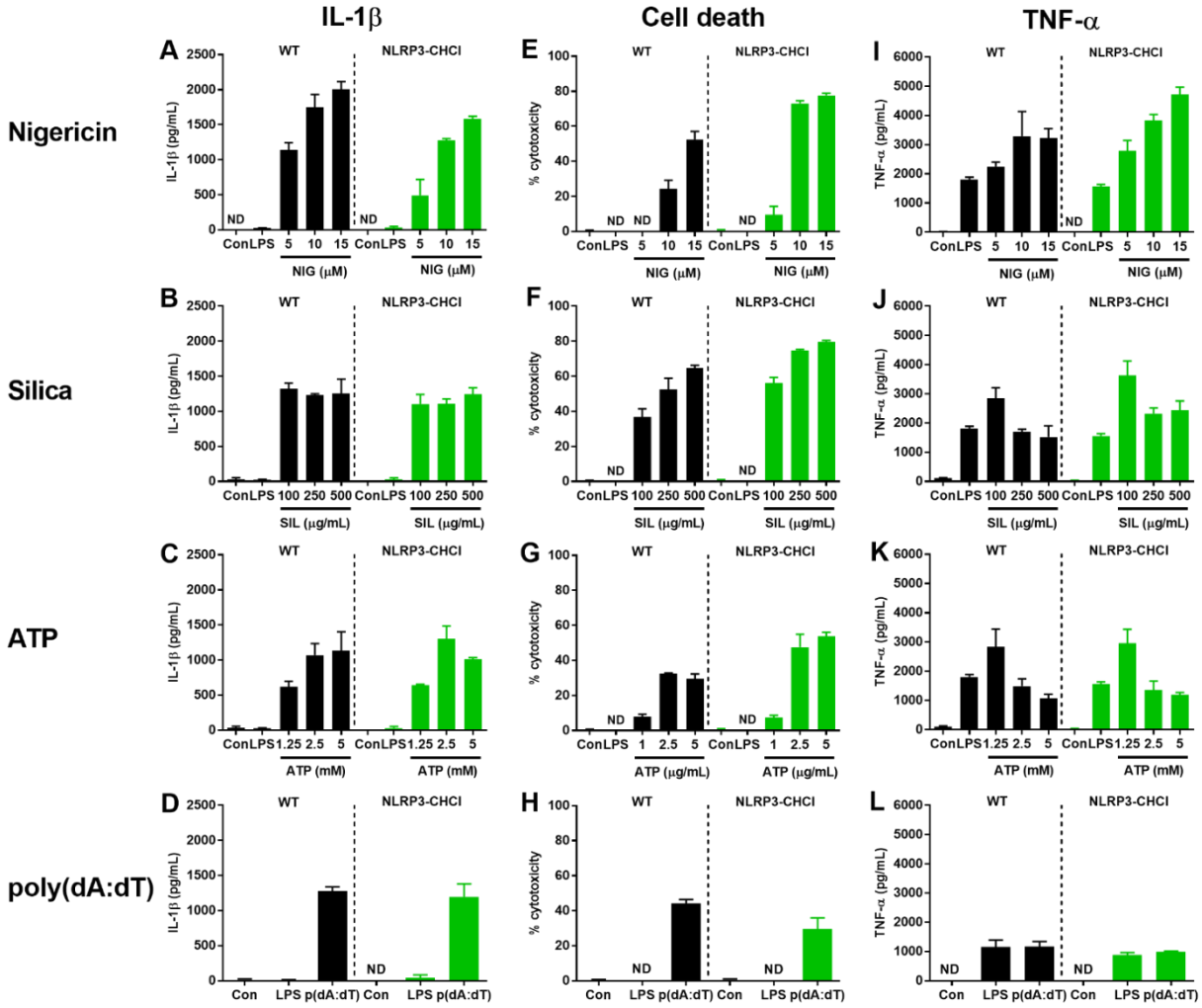

Figure 4.6: The fluorescently-tagged NLRP3 protein still enables IL-1β secretion and cell death in NLRP3-CHCI pBMDMs treated with LPS and inflammasome activators.

WT and NLRP3-CHCI pBMDMs were plated at 1 x 10^5 cells/well in 96-well plates 24 hours prior to the experiment. pBMDMs were treated with LPS (100ng/mL) for 3 hours and stimulated with nigericin (NIG), silica (SIL), ATP or poly(dA:dT) (p(dA:dT), 200ng) in triplicate at the indicated concentrations for 6 hours. Cell-free supernatants were harvested and IL-1β (A-D) and TNF-α (I-L) were assayed via ELISA following the manufacturer's instructions. Cell death (E-H) was measured via a non-radioactive LDH assay kit following the manufacturer's instructions and normalised to the untreated control (con). Data depicted as mean ± SEM and are representative of three independent experiments. Con = pBMDMs not treated with LPS and nigericin, silica, ATP or poly(dA:dT); LPS = pBMDMs treated with LPS only and ND = not detected.

Compared to WT pBMDMs, LPS-primed NLRP3-CHCI pBMDMs exhibited similar dose-dependent IL-1β secretory (Figure 4.6A-C) and cell death (Figure 4.6E-G) responses to nigericin, silica and ATP. WT and NLRP3-CHCI pBMDMs also exhibited comparable IL-1β secretion (Figure 4.6D) and cell death responses (Figure 4.6H) after LPS and poly(dA:dT) treatment, confirming the functionality of the AIM2 inflammasome in NLRP3-CHCI pBMDMs. LPS-treated NLRP3-CHCI pBMDMs secreted equivalent amounts of TNF-α as LPS-primed WT pBMDMs (Figure 4.6I-L) regardless of the inflammasome activator, signifying that the NLRP3-CHCI reporter does not impede NF-κB activation. Taken together, these findings show that the NLRP3-CHCI reporter does not affect inflammasome activation as measured by IL-1β secretion and cell death.

Besides IL-1β secretion and cell death, inflammasome activity is also associated with caspase-1 activation and IL-1β maturation. These can be assessed by immunoblotting for cleaved caspase-1 and IL-1β in supernatant samples respectively (Groß, 2012). Therefore, I assayed for caspase-1 and IL-1β maturation in supernatant and lysate samples from WT and NLRP3-CHCI pBMDMs. LPS treatment was associated with increased caspase-1 and IL-1β protein expression in lysate samples from WT and NLRP3-CHCI pBMDMs (Figure 4.7, caspase-1 p20 and IL-1β lysate panels, lanes 1-2 for WT and lanes 7-8 for NLRP3-CHCI), highlighting the conservation of inflammasome priming. LPS-treated NLRP3-CHCI pBMDMs additionally treated with nigericin, silica, ATP or poly(dA:dT) secreted comparable amounts of mature IL-1β and caspase-1 into the supernatant as WT pBMDMs (Figure 4.7, caspase-1 and IL-1β supernatant panels, lanes 9-12). These findings support my previous results (Figure 4.6) in that the NLRP3-CHCI protein does not impede NLRP3 inflammasome activation and function, validating the NLRP3-CHCI mice as a biologically representative model to study NLRP3 inflammasome expression and activation.

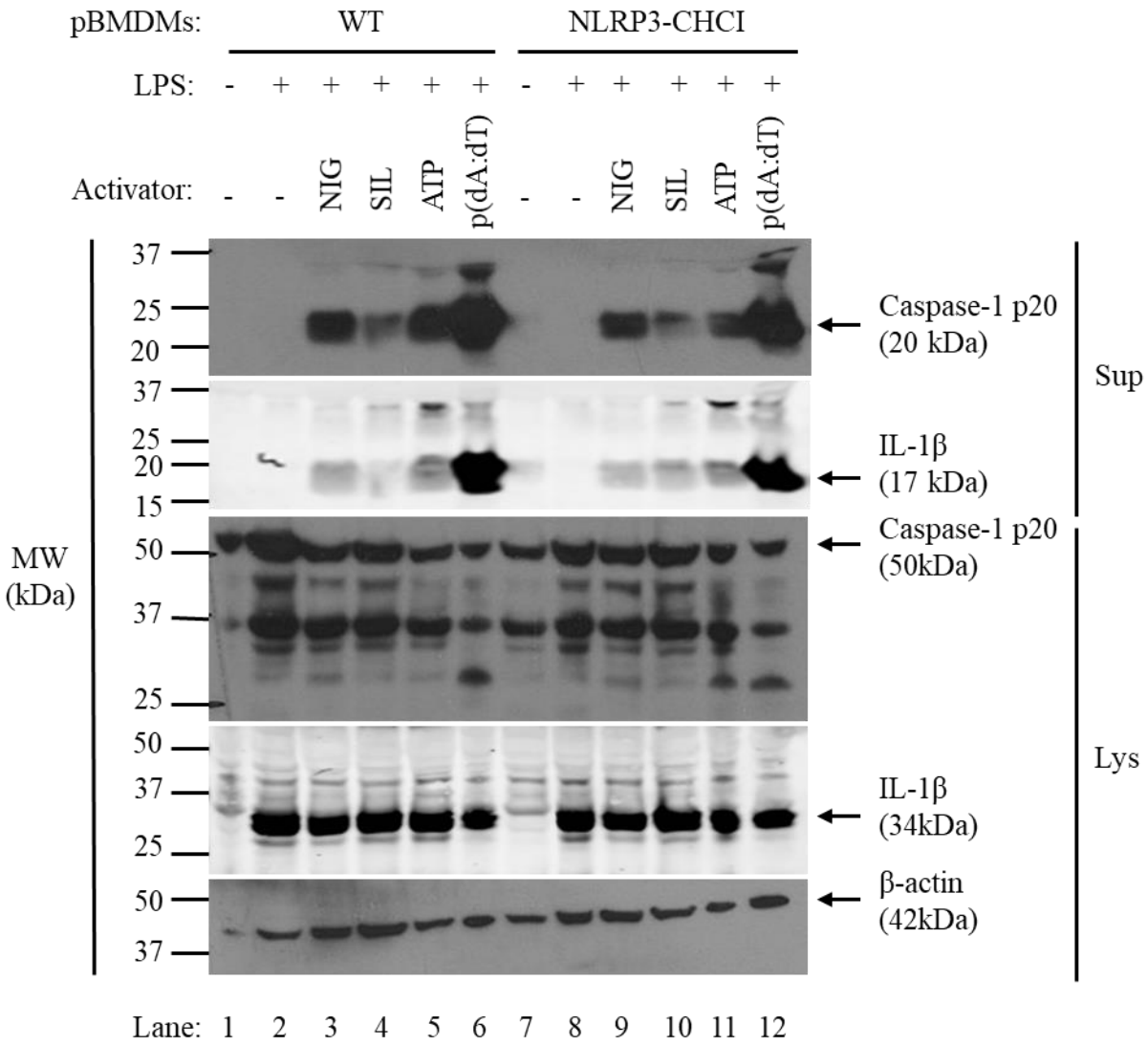

Figure 4.7: The fluorescently-tagged NLRP3 protein still enables caspase-1 and IL-1β maturation

WT and NLRP3-CHCI pBMDMs were seeded at 5 x 10^5 cells/well in 12-well plates and left to settle for 24 hours. pBMDMs were treated with LPS (100ng/mL) for 3 hours and/or stimulated with nigericin (NIG; 10µM), silica (SIL; 250µg/mL), ATP (5mM) or poly(dA:dT) (p(dA:dT), 500ng) for six hours. Supernatant samples (sup) were concentrated in Strataclean resin and resuspended in 5X SDS buffer. Lysate samples (lys) were prepared by lysing cells in 5X SDS buffer. Samples were boiled at 95°C for 10 minutes before proteins were resolved by SDS-PAGE, transferred onto PVDF membrane and immunoblotted independently with the indicated antibodies (anti-mouse caspase-1 monoclonal antibody, goat anti-mouse IL-1β-biotinylated antibody or anti-mouse β-actin monoclonal antibody). Caspase-1 and β-actin immunoblots were visualised via enhanced chemiluminescence with the rabbit anti-mouse IgG-HRP secondary antibody while the IL-1β immunoblot was observed via Odyssey using strep-Alexa Fluor 680. Immunoblot results are representative of three independent experiments. Arrows in each immunoblot indicate the band of interest. MW = molecular weight.

4.2.4 NLRP3-CHCI cells still exhibit inhibition of inflammasome activation

MCC950 is a small molecule inhibitor of the NLRP3 inflammasome that reduces measures of inflammasome activation such as IL-1β maturation and caspase-1 cleavage (Coll et al., 2015). I showed previously that the fluorescent tags in the NLRP3-CHCI reporter do not block inflammasome activation, but they may still sterically impede MCC950 from inhibiting inflammasome activity. To test this, I administered MCC950 to WT and NLRP3-CHCI pBMDMs prior to nigericin or silica treatments. MCC950 dose-dependently inhibited IL-1β secretion in NLRP3-CHCI pBMDMs treated with LPS and nigericin (Figure 4.8A) or silica (Figure 4.8B) commensurate to WT cells. MCC950 did not affect TNF-α secretion in WT and NLRP3-CHCI pBMDMs (Figure 4.8C-D) which confirm previous studies (Coll et al., 2015). MCC950 also reduced cell death in WT and NLRP3-CHCI pBMDMs treated with LPS and nigericin (Figure 4.8E) but not silica (Figure 4.8F). Overall, these experiments show that the fluorescently-tagged NLRP3 protein does not prevent MCC950 from inhibiting NLRP3 inflammasome-induced IL-1β secretion and cell death.

I further examined via immunoblots whether the NLRP3-CHCI reporter prevents MCC950 from suppressing caspase-1 and IL-1β maturation (Figure 4.9). NLRP3-CHCI pBMDMs secreted mature caspase-1 and IL-1β when treated with LPS and nigericin or silica (Figure 4.9, caspase-1 p20 and IL-1β supernatant panels, lanes 9 and 11). These responses were suppressed when NLRP3-CHCI pBMDMs were pre-treated with MCC950 before nigericin or silica stimulation (Figure 4.9, caspase-1 p20 and IL-1β supernatant panels, lanes 10 and 12), similar to WT pBMDMs (Figure 4.9, caspase-1 p20 and IL-1β supernatant panels, lanes 3-6).

Collectively, the fluorescently-tagged NLRP3 protein does not prevent MCC950 from targeting and inhibiting NLRP3 inflammasome activation. As such, the model can be used to screen and study potential inflammasome inhibitors.

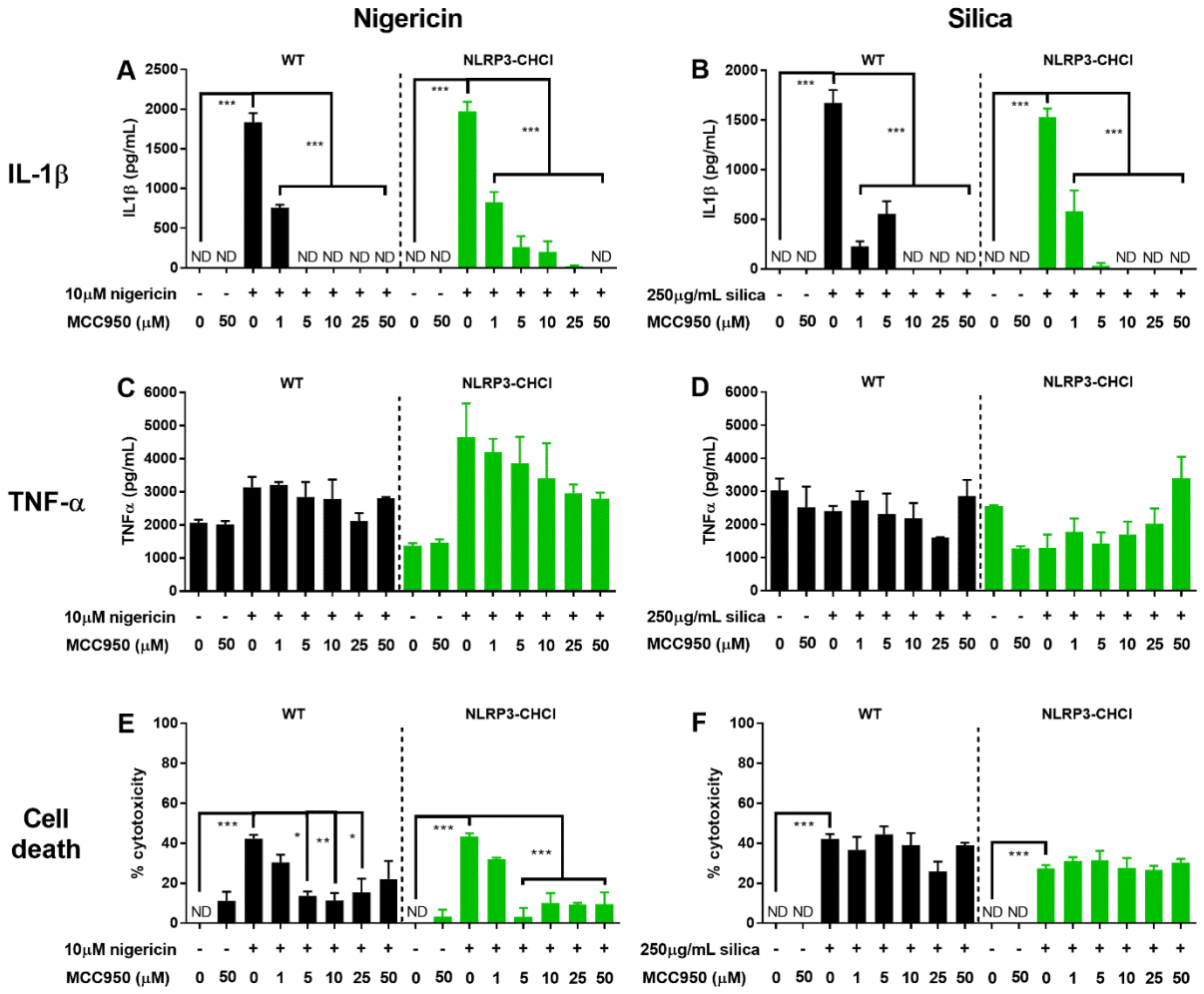

Figure 4.8: MCC950 can inhibit NLRP3 inflammasome activity in NLRP3-CHCI pBMDMs

WT and NLRP3-CHCI pBMDMs were plated at 1 x 10^5 cells/well in a 96 well-plate 24 hours before being primed with LPS (100ng/mL) for 3 hours. MCC950 was added to the wells at the indicated concentrations 30 minutes before pBMDMs were stimulated with nigericin (NIG; 10µM) or silica (SIL; 250µg/mL) in triplicate for 6 hours. Supernatants were harvested and assayed for IL-1β (A-B) and TNF-α (C-D) via ELISA. Cell death was measured using a non-radioactive LDH kit and normalised to the non-MCC950, non-nigericin/silica-stimulated control. Data were compared via one-ANOVA with Tukey's post-hoc test and significance represented as $^{*}p<0.05$, $^{**}p<0.01$ and $^{***}p<0.001$. ND = not detected. Results are representative of three independent experiments.

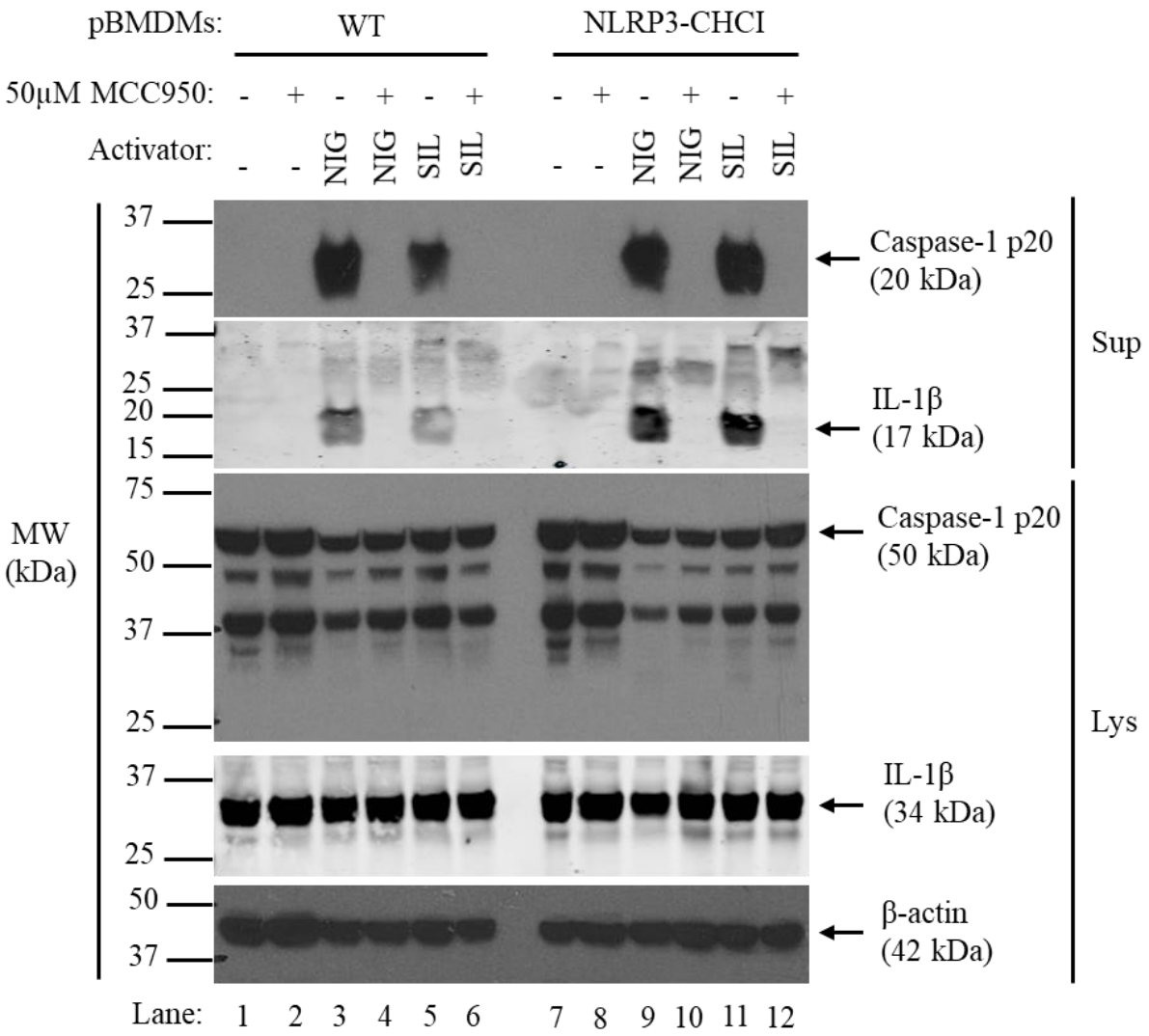

Figure 4.9: NLRP3-CHCI pBMDMs showed MCC950-induced inhibition of NLRP3 inflammasome activity similar to WT pBMDMs

WT and NLRP3-CHCI pBMDMs were plated at 5 x 105 cells/well in a 12-well plate 24 hours before being primed with LPS (100ng/mL) for 3 hours. MCC950 (50μM) was added to each well 30 minutes before pBMDMs were stimulated with nigericin (NIG; 10μM) or silica (SIL; 250μg/mL) in triplicate for 6 hours. Supernatant proteins (sup) were concentrated onto Strataclean resin and resuspended in 5X SDS buffer. Lysate samples (lys) were collected by lysing cells in 5X SDS buffer. Samples were boiled at 95°C for 10 minutes before proteins were resolved vis SDS-PAGE, transferred onto a PVDF membrane and immunoblotted independently overnight (anti-mouse caspase-1 monoclonal antibody, goat anti-mouse IL-1β-biotinylated antibody or anti-mouse β-actin monoclonal antibody). The caspase-1 and β-actin immunoblots were generated via enhanced chemiluminescence with the rabbit anti-mouse IgG-HRP secondary antibody while the IL-1β blots were visualised on Odyssey using strep-Alexa Fluor 680. Arrows indicate the band of interest for each immunoblot. Results are representative of three independent experiments. MW = molecular weight.

4.2.5 Visualising LPS-induced increases in NLRP3 protein expression

Previous experiments have successfully validated biochemical activation of the inflammasome in NLRP3-CHCI cells. Consequently, NLRP3-CHCI cells and mice can be used to discover novel aspects of NLRP3 expression and activation. Initially, I utilised NLRP3-CHCI pBMDMs to explore the effect of LPS on NLRP3 protein expression by measuring the changes in fluorescence intensity of mCitrine and mCherry.

Confocal imaging of untreated NLRP3-CHCI pBMDMs identified low expression of NLRP3 as indicated by detectable mCitrine and mCherry fluorescence within cells (Figure 4.10A, 0 minute row). LPS induced a rapid increase in NLRP3 expression from 60 minutes post-administration (Figure 4.10A, 60-270 minute rows). This was reflected in changes to the mCitrine and mCherry MFIs during LPS treatment (Figure 4.10B-C). Here, LPS significantly increased mCitrine (Figure 4.10B) and mCherry (Figure 4.10C) MFIs in a time-dependent manner. From baseline, these MFIs increased by around 1.5-fold after 270 minutes of LPS treatment.

To further support the confocal imaging findings, I processed WT and NLRP3-CHCI pBMDMs via flow cytometry to measure NLRP3 protein expression at the single-cell level. Similar to Figure 4.5B-C, mCitrine and mCherry fluorescence intensities are higher in untreated NLRP3-CHCI pBMDMs (Figure 4.11A-B, black lines) than WT pBMDMs (Figure 4.11A-B, shaded areas), implying basal expression of NLRP3 in resting pBMDMs. Furthermore, LPS (red lines) but not PBS (blue lines) treatment of NLRP3-CHCI pBMDMs augmented mCitrine and mCherry fluorescence intensities (Figure 4.11A-B), indicating increases in NLRP3 protein expression. The MFI measurements of the samples mirror the histograms. NLRP3-CHCI pBMDMs exhibited significantly higher mCitrine (Figure 4.11C) and mCherry (Figure 4.11D) MFIs compared to WT pBMDMs. Furthermore, LPS (solid lines) but not PBS (dashed lines) induced a time-dependent increase in mCitrine and mCherry MFIs of NLRP3-CHCI pBMDMs (Figure 4.11C-D). The flow cytometry experiments confirm the confocal imaging results in that LPS increases NLRP3 expression.

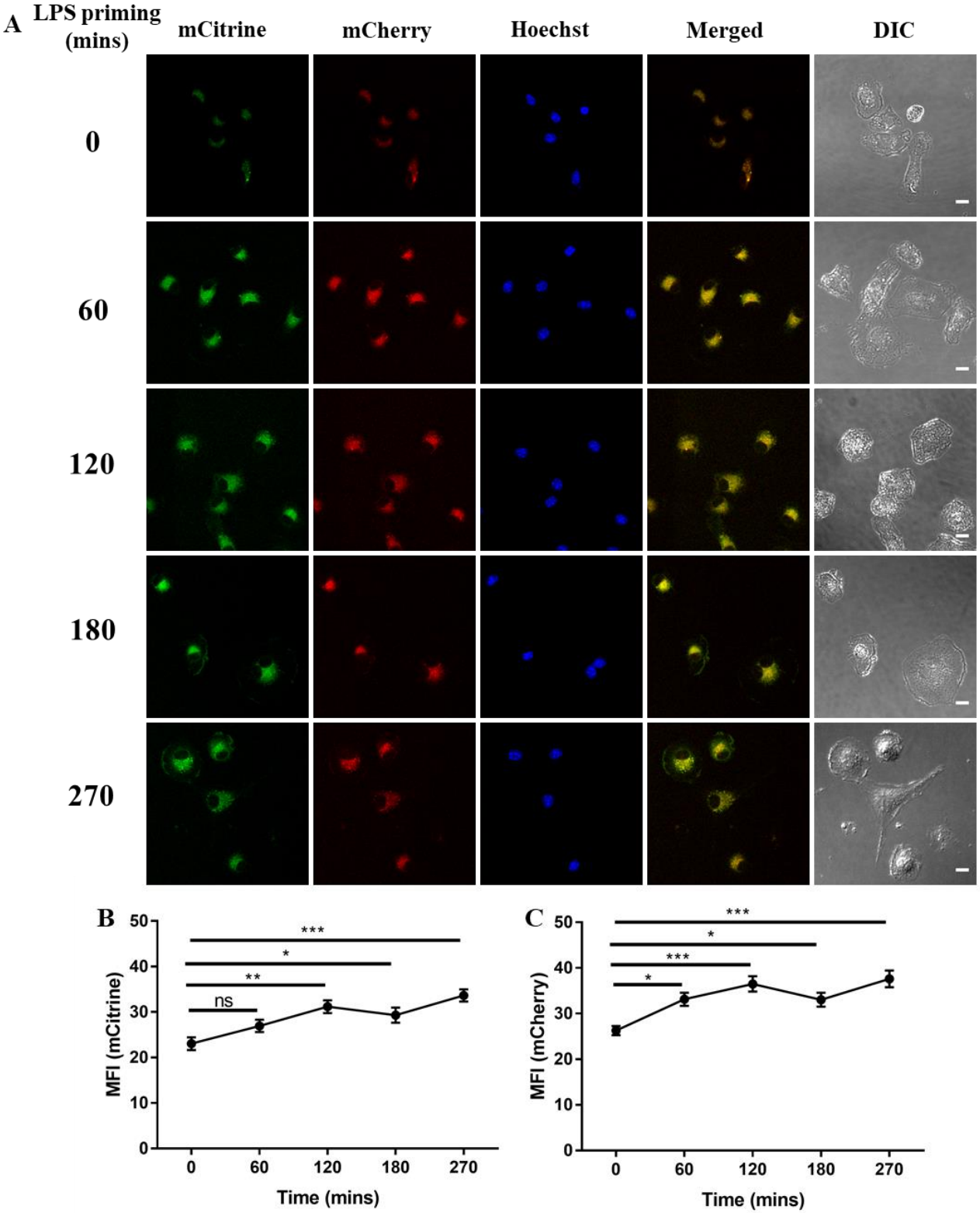
A
LPS priming (mins)
mCitrine
mCherry
Hoechst
Merged
DIC
0
60
120
180
270
B
MFI (mCitrine)
Time (mins)
ns
**
*
***
C
MFI (mCherry)
Time (mins)
*
***
*
***

Figure 4.10: LPS increases NLRP3 protein expression in NLRP3-CHCI pBMDMs as measured by mCitrine and mCherry fluorescence intensities

NLRP3-CHCI pBMDMs were seeded at 2 x 104 cells/well 24 hours before treatment with LPS (100ng/mL) for the indicated times. Cells were stained with Hoechst 15 minutes before they were fixed in 4% PFA for 15 minutes. Fluorescent and differential interference contrast (DIC) z-stack images were taken at 400x magnification (oil-based objective) on the Olympus FV1200 Laser Scanning Microscope. (A) Representative images were generated via deconvolution of z-stacks with maximum intensity projection in Fiji software. Scale bar is 10µm. Mean fluorescence intensities (MFIs) of mCitrine (B) and mCherry (C) were obtained by measuring the threshold of mCitrine and mCherry images in Fiji software. Data is represented by mean ± SEM with N = 9 fields/group. MFI of a fluorescent protein at an LPS priming time was compared to MFI at 0 minutes via one-way ANOVA with Tukey's post-hoc test and significance represented as ns = not significant, *P<0.05, **P<0.01 and ***P<0.001. Results are representative of three independent experiments.

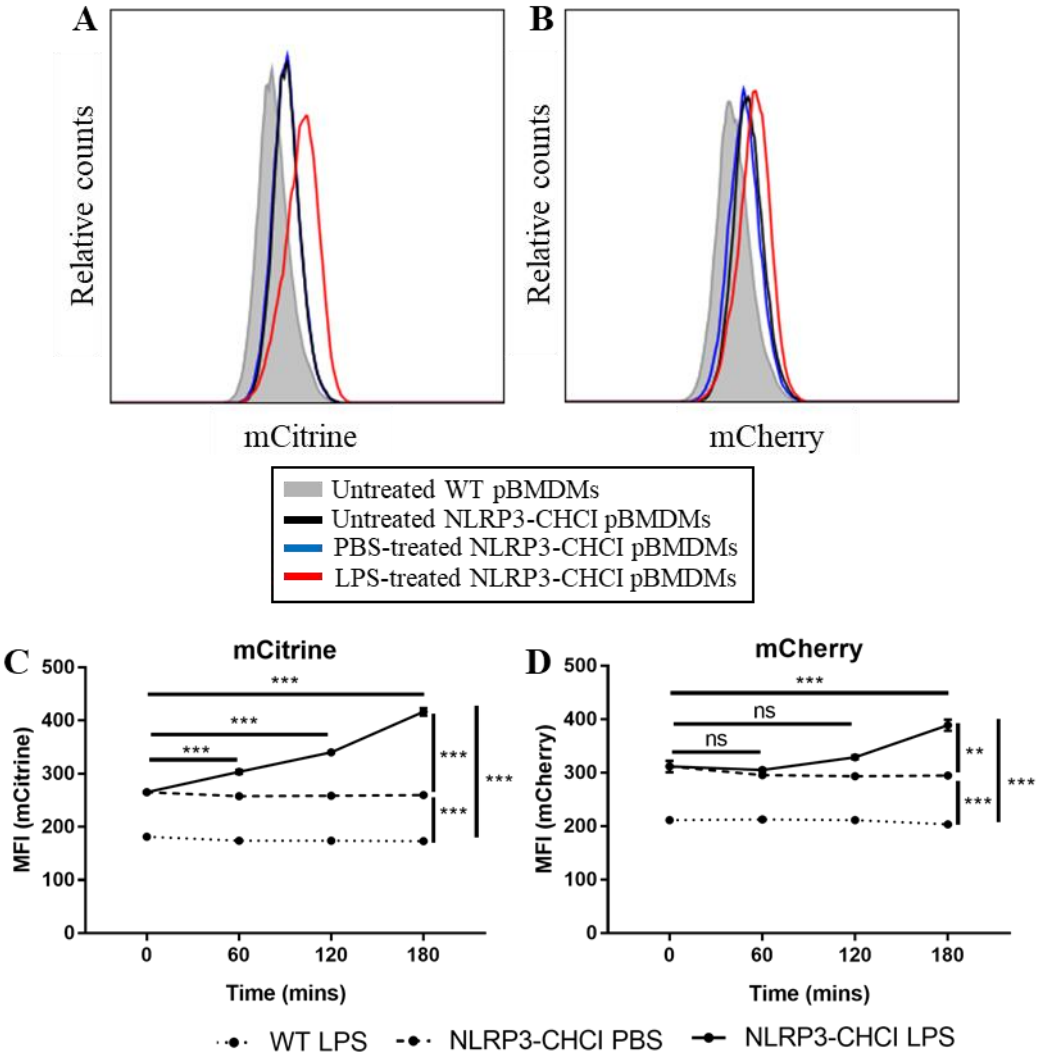

Figure 4.11: NLRP3 is upregulated during LPS treatment at the single-cell level

NLRP3-CHCI pBMDMs were seeded at 5 x 105 cells/well in 12-well plates 24 hours before being primed with LPS (100ng/mL) in triplicate for 60-180 minutes. pBMDMs were released from wells with 5mM EDTA (in PBS) and centrifuged to decant EDTA. pBMDMs were resuspended in 2% FCS and processed on the BD LSRFortessa. Representative mCitrine (A) and mCherry (B) histograms were shown from each group. From the histograms, mean fluorescence intensities (MFIs) of mCitrine (C) and mCherry (D) were measured. Data represented as mean ± SEM. Comparisons were made via one-way ANOVA with Tukey's post-hoc test with significance represented as *P<0.05, **P<0.01 and ***P<0.001. Results are representative of three independent experiments.

To note, LPS only induced a 30% increase in NLRP3 protein expression as measured by mCitrine (Figure 4.11C) and mCherry MFIs (Figure 4.11D) in NLRP3-CHCI pBMDMs. One possibility behind LPS inducing a small increase in NLRP3 protein expression might be that only a small proportion of pBMDMs have responded to LPS. To test this possibility, I gated for LPS-responsive NLRP3-CHCI pBMDMs in the mCitrine vs side scatter (SSC) dot plot based on their shift away from the non-LPS-responsive cell population as defined in the untreated control (Figure 4.12A). Based on this gating strategy, an LPS-responsive cell population emerged in LPS-treated but not PBS-treated NLRP3-CHCI pBMDMs (Figure 4.12B). Seen over a three-hour time course, there was a time-dependent increase in the percentage (Figure 4.12C) and number (Figure 4.12D) of LPS-responsive NLRP3-CHCI pBMDMs. Nevertheless, by the end of the three-hour period, only 20% of NLRP3-CHCI pBMDMs responded to LPS (Figure 4.12C). LPS-responsive cells had twice the NLRP3 protein expression as non-LPS-responsive cells as measured by mCitrine MFIs (Figure 4.12E)

Collectively, these findings indicate that NLRP3 is basally expressed in resting cells and that LPS upregulates NLRP3 protein expression in a small number of cells.

4.2.6 Investigation of NLRP3 speck formation as a measure of NLRP3 inflammasome activation

Having confirmed that LPS upregulates NLRP3, I next investigated how NLRP3 inflammasome activation can be detected in NLRP3-CHCI pBMDMs. It is known that all inflammasome components condense into a large oligomeric speck upon exposure to priming and activating signals (Beilharz et al., 2016; Stutz et al., 2013). Therefore, I initially reasoned that, similar to ASC, NLRP3 could form specks representing inflammasome activation. To test this hypothesis, I imaged LPS-treated cells stimulated with the activator nigericin (Figure 4.13) or the particulate activator silica (Figure 4.14). In response to both activators, NLRP3-CHCI pBMDMs exhibited distinct NLRP3 specks (Figure 4.13 and Figure 4.14, *NLRP3* column) that colocalised with ASC specks (Figure 4.13 and Figure 4.14, *merged* column). The size of the NLRP3 specks ranged from 1µm to 5µm.

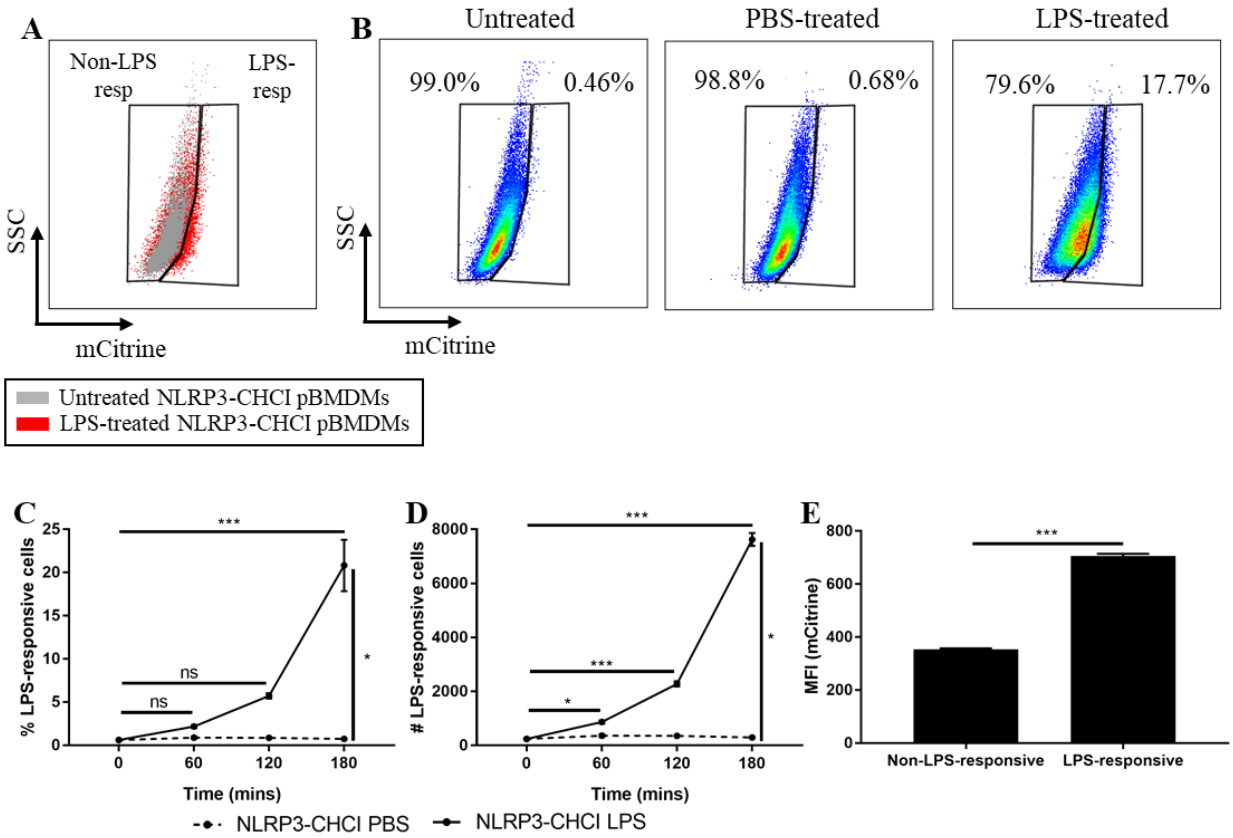

Figure 4.12: NLRP3 is upregulated in a small percentage of LPS-responsive NLRP3-CHCI pBMDMs

NLRP3-CHCI pBMDMs were seeded at 5 x 10^5 cells/well in 12-well plates 24 hours before being primed with LPS (100ng/mL) in triplicate for 60-180 minutes. pBMDMs were released from wells with 5mM EDTA (in PBS) and centrifuged to decant EDTA. pBMDMs were resuspended in 2% FCS and processed on the BD LSRFortessa. (A) LPS-responsive cells were gated based on their shift away from the non-LPS responsive cell population in untreated cells in the mCitrine vs side scatter (SSC) plot. (B) Representative dotplots of mCitrine vs SSC in untreated, PBS-treated and LPS-treated NLRP3-CHCI pBMDMs. (C, D) Graphs of the percentage (C) and counts (D) of LPS-responsive cells. Data represented as mean ± SEM. Comparison between PBS- and LPS-treated NLRP3-CHCI pBMDMs were made via unpaired t-test. Comparisons between zero minute and other timepoints within LPS-treated NLRP3-CHCI pBMDMs were made via one-way ANOVA with Tukey's post-hoc test. Significance represented as *P<0.05 and ***P<0.001. (E) mCitrine MFIs between non-LPS-responsive and LPS-responsive cell populations within LPS-treated NLRP3-CHCI pBMDMs were calculated. Groups were represented as mean ± SEM and compared via unpaired t-test with significance represented as ***P<0.001. Results are representative of three independent experiments.

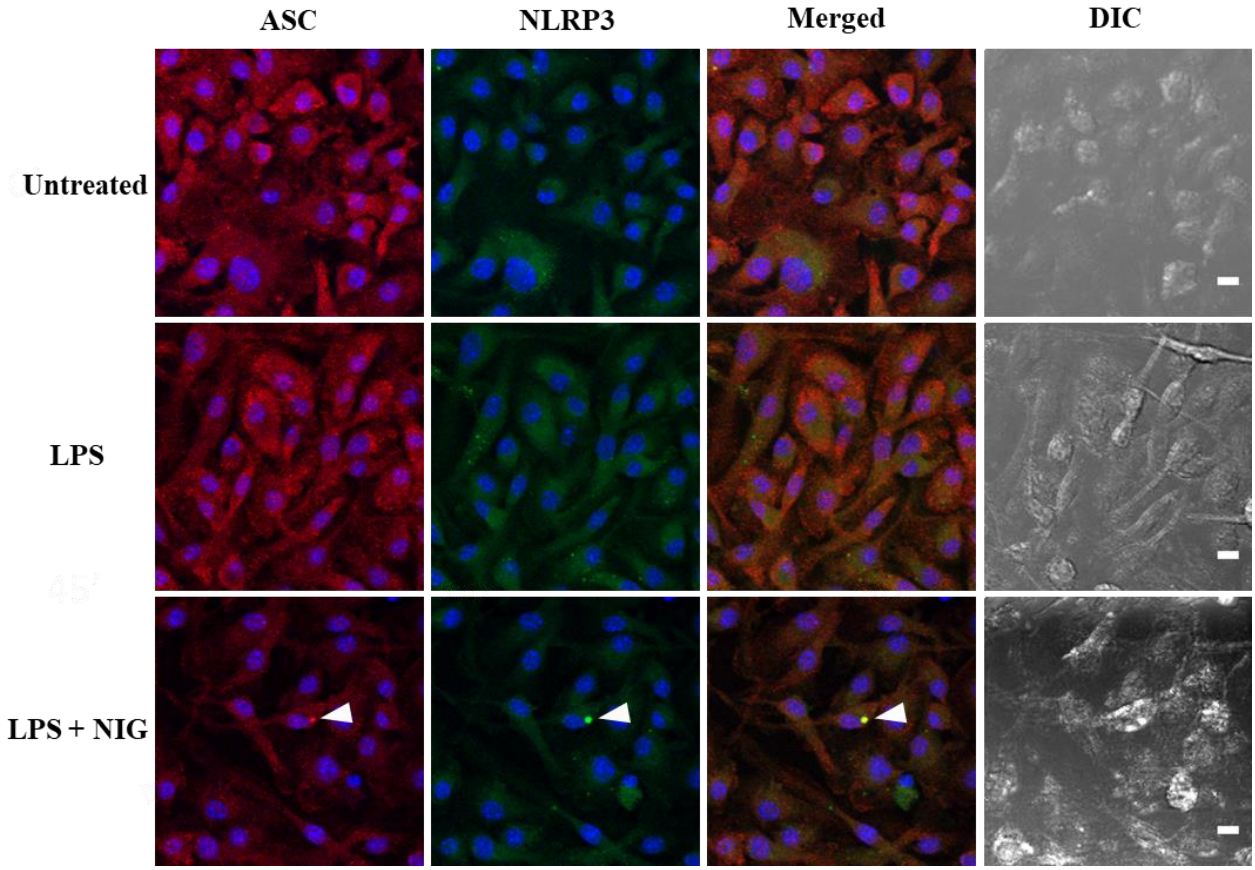

Figure 4.13: NLRP3-CHCI pBMDMs form NLRP3 specks that co-localise with ASC specks upon nigericin stimulation

NLRP3-CHCI pBMDMs were seeded at 4 x 104 cells/well 24 hours before being primed with 100ng/mL LPS for 3 hours. pBMDMs were then stimulated with 30µM nigericin (NIG) for 30 minutes. Cells were fixed in 4% PFA at room temperature for 15 minutes, permeabilised at room temperature for one hour and incubated with rabbit anti-ASC polyclonal antibody at 4°C overnight. The next day, cells were stained with Alexa Fluor 680 goat anti-rabbit IgG at room temperature for one hour and Hoechst at room temperature for 15 minutes before being mounted in PBS. z-stacks of fluorescent and differential interference contrast (DIC) images were taken at 400X magnification (oil-based objective) on the Olympus FV1200 Laser Scanning Microscope. Representative images were generated via deconvolution of z-stacks with maximum intensity projection on Fiji software. Scale bar is 10µm and arrows point to NLRP3 or ASC specks on images. Results are representative of a 3x3 field across three independent experiments.

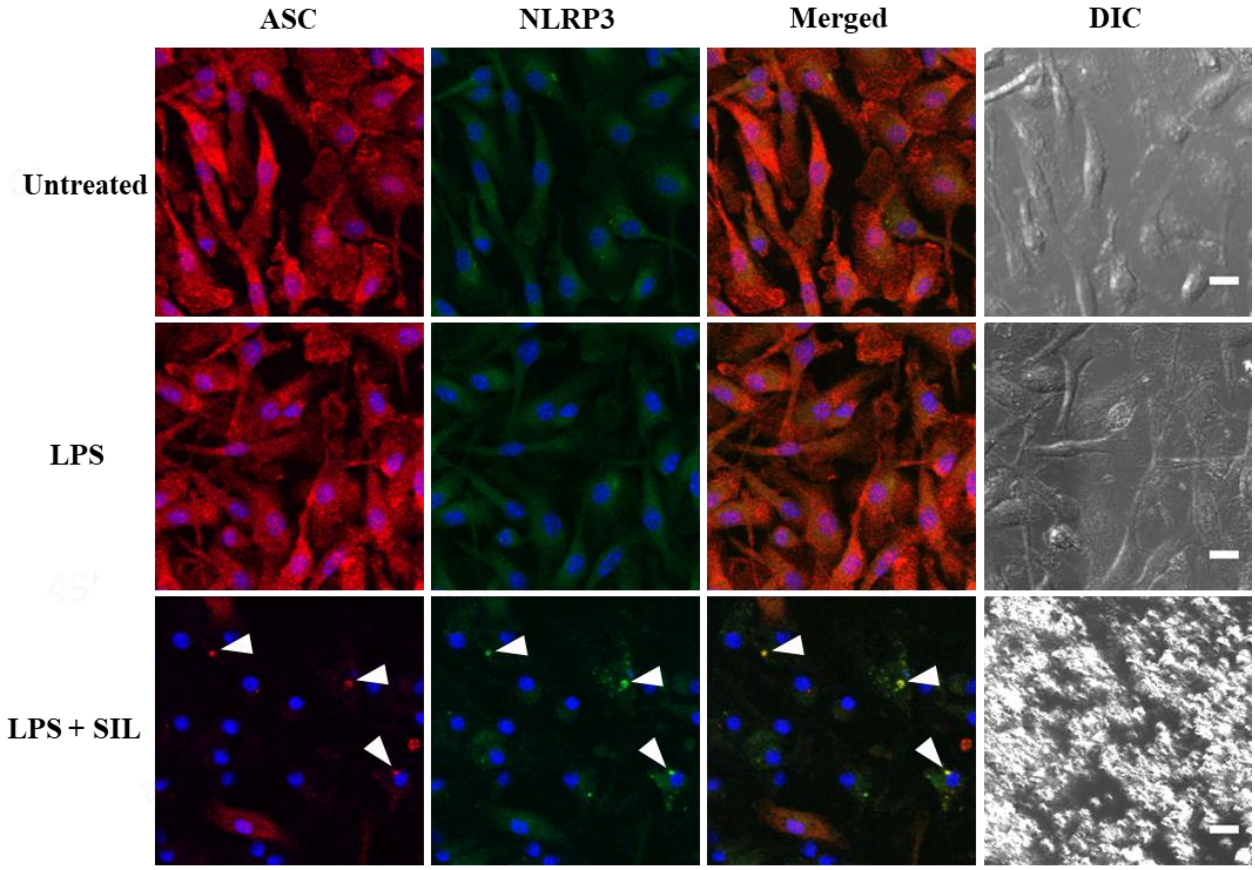

Figure 4.14: LPS-primed NLRP3-CHCI pBMDMs form specks upon silica stimulation

NLRP3-CHCI pBMDMs were seeded at 4 x 10^4 cells/well 24 hours before being primed with 100ng/mL LPS for 3 hours. pBMDMs were then stimulated with 150µg/mL silica (SIL) for 4 hours. Cells were fixed in 4% PFA at room temperature for 15 minutes, permeabilised at room temperature for one hour and incubated with rabbit anti-ASC polyclonal antibody at 4°C overnight. The next day, cells were stained with Alexa Fluor 680 goat anti-rabbit IgG at room temperature for one hour and Hoechst at room temperature for 15 minutes before being mounted in PBS. z-stacks of fluorescent and differential interference contrast (DIC) images were taken at 400X magnification (oil-based objective) on the Olympus FV1200 Laser Scanning Microscope. Representative images were generated via deconvolution of z-stacks with maximum intensity projection on Fiji software. Scale bar is 10µm and arrows point to NLRP3 or ASC specks on images. Results are representative of a 3x3 field across three independent experiments.

It should be noted; however, that only a small proportion of these cells exhibited NLRP3 specks during inflammasome activation (around 1.0-2.5% total cell population). Also, only a small proportion of NLRP3 and ASC is used to form these specks with most ASC and NLRP3 still dispersed within the cytosol (Figure 4.13 and Figure 4.14, *ASC* and *NLRP3* columns respectively). This implies that not all NLRP3 and ASC participate in the formation of an NLRP3 and ASC speck respectively.

Having identified NLRP3 specks in fixed cells, I next conducted live-cell imaging of NLRP3-CHCI pBMDMs to track NLRP3 speck formation. Cells that were treated with LPS and nigericin initially exhibited NLRP3 specks from zero minutes post-nigericin treatment (Figure 4.15, Video 4.1). However, throughout the 90-minute period I could not observe formation of new, distinct NLRP3 specks (Figure 4.15, Video 4.1). Treatment of LPS-primed NLRP3-CHCI pBMDMs with silica also did not lead to the formation of new NLRP3 specks (Figure 4.16, Video 4.2). To note, there was detectable signal noise from the mCherry reporter following silica stimulation due to the refractory nature of silica (Tan and Arndt, 2001). Nevertheless, these observations imply that it is hard to detect NLRP3 speck formation in live NLRP3-CHCI pBMDMs during inflammasome activation.

So far, although distinct NLRP3 specks can be identified in fixed NLRP3-CHCI pBMDMs, they are difficult to recognise in live NLRP3-CHCI pBMDMs, possibly due to their size-transient nature. To detect NLRP3 specks in a larger sample of NLRP3-CHCI pBMDMs, I utilised flow cytometry. WT and NLRP3-CHCI pBMDMs were treated with LPS and/or nigericin, counterstained with anti-ASC antibody and analysed for the presence of an NLRP3 and/or ASC speck positive population (Figure 4.17). I initially confirmed that ASC-Cerulean iBMDMs exhibited an ASC-speck positive cell population when treated with nigericin (0.39±0.10% in untreated cells vs 23.28±1.36% in nigericin-treated cells, $p < 0.001$) (Figure 4.17A), indicative of inflammasome-activated cells in these flow cytometry experiments. I hence applied the technique to identifying NLRP3 and/or ASC speck-positive populations in LPS-treated, nigericin-stimulated NLRP3-CHCI pBMDMs.

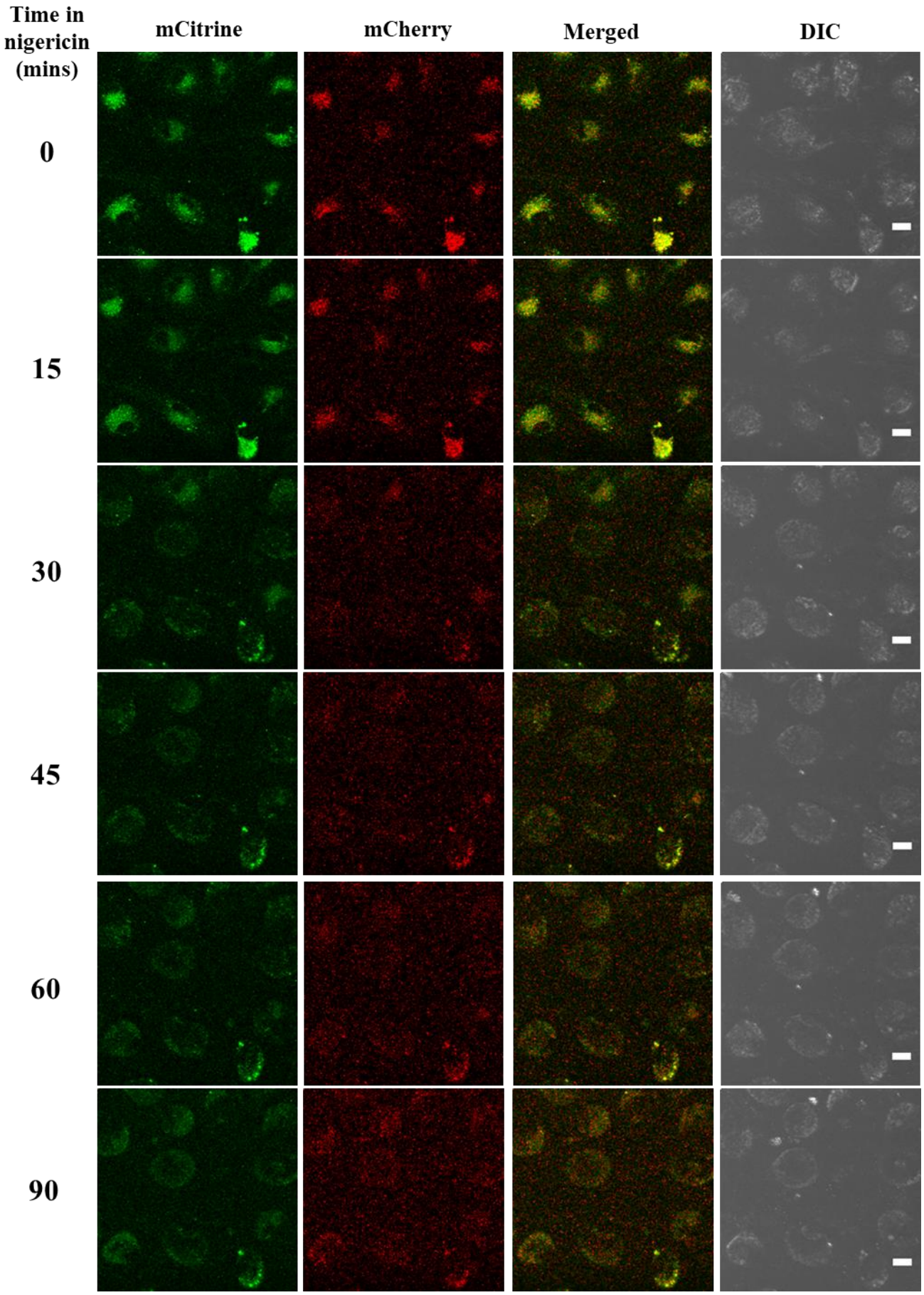
Time in nigericin (mins)
mCitrine
mCherry
Merged
DIC
0
15
30
45
60
90

Figure 4.15: Visualisation of NLRP3 specks in live nigericin-treated NLRP3-CHCI pBMDMs

NLRP3-CHCI pBMDMs were seeded in a Fluorodish at 2 x 10^4 cells 24 hours before the experiment. pBMDMs were primed with LPS (100ng/mL) for 3 hours and stimulated with nigericin (30µM) for 2 hours. Z-stack images were taken on the Olympus FV1200 Laser Scanning Microscope at 400X magnification (oil-based objective) every 5 minutes. Representative images from deconvoluted video of live cells were generated on Fiji with the scale bar being 10µm. Result is representative of a 3x3 field across three independent experiments.

Discovering new aspects of NLRP3 inflammasomes using NLRP3-CHCI mice

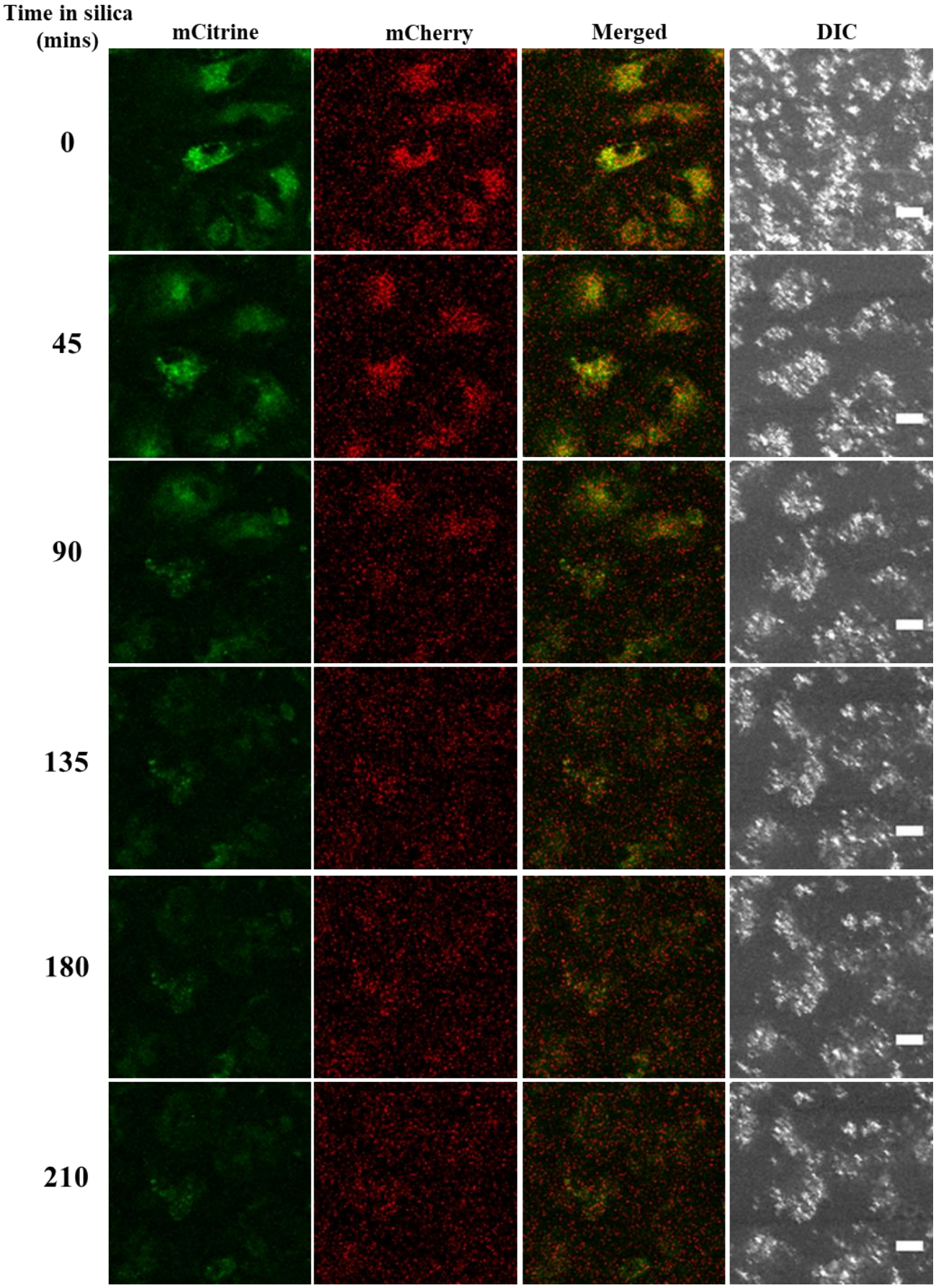

Figure 4.16: Tracking NLRP3 speck formation in NLRP3-CHCI pBMDMs treated with LPS and silica

NLRP3-CHCI pBMDMs were seeded in a Fluorodish at 4 x 10^4 cells 24 hours before the experiment. pBMDMs were primed with LPS (100ng/mL) for 3 hours and stimulated with silica (150µg/mL) for 4 hours. Z-stack images were taken on the Olympus FV1200 Laser Scanning Microscope at 400X magnification (oil-based objective) every 7.5 minutes. Representative images from deconvoluted video of live cells were generated via Fiji with scale bar being 10µm. Result is representative of a 3x3 field across three independent experiments.

Discovering new aspects of NLRP3 inflammasomes using NLRP3-CHCI mice

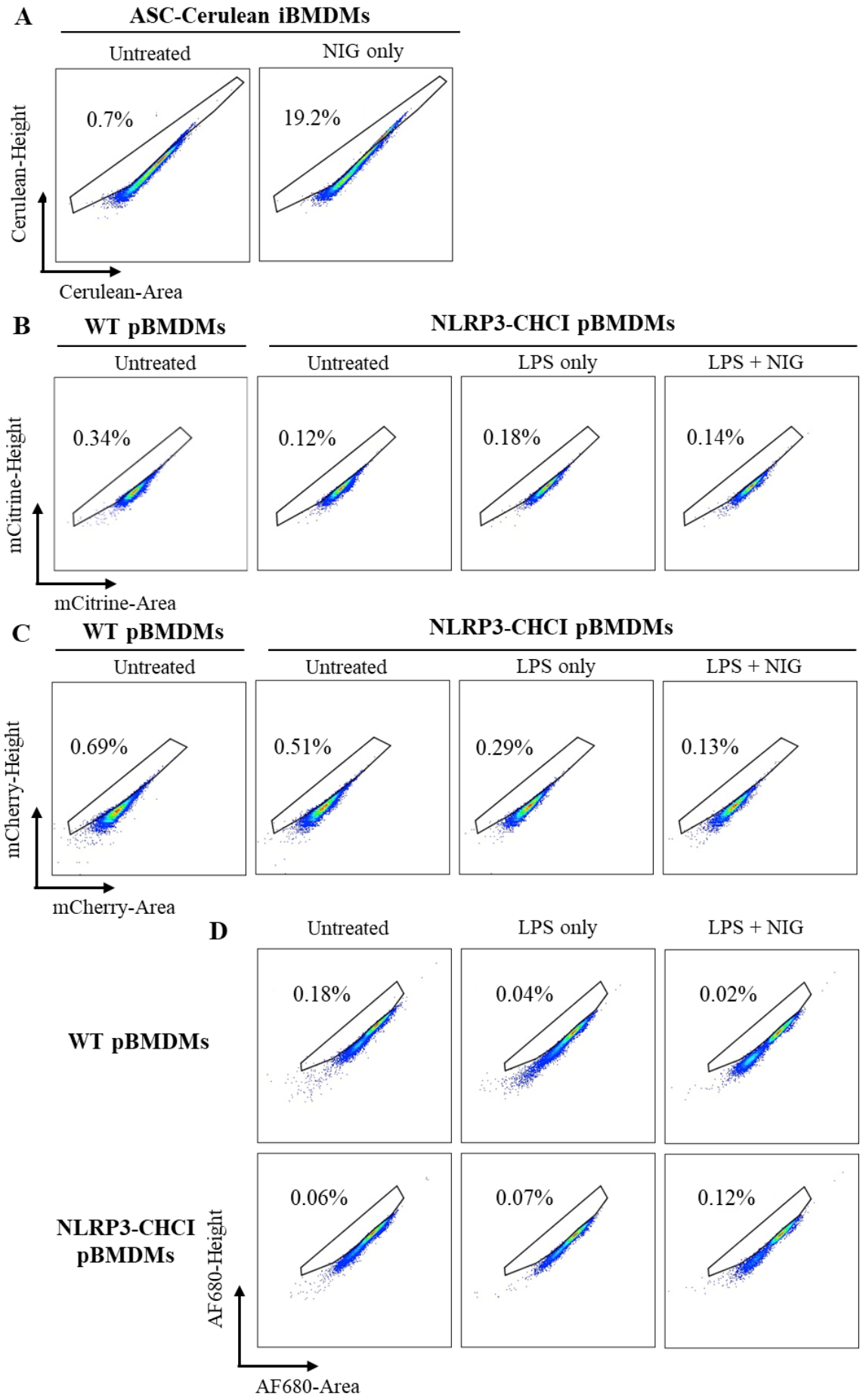

Figure 4.17: Detection of NLRP3 speck-positive and ASC speck-positive populations in NLRP3-CHCI pBMDMs via flow cytometry

WT and NLRP3-CHCI pBMDMs were seeded at 3 x 10^5 cells/well in 24-well plates 24 hours before being primed with LPS (100ng/mL) for 3 hours. pBMDMs were released from wells with 5mM EDTA (in PBS) and stimulated with nigericin (NIG, 30µM) for 30 minutes. Cells were fixed in 4% PFA for 5 minutes at 4°C before they were permeabilised and blocked. Cells were incubated with rabbit anti-ASC polyclonal antibody at 4°C overnight before being stained with Alexa Fluor 680 (AF680)-goat anti-rabbit IgG for one hour. pBMDMs were processed on the BDLSRFortessa and analysed via FlowJo, ASC-Cerulean iBMDMs (A) were also processed for the presence of an ASC speck-positive population. WT and NLRP3-CHCI pBMDMs were analysed for the presence of an NLRP3 speck-positive population in the mCitrine (B) and mCherry (C) channels as well as for an ASC speck-positive population in the Alexa Fluor 680 (AF680) channel (D). Numbers represent percentage of singlet cells that reside in the speck-positive gate. Results are representative of three independent experiments.

Compared to untreated and LPS-treated NLRP3-CHCI pBMDM controls, LPS and nigericin stimulation did not increase the size of the NLRP3 speck-positive population in either the mCitrine (0.16±0.02% in LPS-treated cells vs 0.11±0.02% in LPS and nigericin-treated cells, $p > 0.05$) (Figure 4.17B) or mCherry (0.28±0.02% in LPS-treated cells vs 0.12±0.01% in LPS and nigericin-treated cells, $p < 0.05$) (Figure 4.17C) channels. The ASC speck-positive population in NLRP3-CHCI pBMDMs also did not increase following LPS and nigericin treatment (0.08±0.02% in LPS-treated cells vs 0.29±0.15% in LPS and nigericin-treated cells, $p > 0.05$ (Figure 4.17D). In conjunction with my earlier observations, the NLRP3 specks may not be large enough to be a detectable and reliable measure of inflammasome activation.

4.2.7 NLRP3 inflammasome activation is associated with NLRP3 unfolding

I next examined an alternative method of detecting active NLRP3 inflammasomes. Priming signals induce NLRP3 expression which is initially auto-inhibited because the PYD domain is folded back onto its own NBD domain, impeding recruitment of ASC (Hafner-Bratkovic et al., 2018; Martín-Sánchez et al., 2016). Activating signals stimulate NLRP3 unfolding, leading to NLRP3 oligomerisation (Compan et al., 2012; Hafner-Bratkovic et al., 2018). With these principles, the NLRP3-CHCI reporter is designed to detect the conformation and hence activation state of NLRP3 depending on the proximity of mCitrine and mCherry. The proximity between these two fluorescent proteins is dependent on mCitrine fluorescence lifetime which is measured via FLIM-FRET. Increases in mCitrine fluorescence lifetime indicate that mCitrine is becoming more distant from mCherry, implying NLRP3 unfolding. Therefore, I used FLIM-FRET to track the conformation and hence activation status of NLRP3 in NLRP3-CHCI pBMDMs treated with LPS and nigericin.

mCitrine fluorescence lifetime can be denoted by a colour scale (Figure 4.18A). Blue and green colours indicate low mCitrine fluorescence lifetimes while yellow and red colours represent higher mCitrine fluorescence lifetimes. Using this colour scale, NLRP3-CHCI pBMDMs treated with LPS only displayed no change in mCitrine fluorescence lifetime (Figure 4.18A).

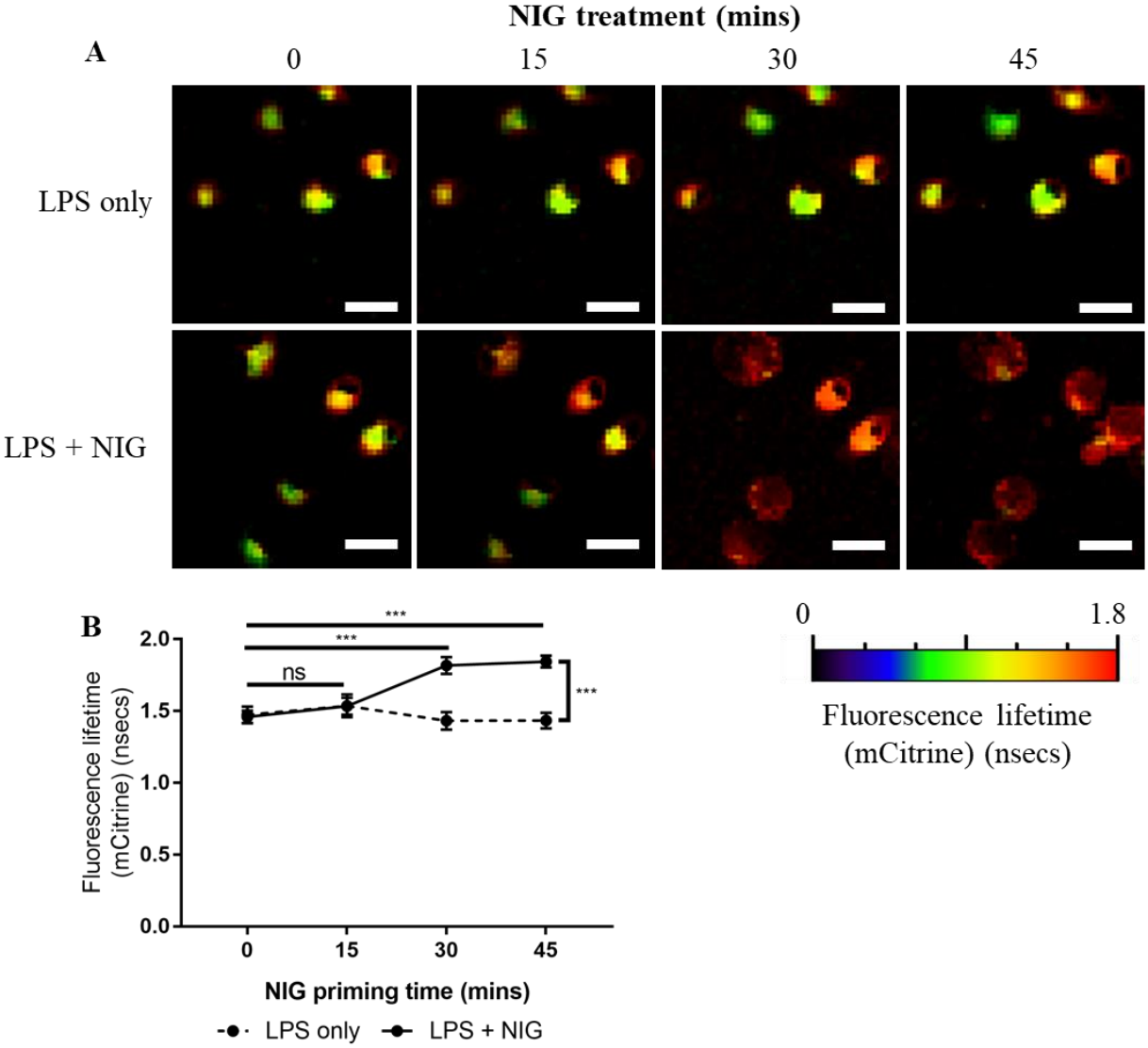

Figure 4.18: The NLRP3-CHCI reporter is unfolded upon LPS and nigericin treatment

NLRP3-CHCI pBMDMs were seeded at 4 x 10^4 cells/well 24 hours before they were primed with 100ng/mL LPS for 3 hours. pBMDMs were pre-treated with 5µM z-YVAD one hour before they were stimulated with 10µM nigericin (NIG) for 45 minutes. NLRP3-CHCI pBMDMs were visualised on the Olympus FV1000 Confocal Laser Scanning Microscope. (A) Representative images of mCitrine fluorescence lifetime within cells. (B) mCitrine fluorescence lifetime was measured on the Picoquant Picoharp300 FLIM system and analysed via SymPhoTime 64 software. Data represented as mean ± SEM with N = 9 cells/group. Data between LPS-treated and LPS + nigericin (NIG)-treated pBMDMs were compared by unpaired t-test. Data between zero minute and a specific timepoint within LPS + NIG-treated pBMDMs were compared via repeated-measures ANOVA with Tukey's post-hoc test. Significance represented as ns = not significant, $^{***}P<0.001$. Results are representative of three independent experiments.

Discovering new aspects of NLRP3 inflammasomes using NLRP3-CHCI mice

Importantly, NLRP3-CHCI pBMDMs treated with LPS and nigericin exhibited time-dependent increases in mCitrine fluorescence lifetime which occurred throughout the whole cell (Figure 4.18A). This can be represented graphically (Figure 4.18B). Here, mCitrine fluorescence lifetime remains stable in LPS-treated NLRP3-CHCI pBMDMs (Figure 4.18B, dashed line) but significantly increases when nigericin is added (Figure 4.18B, solid line).

Collectively, these findings suggest that NLRP3 changes conformation to an unfolded state upon treatment with an inflammasome activator, representing a valid measure of inflammasome activation. Furthermore, the unfolding of NLRP3 seems to occur throughout the whole cell instead of localised to one small area within the cell.

Having identified NLRP3 unfolding as a sign of inflammasome activation, I further tested whether MCC950 could inhibit inflammasome activation to prevent increases in mCitrine fluorescence lifetime. MCC950 was administered to NLRP3-CHCI pBMDMs one hour before nigericin was added. Interestingly, MCC950 did not affect nigericin-induced increases in mCitrine fluorescence lifetime in LPS-primed NLRP3-CHCI pBMDMs (Figure 4.19). This implies that despite MCC950 inhibiting NLRP3 inflammasome function (Figure 4.8), it was unable to prevent NLRP3 unfolding. This suggests that MCC950 may act proximal or downstream to NLRP3 unfolding.

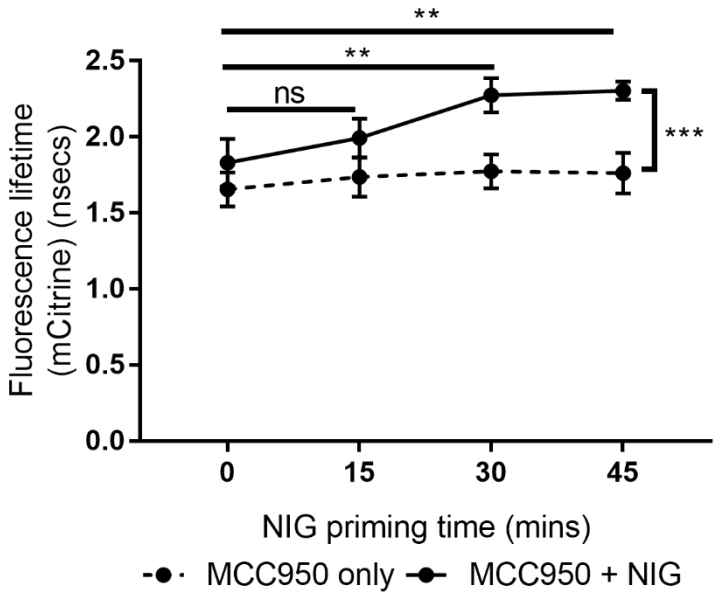

Figure 4.19: MCC950 does not inhibit increases in mCitrine fluorescence lifetime induced by nigericin

NLRP3-CHCI pBMDMs were seeded at 4 x 104 cells 24 hours before they were primed with 100ng/mL LPS for 3 hours. pBMDMs were pre-treated with 50µM MCC950 one hour before they were stimulated with 10µM nigericin (NIG) for 45 minutes. mCitrine fluorescence lifetime was measured on the Picoquant Picoharp300 FLIM system and analysed via SymPhoTime 64 software. Data represented as mean ± SEM with N = 9-10 cells/group. Data between MCC950 only and MCC950 + nigericin (NIG)-treated pBMDMs were compared by unpaired t-test. Data between zero minute and a specific timepoint within MCC950 + NIG-treated pBMDMs were compared via repeated-measures ANOVA with Tukey's post-hoc test. Significance represented as ns = not significant, **P<0.01 and ***P<0.001. Results are representative of three independent experiments.

4.3 Discussion

In chapter three, I found that results from experiments using mCherry-ASC cells were different from past studies that have used overexpressed ASC reporter models. These inferences not only challenge the current paradigm of how ASC functions during inflammasome activation but also highlight the limitations of existing overexpressed ASC reporter models and the utility of endogenously-expressed mCherry-ASC cells to study the inflammasome. In this chapter, I used NLRP3-CHCI reporter cells to study the NLRP3 inflammasome. To my knowledge, this is the first time that an NLRP3 reporter has been generated. These cells have the reporter placed under its native promoter to mirror how NLRP3 behaves in a biological context. The attachment of two fluorescent proteins: mCitrine and mCherry, on opposite ends of NLRP3 allows NLRP3 protein expression to be measured and NLRP3 conformation, which is linked to its activation state, to be determined.

I initially confirmed that NLRP3-CHCI pBMDMs exhibited commensurate inflammasome activation as WT pBMDMs when exposed to prototypic inflammasome activators such as nigericin, silica and ATP (Groß, 2012). NLRP3-CHCI pBMDMs could mature (Figure 4.7, lanes 9-12) and secrete (Figure 4.6A-D) IL-1β, activate caspase-1 (Figure 4.7, lanes 9-12) and exhibit cell death (Figure 4.6E-H) when exposed to LPS and an inflammasome activator. Furthermore, the specific NLRP3 inflammasome inhibitor MCC950 (Coll et al., 2015) could impede caspase-1 activation (Figure 4.9, lanes 10 and 12), IL-1β maturation (Figure 4.9, lanes 10 and 12) and cell death (Figure 4.8E) in NLRP3-CHCI pBMDMs similarly to WT pBMDMs. Collectively, these results imply that despite the attachment of two fluorescent proteins to NLRP3, NLRP3-CHCI cells can still exhibit inflammasome activity in the presence of inflammasome activators which can be blocked by inhibitors such as MCC950. These conclusions support the use of NLRP3-CHCI cells and mice to study NLRP3 expression and activation in health and disease.

NLRP3 is expressed in both myeloid-derived cell populations such as neutrophils and macrophages (Guarda et al., 2011; Sutterwala et al., 2006) as well as non-myeloid-derived cells such as endothelial

cells (Tran et al., 2012). In resting myeloid-derived cells, it has been reported that NLRP3 is lowly expressed, if at all (Bauernfeind et al., 2009; Song et al., 2016). Exposure to priming signals of inflammasome activation such as LPS and TNF-α (Bauernfeind et al., 2009; Franchi et al., 2009; Ichinohe et al., 2011); however, leads to NLRP3 mRNA and protein being upregulated. In the present study, I found that untreated NLRP3-CHCI pBMDMs express NLRP3 (Figure 4.10, and Figure 4.11A-B), implying that resting cells have a basal amount of NLRP3 protein. This is concordant with previous studies showing that a low level of NLRP3 is expressed in untreated pBMDMs and cDCs (Guarda et al., 2011; Sutterwala et al., 2006).

Furthermore, I confirmed that LPS induced a time-dependent increase in NLRP3 protein expression (Figure 4.11C-D). These results are consistent with previous biochemical studies that showed an upregulation of NLRP3 upon exposure to priming signals of inflammasome activation (Bauernfeind et al., 2009; Franchi et al., 2009; Ichinohe et al., 2011). To note, increases in NLRP3 protein expression varied in examining either mCitrine or mCherry fluorescence (Figure 4.11C-D) due to differences in their emission spectra. Compared to mCitrine, mCherry has a lower quantum yield with weaker fluorescence at its peak emission wavelength of 610nm (Griesbeck et al., 2001; Shaner et al., 2004). This is complicated by the use of a narrow bandwidth filter in the flow cytometer machine that only detects a small proportion of the mCherry fluorescence. Future studies could use a filter that optimally captures the mCherry emission spectrum from the peak emission wavelength of 610nm and beyond.

However, across the whole cell population, NLRP3 protein expression only increased by approximately 30% during LPS treatment (Figure 4.11C-D). Compared to previous studies that used LPS-treated pBMDMs, this is less than the 10-fold or more increase in *Nlrp3* mRNA expression (Bauernfeind et al., 2009; Zhao et al., 2017) but is comparable to the 10% increase in NLRP3 protein expression (Guarda et al., 2011). Given the transcription-translation process of expressing NLRP3 in

cells, it is likely that not all *Nlrp3* mRNA is translated to upregulate an equivalent amount of NLRP3 protein.

Investigating further, I discovered that only about 20% of NLRP3-CHCI pBMDMs responded to LPS by upregulating NLRP3 (Figure 4.12C). These findings mirrored those of Xue et al. (2015) which measured TNF-α secretion in human U937 monocytic cells as a readout of LPS responses. They identified that only 24% of the total cell population secreted TNF-α above the untreated background threshold after a four-hour LPS treatment period. The same study also found that about 5% of the total cell population released 60% of the TNF-α which induced or amplified the secretion of other cytokines such as IL-6 and IL-10 from other cells. These cells may also secrete other cytokines such as IL-1β that can control inflammation at the local level via paracrine signalling (Xue et al., 2015). TNF-α and IL-10 as pro- and anti-inflammatory cytokines respectively act as controllers in sentinel sensing, where varying the concentrations of these proteins coordinate cytokine secretion within a group of cells (Antonioli et al., 2018). The presence of a very small number of super-secretory cells enables inflammation to slowly spread depending on the strength of the priming signal, preventing excessive inflammation from being spontaneously induced towards an inappropriate stimulus such as an allergen (Shalek et al., 2014). With this idea in mind, in the NLRP3-CHCI mice, it might be sufficient to have a small number of LPS-responsive pBMDMs to promote strong overall inflammatory responses. These cells may initially release cytokines such as TNF-α that act on cytokine receptors in nearby cells to induce pro-inflammatory responses such as cytokine secretion. At the same time, given that inflammasome activation requires exposure to priming and activating signals (Bauernfeind et al., 2009; Franchi et al., 2009), an even smaller population of cells may secrete mature IL-1β because only LPS-responsive pBMDMs or a subset of them are primed to activate the inflammasome when exposed to activating signals. The idea of super-secretory LPS-responsive cells being present within a cell population may lead to the targeting of these cells to modulate inflammatory and immune responses. These cells could either be removed to treat inflammatory

diseases such as arthritis or augmented to overcome immunosuppressive environments produced by cancer.

These NLRP3 expression results in resting and LPS-treated pBMDMs may give insights into how the NLRP3 inflammasome is assembled. Initially, untreated cells express a small amount of NLRP3 that is insufficient to assemble the inflammasome. Priming signals upregulate NLRP3 to a level that is sufficient for NLRP3 oligomers to quickly form upon the addition of activating signals. This enables the inflammasome to be assembled and activated within minutes of exposure to soluble activators such as nigericin and ATP (Kahlenberg and Dubyak, 2004; Perregaux and Gabel, 1994). Hence, basal expression of NLRP3 in resting cells could reduce the threshold and time taken for inflammasome activation to occur.

It is widely reported and accepted that all NLRP3, ASC and caspase-1 in the cell condense into a large, oligomeric speck upon inflammasome activation (Beilharz et al., 2016; Stutz et al., 2013). This is the basis of ASC speck formation as an indicative measure of inflammasome activation. In contrast, I have failed to find NLRP3 specks in live LPS-primed NLRP3-CHCI pBMDMs during nigericin (

Figure 4.15) or silica (Figure 4.16) treatment. The live cell imaging experiments were confirmed by flow cytometry experiments, where NLRP3-CHCI pBMDMs treated with LPS and nigericin did not form an NLRP3 speck-positive population at the single-cell level (Figure 4.17B-C). Although these results disagree with the notion that all NLRP3, along with other inflammasome components, are condensed into one speck (Beilharz et al., 2016; Stutz et al., 2013), they are concordant with recent studies describing that only a small amount of cellular NLRP3 is required to form multiple puncta in the cell during inflammasome activation (Chen and Chen, 2018; Stutz et al., 2017). These NLRP3 puncta might contain NLRP3 oligomers that nucleate ASC, forming ASC complexes in different areas of the cell that recruit and activate caspase-1 (Boucher et al., 2018; Gambin et al., 2018). In addition, WT and NLRP3-CHCI pBMDMs did not form an ASC speck-positive population during inflammasome activation (Figure 4.17D), consistent with the flow cytometry results of nigericin-

stimulated mCherry-ASC pBMDMs from the previous chapter (Figure 3.17). This reinforces the notion that ASC forms a small, ASC-enriched area during inflammasome activation that cannot be detected by flow cytometry. Collectively, these results suggest that only a small amount of NLRP3 is required to initiate inflammasome assembly and activation upon exposure to activating signals. The response to activating signals is amplified by the enrichment of ASC in small areas that recruit caspase-1 to mature and secrete pro-inflammatory cytokines IL-1β and IL-18.

Interestingly, the observations of fixed NLRP3-CHCI pBMDMs contrasted those of live NLRP3-CHCI pBMDMs in that small NLRP3 specks were identified during treatment with LPS and nigericin (Figure 4.13) or silica (Figure 4.14). These images do show that not all cellular NLRP3 is used to form these specks, still conforming to past studies that describe the formation of multiple small puncta by a subset of cellular NLRP3 (Chen and Chen, 2018; Stutz et al., 2017). It should be noted; though, that the fixation of cells may introduce artefacts such as cellular debris that could be mistaken for NLRP3 specks (Nagar et al., 2019). This may explain why no NLRP3 specks were found in live NLRP3-CHCI pBMDMs when imaged. It should also be noted that silica produced increased signal-to-noise interference in the mCherry reporter due to the refractory nature of silica (Figure 4.16) (Tan and Arndt, 2001). Future studies could combine confocal fluorescence and reflection microscopy as used by Duewell et al. (2010) to remove signal noise from the refraction of crystalline compounds, allowing inflammasome activation from crystalline compounds to be more clearly observed.

Previous studies have shown that during inflammasome activation, NLRC4 unfolds, exposing the NBD domain. This leads to NLRC4 oligomerisation which initiates formation of the NLRC4 inflammasome (Halff et al., 2012; Hu et al., 2015). In the present study, I observed that NLRP3 also unfolds during inflammasome activation (Figure 4.18A-B) which is in agreement with previous studies (Hafner-Bratkovic et al., 2018; Martín-Sánchez et al., 2016). This process might be mediated by post-translational modifications on NLRP3 such as deubiquitination (Juliana et al., 2012; Py et al., 2013) and dephosphorylation (Stutz et al., 2017). As well as that, NLRP3 was unfolding throughout

the whole cell (Figure 4.18A). This is in contrast to previous studies which found that NLRP3 is localised to one area such as the microtubule-organising centre (Li et al., 2017) and the endoplasmic reticulum (Misawa et al., 2013) during inflammasome assembly. With the unfolding of NLRP3 throughout the whole cell, it would seem that NLRP3 can oligomerise and assemble the inflammasome in any area of the cell instead of within one small area. This opens the possibility of multiple small, discrete inflammasome complexes formed within the cell that can mature IL-1β, contributing to the IL-1β of the single cell. Interestingly, pre-treating pBMDMs with MCC950 did not prevent NLRP3 unfolding (Figure 4.19). Given that MCC950 still inhibited inflammasome activation in NLRP3-CHCI pBMDMs (Figure 4.8-Figure 4.9), this result implies that MCC950 may act proximally or downstream to NLRP3 unfolding such as NLRP3 oligomerisation or ASC recruitment.

These findings highlight the viability of NLRP3 unfolding as a readout of inflammasome activation which could be used to identify novel NLRP3 inflammasome activators. In addition, the NLRP3-CHCI reporter can be used track structural changes in NLRP3 during inflammasome activation. This could be used to introduce mutations associated with CAPS into the NLRP3-CHCI reporter. From there, the effects of these mutations on NLRP3 unfolding and hence NLRP3 inflammasome activity can be investigated. As well as that, NLRP3 unfolding could be a target for inhibiting NLRP3 inflammasome activity. Potential inflammasome inhibitors could be screened to elucidate the molecular mechanism behind their inhibition of inflammasome activity and whether they affect NLRP3 unfolding. Candidate molecules that specifically target NLRP3 unfolding could then be identified and rationally designed to exclusively inhibit the NLRP3 inflammasome. This is useful for treating diseases associated with the NLRP3 inflammasome such as influenza or gout without inhibiting other inflammasomes such as the NLRC4 inflammasome that are required for immune defence against pathogens.

In summary, I have shown that the NLRP3-CHCI reporter is a valid model to study the NLRP3 inflammasome. I initially confirmed that cells expressing the NLRP3-CHCI reporter could exhibit biochemical signs of NLRP3 inflammasome activation by inflammasome activators and its inhibition by MCC950. This highlights the capacity of using the NLRP3-CHCI reporter and its cells to study the biology of the NLRP3 inflammasome, particularly on NLRP3 expression and activation. Using NLRP3-CHCI pBMDMs, I found that NLRP3 is expressed in resting cells and that a small proportion of these cells could upregulate NLRP3 when treated with LPS. This has implications in terms of the proportion of cells that will exhibit inflammasome activation due to the need to be exposed to both signals of inflammasome activation. I also applied NLRP3-CHCI cells to identify a potential readout of NLRP3 inflammasome activation. Critically, I could not definitively identify the formation of discernible NLRP3 specks in flow cytometry. Nevertheless, inflammasome activation could be assessed by NLRP3 unfolding which could be measured by FLIM-FRET. The reporter can be used; therefore, to investigate NLRP3 unfolding during inflammasome activation and how mutations in NLRP3 might impact this process. The reporter also provides a readout in which to screen potential NLRP3 inflammasome activators and inhibitors. Furthermore, the reporter can be used to elucidate the molecular mechanisms of inhibitors blocking inflammasome activation, particularly on whether they impede NLRP3 unfolding. This may lead to the development of specific NLRP3 inflammasome inhibitors that prevent NLRP3 unfolding to treat disease.

The NLRP3-CHCI reporter cells are collected from NLRP3-CHCI reporter mice, where the reporter gene is integrated into the mouse's genome. This means that NLRP3-CHCI mice can also be used to conduct *in vivo* studies on the function and role of NLRP3 in health and disease. In the next chapter, I explain how the conclusions drawn from experiments with NLRP3-CHCI cells can be extended to an *in vivo* context.

5 Examining expression and activation of NLRP3 inflammasomes *in vivo*

5.1 Introduction

The NLRP3 inflammasome has both beneficial and detrimental roles in disease. The NLRP3 inflammasome contributes to protective immune responses against pathogenic bacteria such as *Staphylococcus aureus* (Mariathasan et al., 2006) and *Neisseria gonorrhoeae* (Duncan et al., 2009) as well as viruses such as IAV (Kanneganti et al., 2006b) and Dengue (Wu et al., 2013).

At the same time, the NLRP3 inflammasome is linked to a variety of inflammatory diseases such as CAPS, a group of autoinflammatory diseases (Aksentijevich et al., 2007). The presence of NLRP3 mutants in CAPS is associated with the upregulation of *Nlrp3* mRNA in leukocytes (Feldmann et al., 2002) and the continuous secretion of IL-1β from monocytes (Aksentijevich et al., 2002). This promotes a chronic inflammatory state that results in symptoms such as fever and skin rash (Feldmann et al., 2002; Hoffman et al., 2001). Later studies have linked the NLRP3 inflammasome to more common inflammatory diseases. These include arthritic diseases gout and pseudogout (Martinon et al., 2006), respiratory diseases silicosis and asbestosis (Cassel et al., 2008; Dostert et al., 2008) and neurodegenerative disease Alzheimer's disease (Halle et al., 2008; Heneka et al., 2013). The NLRP3 inflammasome also contributes to metabolic diseases. This is indicated by the heightened inflammasome activity in obese individuals (Esser et al., 2013) and enhanced mRNA expression of NLRP3 inflammasome components such as *Nlrp3* and *caspase-1* in type II diabetes (Lee et al., 2013) and atherosclerosis (Wang et al., 2014a) patients.

There are conflicting results on the role of the NLRP3 inflammasome in IAV infection due to the different IAV strains used. Initial studies with inflammasome-deficient mice established that the absence of a functional NLRP3 inflammasome increased the susceptibility of mice to lethal PR8 infection due to reduced pulmonary inflammation which promoted primary viral pneumonia and lung injury (Allen et al., 2009; Ichinohe et al., 2009; Thomas et al., 2009). Later studies with other IAV strains such as A/Shanghai/4664T/2013 (H7N9); however, found that inflammasome-deficient mice were less susceptible to infection due to the NLRP3 inflammasome contributing to hyper-

inflammatory responses against IAV that may lead to lung injury (Coates et al., 2018; Ren et al., 2017; Robinson et al., 2018). In summary, the NLRP3 inflammasome may have protective or pathological roles under varying conditions of IAV infection.

Our laboratory had identified a dual role of the NLRP3 inflammasome in IAV infection using the small molecule inhibitor MCC950 (Tate et al., 2016). Intranasal administration of MCC950 allowed inhibition of the NLRP3 inflammasome at any stage of IAV infection, different from inflammasome-deficient mice where inflammasome activity is constitutively absent. We discovered that the timepoint at which MCC950 is intranasally administered to mice influences the outcome of IAV infection. Administering MCC950 from one day post-HKx31 or PR8 infection rendered the mice hyper-susceptible to IAV infection consistent with inflammasome-deficient studies (Allen et al., 2009; Ichinohe et al., 2009; Thomas et al., 2009), indicative of the NLRP3 inflammasome having a protective role in the early stages of IAV infection. Crucially, administering MCC950 from three days post-HKx31 infection prolonged survival by suppressing pulmonary hyper-inflammation at the height of infection, implying that the NLRP3 inflammasome may promote pathology in the later stages of IAV infection. This study highlights that the NLRP3 inflammasome may adopt a protective or pathological role depending on the stage of IAV infection.

Due to the association of the NLRP3 inflammasome with a broad range of infectious and inflammatory diseases, the protein complex has been identified as a potential therapeutic target. Small molecule inhibitors of the NLRP3 inflammasome are currently being developed to impede inflammatory activity that will treat disease (reviewed in Yang et al. (2019)). Given the ubiquity of NLRP3 expression in not only leukocytes such as macrophages and DCs (Guarda et al., 2011; Sutterwala et al., 2006) but also in non-myeloid-derived cells such as type I AECs and splenic endothelial cells (Kummer et al., 2007; Tran et al., 2012), it is important to measure NLRP3 expression in homeostasis and pathology to identify cell populations that have an NLRP3 inflammasome-dependent role in disease. Cell-specific inflammasome inhibitors could then be

developed to potentially redirect inflammasome activity towards a protective response against infection or disease.

Individual cell populations such as macrophages (Ichinohe et al., 2009) and epithelial cells (Pothlichet et al., 2013) have been shown to exhibit NLRP3 inflammasome activity during IAV infection. However, these cells have only been studied in isolation to each other and not in a whole lung context. This study characterises the *in vivo* properties and practicalities of observing NLRP3 expression during infection. I initially validated the functionality of the reporter mouse in an *in vivo* model using the intranasal nigericin model. I then conducted a pilot study on the intranasal LPS model to identify cells in the lung that responded to LPS. I further hypothesised that specific cell populations in the lung may adopt a dual role of the NLRP3 inflammasome in inducing protection or pathology against IAV infection. I am examining this hypothesis using NLRP3-CHCI mice, tracking changes in NLRP3 expression before and after infection.

5.2 Results

5.2.1 Intranasal nigericin model of NLRP3-CHCI mice

In chapter four, I utilised cells from NLRP3-CHCI mice to examine the expression and activation of NLRP3 *in vitro*. In this chapter, I used NLRP3-CHCI mice to investigate the *in vivo* role and expression of the NLRP3 inflammasome in health and disease. Initially, I tested that NLRP3-CHCI mice elicited similar responses as WT mice to an exogenous substance in the respiratory tract. This was tested with an intranasal dose of nigericin.

Intranasal administration of nigericin into WT and NLRP3-CHCI mice increased commensurate cell numbers in the airways (via BAL) (Figure 5.1A). This was associated with increased infiltration of neutrophils (Figure 5.1B) and DCs (Figure 5.1C) into the airways during treatment but not macrophages (Figure 5.1D). These increases in cell numbers were similar between WT and NLRP3-CHCI mice (Figure 5.1). Importantly, intranasal administration of nigericin increased BAL IL-1β concentrations in NLRP3-CHCI mice commensurate to WT mice (Figure 5.2A). In contrast, BAL IL-6 concentrations remained the same during intranasal nigericin treatment in WT and NLRP3-CHCI mice (Figure 5.2B).

Taken together, these results suggest that NLRP3-CHCI mice exhibit comparable pulmonary inflammation *in vivo* in comparison to WT mice following NLRP3 inflammasome challenge.

5.2.2 NLRP3 expression single-cell studies on LPS-treated lungs

In chapter four, I confirmed that LPS upregulates NLRP3 protein expression in pBMDMs. From this result, I next tracked NLRP3 protein expression in specific cell populations of the whole lung before and after intranasal treatment of LPS. Intranasal administration of LPS into mice did not affect airway IL-1β concentrations (Figure 5.3A) but did comparably increase airway IL-6 concentrations in both WT and NLRP3-CHCI mice (Figure 5.3B).

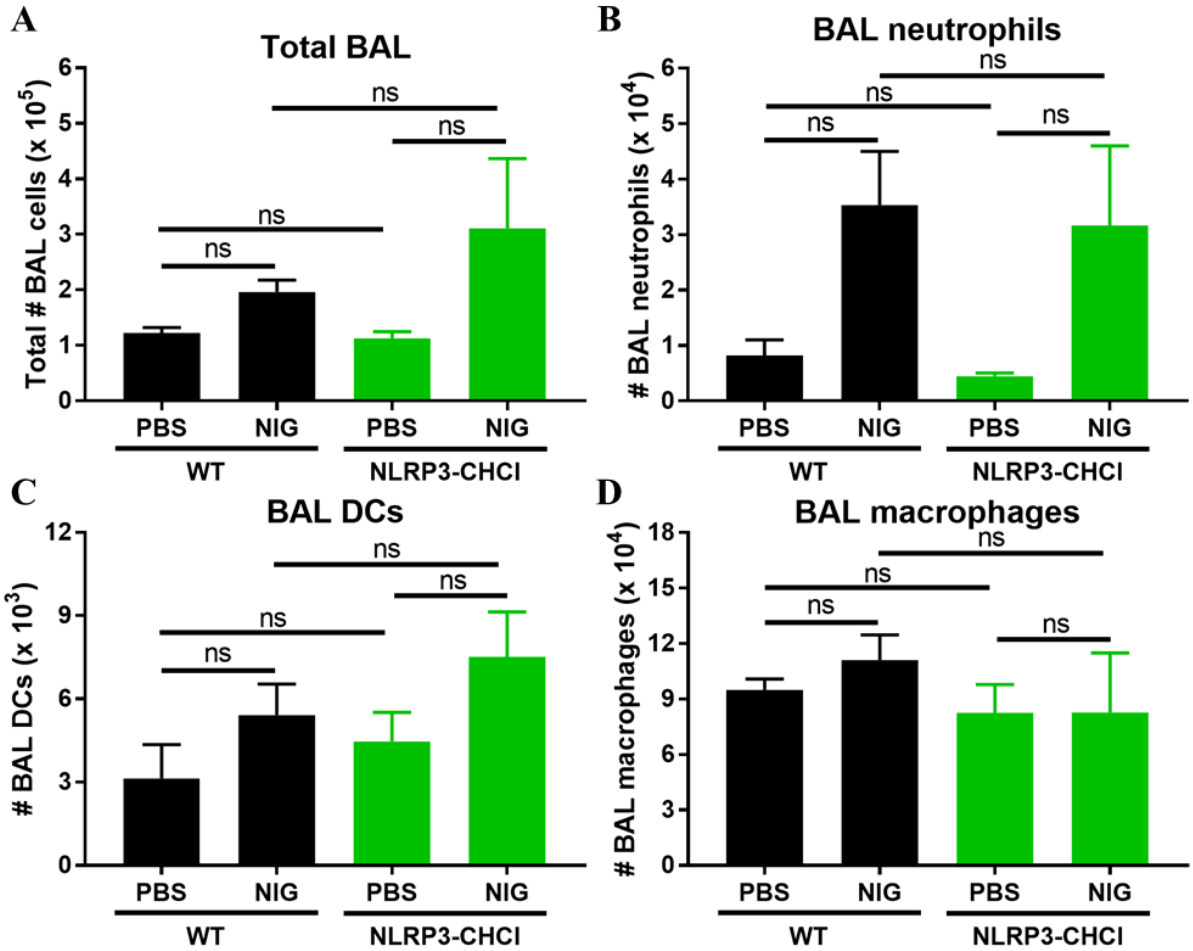

Figure 5.1: NLRP3-CHCI mice exhibit inflammatory cell infiltration in the airways during intranasal nigericin challenge

Nigericin was given intranasally to WT and NLRP3-CHCI mice at 5mg nigericin/kg mouse. Mice were euthanised fourteen hours after administration and bronchoalveolar lavage (BAL) samples were harvested. After the samples were centrifuged, cells were resuspended in 2% FCS and counted via Trypan Blue exclusion. Fc receptors on cells were blocked before surface markers were stained. Cells were processed on the FACSCanto and analysed on FlowJo with specific cell populations gated according to Table 2.4 of Section 2.16 (Flow cytometry of lung and BAL samples) of the *General Materials and Methods* chapter. Data represented as mean ± SEM with N = 3-5 mice/group. Data analysed via one-way ANOVA with Tukey's post-hoc test. ns = not significant

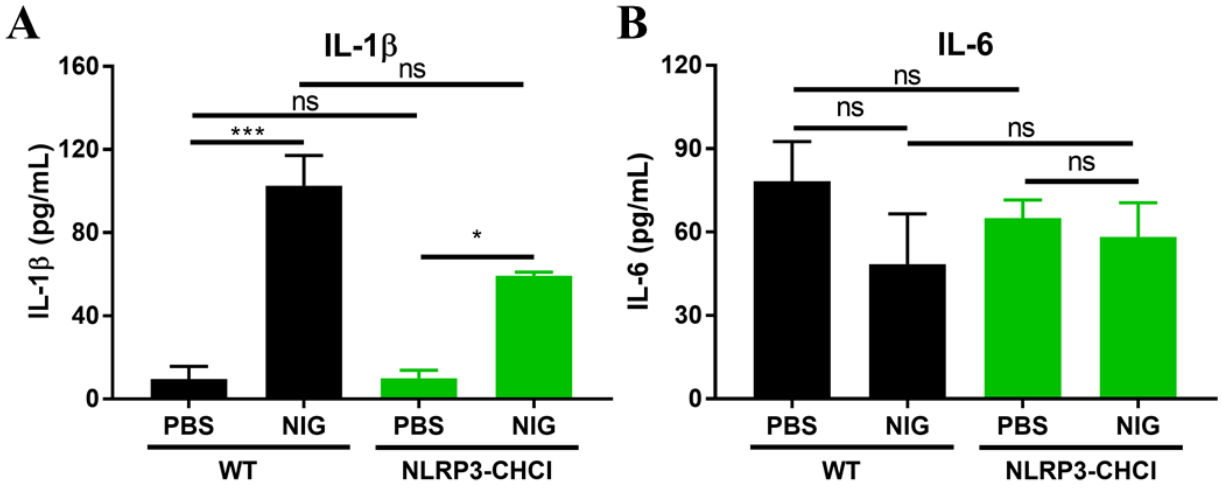

Figure 5.2: NLRP3-CHCI mice exhibit nigericin-induced airway inflammation via pro-inflammatory cytokine secretion

Nigericin was given intranasally to WT and NLRP3-CHCI mice at 5mg nigericin/kg mouse. Mice were euthanised fourteen hours after administration and bronchoalveolar lavage (BAL) samples were harvested. After the samples were centrifuged, supernatant samples were collected and IL-1β and IL-6 concentrations were measured via ELISA following the manufacturer's instructions. Data represented as mean ± SEM with N = 3-5 mice/group and analysed via one-way ANOVA with Tukey's post-hoc test. ns = not significant, *P<0.05 and ***P<0.001.

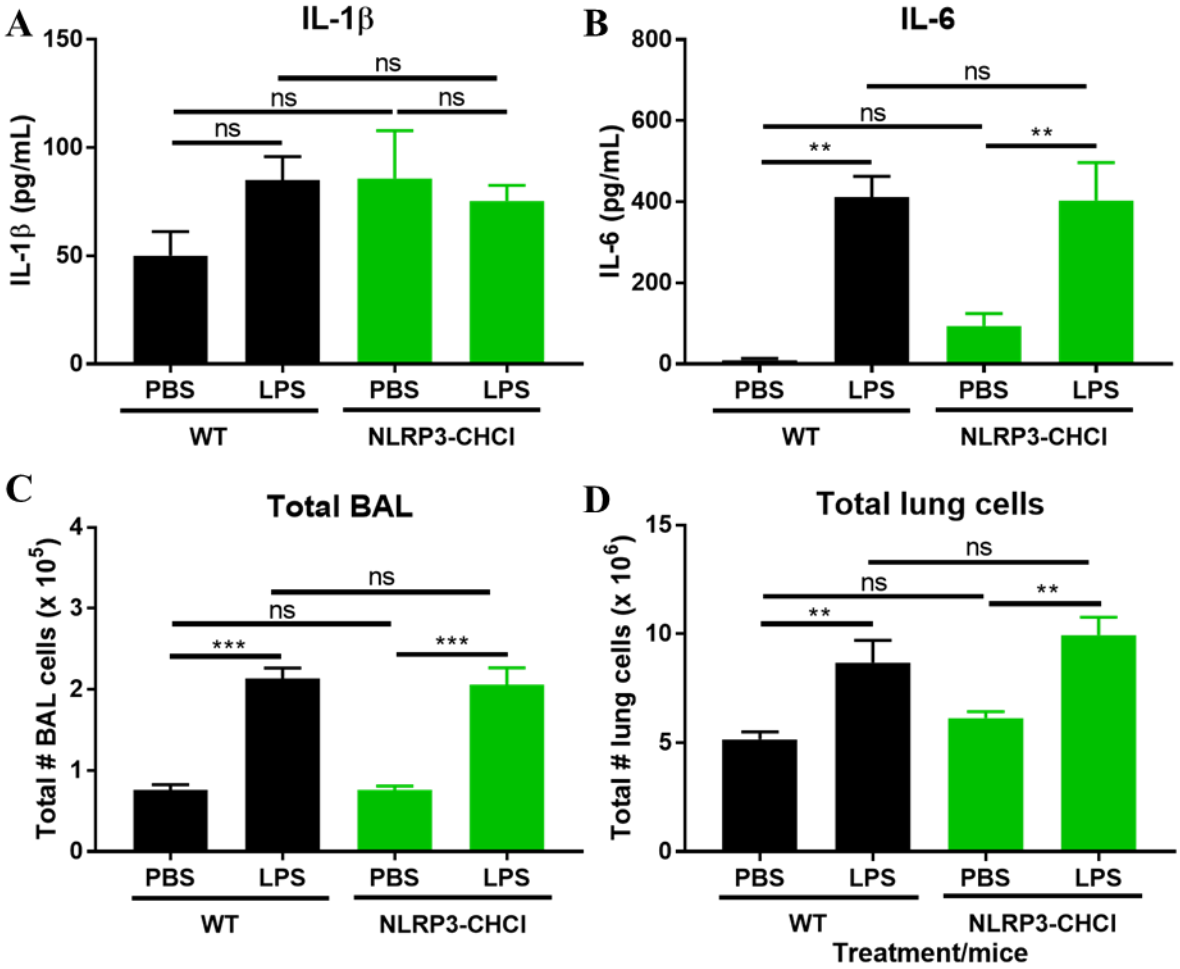

Figure 5.3: Intranasal LPS challenge induces pulmonary inflammation in WT and NLRP3-CHCI mice

WT and NLRP3-CHCI mice were challenged with an intranasal dose of 75µg LPS in 50µL PBS. Mice were euthanised three hours post-administration and bronchoalveolar lavage (BAL) samples and lungs were harvested. After centrifugation, BAL supernatant samples were collected and assayed for IL-1β (A) and IL-6 (B) via ELISA. Lungs were digested, processed through a cell filter and centrifuged. Pelleted cells from BAL and lung samples underwent red blood cell lysis before they were resuspended in FACS buffer and counted via Trypan Blue exclusion (C, D). Data presented as mean ± SEM with N = 5 mice/group for BAL samples and N = 8-10 mice/group for lung samples. Data analysed via one-way ANOVA with Tukey's post-hoc test and significance represented as ns = not significant, **$p<0.01$ and ***$p<0.001$.

Examining expression and activation of NLRP3 inflammasomes in vivo

The presence of LPS in the airways also induced inflammatory cell infiltration as indicated by increased total BAL (Figure 5.3C) and lung (Figure 5.3D) cell counts in both WT and NLRP3-CHCI mice. Importantly, there was no difference in airway pro-inflammatory cytokine concentrations (Figure 5.3A-B) or inflammatory cell counts (Figure 5.3C-D) between LPS-treated WT and NLRP3-CHCI mice, implying that NLRP3-CHCI exhibited similar pulmonary inflammation as WT mice to an intranasal dose of LPS.

I next investigated NLRP3 protein expression in different cell types of the lung following intranasal LPS challenge by mean mCitrine and mCherry fluorescence intensities. Intranasal LPS challenge tended to increase myeloid-derived cell counts in the lungs of WT and NLRP3-CHCI mice (Figure 5.4A) but did not affect non-myeloid-derived or epithelial cell counts (Figure 5.4B-C). Intranasal LPS challenge did not alter lung T cell counts as well (Figure 5.4D) but did increase lung NK cell counts in NLRP3-CHCI mice (Figure 5.4E).

Measuring mCitrine MFIs as a readout of NLRP3 protein expression, LPS did not upregulate NLRP3 in $CD45^+$ myeloid-derived (Figure 5.4F) and $CD45^-$ non-myeloid-derived (Figure 5.4G) cells of NLRP3-CHCI mice as well as epithelial (Figure 5.4H) and T (Figure 5.4I) cells. To note, myeloid-derived cells from LPS-treated NLRP3-CHCI mice had higher mCitrine MFIs compared to those from LPS-treated WT mice (Figure 5.4F). NK cells from untreated NLRP3-CHCI lungs had higher mCitrine MFIs compared to WT lungs which was reduced following LPS challenge (Figure 5.4J). In terms of mCherry MFIs, LPS challenge was associated with an increase in NLRP3 protein expression in myeloid-derived cells from NLRP3-CHCI mice (Figure 5.4K). This upregulation was not seen in non-myeloid-derived, epithelial, T or NK cells (Figure 5.4L-O), though untreated NLRP3-CHCI lung epithelial cells had significantly higher mCherry MFIs than their WT counterparts (Figure 5.4M).

Examining other myeloid-derived cells of the lung that are part of the innate immune system, LPS treatment was associated with an increase in the number of neutrophils in the lung (Figure 5.5A) but not DCs (Figure 5.5B) or macrophages (Figure 5.5C).

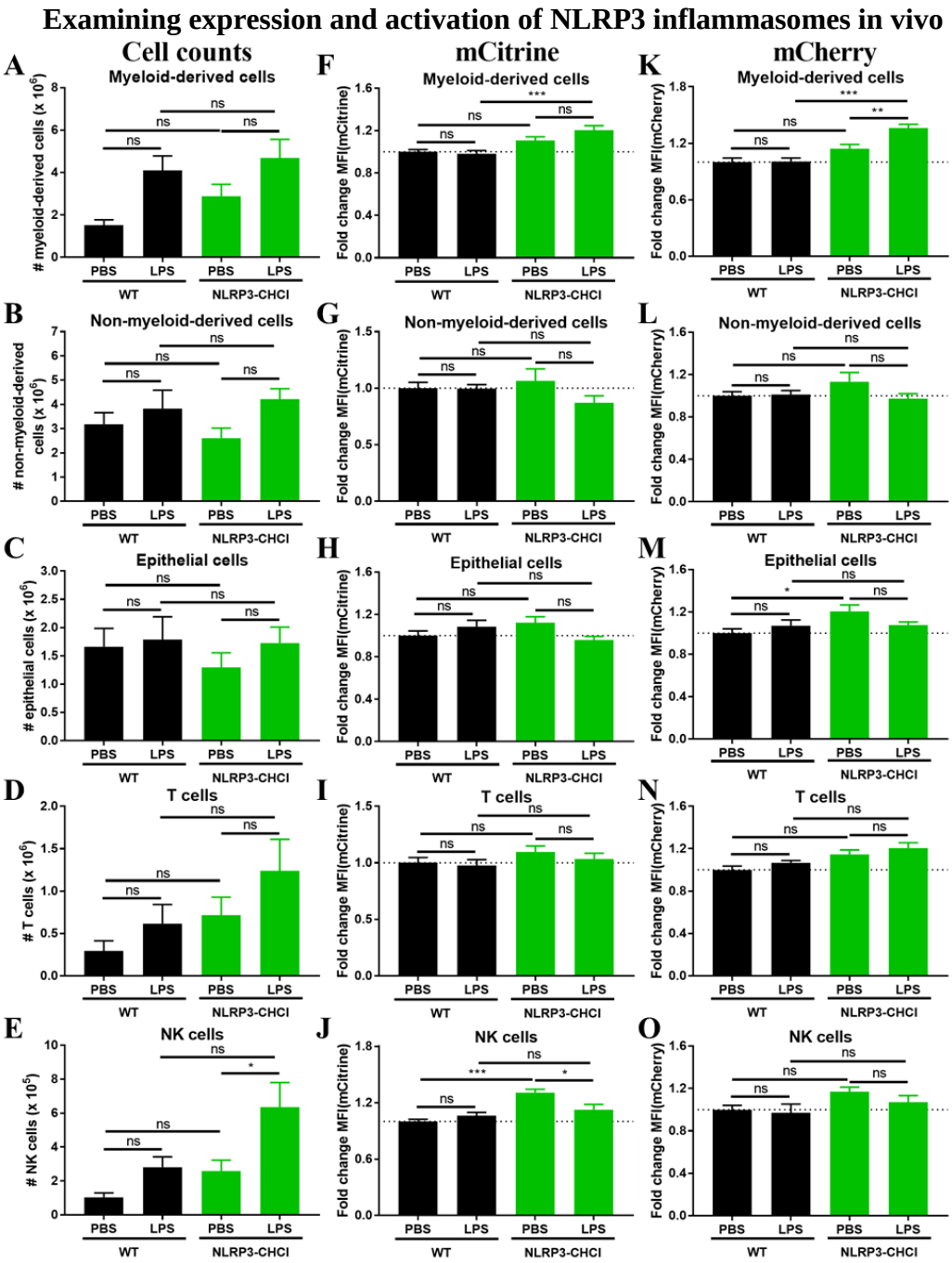

Figure 5.4: Intranasal LPS challenge induces an upregulation of NLRP3 in myeloid-derived cells of NLRP3-CHCI lungs

WT and NLRP3-CHCI mice were challenged with an intranasal dose of 75µg LPS in 50µL PBS. Mice were euthanised three hours post-administration and lungs were harvested. Lungs were digested, processed through a cell filter and red blood cell-lysed. Lung cells were counted via Trypan Blue exclusion before they were Fc receptor-blocked and stained for surface markers. These cells were analysed by flow cytometry on the LSRFortessa with specific cell populations gated according to Table 2.4 of Section 2.16 (Flow cytometry of lung and BAL samples) of the *General Materials and Methods* chapter. Based on the flow cytometry results, a cell count was conducted for each cell subset (A-E) and mCitrine (F-J) and mCherry (K-O) fluorescence intensities were measured which were normalized to the mean of the WT PBS control. Data presented as mean ± SEM and represent pooled data of two independent experiments with 8-10 mice/group. Data analysed via one-way ANOVA with Tukey's post-hoc test and significance represented as ns = not significant, *$p<0.05$, **$p<0.01$ and ***$p<0.001$. Dotted line represents one-fold change in MFI.

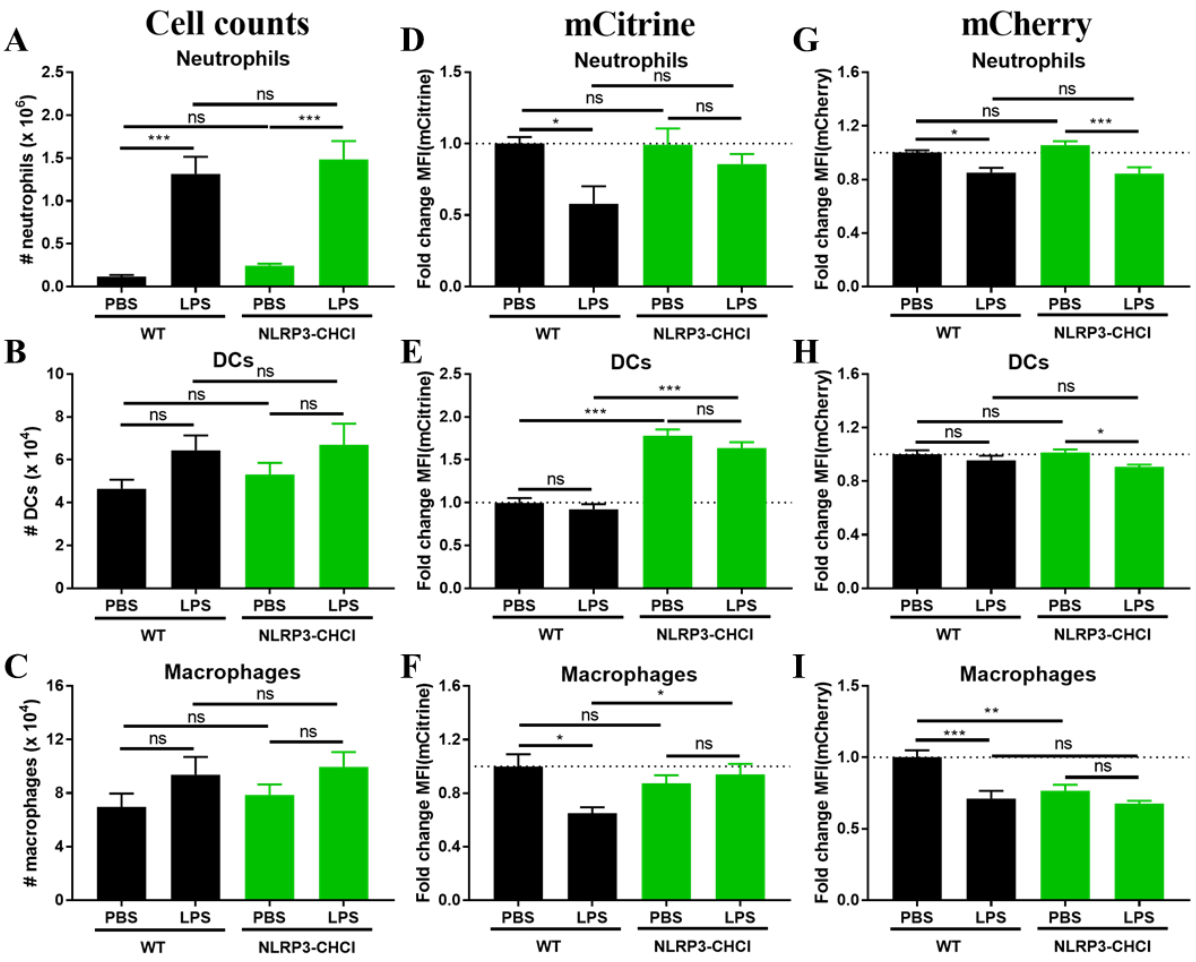

Figure 5.5: Expression of NLRP3 in innate immune cells of the lung following intranasal LPS challenge

WT and NLRP3-CHCI mice were challenged with an intranasal dose of 75µg LPS in 50µL PBS. Mice were euthanised three hours post-administration and lungs were harvested. Lungs were digested, processed through a cell filter and red blood cell-lysed. Lung cells were counted via Trypan Blue exclusion before they were Fc receptor-blocked and stained for surface markers. These cells were analysed by flow cytometry on the LSRFortessa with specific cell populations gated according to Table 2.4 of Section 2.16 (Flow cytometry of lung and BAL samples) of the *General Materials and Methods* chapter. Based on the flow cytometry results, a cell count was conducted for each cell subset (A-C) and mCitrine (D-F) and mCherry (G-I) fluorescence intensities were measured which were normalized to the mean of the WT PBS control. Data presented as mean ± SEM and represent pooled data of two independent experiments with 8-10 mice/group. Data analysed via one-way ANOVA with Tukey's post-hoc test and significance represented as ns = not significant, *$p<0.05$, **$p<0.01$ and ***$p<0.001$. Dotted line represents one-fold change in MFI.

LPS challenge in the lung did not upregulate NLRP3 in lung neutrophils, DCs and macrophages as measured by both mCitrine (Figure 5.5D-F) and mCherry (Figure 5.5G-I) MFIs. Most notably, there was a reduction in mCherry MFIs in NLRP3-CHCI neutrophils and DCs during LPS challenge (Figure 5.5G-H). Nevertheless, within the mCitrine channel, DCs (Figure 5.5E) and macrophages (Figure 5.5F) from LPS-treated NLRP3-CHCI lungs exhibited higher mCitrine MFIs compared to their WT counterparts.

I also analysed the same innate immune cell populations in BAL samples. LPS challenge increased the cell counts of BAL neutrophils (Figure 5.6A) but not DCs (Figure 5.6B) or macrophages (Figure 5.6C) in both WT and NLRP3-CHCI mice. In terms of mCitrine MFI measurements, LPS challenge did not affect NLRP3 protein expression in neutrophils (Figure 5.6D) and DCs (Figure 5.6E) but did upregulate NLRP3 for macrophages from NLRP3-CHCI mice, where they had higher mCitrine MFIs compared to their LPS-treated WT BAL counterparts (Figure 5.6F). Within the mCherry channel, LPS treatment did not increase NLRP3 protein expression in BAL neutrophils, DCs and macrophages (Figure 5.6G-I), though macrophages from LPS-treated NLRP3-CHCI BAL samples had higher mCherry MFIs compared to their LPS-treated WT BAL counterparts (Figure 5.6I).

Taken together, these results imply that LPS upregulates NLRP3 in a small subset of leukocytes within the lung and not non-myeloid-derived populations such as epithelial cells *in vivo.*

5.2.3 Single-cell analysis of NLRP3 expression in IAV-infected lungs

The NLRP3 inflammasome can contribute to the protection or pathology of IAV infection depending on the stage of disease (Tate et al., 2016). Individual cells in the lung such as macrophages have been shown to influence the prognosis of IAV infection by exhibiting NLRP3 inflammasome activity (Ichinohe et al., 2009; Pothlichet et al., 2013). However, these studies have only examined or assessed inflammasome expression or activity in individual cell populations in isolation to each other.

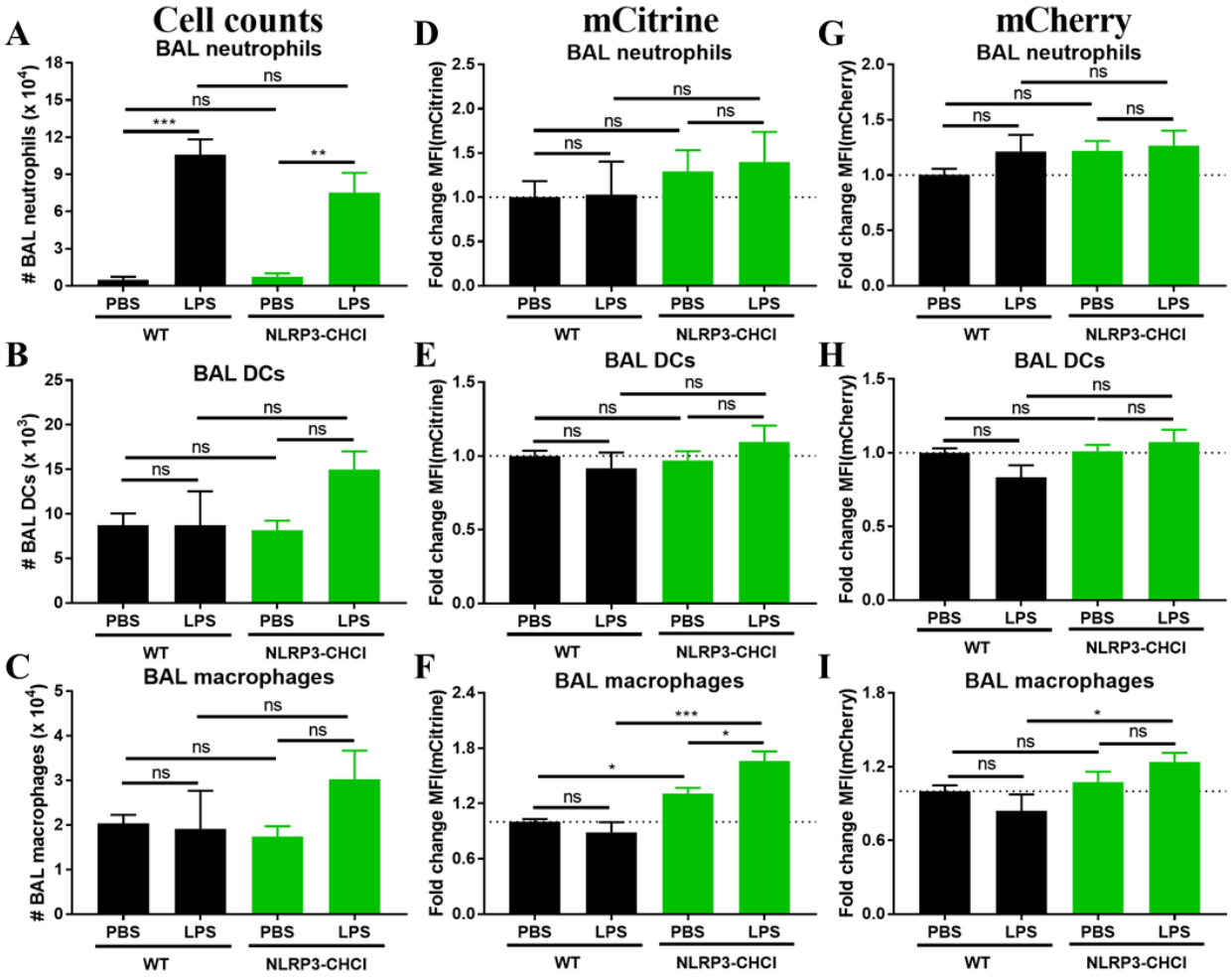

Figure 5.6: Expression of NLRP3 in innate immune cells of BAL samples before and after intranasal LPS challenge

WT and NLRP3-CHCI mice were challenged with an intranasal dose of 75µg LPS in 50µL PBS. Mice were euthanised three hours post-administration and bronchoalveolar lavage (BAL) samples were harvested. After centrifugation, the pelleted cells underwent red blood cell lysis before they were counted via Trypan Blue exclusion, resuspended in FACS buffer, Fc receptor-blocked and stained for surface markers. The stained BAL cells were analysed on the LSRFortessa with specific cell populations gated according to Table 2.4 of Section 2.16 (Flow cytometry of lung and BAL samples) of the *General Materials and Methods* chapter. Based on the flow cytometry results, a cell count was conducted for each cell subset (A-C) and mCitrine (D-F) and mCherry (G-I) fluorescence intensities were measured which were normalized to the mean of the WT PBS control. Data analysed via one-way ANOVA with Tukey's post-hoc test and significance represented as ns = not significant, *$p<0.05$ and ***$p<0.001$. Dotted line represents one-fold change in MFI.

In addition, multiple cell types are involved in the immune response to infection (reviewed in McGill et al. (2009)). Therefore, to address this, I used NLRP3-CHCI reporter mice to identify cells that may exhibit inflammasome activity in a whole lung context via NLRP3 upregulation.

Initially, I compared NLRP3-CHCI and WT mice responses to IAV infection (Figure 5.7). NLRP3-CHCI mice showed comparable weight loss (Figure 5.7A, solid lines) and clinical signs of infection as WT mice (Figure 5.7B-C) during IAV infection. NLRP3-CHCI mice also exhibited pulmonary inflammation during IAV infection, secreting similar amounts of IL-1β (Figure 5.7D) and IL-6 (Figure 5.7E) as WT mice into the airways. Inflammatory cell infiltration into the lung and airways during IAV infection were also similar between WT and NLRP3-CHCI mice as shown by commensurate increases in BAL (Figure 5.7F) and lung (Figure 5.7G) cell counts. These results demonstrate that NLRP3-CHCI mice respond similarly as WT mice to IAV infection by inducing pulmonary inflammation.

I next quantified the expression of NLRP3 in specific cell populations of the lung by measuring mCitrine and mCherry fluorescence intensities via flow cytometry. IAV infection was associated with an increase in $CD45^+$ myeloid-derived and $CD45^-$ non-myeloid-derived cells cell counts in the lungs of both WT and NLRP3-CHCI mice (Figure 5.8A-B). IAV infection did not affect epithelial (Figure 5.8C) or T (Figure 5.8D) cell counts in WT mice but both were found to increase in NLRP3-CHCI lungs (Figure 5.8C-D). Conversely, both WT and NLRP3-CHCI lungs showed increased NK cell counts during IAV infection (Figure 5.8E). Within the mCitrine channel, IAV infection was associated with an upregulation of NLRP3 in myeloid-derived (Figure 5.8F) but not non-myeloid-derived (Figure 5.8G), epithelial (Figure 5.8H) or T (Figure 5.8I) cells from NLRP3-CHCI lungs. Moreover, NLRP3 is also upregulated in NK cells from NLRP3-CHCI lungs as shown by increases in mCitrine MFI during IAV infection (Figure 5.8J). It was noted that IAV increased the mCitrine MFI of WT myeloid-derived cells due to the infiltration of leukocytes into the lung during IAV infection and subsequent increase in autofluorescence (Figure 5.8A) (Monici et al., 1995).

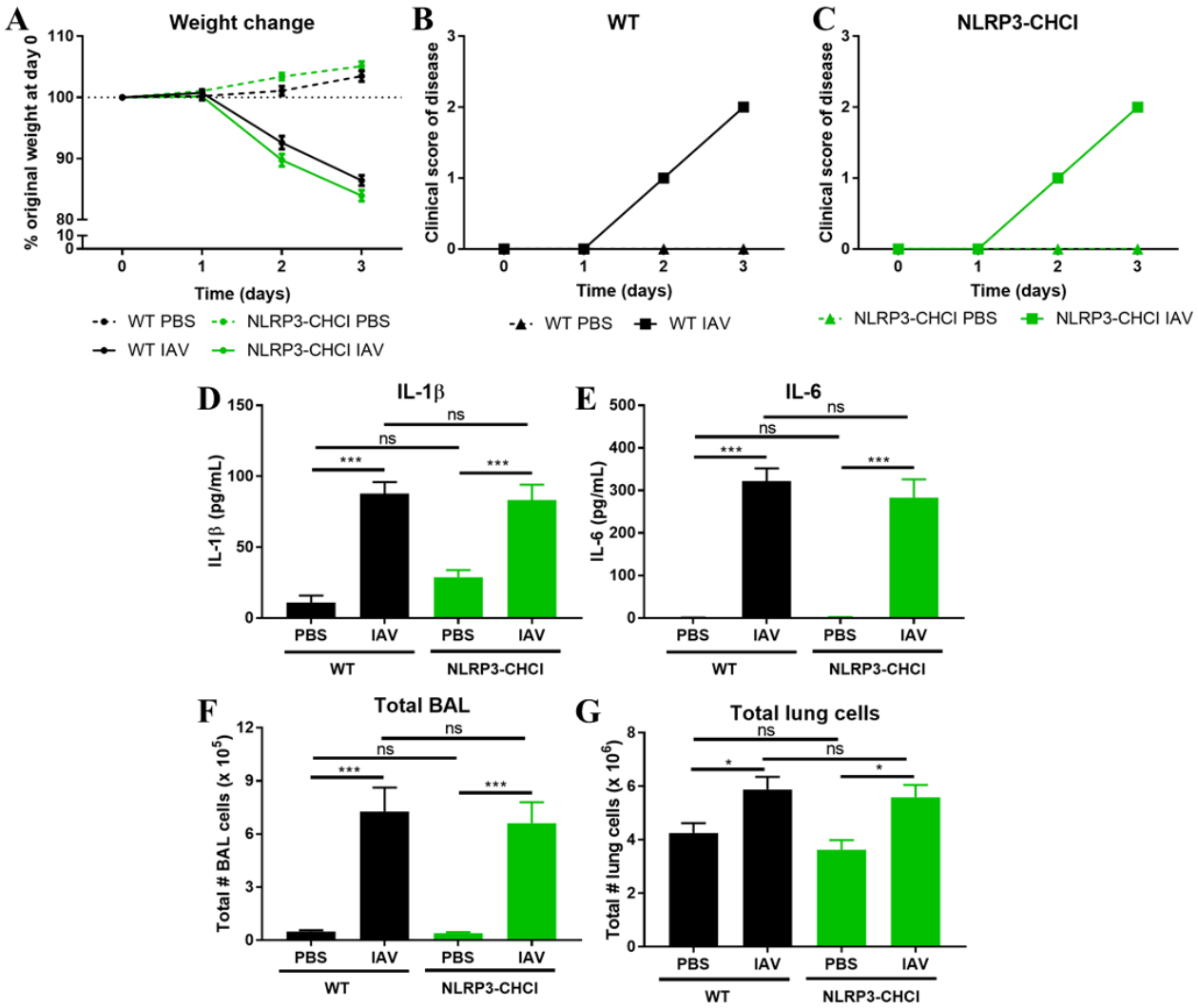

Figure 5.7: NLRP3-CHCI mice exhibit comparable clinical signs of IAV infection to WT mice

WT and NLRP3-CHCI mice were infected with 1 x 10^5 PFU HKx31 (H3N2) and monitored for three days. (A) Mice were weighed daily and the percentage (%) of the original weight at day 0 was calculated. (B, C) WT and NLRP3-CHCI mice were scored for clinical signs of disease according to Table 2.3 of Section 2.14 (IAV infection) of the *General Materials and Methods* chapter. (D-G) Mice were euthanised three days post-infection and bronchoalveolar lavage (BAL) and lung samples were collected. After centrifugation, BAL supernatant samples were collected and assayed for IL-1β (D) and IL-6 (E) via ELISA. Lungs were digested and processed through a cell filter. The pelleted cells from BAL and lung samples underwent red blood cell lysis before they were resuspended in FACS buffer and counted via Trypan Blue exclusion (F, G). Data presented as mean ± SEM and represent pooled data of two independent experiments of 9-10 mice/group. All data analysed via one-way ANOVA with Tukey's post-hoc test and significance represented as ns = not significant, *$p<0.05$, **$p<0.01$ and ***$p<0.001$.

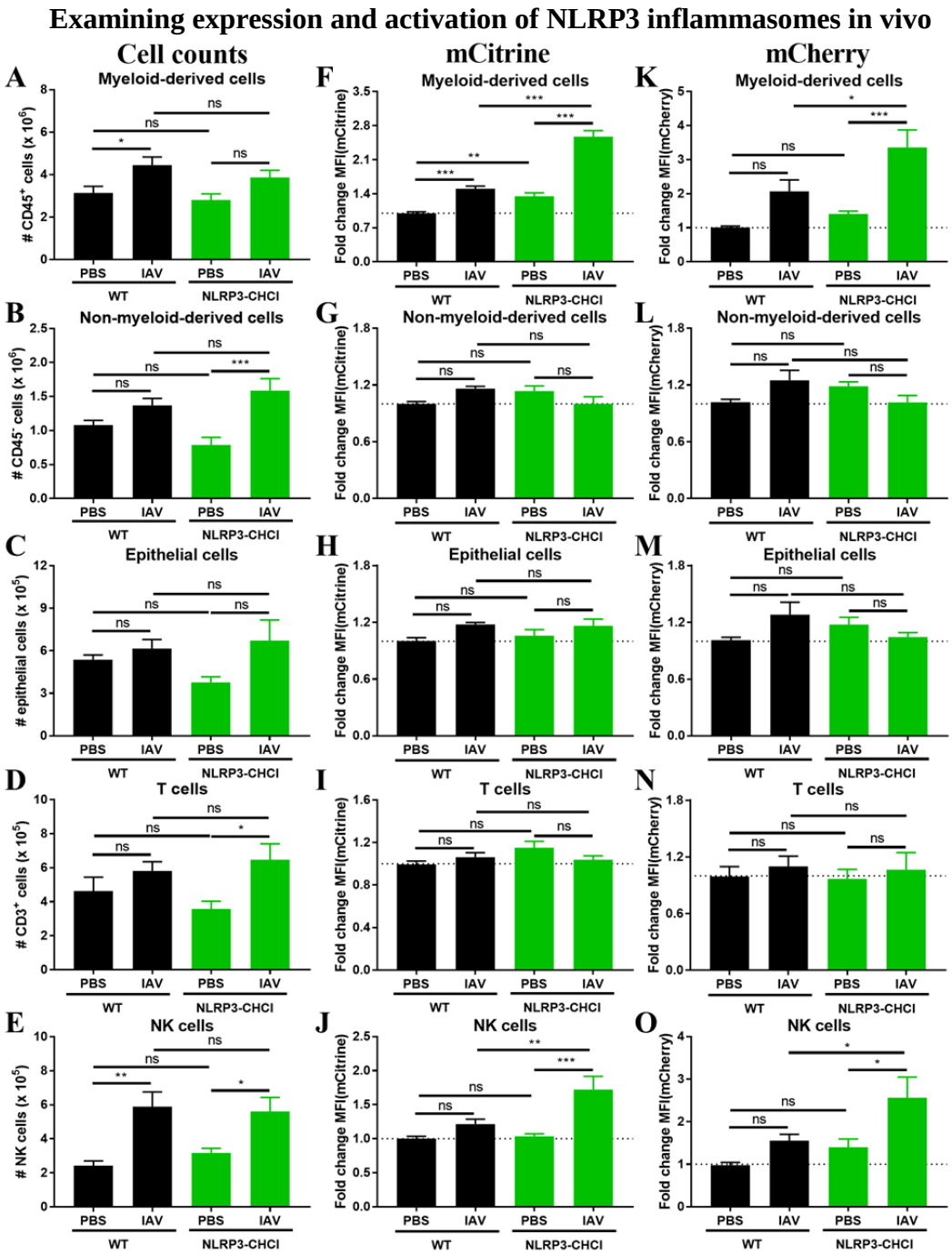

Figure 5.8: NLRP3 is upregulated in myeloid-derived cells of the lung during IAV infection

WT and NLRP3-CHCI mice were intranasally infected with 1 x 10^5 PFU HKx31 (H3N2). Mice were euthanised three days post-infection and lung samples were collected, digested, processed through a cell filter and red blood cell-lysed. Cells were counted via Trypan Blue exclusion before they were Fc receptor-blocked with anti-mouse CD16/32 antibody, stained for surface markers and processed on the LSRFortessa with specific cell populations gated according to Table 2.4 of Section 2.16 (Flow cytometry of lung and BAL samples) of the *General Materials and Methods* chapter. Based on the flow cytometry results, a cell count was conducted for each cell subset (A-E) and mCitrine (F-J) and mCherry (K-O) fluorescence intensities were measured which were normalized to the mean of the WT PBS control. Data are presented as mean ± SEM and represent pooled data of two independent experiments of 9-10 mice/group. Data analysed via one-way ANOVA with Tukey's post-hoc test and significance represented as ns = not significant, *$p<0.05$, **$p<0.01$ and ***$p<0.001$. Dotted line represents one-fold change in MFI.

Examining expression and activation of NLRP3 inflammasomes in vivo

Changes in NLRP3 protein expression during IAV infection were similar when mCherry MFIs were used a readout (Figure 5.8K-O).

I next measured NLRP3 protein expression in specific leukocyte populations of the innate immune system. IAV infection of the lung did not influence lung-resident macrophage cell counts in both WT and NLRP3-CHCI mice (Figure 5.9A) but did increase inflammatory macrophage (Figure 5.9B), neutrophil (Figure 5.9C) and DC (Figure 5.9D) cell counts in both groups of mice. Uninfected lung-resident macrophages from NLRP3-CHCI mice initially had higher NLRP3 expression compared to WT mice as measured by mCitrine MFI which was downregulated during IAV infection (Figure 5.9E). In contrast, NLRP3 was upregulated in inflammatory macrophages (Figure 5.9F), neutrophils (Figure 5.9G) and DCs (Figure 5.9H) from NLRP3-CHCI lungs during IAV infection. Within the mCherry channel, NLRP3 expression was similar in lung-resident macrophages of NLRP3-CHCI lungs (Figure 5.9I) but was upregulated in inflammatory macrophages (Figure 5.9J). mCherry MFIs did not change in neutrophils (Figure 5.9K) and DCs (Figure 5.9L) from IAV-infected NLRP3-CHCI lungs.

I further measured NLRP3 expression in innate immune cells that have infiltrated BAL samples. IAV infection did not affect macrophage cell counts in the BAL of WT and NLRP3-CHCI mice (Figure 5.10A) but did increase inflammatory macrophage, neutrophil and DC cell counts (Figure 5.10B-D). Due to the negligible numbers of inflammatory macrophages and neutrophils found in PBS-treated BAL samples of WT and NLRP3-CHCI mice, mCitrine and mCherry MFIs were not measured for these cell populations. Macrophages (Figure 5.10E), inflammatory macrophages (Figure 5.10F), neutrophils (Figure 5.10G) and DCs (Figure 5.10H) from IAV-infected NLRP3-CHCI BAL samples had significantly higher mCitrine MFIs compared to their WT counterparts.

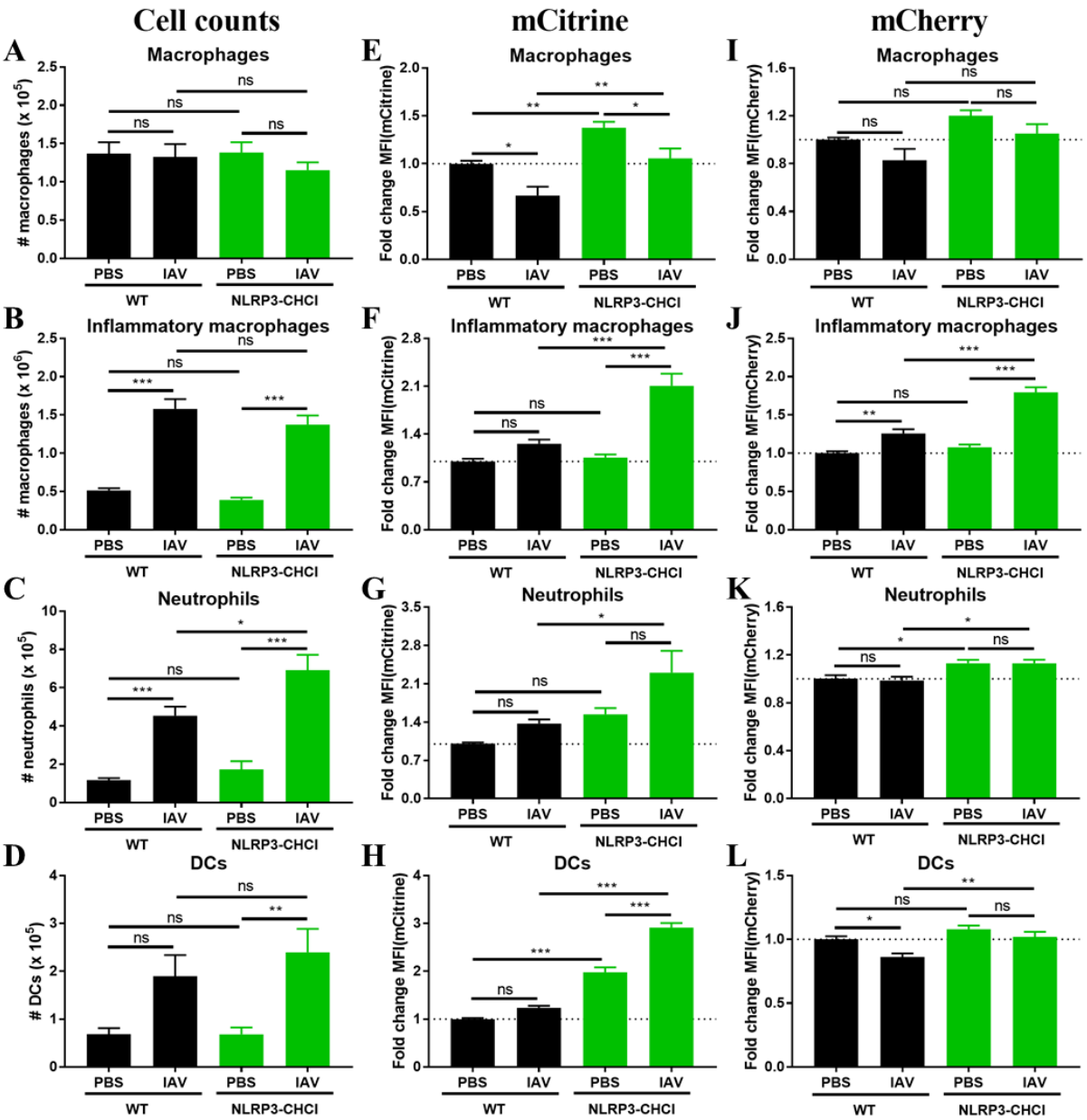

Figure 5.9: NLRP3 is upregulated in various resident and infiltrating leukocytes of the lung during IAV infection

WT and NLRP3-CHCI mice were intranasally infected with 1 x 10^5 PFU HKx31 (H3N2). Mice were euthanised three days post-infection and lung samples were collected, digested, processed through a cell filter and red blood cell-lysed. Cells were counted via Trypan Blue exclusion before they were Fc receptor-blocked with anti-mouse CD16/32 antibody, stained for surface markers and processed on the LSRFortessa with specific cell populations gated according to Table 2.4 of Section 2.16 (Flow cytometry of lung and BAL samples) of the *General Materials and Methods* chapter. Based on the flow cytometry results, a cell count was conducted for each cell subset (A-D) and mCitrine (E-H) and mCherry (I-L) fluorescence intensities were measured which were normalized to the mean of the WT PBS control. Data are presented as mean ± SEM and represent pooled data of two independent experiments of 9-10 mice/group. Data analysed via one-way ANOVA with Tukey's post-hoc test and significance represented as ns = not significant, *p<0.05, **p<0.01 and ***p<0.001. Dotted line represents one-fold change in MFI.

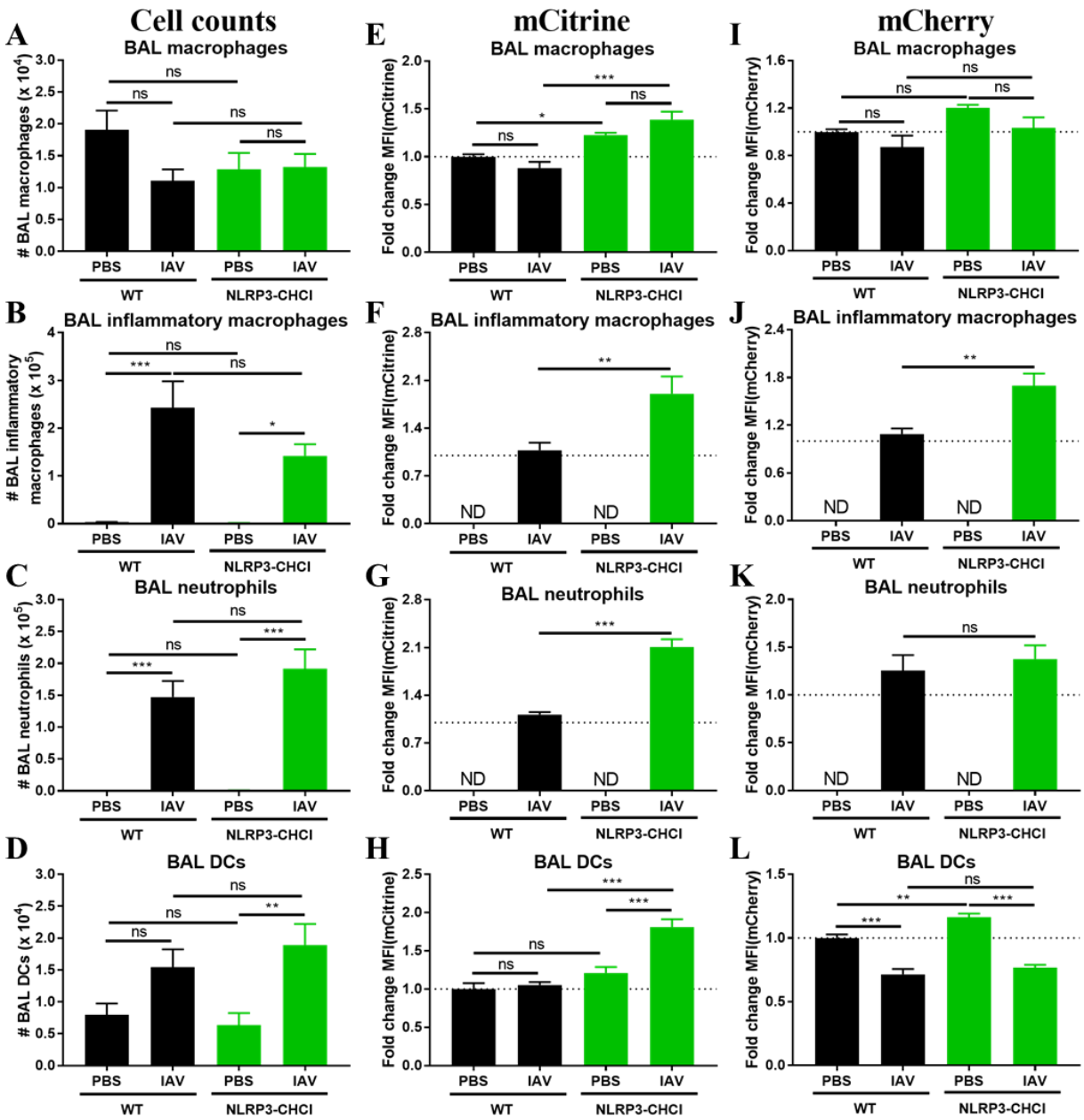

Figure 5.10: NLRP3 is upregulated in infiltrating leukocytes of BAL during IAV infection

WT and NLRP3-CHCI mice were intranasally infected with 1 x 10^5 PFU HKx31 (H3N2). Mice were euthanised three days post-infection and bronchoalveolar lavage (BAL) fluid samples were collected. After centrifugation, the pelleted cells underwent red blood cell lysis before they were resuspended in FACS buffer. Cells were counted via Trypan Blue exclusion before they were Fc receptor-blocked with anti-mouse CD16/32 antibody, stained for surface markers and processed on the LSRFortessa with specific cell populations gated according to Table 2.4 of Section 2.16 (Flow cytometry of lung and BAL samples) of the *General Materials and Methods* chapter. Based on the flow cytometry results, a cell count was conducted for each cell subset (A-D) and mCitrine (E-H) and mCherry (I-L) fluorescence intensities were measured which were normalized to the mean of the WT PBS control. Data presented as mean ± SEM and represent pooled data of two independent experiments of 9-10 mice/group. Data analysed via one-way ANOVA with Tukey's post-hoc test and significance represented as ns = not significant, *$p<0.05$, **$p<0.01$ and ***$p<0.001$. Dotted line represents one-fold change in MFI. ND = not determined due to low cell numbers.

There was also an upregulation of NLRP3 in DCs from NLRP3-CHCI BAL samples (Figure 5.10H) which was not seen in macrophages (Figure 5.10E). NLRP3 protein expression results in macrophages, inflammatory macrophages and neutrophils were similar when mCherry MFIs were used as the readout of expression (Figure 5.10I-K). To note, NLRP3-CHCI DCs showed a significant downregulation of NLRP3 during IAV infection as measured by mCherry MFIs (Figure 5.10L).

Taken together, these results highlight that IAV infection primarily upregulates NLRP3 in leukocytes of myeloid-derived cells with limited to no upregulation in non-myeloid-derived cells.

5.2.4 Pulmonary cellular uptake of MCC950- in IAV-infected mice

MCC950, a small molecule inhibitor of the NLRP3 inflammasome, has different effects on the survival of mice to IAV infection depending on which stage of disease it is administered (Tate et al., 2016). The mechanisms behind this; though, are unknown. One possible mechanism behind the dual effects of MCC950 might be that MCC950 enters various cell populations of the lung at different stages of IAV infection. Given my identification of NLRP3 expression and upregulation in cellular subsets during LPS and IAV challenge, it is important to identify cell populations that NLRP3 inhibitors may be targeting. Hence, I investigated and identified the specific cells in the lung in which MCC950 enters by visualising MCC950-rhodamine uptake into cell subsets, where the rhodamine fluorescent dye is attached to MCC950.

Initially, MCC950-rhodamine was intranasally administered to un-infected mice to measure MCC950 uptake in the lung. Flow cytometry was used to measure the fluorescence intensity of rhodamine as a readout of MCC950 uptake (Figure 5.11A). As can be observed, MCC950 was seen in total lung cell populations from one hour post-administration (6.4% cells being MCC950-rhodamine positive, Figure 5.11B) and was cleared by six hours post-administration (6.2% MCC950-rhodamine positive cells, Figure 5.11B). Maximum MCC950 uptake in the lung was observed at three hours post-administration (11.8% MCC950-rhodamine positive cells, Figure 5.11B).

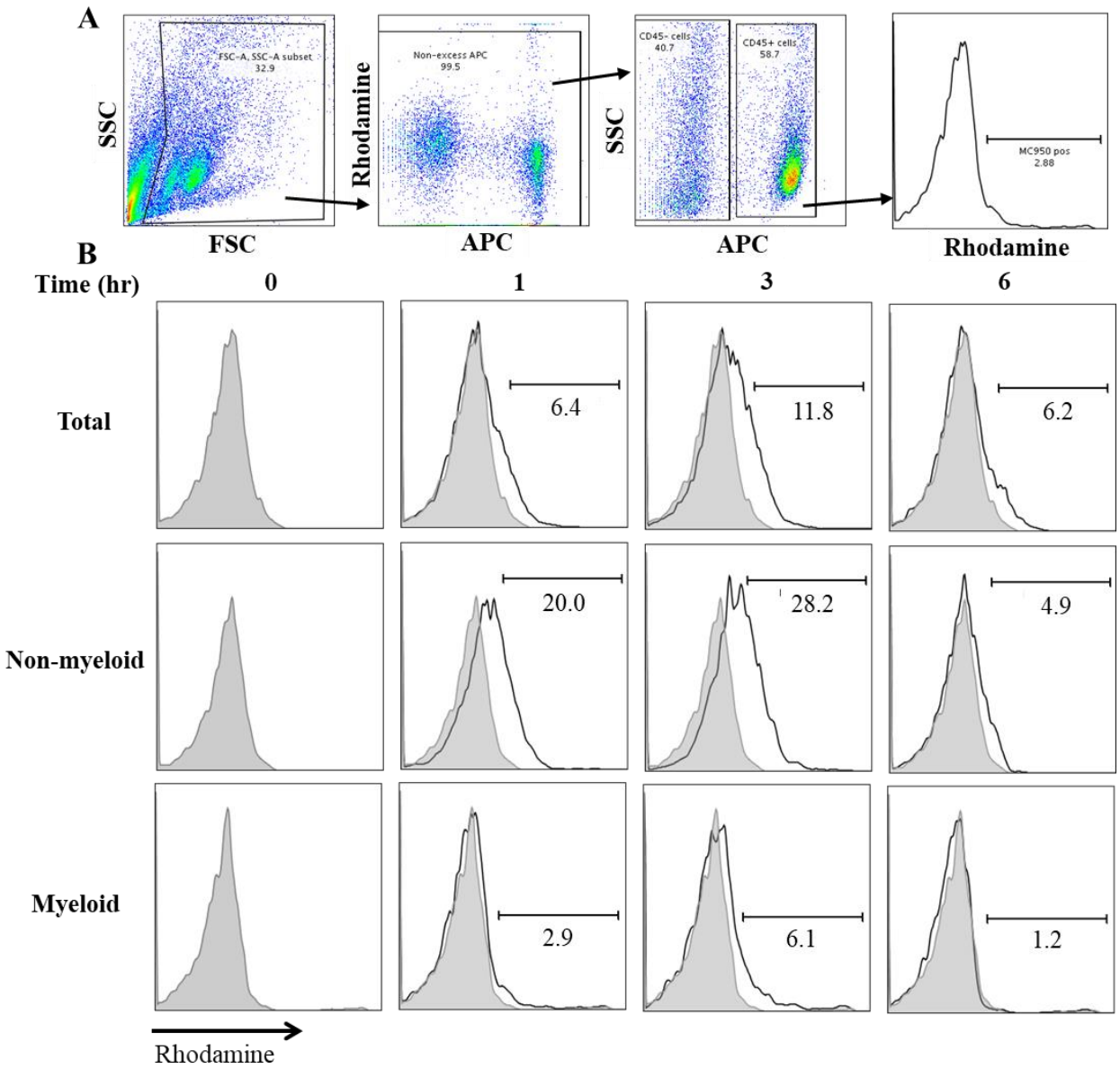

Figure 5.11: MCC950 accumulates in myeloid and non-myeloid-derived cells of the lung.

MCC950-rhodamine (100µg/mouse) was administered intranasally into WT mice 1, 3 or 6 hours before they were euthanised. Lungs were harvested, digested, filtered and red blood cell-lysed. The resultant cells were resuspended in 2% FCS, Fc receptor-blocked with anti-mouse CD16/CD32 antibody and stained with antibodies for surface markers. Cells were processed on the BD FACSCanto II with specific cell populations gated according to Table 2.4 of Section 2.16 (Flow cytometry of lung and BAL samples) of the *General Materials and Methods* chapter. Gates (A) and histograms (B) were produced in FlowJo. For histograms in B, shaded area represent cells from a PBS control mouse and black line represents cells from a MCC950-rhodamine-administered mouse. Bar represents percentage of cells that are MCC950-rhodamine positive. FSC = forward scatter and SSC = side scatter.

Both $CD45^-$ non-myeloid and $CD45^+$ myeloid-derived cells took up MCC950, though in the uninfected state MCC950 uptake within 3 hours of administration was higher in non-myeloid-derived cells of the lung (28.2% non-myeloid-derived cells being MCC950-rhodamine positive, Figure 5.11B) compared to myeloid-derived cells (6.1% myeloid-derived cells being MCC950-rhodamine positive, Figure 5.11B). Looking at specific cell populations, MCC950 uptake was substantial in epithelial cells (29.8% MCC905-rhodamine positive by 3 hours) and macrophages (16.2%) but small for inflammatory macrophages (4.8%) and B cells (5.7%) (Figure 5.12). Nevertheless, for each cell population, MCC950 uptake was seen from one hour post-administration and peaked at the three hour timepoint before it was cleared by six hours (Figure 5.12).

These results imply that in an uninfected state, MCC950 is taken up by both non-myeloid and myeloid-derived cells of the lung and is retained in the lung for a maximum of six hours.

Having identified where MCC950 is taken up in uninfected lungs, I next examined if IAV infection altered the uptake or cellular preference of MCC950. I decided to measure MCC950 uptake in the lung at one and three days post-infection because these timepoints correspond to asymptomatic and symptomatic IAV infection where the NLRP3 inflammasome plays a protective and detrimental role respectively (Tate et al., 2016; Yatmaz et al., 2013). MCC950 was seen in the lung at both infection timepoints, though the three day infection period was associated with higher MCC950 uptake in the lung (22.9% lung cells being MCC950-rhodamine positive) compared to the one day timepoint (6.7%, Figure 5.13A). MCC950 uptake in non-myeloid-derived cells was similar between one and three days post-infection (10.1% at one day vs 13.4% at three days, Figure 5.13B). In contrast, more MCC950 was taken up by myeloid-derived cells at three days post-infection compared to one day post-infection (5.4% at one day to 20.2% at three days, Figure 5.13C).

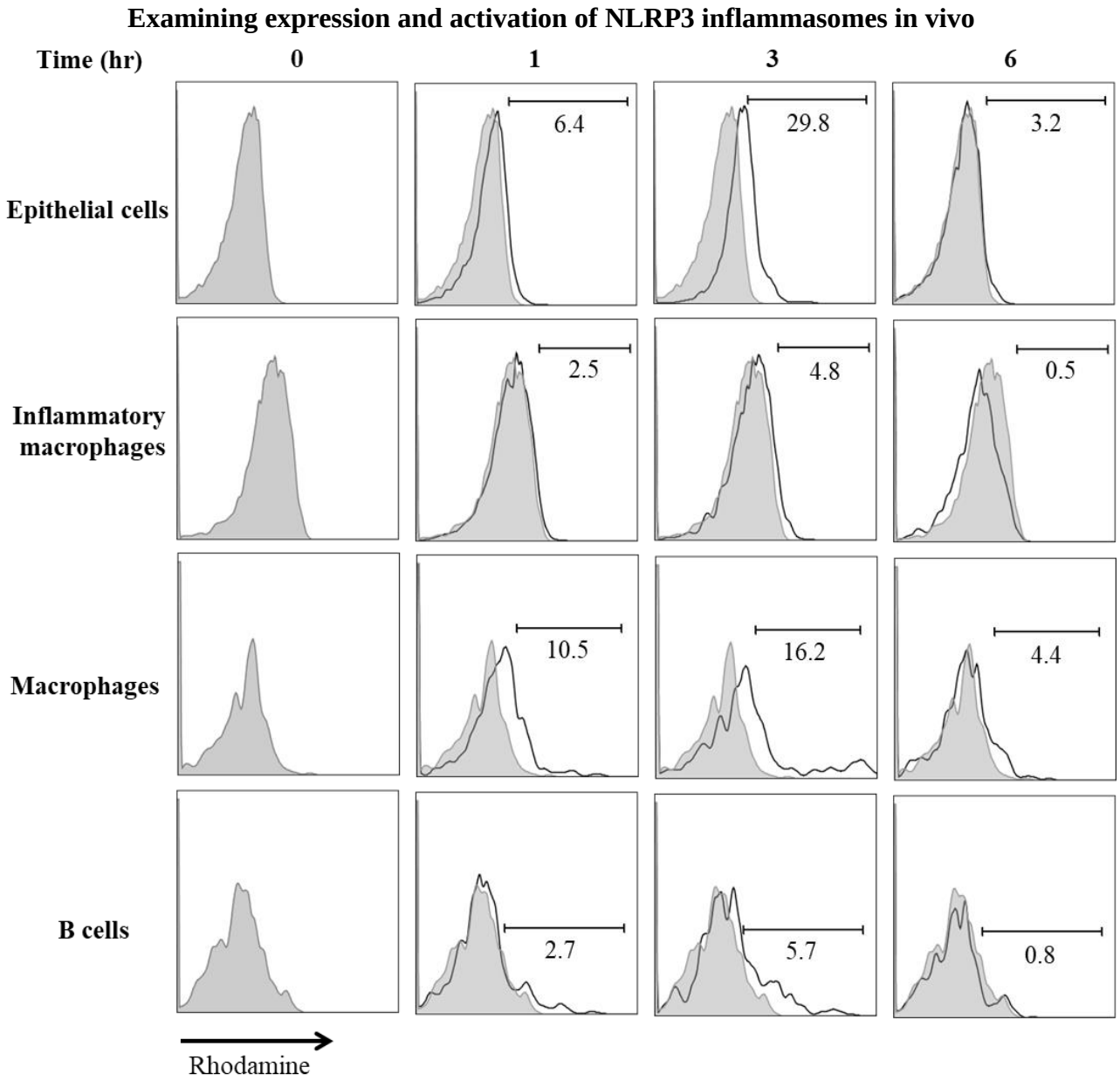

Figure 5.12: MCC950 accumulates in epithelial and immune cells of the lung.

MCC950-rhodamine (100µg/mouse) was administered intranasally into WT mice 1, 3 or 6 hours before they were euthanised. Lungs were harvested, digested, filtered and red blood cell-lysed. The resultant cells were resuspended in 2% FCS, Fc receptor-blocked with anti-mouse CD16/CD32 antibody and stained with antibodies for surface markers. Epithelial cells were fixed and permeabilised before they were stained for the intracellular marker cytokeratin c. Cells were processed on the BD FACSCanto II with specific cell populations gated according to Table 2.4 of Section 2.16 (Flow cytometry of lung and BAL samples) of the *General Materials and Methods* chapter. Histograms for each cell population were produced on FlowJo. Shaded area represent cells from a PBS control mouse and black line represents cells from a MCC950-rhodamine-administered mouse. Bar represents percentage of cells that are MCC950-rhodamine positive.

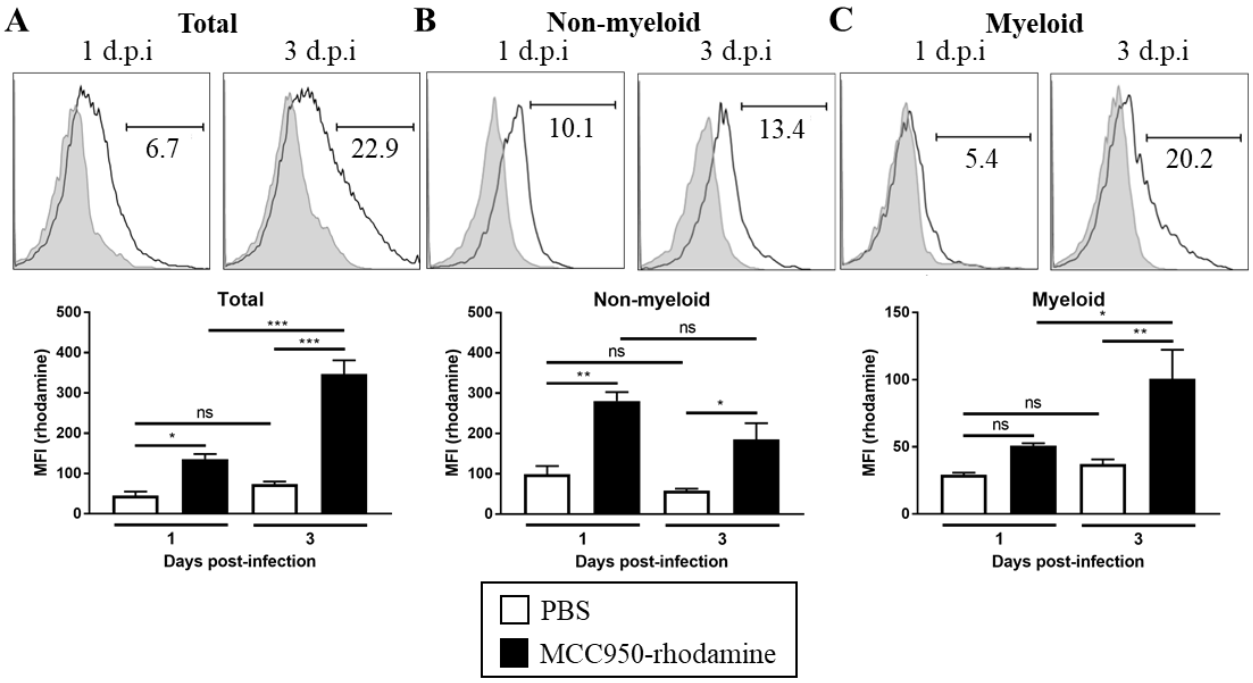

Figure 5.13: MCC950 accumulates in both myeloid- and non-myeloid-derived cell populations of the lung during IAV infection

Mice were infected with 1 x 10^4 PFU HKx31 (H3N2) one or three days before the experiment. On the day of the experiment, mice were given MCC950-rhodamine (100µg/mouse) intranasally three hours before they were euthanised. Lungs were harvested, digested, filtered and red blood cell-lysed. The resultant cells were then resuspended in 2% FCS, Fc receptor-blocked with anti-mouse CD16/CD32 antibodies and stained with antibodies for surface markers. Cells were processed on the BD FACSCanto II with specific cell populations gated according to Table 2.4 of Section 2.16 (Flow cytometry of lung and BAL samples) of the *General Materials and Methods* chapter. Data was analysed via FlowJo. Representative histograms for unstained (A), non-myeloid-derived (B) and myeloid-derived cell populations (C) were generated. Shaded area represents cells from a PBS control mouse and black line represents cells from a MCC950-rhodamine-administered mouse. Bar on histogram represents percentage of cells that are MCC950-rhodamine positive. Mean fluorescence intensity (MFI) of rhodamine for each cell population (A-C) was also calculated for each PBS control and MCC950-rhodamine-administered mouse. Data represented as mean ± SEM with N = 4 mice/group. Data was analysed via one-way ANOVA with Tukey's post-hoc test. ns = not significant, *$p<0.05$, **$p<0.01$ and ***$p<0.001$. d.p.i = days post-infection.

Examining expression and activation of NLRP3 inflammasomes in vivo

Among specific cell populations, at one day post-infection MCC950 uptake was seen in macrophages and DCs (Figure 5.14A-B) but not epithelial cells, inflammatory macrophages, neutrophils or B cells which had similar rhodamine MFIs to the PBS control (Figure 5.14C-F). By three days post-infection, DCs, inflammatory macrophages, neutrophils and B cells took up MCC950 as measured by significantly higher rhodamine MFIs compared to the PBS control (Figure 5.14B, D-F). Macrophages (Figure 5.14A) and epithelial cells (Figure 5.14C) displayed a tendency to take up MCC950 at three days post-infection, but this was not statistically significant compared to the PBS control. Interestingly, MCC950 uptake into macrophages was lower 3 days post-infection compared to 1 day post-infection (from 50.9% MCC950-rhodamine positive one day post-infection to 39.4% three days post-infection, Figure 5.14A).

These results highlight that MCC950 is taken up by various leukocyte cell populations in the healthy and IAV-infected lung to exert its inhibitory actions.

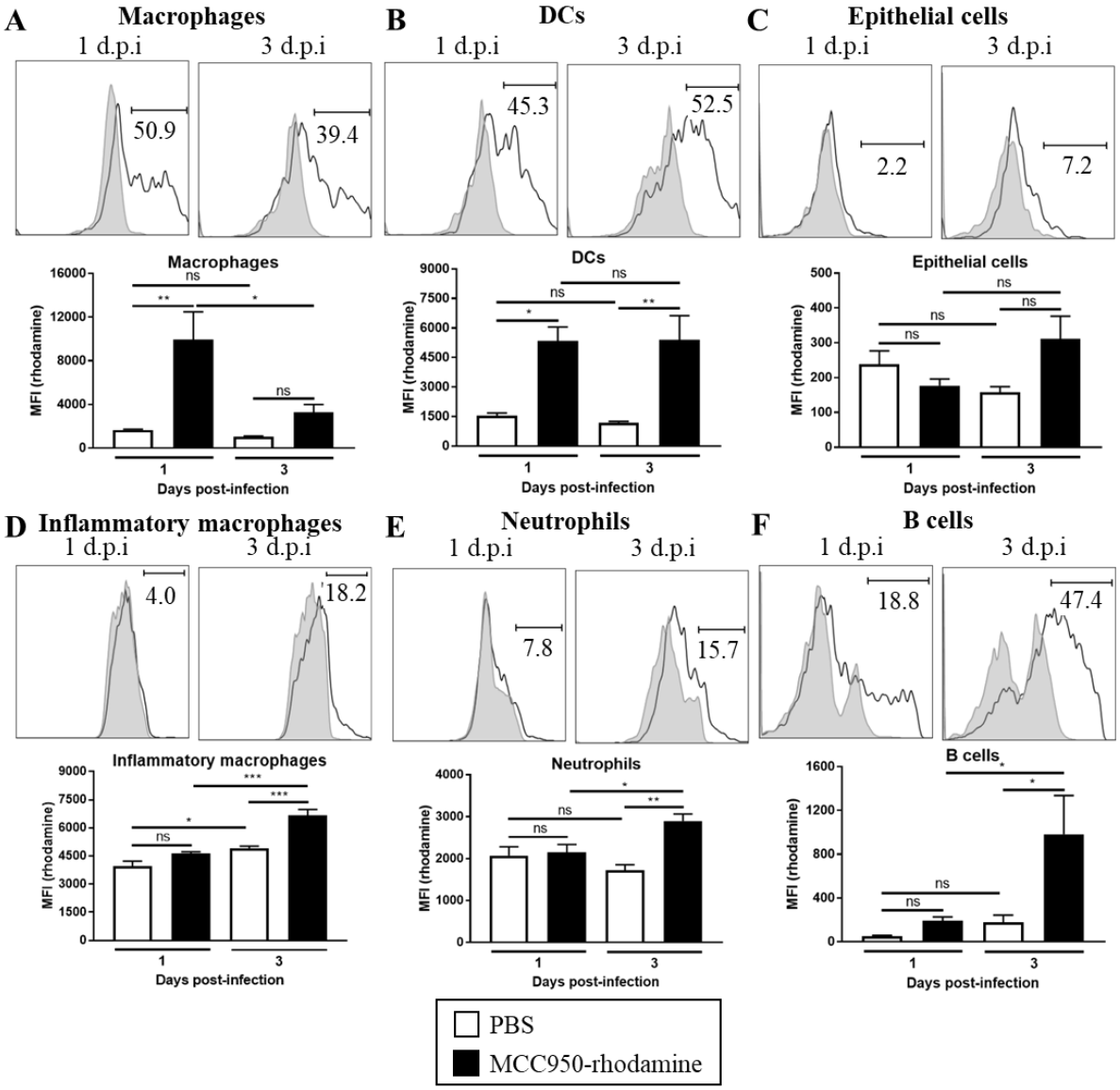

Figure 5.14: MCC950 accumulates in immune cells during IAV infection

Mice were infected with 1 x 10^4 PFU HKx31 (H3N2) one or three days before the experiment. On the day of the experiment, mice were given MCC950-rhodamine (100µg/mouse) intranasally three hours before they were euthanised. Lungs were harvested, digested, filtered and red blood cell-lysed. The resultant cells were then resuspended in 2% FCS, Fc receptor-blocked with anti-mouse CD16/CD32 antibodies and stained with antibodies for surface markers. Epithelial cells were fixed and permeabilised before they were stained for the intracellular marker cytokeratin c. Rhodamine fluorescence was measured on the BD FACSCanto II with specific cell populations gated according to Table 2.4 of Section 2.16 (Flow cytometry of lung and BAL samples) of the *General Materials and Methods* chapter. Data was analysed via FlowJo. Each cell population (A-F) has representative rhodamine histograms with shaded area and black line representing cells from a PBS control and MCC950-rhodamine-administered mouse respectively. Bar on histogram represents percentage of cells that are MCC950-rhodamine positive. Rhodamine mean fluorescence intensities (MFI) (A-F) were also calculated for each mouse. Data represented as mean ± SEM with N = 4 mice/group. Data was analysed via one-way ANOVA with Tukey's post-hoc test. ns = not significant, *$p<0.05$, **$p<0.01$ and ***$p<0.001$. d.p.i = days post-infection.

5.3 Discussion

The NLRP3 inflammasome is expressed and active in a variety of organs and cells. Notably, *Nlrp3* mRNA is expressed in the lung (Guarda et al., 2011; Huang et al., 2014) with NLRP3 protein being found in alveolar macrophages and AECs (Huang et al., 2014; Tran et al., 2012). These cells have been found to exhibit NLRP3 inflammasome activity and to contribute to pulmonary inflammation during IAV infection (Ichinohe et al., 2009; Pothlichet et al., 2013). To date; however, these cells have been studied in isolation to each other, so it is unknown whether these cells will exhibit inflammasome activity in the context of the whole lung. In this chapter, I used NLRP3-CHCI mice to identify the cellular subsets in the lung that exhibit NLRP3 expression and upregulation during pulmonary inflammation.

I initially confirmed that intranasal nigericin challenge induced comparable pulmonary inflammatory responses in WT and NLRP3-CHCI mice as measured by inflammatory cell infiltration (Figure 5.1) and cytokine secretion (Figure 5.2) into the airways. These responses are similar to those seen in silica administration into the lung (Fang et al., 2017; Kato et al., 2017). One major difference however, is that while nigericin challenge stimulates pulmonary inflammation within fourteen hours, experiments involving silica require 7 to 14 days for pulmonary inflammation to be observed (Fang et al., 2017; Kato et al., 2017). Other pro-inflammatory cytokines such as KC and IL-12 are also released during pulmonary inflammation against silica (Dostert et al., 2008) and IAV (Tate et al., 2016). In contrast, the pro-inflammatory cytokine IL-6 was not secreted into the airways during intranasal nigericin challenge (Figure 5.2B). A longer treatment time with nigericin might be required to prolong pulmonary inflammation so that other pro-inflammatory cytokines such as IL-6 can be released.

Regardless, to my knowledge, this is the first instance of nigericin being intranasally administered to mice. Previous studies of nigericin have administered it intrapleurally (Burgy et al., 2016) or intraperitoneally (Stout-Delgado et al., 2012) into mice or given *ex vivo* to human lung tissue (Rotta

Detto Loria et al., 2013). Given that intranasal nigericin challenge produced prominent pulmonary inflammatory responses over a short period of time, the model could be used to simulate acute pulmonary inflammation. Importantly, the results show that the attachment of fluorescent tags to NLRP3 in NLRP3-CHCI mice does not prevent mice from exhibiting pulmonary inflammation against an exogenous substance such as nigericin, consistent with my earlier in vitro observations in the previous chapter.

Similar to intranasal nigericin challenge, intranasal LPS challenge promoted pulmonary inflammation with neutrophils infiltrating the lung and airways within three hours of administration (Figure 5.5A, Figure 5.6A). This is consistent with the notion that neutrophils are the first inflammatory cells to arrive at the injured or inflamed site, including the lung (Abraham, 2003). Intranasal LPS treatment also increased the airway concentrations of IL-6 (Figure 5.3B) but, unexpectedly, not IL-1β (Figure 5.3A). These results contradict previous studies which found that intranasal LPS challenge induced acute lung injury due to pulmonary inflammation. This pulmonary inflammation was associated with the infiltration of macrophages and neutrophils into the lung and the increase in BAL IL-1β, IL-6 and TNF-α concentrations, in part due to NLRP3 inflammasome activity (Jiang et al., 2013; Liu et al., 2016a; Zhang et al., 2016). The difference in results might be due to how mice were treated with LPS. In my experiments, LPS was given intranasally to mice while in previous studies, LPS was administered intratracheally (Liu et al., 2016a; Zhang et al., 2017a; Zhang et al., 2016). This may allow more LPS to enter the lung. Also, while mice in my experiment were only treated with LPS for 3 hours before they were euthanised, other studies have exposed mice to LPS for longer periods of time from 6 (Liu et al., 2016a) to 48 hours (Zhang et al., 2016). This may allow LPS to disperse throughout the lung over an extended period of time, promoting widespread lung injury. While IL-6 can be expressed and secreted shortly after LPS-induced NF-κB activation (Shurety et al., 2000), IL-1β and IL-18 secretion require exposure of cells to DAMPs indicating lung injury to activate the inflammasome and mature and secrete these cytokines (Chi et al., 2015). Future studies may treat mice with a higher dose of LPS for a longer period of time to induce more extensive pulmonary

inflammation, allowing the inflammasome to exert a broader influence on lung injury. Nevertheless, pulmonary inflammation could still be observed within a three-hour LPS challenge period indicating that NLRP3-CHCI mice are a valid tool to examine pulmonary inflammation.

While it has been widely reported that NLRP3 is very lowly, if at all, expressed in non-primed cells (Bauernfeind et al., 2009; Sutterwala et al., 2006), I observed that untreated BAL macrophages (Figure 5.6F) and lung DCs (Figure 5.5E) express NLRP3. The expression of NLRP3 in BAL macrophages is consistent with previous reports that macrophages express NLRP3 and have strong inflammasome activity following challenge (Bauernfeind et al., 2009; Luo et al., 2017). In contrast, NLRP3 was expressed in resting lung DCs (Figure 5.5E) but not in BAL DCs (Figure 5.6E). It is assumed that priming signals would upregulate NLRP3 in DCs (Arnold et al., 2017; Chang et al., 2017). However, a recent study which separated pBMDCs from pBMDMs after granulocyte-macrophage colony-stimulating factor (GM-CSF) culture of bone marrow cells found that pBMDCs neither expressed NLRP3 in the basal state nor upregulated NLRP3 when exposed to priming signals (Erlich et al., 2019) (Figure 2C-D of study). Conversely, splenic cDCs express a basal amount of NLRP3 which is upregulated by priming signals (Erlich et al., 2019) (Figure 5B of study). pBMDCs might not express or upregulate NLRP3 due to the sterile *in vitro* conditions that may impede expression or activation of the NLRP3 inflammasome. In contrast, tissue-resident DCs may express a basal level of NLRP3 as it continually senses for danger signals within the body or pathogen components or environmental agents from the external environment (Jahnsen et al., 2006; Sung et al., 2006). This may enable tissue-resident DCs to readily respond to infection or damage by engulfing antigens within the tissue and organ and secreting cytokines, possibly via the NLRP3 inflammasome. It would be interesting; therefore, to measure NLRP3 protein expression in different tissue-resident DC subsets and compare them to *in vitro*-grown pBMDCs.

It is worthy to note that myeloid-derived cells upregulated NLRP3 protein during LPS challenge (Figure 5.4K) but not non-myeloid-derived cells, including epithelial cells (Figure 5.4G-H, L-M).

Examining expression and activation of NLRP3 inflammasomes in vivo

Previous *in vitro* studies have found that AECs need to be incubated with LPS for 18 to 24 hours to upregulate *Nlrp3* mRNA and protein expression (Sebag et al., 2017; Tran et al., 2012). In an LPS-induced lung injury setting, the delay in NLRP3 inflammasome expression and activation in epithelial cells may indicate the later secretion of IL-1β from these cells. Nevertheless, epithelial cell-derived IL-1β may further promote pulmonary damage in LPS-induced lung injury that was initiated by myeloid-derived cells (Kim et al., 2015). Therefore, prolonging the LPS treatment time in mice may induce NLRP3 upregulation in respiratory epithelial cells so that more pronounced lung injury can be observed.

It is of considerable interest that of the lung and BAL myeloid-derived cell populations analysed, only the BAL macrophages, which represent alveolar macrophages, upregulated NLRP3 (Figure 5.6E). This is concordant with *in vitro* studies stating that alveolar macrophages increase *Nlrp3* mRNA and protein expression during LPS (Luo et al., 2017) or imiquimod (Peiró et al., 2017) treatment to activate TLRs. The small increase in NLRP3 protein expression in alveolar macrophages during LPS challenge matches the *in vitro* pBMDM results from the previous chapter where NLRP3 protein was only upregulated by a small amount following LPS priming. This indicates that the ten-fold increases in *Nlrp3* mRNA expression upon exposure to a priming signal may not translate to an equivalent increase in NLRP3 protein expression (Bauernfeind et al., 2009; Zhao et al., 2017).

Somewhat surprisingly, no other immune cell population upregulated NLRP3 during LPS challenge. Lung NK cells (Figure 5.4J), neutrophils (Figure 5.5G) and DCs (Figure 5.5H) reduced NLRP3 protein expression during LPS treatment. Presumably, this was not due to accelerated cell death during LPS challenge as lung cell counts increased during the experiment (Figure 5.3D). These results do not agree with previous studies that describe how NLRP3 upregulation and inflammasome activity are found in T cells (Eleftheriadis et al., 2015; Martin et al., 2016), neutrophils (Cho et al., 2012; Karmakar et al., 2015) and tissue-resident DCs (Erlich et al., 2019; Mulay et al., 2013).

Examining expression and activation of NLRP3 inflammasomes in vivo

Previous *in vitro* studies demonstrated that LPS administered in media can directly interact with TLR4 in cells to initiate the process of NF-κB activation (Sebag et al., 2017). NLRP3 was upregulated in BAL macrophages as alveolar macrophages reside in the alveolar air spaces (Breeze and Turk, 1984), enabling immediate response to LPS in the airways. In contrast, given the long period of time needed for LPS to induce acute lung injury (Liu et al., 2016a; Zhang et al., 2016), it is possible that prolonged LPS exposure is needed for LPS to enter lung tissue and interact with TLR4 on leukocytes within lung tissue to upregulate NLRP3. Hence, a longer LPS challenge may allow LPS to induce stronger pulmonary inflammation by interacting with TLR4 in more cells to upregulate NLRP3. Nevertheless, early pulmonary responses to LPS appear to be driven by alveolar macrophages consistent with their role as key sentinels of lung homeostasis (Mathie et al., 2015).

Similar to LPS challenge in the lung, myeloid-derived cells, which express NLRP3 in the basal state, upregulated NLRP3 during IAV infection (Figure 5.8F, K). In contrast, non-myeloid-derived (Figure 5.8G, L) and epithelial cells (Figure 5.8H, M) neither basally express NLRP3 nor upregulate NLRP3 during IAV infection. This result matched the very low levels of *Nlrp3* mRNA in untreated primary human AECs but not its upregulation during IAV infection (Allen et al., 2009; Hirota et al., 2012). One reason for this might be that NLRP3 was found in well-preserved cell bodies that budded off from the apical surface of the epithelium during ovalbumin-induced airway inflammation (Tran et al., 2012). Given that epithelial cells are the primary site of infection (Kebaabetswe et al., 2013; Matrosovich et al., 2004; Tate et al., 2011d) and are continually overturned (Soderberg et al., 1990), it is possible that epithelial cells with upregulated NLRP3 expression might be in the process of IAV-induced cell death and shedding. The remaining uninfected epithelial cells in the lung may not have yet upregulated NLRP3, explaining the absence of NLRP3 upregulation in lung non-myeloid-derived and epithelial cells during IAV infection.

Among leukocytes in the lung and airways, I observed that innate immune cells such as neutrophils (Figure 5.10G), inflammatory macrophages (Figure 5.9F, J, Figure 5.10F, J), DCs (Figure 5.9H,

Figure 5.10H) and NK cells (Figure 5.8J, O) upregulated NLRP3 during IAV infection. In contrast, NLRP3 is not upregulated in T lymphocytes (Figure 5.8I, N) and lung-resident and BAL macrophages (Figure 5.9E, I; Figure 5.10E, I). Nonetheless, compared to LPS challenge, IAV infection upregulated NLRP3 in more cell types; presumably because the kinetics of IAV infection and damage to the lung promote widespread pulmonary inflammation, activating more leukocytes.

The cells that upregulated NLRP3 during IAV infection have been previously shown to contribute to protective or detrimental responses to IAV infection. Neutrophils protect mice by phagocytosing IAV virions and producing ROS (Tate et al., 2008; Tate et al., 2009). Later in infection; however, neutrophils can contribute to the pathology of IAV infection by secreting NETs that damage the respiratory epithelium (Narasaraju et al., 2011; Sakai et al., 2000). NETs can also activate the NLRP3 inflammasome in human and murine macrophages, inducing IL-1β release (Kahlenberg et al., 2013). Interestingly, neutrophils themselves can activate the NLRP3 inflammasome, maturing and secreting IL-1β, when treated with LPS and soluble activators such as nigericin and ATP but not particulate activators such as alum and silica (Chen et al., 2016; Goldberg et al., 2017). The failure of neutrophils to activate the NLRP3 inflammasome against particulate activators was due to lysosomal rupture being a weak stimulus to NLRP3 inflammasome activation in neutrophils (Chen et al., 2016), suggesting that phagocytosis might be a determining factor in the degree of inflammasome activation. In the context of IAV infection, IAV virions may upregulate or activate the NLRP3 inflammasome in neutrophils via a phagocytosis-independent mechanism with viral RNA, M2 channel protein or an unidentified IAV component or cofactor.

It is well-accepted that inflammatory macrophages infiltrate the lung to limit primary viral pneumonia by secreting pro-inflammatory cytokines such as TNF-α to promote pulmonary inflammation (Lin et al., 2008; van Riel et al., 2011) and priming $CD4^+$ T cells to activate adaptive immune responses (Diao et al., 2014). Inflammatory macrophages are also known for their expression and hyper-secretion of various pro-inflammatory cytokines such as IL-1β, IL-6 and TNF-α during IAV infection

(Hui et al., 2009; Perrone et al., 2008). Importantly, inflammatory macrophages exhibit NLRP3 inflammasome activity, expressing, maturing and secreting substantial amounts of IL-1β and IL-18 (Shaw et al., 2014; Wu et al., 2013)**.** The resultant hyper-cytokinaemia drives inflammation and epithelium damage, contributing to pathology (Herold et al., 2008; van Riel et al., 2011). Given the upregulation of NLRP3 protein in inflammatory macrophages three days post-infection, a timepoint where the NLRP3 inflammasome plays a pathological role (Tate et al., 2016), inflammatory macrophages might have an NLRP3 inflammasome that promotes IL-1β and IL-18 hyper-secretion, contributing to pulmonary hyper-inflammation that causes lung injury.

Surprisingly, during IAV infection, NLRP3 was not upregulated in lung-resident macrophages in BAL samples (Figure 5.10E, I) and the lung (Figure 5.9E). These results contrast those of intranasal LPS challenge which upregulated NLRP3 in these cells (Figure 5.6F) and a previous study which found that HKx31 infection upregulated *Nlrp3, Il1β and caspase-1* mRNA in alveolar macrophages within 24 hours (Peiró et al., 2017). Given that mice were infected with influenza over a three-day period, it is possible that lung-resident macrophages exhibit NLRP3 inflammasome activity one to two days after infection but is then dampened beyond two days post-infection. This may imply that lung-resident macrophages may have an acute NLRP3 inflammasome response that is dampened in late-stage IAV infection. During this time, the majority of NLRP3 inflammasome activity in macrophages might be seen in the newly-infiltrated inflammatory macrophages.

During IAV infection, monocyte-derived and RDCs phagocytose IAV virions and IAV-infected cells to activate adaptive immune responses (Cruz et al., 2007; GeurtsvanKessel et al., 2008; Kim and Braciale, 2009). Monocyte-derived DCs also secrete a variety of cytokines and chemokines such as IL-1β and RANTES (Erlich et al., 2019; Hao et al., 2008) and express nitric oxide synthase 2 (NOS2) (Lin et al., 2008) during IAV infection, promoting a hyper-inflammatory response and lung injury. The upregulation of NLRP3 in lung (Figure 5.9H) and BAL DCs (Figure 5.10H) conforms to previous results that DCs secrete substantial amounts of IL-1β following viral infection such as HIV (Pontillo

et al., 2012). Therefore, it is possible that DCs may contribute to the pathophysiology of IAV infection by expressing and secreting pro-inflammatory proteins, including IL-1β, via an NLRP3 inflammasome-dependent mechanism, contributing to the pulmonary hyper-inflammatory state.

NK cells limit primary viral pneumonia by killing IAV-infected cells (Achdout et al., 2010; Glasner et al., 2012) and promoting cytotoxic T cell responses (Liu et al., 2018; Zamora et al., 2017). NK cells can also contribute to the pathology of lethal PR8 infection in mice (Abdul-Careem et al., 2012; Zhou et al., 2013), though the mechanisms behind this are unknown. In my experiments, I found that NLRP3 protein is expressed in untreated NK cells in the lung (Figure 5.4J). Previous studies on resting NK cells found that *Nlrp3* mRNA and protein are expressed in peripheral human NK cells (Qiu et al., 2011) but not splenic murine NK cells (Guarda et al., 2011). The various techniques used to measure NLRP3 expression in NK cells may explain the difference in results. Biochemical approaches were used by Qiu et al. (2011) to measure NLRP3 expression while Guarda et al. (2011) knocked-in a fluorescent protein into the *Nlrp3* locus to measure fluorescence intensity as a readout of NLRP3 expression. The conflict in results highlights the need for further experiments on NLRP3 expression in resting NK cells.

Nevertheless, I found that IAV infection upregulates NLRP3 in NK cells (Figure 5.8J, O). NK cells can secrete pro-inflammatory cytokines and chemokines such as IFN-γ, TNF-α and CCL2 (Almishri et al., 2016; Fauriat et al., 2010; Lauwerys et al., 2000; Qiu et al., 2011). In the context of IAV infection, this may suggest that NK cells could contribute to the hyper-cytokinaemia of IAV-induced pulmonary inflammation. Interestingly, peripheral human NK cells do not secrete IL-1β when exposed to a human K562 leukaemia cell line (Fauriat et al., 2010) which is inconsistent with NLRP3 upregulation in murine NK cells during IAV infection. The contrast in studies might be due to differences in how viral and cancerous activating signals may affect NLRP3 inflammasome expression and activity in NK cells. In terms of viral activating signals, there have been no studies on the role of the NLRP3 inflammasome in NK cells and how that may impact their responses against

IAV. Further research needs to be conducted to investigate the role of NLRP3 inflammasome activity in NK cell function and whether they may contribute to the protection or pathology of IAV infection.

Collectively, these results imply that specific innate immune cell populations that have upregulated NLRP3 during IAV infection might be candidates for a dual role of the inflammasome in IAV infection. This is made possible by the use of reporter mice which enable NLRP3 expression to be measured *in vivo* before and during IAV infection in multiple cell populations temporally, something that has not been examined in previous studies. It has previously been proposed that NLRP3 upregulation primes cells to assemble the inflammasome which is required for inflammasome activity (Bauernfeind et al., 2009). Given that mice were infected with IAV for three days, which we previously suggested might be the timepoint where the NLRP3 inflammasome transitions from a protective to a pathological role (Tate et al., 2016), the cell subsets that upregulate NLRP3 at this period would allow them to assemble inflammasome complexes upon exposure to PAMPs from IAV or DAMPs from lung injury. Priming of NLRP3, coinciding with presumed upregulated pro-IL-1β expression, from three days post-infection would therefore increase the capability of these cells to exhibit inflammasome activity that could contribute to IAV-induced pulmonary hyper-inflammation, causing morbidity and mortality. Future studies could further dissect the association between IAV infection, NLRP3 upregulation and activity in individual cells via immunofluorescence and FLIM-FRET of NLRP3-CHCI lung tissue with fluorescently-tagged IAV virions.

MCC950 is a small molecule inhibitor of the NLRP3 inflammasome, able to suppress inflammasome activity such as IL-1β and caspase-1 maturation (Coll et al., 2015). Our laboratory has previously used MCC950 to highlight a dual role of the NLRP3 inflammasome in IAV infection, adopting protective or pathological roles at different stages of IAV infection (Tate et al., 2016). How the administration of MCC950 influences the outcome of IAV infection *in vivo* is unknown, but it is possible that MCC950 could enter different cell populations at various stages of infection. I observed that MCC950 uptake in the lung peaked at 3 hours post-administration before it is cleared within 6

hours (Figure 5.11B). This is comparable to the plasma half-life of MCC950 which has been reported to be 3.27 hours upon oral or intravenous administration (Coll et al., 2015). Given the reduced IAV-induced inflammatory cell infiltration and airway cytokine secretion in mice 7 (Pinar et al., 2017) and 24 hours (Tate et al., 2016) after MCC950 administration, the short half-life of MCC950 does not seem to reduce the potency of MCC950 in inhibiting the downstream effects of NLRP3 inflammasome activity. MCC950's short half-life; though, may indicate the need for continual administration of the inhibitor into the lungs to limit pulmonary inflammation and prevent pulmonary damage during IAV infection. Conversely, the rapid clearance of MCC950 from the lung due to its short half-life could be beneficial in a clinical trial setting if administration of MCC950 needs to be halted due to unforeseen adverse events and reactions.

Furthermore, I found that MCC950 enters both myeloid and non-myeloid-derived populations of the uninfected lung (Figure 5.11B, Figure 5.12), implying that MCC950 can non-specifically enter any cell in the lung. This is possible because MCC950 is lipophilic, allowing it to pass through plasma membranes in tissue. It has previously been described that MCC950 can inhibit NLRP3 inflammasome activity in myeloid-derived cells such as macrophages and DCs (Coll et al., 2015; Gov et al., 2017; van der Heijden et al., 2017). More recently, MCC950 was also found to inhibit NLRP3 inflammasome activity in non-myeloid-derived cells of the human and mouse retina *in vitro* such as endothelial cells (Zhang et al., 2017b) and pigment epithelial cells (Wang et al., 2019), impeding macular degeneration. These results indicate that MCC950 may also inhibit NLRP3 inflammasome activity in non-myeloid-derived cells. Given that MCC950 was readily absorbed into lung epithelial cells (Figure 5.12), MCC950 might have the capacity to target NLRP3 inflammasome activity in these cells. Critically, these results demonstrate proof-of-concept that fluorescently-tagged MCC950 can be used to measure the duration at which MCC950 is retained in an organ and to identify MCC950 uptake in individual cell populations.

During IAV infection, while MCC950 uptake into non-myeloid-derived cells remained similar between one and three days post-infection (Figure 5.13B), MCC950 influx into myeloid-derived cells increased at three days post-infection (Figure 5.13C). This was due to increased MCC950 intake into inflammatory macrophages and neutrophils (Figure 5.14D-F) that appear days after infection (Tate et al., 2011c). In contrast, MCC950 uptake into lung-resident cells such as macrophages and DCs remained the same at both infection timepoints (Figure 5.14A-C). The results show a shift in MCC950 uptake from non-myeloid-derived cells and lung-resident leukocytes in the early stages of infection to infiltrating blood-derived inflammatory cells such as neutrophils in the later stages of infection.

This may explain the difference in prognosis of IAV infection via variations in the timing of MCC950 administration as described by Tate et al. (2016). If MCC950 was administered into mice from one day post-infection, MCC950 may suppress IL-1β secretion from non-myeloid-derived cells such as epithelial and endothelial cells (Kim et al., 2015) and lung-resident leukocytes such as alveolar macrophages (Peiró et al., 2017) and RDCs (Arae et al., 2018). This may blunt the initial pulmonary inflammatory response that is required to limit primary viral pneumonia, causing extensive lung damage which may lead to mortality (Thomas et al., 2009). However, from three days post-infection, there is an increase in infiltrating blood-derived leukocytes such as neutrophils and inflammatory macrophages into the lung (Tate et al., 2011b; Tate et al., 2016). These cells have been shown to upregulate NLRP3 (Figure 5.10F-G, J-K), a prerequisite to NLRP3 inflammasome activity. These cells may secrete IL-1β that may raise the IL-1β concentration above a threshold to promote hyper-cytokinaemia and a hyper-inflammatory response. Conversely, there may be a duality in the expression and maturation of IL-18 which may also play a protective or detrimental role. Administering MCC950 at this timepoint; therefore, may suppress excessive IL-1β and/or IL-18 secretion from infiltrating leukocytes, limiting pulmonary inflammation which may prolong survival. At the same time, some IL-1β secretion from lung-resident macrophages which did not upregulate NLRP3 in late-stage IAV infection (Figure 5.9E, I; Figure 5.10E, I) might be required to maintain a protective pulmonary inflammatory response to restrict viral replication. Therefore, there is still a

need to modify small molecule inhibitors to impede inflammasome activity in specific cell populations such as inflammatory macrophages that contribute to the pathology of late-stage IAV infection. Future research could study associations between small molecule inhibitor uptake and IAV-induced NLRP3 upregulation in cells by intranasally administering a fluorescently-tagged small molecule inhibitor into IAV-infected NLRP3-CHCI mice. The challenge would be in finding a fluorescent tag for the inhibitor that does not coincide with the emission spectra of mCitrine and mCherry.

In summary, I found that myeloid- but not non-myeloid-derived cells upregulated NLRP3 in *in vivo* pulmonary challenge models. Critically, NLRP3 was upregulated in cells such as inflammatory macrophages that are known to play a protective or pathological role in IAV infection. Fascinatingly, NK cells display upregulated NLRP3 expression despite the absence of previous studies showing inflammasome activity in these cells. Collectively, these findings open new lines of investigation on how the NLRP3 inflammasome functions in specific cell populations and how that may contribute to its dual roles in IAV infection.

Lastly, studies with MCC950-rhodamine indicated that MCC950 enters both myeloid- and non-myeloid-derived cells of the lung, where they may non-specifically inhibit inflammasome activity. Furthermore, the cells that MCC950 enters at different stages of IAV infection may explain how delayed administration of MCC950 blunts the hyper-inflammatory response in late-stage IAV that contributes to prolonged survival. Therefore, these studies identify that targeting NLRP3 inflammasome inhibitors to specific cellular subsets such as infiltrating macrophages or potentially NK cells may improve drug efficacy and specificity, targeting only ‘detrimental’ inflammasome activity. The NLRP3-CHCI mouse provides a suitable tool to investigate these possibilities. Overall, this chapter demonstrates how NLRP3-CHCI mice represent an important research tool to examine, characterise and visualise the expression and potential inhibitor association of different diseases *in vivo*.

6 General discussion

General discussion

The innate immune system and inflammation are designed to restrict the replication of pathogens, giving the adaptive immune system time to be activated and clear infection (Medzhitov and Janeway, 2000). However, excessive activation of innate immune and inflammatory pathways are causative factors to chronic diseases such as atherosclerosis (Swirski and Nahrendorf, 2013) and arthritis (Banda et al., 2003). The inflammasome is an integral sensor of the innate immune system that matures pro-inflammatory cytokines IL-1β and IL-18 (Dowds et al., 2004; Martinon et al., 2004) and stimulates pyroptosis, an inflammatory form of cell death (Kayagaki et al., 2015; Shi et al., 2015). The NLRP3 inflammasome is required for the clearance of bacterial pathogens such as *Staphylococcus aureus* (Mariathasan et al., 2006) and viruses such as IAV (Allen et al., 2009; Ichinohe et al., 2009; Thomas et al., 2009). However, the NLRP3 inflammasome is also linked to inflammatory diseases such as Alzheimer's disease (Heneka et al., 2013) and contributes to pathology in late-stage IAV infection (Tate et al., 2016). Hence, the NLRP3 inflammasome is a potential therapeutic target for limiting inflammation in infectious and inflammatory diseases.

In my project, I aimed to better understand the expression and mechanisms of activation of the NLRP3 inflammasome. Understanding the biology and mechanism of NLRP3 inflammasome expression and activity in health and disease and how it can be therapeutically targeted would significantly enhance our knowledge and understanding of the discipline. These aspects of NLRP3 inflammasome biology were studied using novel inflammasome reporter mice mCherry-ASC and NLRP3-CHCI. These mice express a full-length, native protein tagged with fluorescent proteins that allow the exploration of domain-domain interactions within the inflammasome component and measurement of protein expression at the single-cell level *in vitro and ex vivo*. The reporters are placed under the control of their native promoters, resulting in endogenous expression levels of the inflammasome component to remove the potential of off-target or non-specific effects due to overexpression. Collectively, these characteristics of both reporter mice allow us to study NLRP3 inflammasome expression and activity in a biologically-relevant model where ASC and NLRP3 are able to behave under native conditions.

General discussion

With these reporter mice, I discovered key information on the expression and activation of the NLRP3 inflammasome that has challenged the current knowledge of inflammasome biology. I was also able to track NLRP3 expression and upregulation in individual cell populations of the lung in different pulmonary inflammation models, particularly IAV infection. This provides detailed insights into the kinetics of inflammasome upregulation and the relationship with infiltrating cell populations during infection. Lastly, I demonstrated a proof-of-concept that inhibitor uptake into specific cell populations of the lung can be tracked with a fluorescent tag. These findings will form the framework towards exploring methods and models to improve targeting of the NLRP3 inflammasome that can be translated into disease therapies and strategies, particularly IAV infection.

The dogma relating to inflammasome activation is that all inflammasome components (i.e., sensor and adaptor proteins and inflammatory caspases) condense into an all-encompassing speck (reviewed in Broz and Dixit (2016); Elliott and Sutterwala (2015)). This paradigm is based upon studies using ASC reporter cells (Beilharz et al., 2016; Stutz et al., 2013) and mice (Sagoo et al., 2016; Tzeng et al., 2016) where overexpressed ASC oligomerises into one, large speck during inflammasome activation. Crucially, the formation of this all-inclusive speck has been linked to inflammasome function and dictates that the formation of the speck "licences" the inflammasome to mature caspase-1, IL-1β and IL-18. The limitation of these systems is that the reporters were overexpressed which may exaggerate the size of ASC specks. Given the prion capacity of ASC (Cheng et al., 2010; Franklin et al., 2014), overexpression of the reporter may "bias" formation towards an extra-ordinary multi-oligomeric structure. Inflammasome assembly has also been studied using recombinant proteins in cell-free systems where ASC filaments are formed (Dick et al., 2016; Lu et al., 2014; Nambayan et al., 2018). However, these studies often use truncated ASC constructs that may form different complexes from full-length ASC in cell-free systems where proteins that may influence inflammasome assembly have been removed. Interestingly; however, these models predominantly identified a less "structured" oligomeric structure, forming a multimeric signalling and enzymatic platform nucleated by a sensor protein such as NLRP3.

The findings from my studies have challenged this doctrine of inflammasome activation, where ASC and NLRP3 specks are not formed in an endogenous system. Crucially, cells from these reporter mice are still able to exhibit inflammasome activity as shown by their ability to activate caspase-1, mature IL-1β and undergo cell death. Moreover, NLRP3-CHCI mice were able to secrete comparable amounts of IL-1β into the airways as WT mice against exogenous compounds and pathogens such as nigericin and IAV respectively, implying that reporter mice are still able to exhibit inflammasome activation and pulmonary inflammation *in vivo.* Contrary to our generally accepted understanding of inflammasome biology; therefore, these results clearly demonstrate that at endogenous concentrations the formation of an all-encompassing speck is not a prerequisite for a functional inflammasome complex. It is feasible that multiple small inflammasome complexes within a cell may mature pro-inflammatory cytokines IL-1β and IL-18 and cleave gasdermin D to induce inflammation and pyroptosis respectively.

By expressing reporters in a cellular environment, regulatory proteins such as POPs and COPs are also able to control the number and size of inflammasome complexes. POPs and COPs bind to PYD and CARD domains respectively to restrict the size of ASC (de Almeida et al., 2015; Dorfleutner et al., 2007; Ratsimandresy et al., 2017) and caspase-1 (Lamkanfi et al., 2004; Lee et al., 2001; Lu et al., 2016) complexes respectively. A murine POP orthologue called PYDC3 was recently discovered to inhibit IL-1β secretion in murine pBMDMs (Vijay et al., 2017), suggesting inflammasome-inhibitory functions are conserved across species. These proteins were obviously absent in cell-free experimental systems (Gambin et al., 2018), and in overexpression systems the prion capacity of abundant ASC overwhelmed the regulatory capacity of native inhibitory proteins such as COPs and POPs (Cheng et al., 2010; Fernandes-Alnemri et al., 2007; Franklin et al., 2014). Endogenous expression of ASC and NLRP3 in our reporter mice may; therefore, allow regulatory proteins in the cell to effectively restrict the number and size of ASC and NLRP3 complexes, resulting in multiple small inflammasomes. This may explain why in some studies only a small amount of ASC and NLRP3 form multiple inflammasome foci within pBMDMs (Bryan et al., 2009; Green et al., 2018;

Subramanian et al., 2013). Consequently, the presence of multiple small inflammasome complexes within an inflammasome-activated cell in an endogenous setting may contribute to the absence of an all-encompassing speck seen in overexpression and cell-free studies.

In place of ASC speck formation, I observed NLRP3 unfolding in inflammasome-activated cells as shown by increased mCitrine fluorescence lifetimes in LPS and nigericin-treated NLRP3-CHCI pBMDMs using FRET analysis (Figure 4.18). This result is consistent with a previous study showing that inactive NLRP3 has the PYD domain folded onto its own NBD domain, acting as an auto-inhibitory domain. Following activation involving post-translational modifications such as deubiquitination (Palazon-Riquelme et al., 2018; Py et al., 2013) and dephosphorylation (Stutz et al., 2017), NLRP3 changes conformation so that the PYD domain no longer inhibits the NBD domain, exposing the latter (Hafner-Bratkovic et al., 2018), and allowing recruitment of downstream adaptor proteins such as ASC. Hence, NLRP3 unfolding could represent a new measure of inflammasome activation which could be useful for studying inflammasome biology and screening potential inflammasome activators and inhibitors. In the context of my project, I observed that NLRP3 appeared to unfold (i.e., reduce fluorescence lifetime) throughout the cytosol of the entire cell. This in itself contradicts previous findings that NLRP3 is localised to a specific area of the cell such as the microtubule-organising centre (Li et al., 2017) and the endoplasmic reticulum (Misawa et al., 2013) during inflammasome activation. However, it does concur with observations of multiple NLRP3 puncta in the cell during inflammasome activation (Chen and Chen, 2018; Stutz et al., 2017; Subramanian et al., 2013). Biologically, the diffuse pattern of NLRP3 unfolding, and hence activation, throughout the cell may lead to the establishment of numerous NLRP3 oligomers and recruitment of ASC, that may form multiple discrete inflammasome complexes distributed throughout the cell. This idea lends further credence to the absence of an all-encompassing speck in a cell and its requirement for biological activity.

These experimental results may; therefore, propose a new “amplification” model of inflammasome assembly, where only a small amount of NLRP3 is required to initiate inflammasome assembly and activation (Figure 6.1). In effect, it supports the unified polymerisation model of Lu et al. (2014) but incorporates the regulatory mechanisms of NLRP3 activation and absence of an unifying speck from my studies. Given that a diverse range of PAMPs and DAMPs can induce NLRP3 inflammasome assembly (reviewed in He et al. (2016)) and NLRP3’s role as a nucleating agent (Yu et al., 2006), the concentration and conformation of NLRP3 may be limiting factors in inflammasome assembly and activation with regulatory checkpoints to ensure the NLRP3 inflammasome is not inappropriately activated. These principles may also be applicable to other inflammasome complexes such as AIM2 and NLRP3 which have also been reported to undergo ASC-encompassing speck formation for biological activity.

Initially, NLRP3 is lowly expressed to prevent premature oligomerisation of NLRP3 and association with existing ASC oligomers (Compan et al., 2015; Green et al., 2018) (Figure 6.1A). NLRP3 is also ubiquitinated (Palazon-Riquelme et al., 2018; Py et al., 2013) and kept in an inactive conformation with its PYD domain folding onto its own NBD domain (Hafner-Bratkovic et al., 2018) to prevent oligomerisation (Figure 6.1A). Engagement of priming signals such as LPS with TLRs or cytokine receptors activate NF-κB, upregulating not only pro-IL-1β, pro-IL-18 and pro-caspase-1 but also NLRP3 (Bauernfeind et al., 2009; Franchi et al., 2009) (Figure 6.1B). This overcomes the checkpoint of low expression that blocks inflammasome assembly and activation.

However, this upregulation is insufficient because NLRP3 is still ubiquitinated and folded. Activating signals from inflammasome activators stimulate post-translational modifications on NLRP3 such as deubiquitination (Palazon-Riquelme et al., 2018; Py et al., 2013) and dephosphorylation (Stutz et al., 2017) (Figure 6.1C). This leads to NLRP3 unfolding which enables NLRP3 oligomer formation (Duncan et al., 2007; Hafner-Bratkovic et al., 2018; Subramanian et al., 2013) (Figure 6.1D).

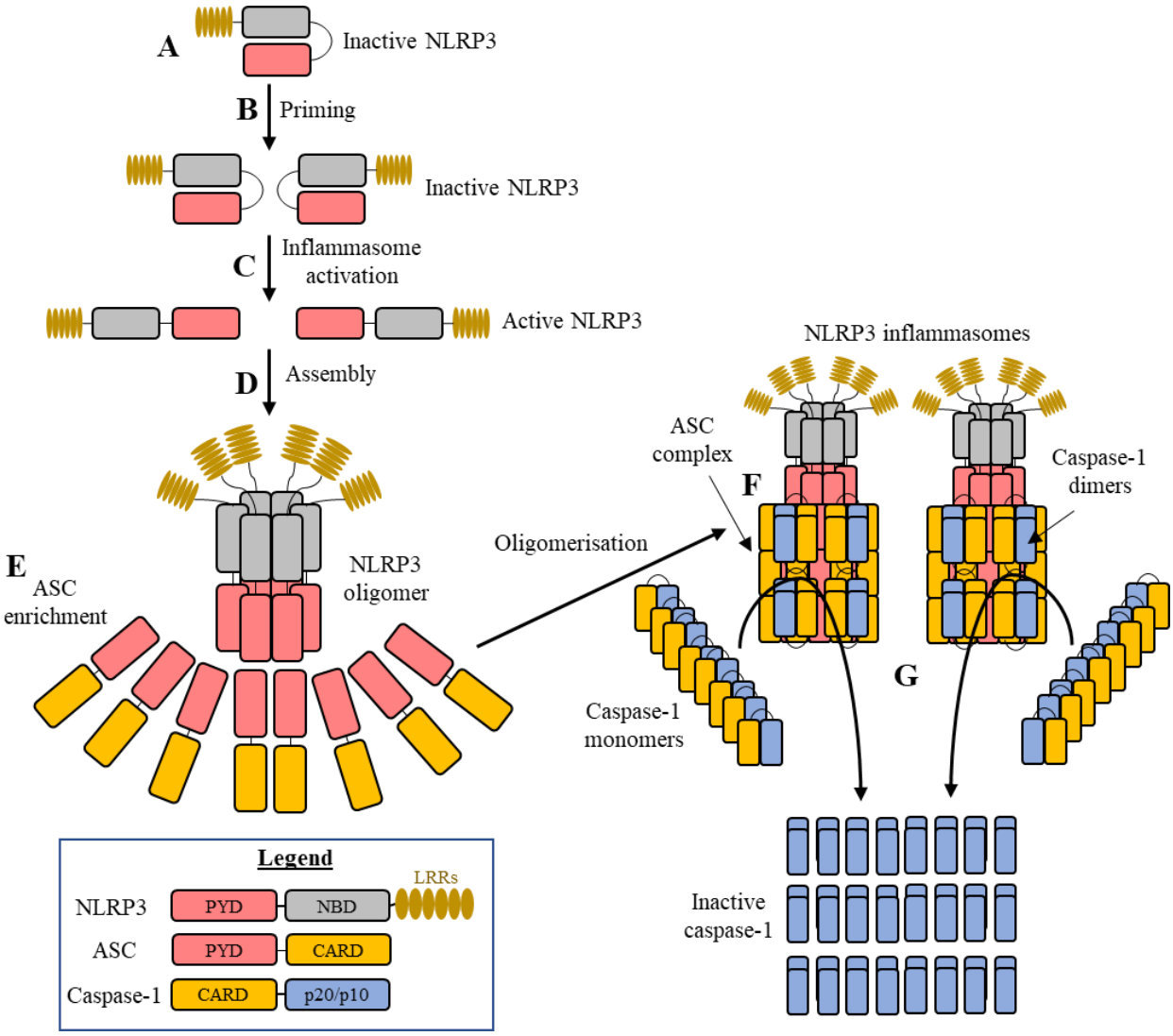

Figure 6.1: The "amplification" model of inflammasome assembly

NLRP3, in its folded conformation, is lowly expressed in untreated cells (A). During LPS priming, NLRP3 is upregulated but still maintains its folded conformation (B). NLRP3 is only unfolded in the presence of inflammasome activators such as nigericin (C), enabling NLRP3 to form an oligomer (D). The NLRP3 oligomer attracts ASC, forming an ASC-enriched area (E). Within the ASC-enriched area, ASC forms complexes across multiple NLRP3 oligomers (F). This enables numerous caspase-1 monomers to dimerise and form active caspase-1 before it is inactivated, allowing copious amounts of IL-1β and IL-18 to be matured (G).

Similar to NLRC4 oligomerisation (Halff et al., 2012; Hu et al., 2015), each NLRP3 oligomer only requires a small number of active, unfolded NLRP3, though that exact number needs to be defined in future experiments. What is important; though, is that inflammasome assembly does not require an all-encompassing NLRP3 speck but is rather mediated by the formation of multiple small NLRP3 oligomers.

The presence of multiple NLRP3 oligomers is sufficient to attract ASC to different points of the cell, forming an ASC-enriched area (Figure 6.1E). Within the ASC-enriched area, multiple ASC complexes are formed whose sizes are restricted by regulatory proteins such as POPs (de Almeida et al., 2015; Dorfleutner et al., 2007) (Figure 6.1F), thus disrupting all NLRP3 and ASC from participating in inflammasome assembly and restricts the size of inflammasome complexes, preventing formation of cross-links that lead to speck formation (Dick et al., 2016; Schmidt et al., 2016). Nevertheless, these ASC complexes are still able to recruit caspase-1 via their CARD domains to form active caspase-1 dimers to facilitate catalytic maturation of IL-1β and IL-18 (Lamkanfi et al., 2004; Lee et al., 2001; Lu et al., 2016) (Figure 6.1G).

Hence, from a small number of NLRP3 forming tiny NLRP3 oligomers, the response to a danger signal can be amplified by assembly of multiple inflammasome complexes involving larger amounts of ASC and caspase-1 proteins, increasing the surface area of the catalytic framework. This leads to maturation of pro-inflammatory cytokines IL-1β and IL-18 and pyroptosis to promote inflammation despite the absence of a single speck.

Our current understanding of NLRP3 expression centres upon its upregulation by priming signals such as LPS and TNF-α (Bauernfeind et al., 2009; Gurung et al., 2015). In my studies, I found that across the cell population, NLRP3 protein expression was only increased by around 30%. Although this is consistent with the less than 2-fold increase in NLRP3 protein expression upon exposure to priming signals (Guarda et al., 2011; Ramani and Awasthi, 2015), it is different from increases in *Nlrp3* mRNA expression which can be 10-fold or more during LPS treatment (Bauernfeind et al.,

2009; Zhao et al., 2017). These previous studies have used genomic and biochemical techniques such as RT-PCR and immunoblots that represent empirical population measurements of NLRP3 expression (Bauernfeind et al., 2009; Gurung et al., 2015). In contrast, I am able to examine and assess NLRP3 protein expression at the single-cell level by using fluorescence intensity, allowing cells that upregulate NLRP3 to be analysed separately.

Using NLRP3 upregulation as a measure of LPS responsiveness, I discovered that only around 20% of macrophages responded to LPS via upregulation of NLRP3. Inflammasome activation requires cells to be exposed to both priming and activating signals such as LPS and nigericin respectively (Bauernfeind et al., 2009; Faustin et al., 2007; Franchi et al., 2009). The low percentage of LPS-responsive cells may suggest an even smaller sample of cells exhibiting inflammasome activation upon exposure to activating signals, accounting for most if not all IL-1β and IL-18 secretion and pyroptosis. This suggests that initially, a small proportion of cells may be responsible for the totality of inflammasome-induced inflammation. Given the role of the inflammasome in disease and the pyrogenic properties of inflammasome substrates such as IL-1β, this mechanism may suggest another level of regulatory control on innate inflammation to restrict the risk of an exaggerated inflammatory response and damage to the host.

These observations are consistent with the concept of sentinel inflammasome sensing, where only a small proportion of super-secretory LPS-responsive cells is required to promote inflammation in a cell population where the majority secrete little or no cytokines (Xue et al., 2015). These super-secretory LPS-responsive cells, upon inflammasome activation, may secrete IL-1β which engages with IL-1R to activate NF-κB. This leads to the expression and secretion of pro-inflammatory cytokines from macrophages (Belisle et al., 2010) and endothelial cells (Kim et al., 2015) which may propagate hyper-cytokinaemia in a “feed-forward” inflammatory loop, leading to a hyper-inflammatory response (Antonioli et al., 2018). Given the capacity of this small subset to promote hyper-inflammatory responses against infection or tissue damage, identifying and targeting these cells

may constitute a therapeutic strategy in limiting inflammation by reducing their pro-inflammatory response and/or promoting anti-inflammatory functions such as IL-10 secretion.

A major aspect of my studies was the analysis and visualisation of inflammasome expression in specific cell populations from mice that have undergone homeostasis or disease. The advantage of this methodology is that any influences from the local cellular environment such as paracrine factors affecting inflammasome expression are reflected. For instance, within the healthy lung, alveolar macrophages basally expressed NLRP3 which is consistent with previous studies (Guarda et al., 2011; Luo et al., 2017) and their roles as sentinels of lung homeostasis (Mathie et al., 2015). RDCs also expressed basal NLRP3, a result previously described in tissue-resident DCs *in vivo* (Guarda et al., 2011) but not in pBMDCs *in vitro* (Erlich et al., 2019). Nevertheless, given the exposure of the respiratory epithelium to the external environment, PAMPs and DAMPs within the airways may engage PRRs in RDCs to maintain a basal level of NLRP3. Unexpectedly; however, was the basal expression of NLRP3 in pulmonary NK cells, something previously observed in resting peripheral human NK cells (Qiu et al., 2011) but not splenic murine NK cells (Guarda et al., 2011). Given that at present no study has investigated how the NLRP3 inflammasome affects the cytokine secretion and cytotoxicity of NK cells, this result opens a new line of investigation on the role of the NLRP3 inflammasome in NK cells. Collectively, these results highlight the potential of using reporter mice to screen various cell populations of different organs for basal NLRP3 expression.

By challenging reporter mice with different disease models, cell populations within a tissue or organ can be isolated and analysed for NLRP3 protein upregulation. Given that increased NLRP3 expression is a required event for inflammasome activation (Bauernfeind et al., 2009; Faustin et al., 2007; Franchi et al., 2009), upregulation of NLRP3 in specific cell populations may represent potential inflammasome activity. For instance, I used NLRP3-CHCI mice to distinguish the kinetics of inflammasome upregulation among various macrophage populations in different models of pulmonary inflammation. From there, small molecule inhibitors of the inflammasome could be

optimised to target specific cell populations that have upregulated an inflammasome component to control the level of inflammasome-dependent inflammation.

For example, I found that MCC950 enters cells from both myeloid and non-myeloid-derived cell populations in uninfected and IAV-infected lungs. In addition, while MCC950 entry into non-myeloid-derived cells remained constant at different stages of IAV infection, MCC950 uptake into myeloid-derived cells increased as IAV infection is prolonged due to the infiltration of inflammatory cells such as inflammatory macrophages and neutrophils. Combined with the possibility that super-secretory cells could propagate inflammation in a cell population, these results highlight the importance of optimising small molecule inhibitors that can target and impede inflammasome activity in specific cell subsets that contribute to the hyper-inflammatory state. These inhibitors could be used to treat a variety of infectious and inflammatory diseases. In the case of IAV infection, these inhibitors could provide a new way to treat severe IAV infection by modulating inflammasome-induced pulmonary inflammation to reduce lung injury. These inflammasome inhibitors could be administered in combination with with antivirals which restrict viral replication and promote virion clearance to improve survival and reduce disease severity as detailed in previous studies (Liu et al., 2012a; Zheng et al., 2008). To further this aim, future studies could challenge reporter mice with a fluorescently-tagged pathogen or exogenous substance with or without a small molecule inhibitor reporter. These studies would allow us to study intersections among host, pathogen and drug by investigating associations between inflammasome expression or activity, inhibitor uptake and/or disease pathogenesis. The results from these studies would assist in the optimisation of small molecule inhibitors as they would provide key insights into the kinetics, dynamics and mechanisms of host-pathogen interactions and potential therapeutic strategies.

The study; however, does present some potential limitations. Firstly, *in vitro* studies of endogenous inflammasome expression and assembly were conducted on pBMDMs as they represent the major and most widely characterised cells related to inflammasome activation (Bauernfeind et al., 2009;

Guarda et al., 2011). Hence, novel findings of inflammasome expression and assembly in the endogenous setting are currently only applicable to pBMDMs. Future studies could test the applicability of novel findings from *in vitro* experiments to other cell types that exhibit inflammasome activation such as neutrophils and NK cells. These studies could then be expanded to non-myeloid-derived cells such as keratinocytes that have previously been demonstrated to express NLRP3 and ASC and display inflammasome activation (Dai et al., 2017; Sand et al., 2018). However, these studies were beyond the scope of this investigation. The small sample sizes of some experiments may also be a limitation, although it is generally acceptable to conduct three biological and three independent experimental replicates to examine the research question (Masters et al., 2010a; Tate et al., 2016). Future studies could increase the sample size of some experiments, particularly those involving mice, to raise their statistical power, providing stronger evidence to confirm the veracity of the findings.

In conclusion, I have used novel inflammasome reporter mice to explore the expression and activation of the inflammasome in health and disease *in vitro* and *in vivo* in an endogenous setting. A crucial finding from my studies was the absence of an all-encompassing speck in functional inflammasomes. Instead, inflammasome activation was associated with the condensation or enrichment of ASC into an ASC-enriched area and the unfolding of NLRP3 diffusely within the cell. These findings fundamentally alter our understanding of inflammasome function and challenges the current dogma of inflammasome biology, predominantly based on overexpression models. I propose a new model whereby small discrete inflammasome complexes are formed throughout the cell that catalytically mature pro-inflammatory cytokines and induce pyroptosis. Furthermore, only a small group of LPS-responsive cells within the cell population are able to upregulate NLRP3, providing sentinel sensing of homeostatic dysregulation. Additionally, these reporter mice could be combined with models of homeostasis and pulmonary inflammation highlight the potential of using them to screen for the expression of inflammasome components across different cell populations in health and disease *in*

vivo. Cell populations that express and/or upregulate inflammasome components in homeostatic and/or challenged conditions may possess latent inflammasome activity.

Altogether, these studies support the use of novel inflammasome reporter cells and mice to examine the structure and function of the inflammasome *in vitro* and their role in health and disease *in vivo.* The results generated from these models will not only establish a new paradigm for inflammasome biology in an endogenous setting but will also become useful tools for investigating the role of the inflammasome in health and disease and how it can be therapeutically targeted.

7 Appendices

Appendix I: video legends

Video 3.1: live-cell imaging of mCherry-ASC pBMDMs treated with LPS and nigericin

mCherry-ASC pBMDMs were seeded in a Fluorodish at 2 x 10^4 cells 24 hours before the experiment. pBMDMs were primed with 100ng/mL LPS for 3 hours and stimulated with 10µM nigericin for 90 minutes. Z-stack images were taken on the Olympus FV1200 Laser Scanning Microscope at 400X magnification (oil-based objective) every 5 minutes for 90 minutes. The video was generated via deconvolution of z-stacks with maximum intensity projection for each timepoint on Fiji. Scale bar is 10µm. Video is representative of one of three independent experiments.

Video 3.2: live-cell imaging of mCherry-ASC pBMDMs treated with LPS and silica

mCherry-ASC pBMDMs were seeded in a Fluorodish at 4 x 104 cells 24 hours before the experiment. pBMDMs were primed with 100ng/mL LPS for 3 hours and stimulated with 150µg/mL silica for 3.5 hours. Z-stack images were taken on the Olympus FV1200 Laser Scanning Microscope at 400X magnification (oil-based objective) every 7.5 minutes for 3.5 hours. The video was generated via deconvolution of z-stacks with maximum intensity projection for each timepoint on Fiji. Scale bar is 10µm. Result is representative of two independent experiments.

Video 4.1: live-cell imaging of NLRP3-CHCI pBMDMs treated with LPS and nigericin

NLRP3-CHCI pBMDMs were seeded in a Fluorodish at 2 x 104 cells 24 hours before the experiment. pBMDMs were primed with 100ng/mL LPS for 3 hours before being stimulated with 30µM nigericin for 2 hours. Z-stack images were taken on the Olympus FV1200 Laser Scanning Microscope at 400X magnification (oil-based objective) every 5 minutes for 2 hours. The video was generated via deconvolution of z-stacks with maximum intensity projection for each timepoint on Fiji. Scale bar is 10µm. Video is representative of one of three independent experiments.

Video 4.2: live-cell imaging of NLRP3-CHCI pBMDMs treated with LPS and silica

NLRP3-CHCI pBMDMs were seeded in a Fluorodish at 4 x 104 cells 24 hours before the experiment. pBMDMs were primed with 100ng/mL LPS for 3 hours and stimulated with 150µg/mL silica for 4 hours. Z-stack images were taken on the Olympus FV1200 Laser Scanning Microscope at 400X magnification (oil-based objective) every 7.5 minutes for 4 hours. The video was generated via deconvolution of z-stacks with maximum intensity projection for each timepoint on Fiji. Scale bar is 10µm. Result is representative of two independent experiments.

Appendix II: cell stimulating reagents and inhibitors

Reagent	Catalogue number	Supplier	Distributor	Location
LPS from *E. coli* O55:B5	tlrl-b5lps	InVivoGen	Jomar Life Research	Carribean Park, VIC, Australia
Nigericin	tlrl-nig	InVivoGen	Jomar Life Research	Carribean Park, VIC, Australia
Silica	S5505	Sigma-Aldrich	Sigma-Aldrich Pty. Ltd.	Sydney, NSW, Australia
ATP	A2383	Sigma-Aldrich	Sigma-Aldrich Pty. Ltd.	Sydney, NSW, Australia
poly(dA:dT)	86828-69-5	InVivoGen	Jomar Life Research	Carribean Park, VIC, Australia
Lipofectamine 2000	11668-019	Life Technologies	Thermo Fisher Scientific Australia Pty. Ltd.	Scoresby, VIC, Australia

Appendix III: immunoblotting antibodies

Antibody	Catalogue number	Concentration	Isotype (Clone)	Dilution	Supplier	Distributor	Location
Anti-mouse caspase-1 monoclonal antibody	AG-20B-0042-C100	1mg/mL	Mouse monoclonal IgG1 (Casper-1)	1:1000	AdipoGen	Sapphire Bioscience Pty. Ltd.	Redfern, NSW, Australia
Anti-mouse NLRP3 monoclonal antibody	AG-20B-0014-C100	1mg/mL	Mouse monoclonal IgG2b (Cryo-2)	1:2000	AdipoGen	Sapphire Bioscience Pty. Ltd.	Redfern, NSW, Australia
Rabbit anti-ASC polyclonal antibody	AG-25B-0006-C100	1mg/mL	Rabbit polyclonal IgG	1:1000	AdipoGen	Sapphire Bioscience Pty. Ltd.	Redfern, NSW, Australia
Rabbit anti-GFP polyclonal antibody	A-11122	2mg/mL	Rabbit polyclonal IgG	1:2000	Thermo Fisher Scientific	Thermo Fisher Scientific Australia Pty. Ltd.	Scoresby, VIC, Australia
Anti-mouse β-actin monoclonal antibody	A2228	2mg/mL	Mouse monoclonal IgG2a (AC-74)	1:25000	Sigma-Aldrich	Sigma-Aldrich Pty. Ltd.	Sydney, NSW, Australia
Goat anti-mouse IL-1β-biotinylated antibody	BAF401	0.2mg/mL	Goat polyclonal IgG	1:2000	R&D Systems	Bio-Scientific Pty. Ltd.	Kirrawee, NSW, Australia
Rat anti-α-tubulin monoclonal antibody	ab6160	1mg/mL	Rat monoclonal IgG2a	1:1000	Abcam	Abcam	Melbourne, VIC, Australia

Rabbit anti-mouse IgG-HRP polyclonal antibody	P026002-2	1.3mg/mL	Rabbit polyclonal IgG	1:2000	Dako (part of Agilent)	Agilent Technologies Australia	Mulgrave, VIC, Australia
Goat anti-rabbit IgG-HRP polyclonal antibody	P044801-2	0.25mg/mL	Goat polyclonal IgG	1:2000	Dako (part of Agilent)	Agilent Technologies Australia	Mulgrave, VIC, Australia
Streptavidin -Alexa Fluor 680	S32358	2mg/ml	N/A	1:2000	Life Technologies	Thermo Fisher Scientific Australia Pty. Ltd.	Scoresby, VIC, Australia
Dylight 800-conjugated goat anti-rat IgG (H+L)	612-145-002	1mg/mL	Goat polyclonal IgG	1:6000	Rockland	Jomar Life Research	Carribean Park, VIC, Australia

Appendix IV: flow cytometry antibodies

Antibody	Catalogue number	Concentration	Isotype (Clone)	Dilution	Supplier	Distributor	Location
Anti-B220-FITC	553087	0.5 mg/ml	Monoclonal rat IgG2a (RA3-6B2)	1:200	BD	Becton Dickinson Pty. Ltd.	North Ryde, NSW, Australia
Anti-CD11c-FITC	553801	0.5 mg/ml	Monoclonal Armenian Hamster IgG1 (HL3)	1:200	BD	Becton Dickinson Pty. Ltd.	North Ryde, NSW, Australia
Anti-CD11c-PE	553802	0.5 mg/ml	Monoclonal Armenian Hamster IgG1 (HL3)	1:200	BD	Becton Dickinson Pty. Ltd.	North Ryde, NSW, Australia
Anti-CD3-PE	561824	0.2 mg/ml	Monoclonal Armenian Hamster IgG (145-2C11)	1:200	BD	Becton Dickinson Pty. Ltd.	North Ryde, NSW, Australia
Anti-CD45-APC	561880	0.2 mg/ml	Monoclonal rat IgG2a (30-F11)	1:200	BD	Becton Dickinson Pty. Ltd.	North Ryde, NSW, Australia
Anti-CD45-BV510	563103	0.2 mg/ml	Monoclonal rat IgG2a (30-F11)	1:200	BD	Becton Dickinson Pty. Ltd.	North Ryde, NSW, Australia
Anti-cytokeratin 18-FITC	MA1-10326	0.1 mg/mL	Mouse monoclonal IgG1 (C-04)	1:200	eBioscience	Thermo Fisher Scientific Australia Pty. Ltd.	Scoresby, VIC, Australia

Anti-EpCAM-APC	563478	0.2 mg/ml	Rat monoclonal IgG2a (G8.8)	1:200	BD	Becton Dickinson Pty. Ltd.	North Ryde, NSW, Australia
Anti-F4/80-biotin	13-4801-82	0.5 mg/mL	Rat monoclonal IgG2a (BM8)	1:200	eBioscience	Thermo Fisher Scientific Australia Pty. Ltd.	Scoresby, VIC, Australia
Anti-I-A^b-APC	562823	0.2 mg/ml	Mouse monoclonal IgG2a (AF6-120.1)	1:200	BD	Becton Dickinson Pty. Ltd.	North Ryde, NSW, Australia
Anti-I-A-biotin	553604	0.5 mg/ml	Mouse monoclonal IgG2a (25-9-17)	1:200	BD	Becton Dickinson Pty. Ltd.	North Ryde, NSW, Australia
Anti-Ly6C/Ly6G-Pac Blue	RM3028	0.2 mg/mL	Rat monoclonal IgG2b (RB6-8C5)	1:400	eBioscience	Thermo Fisher Scientific Australia Pty. Ltd.	Scoresby, VIC, Australia
Anti-Ly6C-APC	560595	0.2 mg/ml	Rat monoclonal IgM (AL-21)	1:400	BD	Becton Dickinson Pty. Ltd.	North Ryde, NSW, Australia
Anti-Ly6C-FITC	561085	0.5 mg/mL	Rat monoclonal IgM (AL-21)	1:400	BD	Becton Dickinson Pty. Ltd.	North Ryde, NSW, Australia
Anti-Ly6G-APC	17-9668-82	0.2 mg/mL	Rat monoclonal IgG2a (1A8-Ly6g)	1:400	eBioscience	Thermo Fisher Scientific Australia Pty. Ltd.	Scoresby, VIC, Australia
Anti-Ly6G-PE	561104	0.2 mg/mL	Rat monoclonal IgG2a (1A8)	1:400	BD	Becton Dickinson Pty. Ltd.	North Ryde, NSW, Australia

Anti-NK1.1-biotin	553163	0.5 mg/ml	Mouse monoclonal IgG2a (PK136)	1:200	BD	Becton Dickinson Pty. Ltd.	North Ryde, NSW, Australia
Strep-APC	17-4317-82	0.2 mg/mL	-	1:200	eBioscience	Thermo Fisher Scientific Australia Pty. Ltd.	Scoresby, VIC, Australia
Strep-APC-Cy7	554063	0.2 mg/ml	-	1:200	BD	Becton Dickinson Pty. Ltd.	North Ryde, NSW, Australia
Strep-PE	554061	0.5 mg/ml	-	1:200	BD	Becton Dickinson Pty. Ltd.	North Ryde, NSW, Australia

8 References

References

A-Gonzalez, N., Bensinger, S.J., Hong, C., Beceiro, S., Bradley, M.N., Zelcer, N., Deniz, J., Ramirez, C., Díaz, M., Gallardo, G., *et al.* (2009). Apoptotic cells promote their own clearance and immune tolerance through activation of LXR. Immunity *31*, 245-258.

Abbate, A., Salloum, F.N., Vecile, E., Das, A., Hoke, N.N., Straino, S., Biondi-Zoccai, G.G., Houser, J.E., Qureshi, I.Z., Ownby, E.D., *et al.* (2008). Anakinra, a recombinant human interleukin-1 receptor antagonist, inhibits apoptosis in experimental acute myocardial infarction. Circulation *117*, 2670-2683.

Abderrazak, A., Syrovets, T., Couchie, D., El Hadri, K., Friguet, B., Simmet, T., and Rouis, M. (2015). NLRP3 inflammasome: From a danger signal sensor to a regulatory node of oxidative stress and inflammatory diseases. Redox Biology *4*, 296-307.

Abdul-Careem, M.F., Mian, M.F., Yue, G., Gillgrass, A., Chenoweth, M.J., Barra, N.G., Chew, M.V., Chan, T., Al-Garawi, A.A., Jordana, M., and Ashkar, A.A. (2012). Critical Role of Natural Killer Cells in Lung Immunopathology During Influenza Infection in Mice. J. Infect. Dis. *206*, 167-177.

Abraham, E. (2003). Neutrophils and acute lung injury. Crit. Care Med. *31*, S195-199.

Achdout, H., Meningher, T., Hirsh, S., Glasner, A., Bar-On, Y., Gur, C., Porgador, A., Mendelson, M., Mandelboim, M., and Mandelboim, O. (2010). Killing of Avian and Swine Influenza Virus by Natural Killer Cells. J. Virol. *84*, 3993-4001.

Aglietti, R.A., Estevez, A., Gupta, A., Ramirez, M.G., Liu, P.S., Kayagaki, N., Ciferri, C., Dixit, V.M., and Dueber, E.C. (2016). GsdmD p30 elicited by caspase-11 during pyroptosis forms pores in membranes. Proc. Natl. Acad. Sci. U. S. A. *113*, 7858-7863.

Agostini, L., Martinon, F., Burns, K., McDermott, M.F., Hawkins, P.N., and Tschopp, J. (2004). NALP3 Forms an IL-1β-Processing Inflammasome with Increased Activity in Muckle-Wells Autoinflammatory Disorder. Immunity *20*, 319-325.

Agrawal, A., and Pulendran, B. (2004). Anthrax lethal toxin: a weapon of multisystem destruction. Cell. Mol. Life Sci. *61*, 2859-2865.

Akinbi, H.T., Epaud, R., Bhatt, H., and Weaver, T.E. (2000). Bacterial killing is enhanced by expression of lysozyme in the lungs of transgenic mice. J. Immunol. *165*, 5760-5766.

Aksentijevich, I., D. Putnam, C., Remmers, E.F., Mueller, J.L., Le, J., Kolodner, R.D., Moak, Z., Chuang, M., Austin, F., Goldbach-Mansky, R., *et al.* (2007). The clinical continuum of cryopyrinopathies: Novel CIAS1 mutations in North American patients and a new cryopyrin model. Arthritis Rheum. *56*, 1273-1285.

Aksentijevich, I., Nowak, M., Mallah, M., Chae, J.J., Watford, W.T., Hofmann, S.R., Stein, L., Russo, R., Goldsmith, D., Dent, P., *et al.* (2002). De novo CIAS1 mutations, cytokine activation, and evidence for genetic heterogeneity in patients with neonatal-onset multisystem inflammatory disease (NOMID): A new member of the expanding family of pyrin-associated autoinflammatory diseases. Arthritis Rheum. *46*, 3340-3348.

References

Alberts, R., Srivastava, B., Wu, H., Viegas, N., Geffers, R., Klawonn, F., Novoselova, N., Zaverucha do Valle, T., Panthier, J.-J., and Schughart, K. (2010). Gene expression changes in the host response between resistant and susceptible inbred mouse strains after influenza A infection. Microbes and Infection *12*, 309-318.

Alexopoulou, L., Holt, A.C., Medzhitov, R., and Flavell, R.A. (2001). Recognition of double-stranded RNA and activation of NF-kappaB by Toll-like receptor 3. Nature *413*, 732-738.

Allen, I.C., Scull, M.A., Moore, C.B., Holl, E.K., McElvania-TeKippe, E., Taxman, D.J., Guthrie, E.H., Pickles, R.J., and Ting, J.P.Y. (2009). The NLRP3 inflammasome mediates in vivo innate immunity to influenza A virus through recognition of viral RNA. Immunity *30*, 556-565.

Almishri, W., Santodomingo-Garzon, T., Le, T., Stack, D., Mody, C.H., and Swain, M.G. (2016). TNFα Augments Cytokine-Induced NK Cell IFNγ Production through TNFR2. J. Innate Immun. *8*, 617-629.

Amano, F., and Akamatsu, Y. (1991). A lipopolysaccharide (LPS)-resistant mutant isolated from a macrophagelike cell line, J774.1, exhibits an altered activated-macrophage phenotype in response to LPS. Infect. Immun. *59*, 2166-2174.

Ank, N., and Paludan, S.R. (2009). Type III IFNs: New layers of complexity in innate antiviral immunity. Biofactors *35*, 82-87.

Ank, N., West, H., Bartholdy, C., Eriksson, K., Thomsen, A.R., and Paludan, S.R. (2006). Lambda Interferon (IFN-λ), a Type III IFN, Is Induced by Viruses and IFNs and Displays Potent Antiviral Activity against Select Virus Infections In Vivo. J. Virol. *80*, 4501-4509.

Antonioli, L., Blandizzi, C., Pacher, P., Guilliams, M., and Haskó, G. (2018). Quorum sensing in the immune system. Nature Reviews Immunology *18*, 537-538.

Aoki, F.Y., Macleod, M.D., Paggiaro, P., Carewicz, O., El Sawy, A., Wat, C., Griffiths, M., Waalberg, E., and Ward, P. (2003). Early administration of oral oseltamivir increases the benefits of influenza treatment. J. Antimicrob. Chemother. *51*, 123-129.

Arae, K., Morita, H., Unno, H., Motomura, K., Toyama, S., Okada, N., Ohno, T., Tamari, M., Orimo, K., Mishima, Y., *et al.* (2018). Chitin promotes antigen-specific Th2 cell-mediated murine asthma through induction of IL-33-mediated IL-1β production by DCs. Sci. Rep. *8*, 11721-11721.

Arankalle, V.A., Lole, K.S., Arya, R.P., Tripathy, A.S., Ramdasi, A.Y., Chadha, M.S., Sangle, S.A., and Kadam, D.B. (2010). Role of Host Immune Response and Viral Load in the Differential Outcome of Pandemic H1N1 (2009) Influenza Virus Infection in Indian Patients. PLoS One *5*, e13099.

Arend, W.P., Palmer, G., and Gabay, C. (2008). IL-1, IL-18, and IL-33 families of cytokines. Immunol. Rev. *223*, 20-38.

Aries, A., Whitcomb, J., Shao, W., Komati, H., Saleh, M., and Nemer, M. (2014). Caspase-1 cleavage of transcription factor GATA4 and regulation of cardiac cell fate. Cell Death Dis. *5*, e1566.

References

Armstrong, S.M., Wang, C., Tigdi, J., Si, X., Dumpit, C., Charles, S., Gamage, A., Moraes, T.J., and Lee, W.L. (2012). Influenza Infects Lung Microvascular Endothelium Leading to Microvascular Leak: Role of Apoptosis and Claudin-5. PLoS One *7*, e47323.

Arnold, I.C., Zhang, X., Urban, S., Artola-Borán, M., Manz, M.G., Ottemann, K.M., and Müller, A. (2017). NLRP3 Controls the Development of Gastrointestinal CD11b+ Dendritic Cells in the Steady State and during Chronic Bacterial Infection. Cell Reports *21*, 3860-3872.

Ashley, N.T., Weil, Z.M., and Nelson, R.J. (2012). Inflammation: Mechanisms, Costs, and Natural Variation. Annu. Rev. Ecol. Evol. Syst. *43*, 385-406.

Asselin-Paturel, C., Boonstra, A., Dalod, M., Durand, I., Yessaad, N., Dezutter-Dambuyant, C., Vicari, A., O'Garra, A., Biron, C., Briere, F., and Trinchieri, G. (2001). Mouse type I IFN-producing cells are immature APCs with plasmacytoid morphology. Nat. Immunol. *2*, 1144-1150.

Bae, J.Y., and Park, H.H. (2011). Crystal Structure of NALP3 Protein Pyrin Domain (PYD) and Its Implications in Inflammasome Assembly. J. Biol. Chem. *286*, 39528-39536.

Baker, P.J., Boucher, D., Bierschenk, D., Tebartz, C., Whitney, P.G., D'Silva, D.B., Tanzer, M.C., Monteleone, M., Robertson, A.A., Cooper, M.A., *et al.* (2015). NLRP3 inflammasome activation downstream of cytoplasmic LPS recognition by both caspase-4 and caspase-5. Eur. J. Immunol. *45*, 2918-2926.

Banda, N.K., Vondracek, A., Kraus, D., Dinarello, C.A., Kim, S.H., Bendele, A., Senaldi, G., and Arend, W.P. (2003). Mechanisms of inhibition of collagen-induced arthritis by murine IL-18 binding protein. J. Immunol. *170*, 2100-2105.

Baranovich, T., Bahl, J., Marathe, B.M., Culhane, M., Stigger-Rosser, E., Darnell, D., Kaplan, B.S., Lowe, J.F., Webby, R.J., and Govorkova, E.A. (2015). Influenza A viruses of swine circulating in the United States during 2009–2014 are susceptible to neuraminidase inhibitors but show lineage-dependent resistance to adamantanes. Antiviral Res. *117*, 10-19.

Barnich, N., Aguirre, J.E., Reinecker, H.-C., Xavier, R., and Podolsky, D.K. (2005). Membrane recruitment of NOD2 in intestinal epithelial cells is essential for nuclear factor–κB activation in muramyl dipeptide recognition. The Journal of Cell Biology *170*, 21-26.

Baroja-Mazo, A., Martin-Sanchez, F., Gomez, A.I., Martinez, C.M., Amores-Iniesta, J., Compan, V., Barbera-Cremades, M., Yague, J., Ruiz-Ortiz, E., Anton, J., *et al.* (2014). The NLRP3 inflammasome is released as a particulate danger signal that amplifies the inflammatory response. Nat. Immunol. *15*, 738-748.

Barsness, K.A., Bensard, D.D., Partrick, D.A., Calkins, C.M., Hendrickson, R.J., Banerjee, A., and McIntyre, R.C. (2004). IL-1β induces an exaggerated pro- and anti-inflammatory response in peritoneal macrophages of children compared with adults. Pediatr. Surg. Int. *20*, 238-242.

Bauernfeind, F.G., Horvath, G., Stutz, A., Alnemri, E.S., MacDonald, K., Speert, D., Fernandes-Alnemri, T., Wu, J., Monks, B.G., Fitzgerald, K.A., *et al.* (2009). Cutting Edge: NF-κB Activating

References

Pattern Recognition and Cytokine Receptors License NLRP3 Inflammasome Activation by Regulating NLRP3 Expression. The Journal of Immunology *183*, 787-791.

Bedoui, S., Whitney, P.G., Waithman, J., Eidsmo, L., Wakim, L., Caminschi, I., Allan, R.S., Wojtasiak, M., Shortman, K., Carbone, F.R., *et al.* (2009). Cross-presentation of viral and self antigens by skin-derived CD103+ dendritic cells. Nat. Immunol. *10*, 488-495.

Beilharz, M., De Nardo, D., Latz, E., and Franklin, B.S. (2016). Measuring NLR Oligomerization II: Detection of ASC Speck Formation by Confocal Microscopy and Immunofluorescence. In NLR Proteins: Methods and Protocols, F. Di Virgilio, and P. Pelegrín, eds. (New York, NY: Springer New York), pp. 145-158.

Belisle, S.E., Tisoncik, J.R., Korth, M.J., Carter, V.S., Proll, S.C., Swayne, D.E., Pantin-Jackwood, M., Tumpey, T.M., and Katze, M.G. (2010). Genomic profiling of tumor necrosis factor alpha (TNF-α) receptor and interleukin-1 receptor knockout mice reveals a link between TNF-α signaling and increased severity of 1918 pandemic influenza virus infection. J. Virol. *84*, 12576-12588.

Belser, J.A., Bridges, C.B., Katz, J.M., and Tumpey, T.M. (2009). Past, Present, and Possible Future Human Infection with Influenza Virus A Subtype H7. Emerg. Infect. Dis. *15*, 859-865.

Belser, J.A., Gustin, K.M., Pearce, M.B., Maines, T.R., Zeng, H., Pappas, C., Sun, X., Carney, P.J., Villanueva, J.M., Stevens, J., *et al.* (2013). Pathogenesis and transmission of avian influenza A (H7N9) virus in ferrets and mice. Nature *501*, 556-559.

Benitez, A.A., Panis, M., Xue, J., Varble, A., Shim, J.V., Frick, A.L., López, C.B., Sachs, D., and TenOever, B.R. (2015). InVivo RNAi Screening Identifies MDA5 as a Significant Contributor to the Cellular Defense against Influenza A Virus. Cell Reports.

Bermejo-Martin, J.F., Martin-Loeches, I., Rello, J., Antón, A., Almansa, R., Xu, L., Lopez-Campos, G., Pumarola, T., Ran, L., Ramirez, P., *et al.* (2010). Host adaptive immunity deficiency in severe pandemic influenza. Critical Care *14*, R167.

Bermejo-Martin, J.F., Ortiz de Lejarazu, R., Pumarola, T., Rello, J., Almansa, R., Ramírez, P., Martin-Loeches, I., Varillas, D., Gallegos, M.C., Serón, C., *et al.* (2009). Th1 and Th17 hypercytokinemia as early host response signature in severe pandemic influenza. Critical Care *13*, R201-R201.

Beutler, B. (2004). Innate immunity: an overview. Mol. Immunol. *40*, 845-859.

Bianchi, M.E. (2007). DAMPs, PAMPs and alarmins: all we need to know about danger. J. Leukoc. Biol. *81*, 1-5.

Black, R.A., Kronheim, S.R., Merriam, J.E., March, C.J., and Hopp, T.P. (1989). A pre-aspartate-specific protease from human leukocytes that cleaves pro-interleukin-1 beta. J. Biol. Chem. *264*, 5323-5326.

References

Boucher, D., Monteleone, M., Coll, R.C., Chen, K.W., Ross, C.M., Teo, J.L., Gomez, G.A., Holley, C.L., Bierschenk, D., Stacey, K.J., *et al.* (2018). Caspase-1 self-cleavage is an intrinsic mechanism to terminate inflammasome activity. The Journal of Experimental Medicine *215*, 827-840.

Bouvier, N.M., and Lowen, A.C. (2010). Animal Models for Influenza Virus Pathogenesis and Transmission. Viruses *2*, 1530-1563.

Bowdish, D.M., Davidson, D.J., and Hancock, R.E. (2005). A re-evaluation of the role of host defence peptides in mammalian immunity. Current protein & peptide science *6*, 35-51.

Boyden, E.D., and Dietrich, W.F. (2006). Nalp1b controls mouse macrophage susceptibility to anthrax lethal toxin. Nat. Genet. *38*, 240-244.

Breeze, R., and Turk, M. (1984). Cellular structure, function and organization in the lower respiratory tract. Environ. Health Perspect. *55*, 3-24.

Brennan, M.A., and Cookson, B.T. (2000). Salmonella induces macrophage death by caspase-1-dependent necrosis. Mol. Microbiol. *38*, 31-40.

Brinkmann, V., Reichard, U., Goosmann, C., Fauler, B., Uhlemann, Y., Weiss, D.S., Weinrauch, Y., and Zychlinsky, A. (2004). Neutrophil extracellular traps kill bacteria. Science *303*, 1532-1535.

Briscoe, J., Rogers, N.C., Witthuhn, B.A., Watling, D., Harpur, A.G., Wilks, A.F., Stark, G.R., Ihle, J.N., and Kerr, I.M. (1996). Kinase-negative mutants of JAK1 can sustain interferon-gamma-inducible gene expression but not an antiviral state. EMBO J. *15*, 799-809.

Brown, E.G. (1990). Increased virulence of a mouse-adapted variant of influenza A/FM/1/47 virus is controlled by mutations in genome segments 4, 5, 7, and 8. J. Virol. *64*, 4523-4533.

Broz, P., and Dixit, V.M. (2016). Inflammasomes: mechanism of assembly, regulation and signalling. Nature Reviews Immunology *16*, 407-420.

Broz, P., Newton, K., Lamkanfi, M., Mariathasan, S., Dixit, V.M., and Monack, D.M. (2010a). Redundant roles for inflammasome receptors NLRP3 and NLRC4 in host defense against Salmonella. J. Exp. Med. *207*, 1745-1755.

Broz, P., von Moltke, J., Jones, J.W., Vance, R.E., and Monack, D.M. (2010b). Differential requirement for Caspase-1 autoproteolysis in pathogen-induced cell death and cytokine processing. Cell host & microbe *8*, 471-483.

Bryan, N.B., Dorfleutner, A., Rojanasakul, Y., and Stehlik, C. (2009). Activation of inflammasomes requires intracellular redistribution of the apoptotic speck-like protein containing a caspase recruitment domain (ASC). Journal of immunology (Baltimore, Md. : 1950) *182*, 3173-3182.

Bryant, C.E., Orr, S., Ferguson, B., Symmons, M.F., Boyle, J.P., and Monie, T.P. (2015). International Union of Basic and Clinical Pharmacology. XCVI. Pattern recognition receptors in health and disease. Pharmacol. Rev. *67*, 462-504.

References

Buchweitz, J.P., Harkema, J.R., and Kaminski, N.E. (2007). Time-dependent airway epithelial and inflammatory cell responses induced by influenza virus A/PR/8/34 in C57BL/6 mice. Toxicol. Pathol. *35*, 424-435.

Bulau, A.M., Nold, M.F., Li, S., Nold-Petry, C.A., Fink, M., Mansell, A., Schwerd, T., Hong, J., Rubartelli, A., Dinarello, C.A., and Bufler, P. (2014). Role of caspase-1 in nuclear translocation of IL-37, release of the cytokine, and IL-37 inhibition of innate immune responses. Proc. Natl. Acad. Sci. U. S. A. *111*, 2650-2655.

Bürckstümmer, T., Baumann, C., Blüml, S., Dixit, E., Dürnberger, G., Jahn, H., Planyavsky, M., Bilban, M., Colinge, J., Bennett, K.L., and Superti-Furga, G. (2009). An orthogonal proteomic-genomic screen identifies AIM2 as a cytoplasmic DNA sensor for the inflammasome. Nat. Immunol. *10*, 266-272.

Burgy, O., Bellaye, P.S., Causse, S., Beltramo, G., Wettstein, G., Boutanquoi, P.M., Goirand, F., Garrido, C., and Bonniaud, P. (2016). Pleural inhibition of the caspase-1/IL-1beta pathway diminishes profibrotic lung toxicity of bleomycin. Respir. Res. *17*, 162.

Bursch, L.S., Wang, L., Igyarto, B., Kissenpfennig, A., Malissen, B., Kaplan, D.H., and Hogquist, K.A. (2007). Identification of a novel population of Langerin+ dendritic cells. The Journal of Experimental Medicine *204*, 3147-3156.

Campbell, G.M., Nicol, M.Q., Dransfield, I., Shaw, D.J., Nash, A.A., and Dutia, B.M. (2015). Susceptibility of bone marrow-derived macrophages to influenza virus infection is dependent on macrophage phenotype. J. Gen. Virol. *96*, 2951-2960.

Cassel, S.L., Eisenbarth, S.C., Iyer, S.S., Sadler, J.J., Colegio, O.R., Tephly, L.A., Carter, A.B., Rothman, P.B., Flavell, R.A., and Sutterwala, F.S. (2008). The Nalp3 inflammasome is essential for the development of silicosis. Proceedings of the National Academy of Sciences *105*, 9035-9040.

Cassidy, L.F., Lyles, D.S., and Abramson, J.S. (1988). Synthesis of viral proteins in polymorphonuclear leukocytes infected with influenza A virus. J. Clin. Microbiol. *26*, 1267-1270.

Ceballos-Olvera, I., Sahoo, M., Miller, M.A., del Barrio, L., and Re, F. (2011). Inflammasome-dependent Pyroptosis and IL-18 Protect against Burkholderia pseudomallei Lung Infection while IL-1β Is Deleterious. PLoS Pathog. *7*, e1002452.

Cerretti, D.P., Kozlosky, C.J., Mosley, B., Nelson, N., Ness, K.V., Greenstreet, T.A., March, C.J., Kronheim, S.R., Druck, T., Cannizzaro, L.A., *et al.* (1992). Molecular Cloning of the Interleukin- 1β Converting Enzyme. Science *256*, 97-100.

Chakrabarti, A., Banerjee, S., Franchi, L., Loo, Y.M., Gale, M., Jr., Nunez, G., and Silverman, R.H. (2015). RNase L activates the NLRP3 inflammasome during viral infections. Cell host & microbe *17*, 466-477.

Chalkiadaki, A., and Guarente, L. (2012). High-fat diet triggers inflammation-induced cleavage of SIRT1 in adipose tissue to promote metabolic dysfunction. Cell Metab. *16*, 180-188.

References

Chamaillard, M., Hashimoto, M., Horie, Y., Masumoto, J., Qiu, S., Saab, L., Ogura, Y., Kawasaki, A., Fukase, K., Kusumoto, S., *et al.* (2003). An essential role for NOD1 in host recognition of bacterial peptidoglycan containing diaminopimelic acid. Nat. Immunol. *4*, 702-707.

Chan, M.C., Chan, R.W., Yu, W.C., Ho, C.C., Chui, W.H., Lo, C.K., Yuen, K.M., Guan, Y.I., Nicholls, J.M., and Peiris, J.S. (2009). Influenza H5N1 virus infection of polarized human alveolar epithelial cells and lung microvascular endothelial cells. Respir. Res. *10*, 102.

Chan, M.C., Cheung, C.Y., Chui, W.H., Tsao, S.W., Nicholls, J.M., Chan, Y.O., Chan, R.W., Long, H.T., Poon, L.L., Guan, Y., and Peiris, J.S. (2005a). Proinflammatory cytokine responses induced by influenza A (H5N1) viruses in primary human alveolar and bronchial epithelial cells. Respir. Res. *6*, 135.

Chan, M.C.W., Cheung, C.Y., Chui, W.H., Tsao, G.S.W., Nicholls, J.M., Chan, Y.O., Chan, R.W.Y., Long, H.T., Poon, L.L.M., Guan, Y., and Peiris, J.S.M. (2005b). Proinflammatory cytokine responses induced by influenza A (H5N1) viruses in primary human alveolar and bronchial epithelial cells. Respir. Res. *6*.

Chang, S.T., Tchitchek, N., Ghosh, D., Benecke, A., and Katze, M.G. (2011). A chemokine gene expression signature derived from meta-analysis predicts the pathogenicity of viral respiratory infections. BMC Syst. Biol. *5*.

Chang, T.-H., Huang, J.-H., Lin, H.-C., Chen, W.-Y., Lee, Y.-H., Hsu, L.-C., Netea, M.G., Ting, J.P.Y., and Wu-Hsieh, B.A. (2017). Dectin-2 is a primary receptor for NLRP3 inflammasome activation in dendritic cell response to Histoplasma capsulatum. PLoS Pathog. *13*, e1006485.

Chen, C.-J., Chen, G.-W., Wang, C.-H., Huang, C.-H., Wang, Y.-C., and Shih, S.-R. (2010). Differential localization and function of PB1-F2 derived from different strains of influenza A virus. J. Virol. *84*, 10051-10062.

Chen, J., and Chen, Z.J. (2018). PtdIns4P on dispersed trans-Golgi network mediates NLRP3 inflammasome activation. Nature *564*, 71-76.

Chen, K.W., Bezbradica, J.S., Gross, C.J., Wall, A.A., Sweet, M.J., Stow, J.L., and Schroder, K. (2016). The murine neutrophil NLRP3 inflammasome is activated by soluble but not particulate or crystalline agonists. Eur. J. Immunol. *46*, 1004-1010.

Chen, W., Xu, Y., Li, H., Tao, W., Xiang, Y., Huang, B., Niu, J., Zhong, J., and Meng, G. (2014). HCV Genomic RNA Activates the NLRP3 Inflammasome in Human Myeloid Cells. PLoS One *9*, e84953.

Chen, Y., Li, X., Boini, K.M., Pitzer, A.L., Gulbins, E., Zhang, Y., and Li, P.L. (2015). Endothelial Nlrp3 inflammasome activation associated with lysosomal destabilization during coronary arteritis. Biochim. Biophys. Acta Mol. Cell Res. *1853*, 396-408.

Cheng, J., Waite, A.L., Tkaczyk, E.R., Ke, K., Richards, N., Hunt, A.J., and Gumucio, D.L. (2010). Kinetic properties of ASC protein aggregation in epithelial cells. J. Cell. Physiol. *222*, 738-747.

References

Cheung, C.Y., Poon, L.L., Lau, A.S., Luk, W., Lau, Y.L., Shortridge, K.F., Gordon, S., Guan, Y., and Peiris, J.S. (2002). Induction of proinflammatory cytokines in human macrophages by influenza A (H5N1) viruses: a mechanism for the unusual severity of human disease? Lancet *360*, 1831-1837.

Chevalier, C., Al Bazzal, A., Vidic, J., Février, V., Bourdieu, C., Bouguyon, E., Le Goffic, R., Vautherot, J.-F., Bernard, J., Moudjou, M., *et al.* (2010). PB1-F2 influenza A virus protein adopts a β-sheet conformation and forms amyloid fibers in membrane environments. J. Biol. Chem. *285*, 13233-13243.

Chi, W., Chen, H., Li, F., Zhu, Y., Yin, W., and Zhuo, Y. (2015). HMGB1 promotes the activation of NLRP3 and caspase-8 inflammasomes via NF-kappaB pathway in acute glaucoma. J. Neuroinflammation *12*, 137.

Chi, Y., Zhu, Y., Wen, T., Cui, L., Ge, Y., Jiao, Y., Wu, T., Ge, A., Ji, H., Xu, K., *et al.* (2013). Cytokine and chemokine levels in patients infected with the novel avian influenza a (H7N9) virus in China. J. Infect. Dis. *208*, 1962-1967.

Chiaretti, A., Pulitanò, S., Barone, G., Ferrara, P., Romano, V., Capozzi, D., and Riccardi, R. (2013). IL-1 β and IL-6 upregulation in children with H1N1 influenza virus infection. Mediators Inflamm. *2013*, 495848-495848.

Cho, J.S., Guo, Y., Ramos, R.I., Hebroni, F., Plaisier, S.B., Xuan, C., Granick, J.L., Matsushima, H., Takashima, A., Iwakura, Y., *et al.* (2012). Neutrophil-derived IL-1β Is Sufficient for Abscess Formation in Immunity against Staphylococcus aureus in Mice. PLoS Pathog. *8*, e1003047.

Cho, M.H., Cho, K., Kang, H.J., Jeon, E.Y., Kim, H.S., Kwon, H.J., Kim, H.M., Kim, D.H., and Yoon, S.Y. (2014). Autophagy in microglia degrades extracellular β-amyloid fibrils and regulates the NLRP3 inflammasome. Autophagy *10*, 1761-1775.

Chotpitayasunondh, T., Ungchusak, K., Hanshaoworakul, W., Chunsuthiwat, S., Sawanpanyalert, P., Kijphati, R., Lochindarat, S., Srisan, P., Suwan, P., Osotthanakorn, Y., *et al.* (2005). Human Disease from Influenza A (H5N1), Thailand, 2004. Emerg. Infect. Dis. *11*, 201-209.

Ciancio, B.C., Meerhoff, T.J., Kramarz, P., Bonmarin, I., Borgen, K., Boucher, C.A., Buchholz, U., Buda, S., Dijkstra, F., Dudman, S., *et al.* (2009). Oseltamivir-resistant influenza A(H1N1) viruses detected in Europe during season 2007-8 had epidemiologic and clinical characteristics similar to co-circulating susceptible A(H1N1) viruses. Euro Surveill. *14*.

Coates, B.M., Staricha, K.L., Koch, C.M., Cheng, Y., Shumaker, D.K., Budinger, G.R.S., Perlman, H., Misharin, A.V., and Ridge, K.M. (2018). Inflammatory Monocytes Drive Influenza A Virus–Mediated Lung Injury in Juvenile Mice. The Journal of Immunology *200*, 2391-2404.

Coates, B.M., Staricha, K.L., Ravindran, N., Koch, C.M., Cheng, Y., Davis, J.M., Shumaker, D.K., and Ridge, K.M. (2017). Inhibition of the NOD-Like Receptor Protein 3 Inflammasome Is Protective in Juvenile Influenza A Virus Infection. Front. Immunol. *8*, 782.

Coccia, E.M., Severa, M., Giacomini, E., Monneron, D., Remoli, M.E., Julkunen, I., Cella, M., Lande, R., and Uzé, G. (2004). Viral infection and Toll-like receptor agonists induce a differential expression

of type I and λ interferons in human plasmacytoid and monocyte-derived dendritic cells. Eur. J. Immunol. *34*, 796-805.

Codolo, G., Plotegher, N., Pozzobon, T., Brucale, M., Tessari, I., Bubacco, L., and de Bernard, M. (2013). Triggering of Inflammasome by Aggregated α-Synuclein, an Inflammatory Response in Synucleinopathies. PLoS One *8*, e55375.

Colak, E., Leslie, A., Zausmer, K., Khatamzas, E., Kubarenko, A.V., Pichulik, T., Klimosch, S.N., Mayer, A., Siggs, O., Hector, A., *et al.* (2014). RNA and imidazoquinolines are sensed by distinct TLR7/8 ectodomain sites resulting in functionally disparate signaling events. J. Immunol. *192*, 5963-5973.

Colden-Stanfield, M., Ratcliffe, D., Cramer, E.B., and Gallin, E.K. (1993). Characterization of influenza virus-induced leukocyte adherence to human umbilical vein endothelial cell monolayers. The Journal of Immunology *151*, 310-321.

Coll, R.C., Robertson, A.A., Chae, J.J., Higgins, S.C., Munoz-Planillo, R., Inserra, M.C., Vetter, I., Dungan, L.S., Monks, B.G., Stutz, A., *et al.* (2015). A small-molecule inhibitor of the NLRP3 inflammasome for the treatment of inflammatory diseases. Nat. Med. *21*, 248-255.

Collins, F.S., Rossant, J., and Wurst, W. (2007). A mouse for all reasons. Cell *128*, 9-13.

Compan, V., Baroja-Mazo, A., Lopez-Castejon, G., Gomez, A.I., Martinez, C.M., Angosto, D., Montero, M.T., Herranz, A.S., Bazan, E., Reimers, D., *et al.* (2012). Cell volume regulation modulates NLRP3 inflammasome activation. Immunity *37*, 487-500.

Compan, V., Martin-Sanchez, F., Baroja-Mazo, A., Lopez-Castejon, G., Gomez, A.I., Verkhratsky, A., Brough, D., and Pelegrin, P. (2015). Apoptosis-associated speck-like protein containing a CARD forms specks but does not activate caspase-1 in the absence of NLRP3 during macrophage swelling. J. Immunol. *194*, 1261-1273.

Costa, A., Gupta, R., Signorino, G., Malara, A., Cardile, F., Biondo, C., Midiri, A., Galbo, R., Trieu-Cuot, P., Papasergi, S., *et al.* (2012). Activation of the NLRP3 Inflammasome by Group B Streptococci. The Journal of Immunology *188*, 1953-1960.

Couturier, J., Stancu, I.-C., Schakman, O., Pierrot, N., Huaux, F., Kienlen-Campard, P., Dewachter, I., and Octave, J.-N. (2016). Activation of phagocytic activity in astrocytes by reduced expression of the inflammasome component ASC and its implication in a mouse model of Alzheimer disease. J. Neuroinflammation *13*, 20.

Crotta, S., Davidson, S., Mahlakoiv, T., Desmet, C.J., Buckwalter, M.R., Albert, M.L., Staeheli, P., and Wack, A. (2013). Type I and Type III Interferons Drive Redundant Amplification Loops to Induce a Transcriptional Signature in Influenza-Infected Airway Epithelia. PLoS Pathog. *9*, e1003773.

Crowley, M., Inaba, K., Witmer-Pack, M., and Steinman, R.M. (1989). The cell surface of mouse dendritic cells: FACS analyses of dendritic cells from different tissues including thymus. Cell. Immunol. *118*, 108-125.

References

Cruz, C.M., Rinna, A., Forman, H.J., Ventura, A.L.M., Persechini, P.M., and Ojcius, D.M. (2007). ATP Activates a Reactive Oxygen Species-dependent Oxidative Stress Response and Secretion of Proinflammatory Cytokines in Macrophages. J. Biol. Chem. *282*, 2871-2879.

Cullinan, E.B., Kwee, L., Nunes, P., Shuster, D.J., Ju, G., McIntyre, K.W., Chizzonite, R.A., and Labow, M.A. (1998). IL-1 receptor accessory protein is an essential component of the IL-1 receptor. J. Immunol. *161*, 5614-5620.

Dai, X., Tohyama, M., Murakami, M., and Sayama, K. (2017). Epidermal keratinocytes sense dsRNA via the NLRP3 inflammasome, mediating interleukin (IL)-1beta and IL-18 release. Exp. Dermatol. *26*, 904-911.

Daigneault, D.E., Hartshorn, K.L., Liou, L.S., Abbruzzi, G.M., White, M.R., Oh, S.K., and Tauber, A.I. (1992). Influenza A virus binding to human neutrophils and cross-linking requirements for activation. Blood *80*, 3227-3234.

Darnell, J.E., Kerr, I.M., and Stark, G.R. (1994). Jak-STAT Pathways and Transcriptional Activation in Response to IFNs and Other Extracellular Signaling Proteins. Science *264*, 1415-1421.

Davidson, S., Crotta, S., McCabe, T.M., and Wack, A. (2014). Pathogenic potential of interferon αβ in acute influenza infection. Nat Commun *5*, 3864.

Davidson, S., McCabe, T.M., Crotta, S., Gad, H.H., Hessel, E.M., Beinke, S., Hartmann, R., and Wack, A. (2016). IFNλ is a potent anti-influenza therapeutic without the inflammatory side effects of IFNalpha treatment. EMBO Mol. Med. *8*, 1099-1112.

Dawson, T.C., Beck, M.A., Kuziel, W.A., Henderson, F., and Maeda, N. (2000). Contrasting effects of CCR5 and CCR2 deficiency in the pulmonary inflammatory response to influenza A virus. Am. J. Pathol. *156*, 1951-1959.

de Alba, E. (2009). Structure and Interdomain Dynamics of Apoptosis-associated Speck-like Protein Containing a CARD (ASC). J. Biol. Chem. *284*, 32932-32941.

De Berge, M.P., Ely, K.H., and Enelow, R.I. (2014). Soluble, but not transmembrane, TNF-α is required during influenza infection to limit the magnitude of immune responses and the extent of immunopathology. J. Immunol. *192*, 5839-5851.

de Jong, M.D., Simmons, C.P., Thanh, T.T., Hien, V.M., Smith, G.J., Chau, T.N., Hoang, D.M., Chau, N.V., Khanh, T.H., Dong, V.C., *et al.* (2006). Fatal outcome of human influenza A (H5N1) is associated with high viral load and hypercytokinemia. Nat. Med. *12*, 1203-1207.

De Los Santos, C., Chang, C.W., Mycek, M.A., and Cardullo, R.A. (2015). FRAP, FLIM, and FRET: Detection and analysis of cellular dynamics on a molecular scale using fluorescence microscopy. Mol. Reprod. Dev. *82*, 587-604.

de Almeida, L., Khare, S., Misharin, Alexander V., Patel, R., Ratsimandresy, Rojo A., Wallin, Melissa C., Perlman, H., Greaves, David R., Hoffman, Hal M., Dorfleutner, A., and Stehlik, C.

(2015). The PYRIN Domain-only Protein POP1 Inhibits Inflammasome Assembly and Ameliorates Inflammatory Disease. Immunity *43*, 264-276.

del Rio, M.L., Rodriguez-Barbosa, J.I., Kremmer, E., and Forster, R. (2007). CD103- and CD103+ bronchial lymph node dendritic cells are specialized in presenting and cross-presenting innocuous antigen to CD4+ and CD8+ T cells. J. Immunol. *178*, 6861-6866.

Demicheli, V., Jefferson, T., Di Pietrantonj, C., Ferroni, E., Thorning, S., Thomas, R.E., and Rivetti, A. (2018a). Vaccines for preventing influenza in the elderly. Cochrane Database of Systematic Reviews *2*, CD004876.

Demicheli, V., Jefferson, T., Ferroni, E., Rivetti, A., and Di Pietrantonj, C. (2018b). Vaccines for preventing influenza in healthy adults. Cochrane Database of Systematic Reviews *2*, CD001269.

Dempsey, C., Rubio Araiz, A., Bryson, K.J., Finucane, O., Larkin, C., Mills, E.L., Robertson, A.A.B., Cooper, M.A., O'Neill, L.A.J., and Lynch, M.A. (2017). Inhibiting the NLRP3 inflammasome with MCC950 promotes non-phlogistic clearance of amyloid-β and cognitive function in APP/PS1 mice. Brain. Behav. Immun. *61*, 306-316.

Denton, A.E., Doherty, P.C., Turner, S.J., and La Gruta, N.L. (2007). IL-18, but not IL-12, is required for optimal cytokine production by influenza virus-specific $CD8^+$ T cells. Eur. J. Immunol. *37*, 368-375.

Dharan, N.J., Gubareva, L.V., Meyer, J.J., and et al. (2009). Infections with oseltamivir-resistant influenza a(h1n1) virus in the united states. JAMA *301*, 1034-1041.

Diao, H., Cui, G., Wei, Y., Chen, J., Zuo, J., Cao, H., Chen, Y., Yao, H., Tian, Z., and Li, L. (2014). Severe H7N9 Infection Is Associated with Decreased Antigen-Presenting Capacity of CD14+ Cells. PLoS One *9*, e92823.

Dick, M.S., Sborgi, L., Ruhl, S., Hiller, S., and Broz, P. (2016). ASC filament formation serves as a signal amplification mechanism for inflammasomes. Nat Commun *7*, 11929.

Dinarello, C.A. (2007). Historical insights into cytokines. Eur. J. Immunol. *37 Suppl 1*, S34-45.

Dong, G., Peng, C., Luo, J., Wang, C., Han, L., Wu, B., Ji, G., and He, H. (2015). Adamantane-Resistant Influenza A Viruses in the World (1902–2013): Frequency and Distribution of M2 Gene Mutations. PLoS One *10*, e0119115.

Dorfleutner, A., Bryan, N.B., Talbott, S.J., Funya, K.N., Rellick, S.L., Reed, J.C., Shi, X., Rojanasakul, Y., Flynn, D.C., and Stehlik, C. (2007). Cellular Pyrin Domain-Only Protein 2 Is a Candidate Regulator of Inflammasome Activation. Infect. Immun. *75*, 1484-1492.

Dostert, C., Pétrilli, V., Van Bruggen, R., Steele, C., Mossman, B.T., and Tschopp, J. (2008). Innate Immune Activation Through Nalp3 Inflammasome Sensing of Asbestos and Silica. Science *320*, 674-677.

References

Dowds, T.A., Masumoto, J., Zhu, L., Inohara, N., and Núñez, G. (2004). Cryopyrin-induced Interleukin 1β Secretion in Monocytic Cells: enhanced activity of disease-associated mutants and requirement for ASC. J. Biol. Chem. *279*, 21924-21928.

Dower, S.K., Kronheim, S.R., Hopp, T.P., Cantrell, M., Deeley, M., Gillis, S., Henney, C.S., and Urdal, D.L. (1986). The cell surface receptors for interleukin-1 alpha and interleukin-1 beta are identical. Nature *324*, 266-268.

Dripps, D.J., Brandhuber, B.J., Thompson, R.C., and Eisenberg, S.P. (1991). Interleukin-1 (IL-1) receptor antagonist binds to the 80-kDa IL-1 receptor but does not initiate IL-1 signal transduction. J. Biol. Chem. *266*, 10331-10336.

Dudziak, D., Kamphorst, A.O., Heidkamp, G.F., Buchholz, V.R., Trumpfheller, C., Yamazaki, S., Cheong, C., Liu, K., Lee, H.W., Park, C.G., *et al.* (2007). Differential antigen processing by dendritic cell subsets in vivo. Science *315*, 107-111.

Duellman, T., Burnett, J., and Yang, J. (2015). Quantitation of secreted proteins using mCherry fusion constructs and a fluorescent microplate reader. Anal. Biochem. *473*, 34-40.

Duewell, P., Kono, H., Rayner, K.J., Sirois, C.M., Vladimer, G., Bauernfeind, F.G., Abela, G.S., Franchi, L., Nũez, G., Schnurr, M., *et al.* (2010). NLRP3 inflammasomes are required for atherogenesis and activated by cholesterol crystals. Nature *464*, 1357-1361.

Dumoutier, L., Tounsi, A., Michiels, T., Sommereyns, C., Kotenko, S.V., and Renauld, J.C. (2004). Role of the interleukin (IL)-28 receptor tyrosine residues for antiviral and antiproliferative activity of IL-29/interferon-lambda 1: similarities with type I interferon signaling. J. Biol. Chem. *279*, 32269-32274.

Duncan, J.A., Bergstralh, D.T., Wang, Y., Willingham, S.B., Ye, Z., Zimmermann, A.G., and Ting, J.P.-Y. (2007). Cryopyrin/NALP3 binds ATP/dATP, is an ATPase, and requires ATP binding to mediate inflammatory signaling. Proceedings of the National Academy of Sciences *104*, 8041-8046.

Duncan, J.A., Gao, X., Huang, M.T.H., O'Connor, B.P., Thomas, C.E., Willingham, S.B., Bergstralh, D.T., Jarvis, G.A., Sparling, P.F., and Ting, J.P.Y. (2009). Neisseria gonorrhoeae activates the proteinase cathepsin B to mediate the signaling activities of the NLRP3 and ASC-containing inflammasome. J. Immunol. *182*, 6460-6469.

Dupuis, S., Jouanguy, E., Al-Hajjar, S., Fieschi, C., Al-Mohsen, I.Z., Al-Jumaah, S., Yang, K., Chapgier, A., Eidenschenk, C., Eid, P., *et al.* (2003). Impaired response to interferon-alpha/beta and lethal viral disease in human STAT1 deficiency. Nat. Genet. *33*, 388-391.

Ekiert, D.C., Bhabha, G., Elsliger, M.A., Friesen, R.H., Jongeneelen, M., Throsby, M., Goudsmit, J., and Wilson, I.A. (2009). Antibody recognition of a highly conserved influenza virus epitope. Science *324*, 246-251.

Ekiert, D.C., Friesen, R.H., Bhabha, G., Kwaks, T., Jongeneelen, M., Yu, W., Ophorst, C., Cox, F., Korse, H.J., Brandenburg, B., *et al.* (2011). A highly conserved neutralizing epitope on group 2 influenza A viruses. Science *333*, 843-850.

References

Eleftheriadis, T., Pissas, G., Antoniadi, G., Makri, P., Liakopoulos, V., and Stefanidis, I. (2015). Urate crystals induce NLRP3 inflammasome-dependent IL-1beta secretion and proliferation in isolated primary human T-cells. Hippokratia *19*, 41-46.

Elliott, E.I., and Sutterwala, F.S. (2015). Initiation and perpetuation of NLRP3 inflammasome activation and assembly. Immunol. Rev. *265*, 35-52.

Erlich, Z., Shlomovitz, I., Edry-Botzer, L., Cohen, H., Frank, D., Wang, H., Lew, A.M., Lawlor, K.E., Zhan, Y., Vince, J.E., and Gerlic, M. (2019). Macrophages, rather than DCs, are responsible for inflammasome activity in the GM-CSF BMDC model. Nat. Immunol. *20*, 397-406.

Esser, N., L'Homme, L., De Roover, A., Kohnen, L., Scheen, A.J., Moutschen, M., Piette, J., Legrand-Poels, S., and Paquot, N. (2013). Obesity phenotype is related to NLRP3 inflammasome activity and immunological profile of visceral adipose tissue. Diabetologia *56*, 2487-2497.

Fang, Y., Zhang, S., Li, X., Jiang, F., Ye, Q., and Ning, W. (2017). Follistatin like-1 aggravates silica-induced mouse lung injury. Sci. Rep. *7*, 399-399.

Fauriat, C., Long, E.O., Ljunggren, H.G., and Bryceson, Y.T. (2010). Regulation of human NK-cell cytokine and chemokine production by target cell recognition. Blood *115*, 2167-2176.

Faustin, B., Lartigue, L., Bruey, J.-M., Luciano, F., Sergienko, E., Bailly-Maitre, B., Volkmann, N., Hanein, D., Rouiller, I., and Reed, J.C. (2007). Reconstituted NALP1 Inflammasome Reveals Two-Step Mechanism of Caspase-1 Activation. Mol. Cell *25*, 713-724.

Feldmann, J., Prieur, A.-M., Quartier, P., Berquin, P., Certain, S., Cortis, E., Teillac-Hamel, D., Fischer, A., and Basile, G.d.S. (2002). Chronic Infantile Neurological Cutaneous and Articular Syndrome Is Caused by Mutations in CIAS1, a Gene Highly Expressed in Polymorphonuclear Cells and Chondrocytes. The American Journal of Human Genetics *71*, 198-203.

Fernandes-Alnemri, T., Wu, J., Yu, J.W., Datta, P., Miller, B., Jankowski, W., Rosenberg, S., Zhang, J., and Alnemri, E.S. (2007). The pyroptosome: a supramolecular assembly of ASC dimers mediating inflammatory cell death via caspase-1 activation. Cell Death Differ. *14*, 1590.

Fernandes-Alnemri, T., Yu, J.W., Datta, P., Wu, J., and Alnemri, E.S. (2009). AIM2 activates the inflammasome and cell death in response to cytoplasmic DNA. Nature *458*, 509-513.

Finger, J.N., Lich, J.D., Dare, L.C., Cook, M.N., Brown, K.K., Duraiswami, C., Bertin, J.J., and Gough, P.J. (2012). Autolytic Proteolysis within the Function to Find Domain (FIIND) Is Required for NLRP1 Inflammasome Activity. J. Biol. Chem. *287*, 25030-25037.

Fink, S.L., and Cookson, B.T. (2006). Caspase-1-dependent pore formation during pyroptosis leads to osmotic lysis of infected host macrophages. Cell. Microbiol. *8*, 1812-1825.

Franchi, L., Eigenbrod, T., and Núñez, G. (2009). Cutting edge: TNF-α mediates sensitization to ATP and silica via the NLRP3 inflammasome in the absence of microbial stimulation. J. Immunol. *183*, 792-796.

References

Franchi, L., and Núñez, G. (2008). The Nlrp3 inflammasome is critical for aluminium hydroxide-mediated IL-1β secretion but dispensable for adjuvant activity. Eur. J. Immunol. *38*, 2085-2089.

Franklin, B.S., Bossaller, L., De Nardo, D., Ratter, J.M., Stutz, A., Engels, G., Brenker, C., Nordhoff, M., Mirandola, S.R., Al-Amoudi, A., *et al.* (2014). The adaptor ASC has extracellular and 'prionoid' activities that propagate inflammation. Nat. Immunol. *15*, 727-737.

Friedrich, G., and Soriano, P. (1991). Promoter traps in embryonic stem cells: a genetic screen to identify and mutate developmental genes in mice. Genes Dev. *5*, 1513-1523.

Fry, A.M., Goswami, D., Nahar, K., Sharmin, A.T., Rahman, M., Gubareva, L., Azim, T., Bresee, J., Luby, S.P., and Brooks, W.A. (2014). Efficacy of oseltamivir treatment started within 5 days of symptom onset to reduce influenza illness duration and virus shedding in an urban setting in Bangladesh: a randomised placebo-controlled trial. Lancet Infect. Dis. *14*, 109-118.

Fujisawa, H. (2008). Neutrophils play an essential role in cooperation with antibody in both protection against and recovery from pulmonary infection with influenza virus in mice. J. Virol. *82*, 2772-2783.

Fujisawa, H., Tsuru, S., Taniguchi, M., Zinnaka, Y., and Nomoto, K. (1987). Protective mechanisms against pulmonary infection with influenza virus. I. Relative contribution of polymorphonuclear leukocytes and of alveolar macrophages to protection during the early phase of intranasal infection. J. Gen. Virol. *68 (Pt 2)*, 425-432.

Fukushi, M., Ito, T., Oka, T., Kitazawa, T., Miyoshi-Akiyama, T., Kirikae, T., Yamashita, M., and Kudo, K. (2011). Serial histopathological examination of the lungs of mice infected with influenza A virus PR8 strain. PLoS One *6*, e21207.

Gaekwad, J., Zhang, Y., Zhang, W., Reeves, J., Wolfert, M.A., and Boons, G.-J. (2010). Differential induction of innate immune responses by synthetic lipid a derivatives. The Journal of biological chemistry *285*, 29375-29386.

Gambin, Y., Giles, N., O'Carroll, A., Polinkovsky, M., Hunter, D., and Sierecki, E. (2018). Single-Molecule Fluorescence Reveals the Oligomerization and Folding Steps Driving the Prion-like Behavior of ASC. J. Mol. Biol. *430*, 491-508.

Gao, D., Madi, M., Ding, C., Fok, M., Steele, T., Ford, C., Hunter, L., and Bing, C. (2014). Interleukin-1beta mediates macrophage-induced impairment of insulin signaling in human primary adipocytes. Am. J. Physiol. Endocrinol. Metab. *307*, E289-304.

Gao, R., Bhatnagar, J., Blau, D.M., Greer, P., Rollin, D.C., Denison, A.M., Deleon-Carnes, M., Shieh, W.J., Sambhara, S., Tumpey, T.M., *et al.* (2013). Cytokine and chemokine profiles in lung tissues from fatal cases of 2009 pandemic influenza A (H1N1): Role of the host immune response in pathogenesis. Am. J. Pathol. *183*, 1258-1268.

Garcia-Ramirez, R.A., Ramirez-Venegas, A., Quintana-Carrillo, R., Camarena, A.E., Falfan-Valencia, R., and Mejia-Arangure, J.M. (2015). TNF, IL6, and IL1B polymorphisms are associated with severe influenza A (H1N1) virus infection in the Mexican population. PLoS One *10*, e0144832.

References

Garlanda, C., Dinarello, Charles A., and Mantovani, A. (2013). The Interleukin-1 Family: Back to the Future. Immunity *39*, 1003-1018.

Gay, N.J., and Keith, F.J. (1991). Drosophila Toll and IL-1 receptor. Nature *351*, 355-356.

Geissmann, F., Jung, S., and Littman, D.R. (2003). Blood monocytes consist of two principal subsets with distinct migratory properties. Immunity *19*, 71-82.

GeurtsvanKessel, C.H., Willart, M.A., van Rijt, L.S., Muskens, F., Kool, M., Baas, C., Thielemans, K., Bennett, C., Clausen, B.E., Hoogsteden, H.C., *et al.* (2008). Clearance of influenza virus from the lung depends on migratory langerin+CD11b- but not plasmacytoid dendritic cells. J. Exp. Med. *205*, 1621-1634.

Gioannini, T.L., Teghanemt, A., Zhang, D., Coussens, N.P., Dockstader, W., Ramaswamy, S., and Weiss, J.P. (2004). Isolation of an endotoxin-MD-2 complex that produces Toll-like receptor 4-dependent cell activation at picomolar concentrations. Proc. Natl. Acad. Sci. U. S. A. *101*, 4186-4191.

Girardin, S.E., Boneca, I.G., Viala, J., Chamaillard, M., Labigne, A., Thomas, G., Philpott, D.J., and Sansonetti, P.J. (2003). Nod2 is a general sensor of peptidoglycan through muramyl dipeptide (MDP) detection. J. Biol. Chem. *278*, 8869-8872.

Girardin, S.E., Tournebize, R., Mavris, M., Page, A.L., Li, X., Stark, G.R., Bertin, J., DiStefano, P.S., Yaniv, M., Sansonetti, P.J., and Philpott, D.J. (2001). CARD4/Nod1 mediates NF-kappaB and JNK activation by invasive Shigella flexneri. EMBO reports *2*, 736-742.

Glasner, A., Zurunic, A., Meningher, T., Lenac Rovis, T., Tsukerman, P., Bar-On, Y., Yamin, R., Meyers, A.F.A., Mandeboim, M., Jonjic, S., and Mandelboim, O. (2012). Elucidating the Mechanisms of Influenza Virus Recognition by Ncr1. PLoS One *7*, e36837.

Goldberg, E.L., Asher, J.L., Molony, R.D., Shaw, A.C., Zeiss, C.J., Wang, C., Morozova-Roche, L.A., Herzog, R.I., Iwasaki, A., and Dixit, V.D. (2017). β-Hydroxybutyrate Deactivates Neutrophil NLRP3 Inflammasome to Relieve Gout Flares. Cell Rep *18*, 2077-2087.

Goubau, D., Schlee, M., Deddouche, S., Pruijssers, A.J., Zillinger, T., Goldeck, M., Schuberth, C., Van der Veen, A.G., Fujimura, T., Rehwinkel, J., *et al.* (2014). Antiviral immunity via RIG-I-mediated recognition of RNA bearing 5'-diphosphates. Nature *514*, 372-375.

Gov, L., Schneider, C.A., Lima, T.S., Pandori, W., and Lodoen, M.B. (2017). NLRP3 and Potassium Efflux Drive Rapid IL-1beta Release from Primary Human Monocytes during Toxoplasma gondii Infection. J. Immunol. *199*, 2855-2864.

Green, J.P., Yu, S., Martin-Sanchez, F., Pelegrin, P., Lopez-Castejon, G., Lawrence, C.B., and Brough, D. (2018). Chloride regulates dynamic NLRP3-dependent ASC oligomerization and inflammasome priming. Proc. Natl. Acad. Sci. U. S. A. *115*, E9371-e9380.

Griesbeck, O., Baird, G.S., Campbell, R.E., Zacharias, D.A., and Tsien, R.Y. (2001). Reducing the Environmental Sensitivity of Yellow Fluorescent Protein: MECHANISM AND APPLICATIONS. J. Biol. Chem. *276*, 29188-29194.

References

Groß, O. (2012). Measuring the Inflammasome. In Leucocytes: Methods and Protocols, R.B. Ashman, ed. (Totowa, NJ: Humana Press), pp. 199-222.

Gu, Y., Kuida, K., Tsutsui, H., Ku, G., Hsiao, K., Fleming, M.A., Hayashi, N., Higashino, K., Okamura, H., Nakanishi, K., *et al.* (1997). Activation of interferon-gamma inducing factor mediated by interleukin-1beta converting enzyme. Science *275*, 206-209.

Guan, X., Sagara, J., Yokoyama, T., Koganehira, Y., Oguchi, M., Saida, T., and Taniguchi, S. (2003). ASC/TMS1, a caspase-1 activating adaptor, is downregulated by aberrant methylation in human melanoma. Int. J. Cancer *107*, 202-208.

Guarda, G., Zenger, M., Yazdi, A.S., Schroder, K., Ferrero, I., Menu, P., Tardivel, A., Mattmann, C., and Tschopp, J. (2011). Differential Expression of NLRP3 among Hematopoietic Cells. The Journal of Immunology *186*, 2529-2534.

Guillot, L., Le Goffic, R., Bloch, S., Escriou, N., Akira, S., Chignard, M., and Si-Tahar, M. (2005). Involvement of Toll-like Receptor 3 in the Immune Response of Lung Epithelial Cells to Double-stranded RNA and Influenza A Virus. J. Biol. Chem. *280*, 5571-5580.

Guo, H., Callaway, J.B., and Ting, J.P.Y. (2015a). Inflammasomes: mechanism of action, role in disease, and therapeutics. Nat. Med. *21*, 677-687.

Guo, H., Petrin, D., Zhang, Y., Bergeron, C., Goodyer, C.G., and LeBlanc, A.C. (2006). Caspase-1 activation of caspase-6 in human apoptotic neurons. Cell Death Differ. *13*, 285-292.

Guo, J., Huang, F., Liu, J., Chen, Y., Wang, W., Cao, B., Zou, Z., Liu, S., Pan, J., Bao, C., *et al.* (2015b). The serum profile of hypercytokinemia factors identified in H7N9-infected patients can predict fatal outcomes. Sci. Rep. *5*, 10942.

Guo, L., Wang, Y.-C., Mei, J.-J., Ning, R.-T., Wang, J.-J., Li, J.-Q., Wang, X., Zheng, H.-W., Fan, H.-T., and Liu, L.-D. (2017). Pulmonary immune cells and inflammatory cytokine dysregulation are associated with mortality of IL-1R1(-/-) mice infected with influenza virus (H1N1). Zoological research *38*, 146-154.

Gupta, R., Ghosh, S., Monks, B., DeOliveira, R.B., Tzeng, T.C., Kalantari, P., Nandy, A., Bhattacharjee, B., Chan, J., Ferreira, F., *et al.* (2014). RNA and beta;-hemolysin of group B streptococcus induce interleukin-1β (IL-1β) by activating NLRP3 inflammasomes in mouse macrophages. J. Biol. Chem. *289*, 13701-13705.

Gurung, P., Li, B., Subbarao Malireddi, R.K., Lamkanfi, M., Geiger, T.L., and Kanneganti, T.-D. (2015). Chronic TLR Stimulation Controls NLRP3 Inflammasome Activation through IL-10 Mediated Regulation of NLRP3 Expression and Caspase-8 Activation. Sci. Rep. *5*, 14488-14488.

Haas, T., Metzger, J., Schmitz, F., Heit, A., Muller, T., Latz, E., and Wagner, H. (2008). The DNA sugar backbone 2' deoxyribose determines toll-like receptor 9 activation. Immunity *28*, 315-323.

References

Hafner-Bratkovič, I., Benčina, M., Fitzgerald, K., Golenbock, D., and Jerala, R. (2012). NLRP3 inflammasome activation in macrophage cell lines by prion protein fibrils as the source of IL-1β and neuronal toxicity. Cell. Mol. Life Sci. *69*, 4215-4228.

Hafner-Bratkovic, I., Susjan, P., Lainscek, D., Tapia-Abellan, A., Cerovic, K., Kadunc, L., Angosto-Bazarra, D., Pelegriotan, P., and Jerala, R. (2018). NLRP3 lacking the leucine-rich repeat domain can be fully activated via the canonical inflammasome pathway. Nat Commun *9*, 5182.

Hagar, J.A., Powell, D.A., Aachoui, Y., Ernst, R.K., and Miao, E.A. (2013). Cytoplasmic LPS activates caspase-11: implications in TLR4-independent endotoxic shock. Science *341*, 1250-1253.

Halff, E.F., Diebolder, C.A., Versteeg, M., Schouten, A., Brondijk, T.H.C., and Huizinga, E.G. (2012). Formation and structure of a NAIP5-NLRC4 inflammasome induced by direct interactions with conserved N- and C-terminal regions of flagellin. J. Biol. Chem. *287*, 38460-38472.

Halle, A., Hornung, V., Petzold, G.C., Stewart, C.R., Monks, B.G., Reinheckel, T., Fitzgerald, K.A., Latz, E., Moore, K.J., and Golenbock, D.T. (2008). The NALP3 inflammasome is involved in the innate immune response to amyloid-beta. Nature immunology *9*, 857-865.

Hao, X., Kim, T.S., and Braciale, T.J. (2008). Differential response of respiratory dendritic cell subsets to influenza virus infection. J. Virol. *82*, 4908-4919.

Hargadon, K.M., Zhou, H., Albrecht, R.A., Dodd, H.A., García-Sastre, A., and Braciale, T.J. (2011). Major histocompatibility complex class II expression and hemagglutinin subtype influence the infectivity of type A influenza virus for respiratory dendritic cells. J. Virol. *85*, 11955-11963.

Hashimoto, C., Hudson, K.L., and Anderson, K.V. (1988). The Toll gene of Drosophila, required for dorsal-ventral embryonic polarity, appears to encode a transmembrane protein. Cell *52*, 269-279.

Hashimoto, D., Chow, A., Noizat, C., Teo, P., Beasley, M.B., Leboeuf, M., Becker, C.D., See, P., Price, J., Lucas, D., *et al.* (2013). Tissue-resident macrophages self-maintain locally throughout adult life with minimal contribution from circulating monocytes. Immunity *38*, 792-804.

Hashimoto, Y., Moki, T., Takizawa, T., Shiratsuchi, A., and Nakanishi, Y. (2007). Evidence for phagocytosis of influenza virus-infected, apoptotic cells by neutrophils and macrophages in mice. J. Immunol. *178*, 2448-2457.

Hause, B.M., Collin, E.A., Liu, R., Huang, B., Sheng, Z., Lu, W., Wang, D., Nelson, E.A., and Li, F. (2014). Characterization of a Novel Influenza Virus in Cattle and Swine: Proposal for a New Genus in the Orthomyxoviridae Family. mBio *5*, e00031-00014.

Hawkins, P.N., Lachmann, H.J., Aganna, E., and McDermott, M.F. (2004). Spectrum of clinical features in Muckle-Wells syndrome and response to anakinra. Arthritis Rheum. *50*, 607-612.

Hayashi, F., Smith, K.D., Ozinsky, A., Hawn, T.R., Yi, E.C., Goodlett, D.R., Eng, J.K., Akira, S., Underhill, D.M., and Aderem, A. (2001). The innate immune response to bacterial flagellin is mediated by Toll-like receptor 5. Nature *410*, 1099-1103.

References

He, W.-t., Wan, H., Hu, L., Chen, P., Wang, X., Huang, Z., Yang, Z.-H., Zhong, C.-Q., and Han, J. (2015). Gasdermin D is an executor of pyroptosis and required for interleukin-1β secretion. Cell Res. *25*, 1285-1298.

He, Y., Hara, H., and Núñez, G. (2016). Mechanism and Regulation of NLRP3 Inflammasome Activation. Trends Biochem. Sci. *41*, 1012-1021.

Headland, S.E., and Norling, L.V. (2015). The resolution of inflammation: Principles and challenges. Semin. Immunol. *27*, 149-160.

Heid, M.E., Keyel, P.A., Kamga, C., Shiva, S., Watkins, S.C., and Salter, R.D. (2013). Mitochondrial reactive oxygen species induces NLRP3-dependent lysosomal damage and inflammasome activation. J. Immunol. *191*, 5230-5238.

Hemmi, H., Kaisho, T., Takeuchi, O., Sato, S., Sanjo, H., Hoshino, K., Horiuchi, T., Tomizawa, H., Takeda, K., and Akira, S. (2002). Small anti-viral compounds activate immune cells via the TLR7 MyD88-dependent signaling pathway. Nat. Immunol. *3*, 196-200.

Hemmi, H., Takeuchi, O., Kawai, T., Kaisho, T., Sato, S., Sanjo, H., Matsumoto, M., Hoshino, K., Wagner, H., Takeda, K., and Akira, S. (2000). A Toll-like receptor recognizes bacterial DNA. Nature *408*, 740-745.

Heneka, M.T., Kummer, M.P., Stutz, A., Delekate, A., Schwartz, S., Saecker, A., Griep, A., Axt, D., Remus, A., Tzeng, T.-C., *et al.* (2013). NLRP3 is activated in Alzheimer´s disease and contributes to pathology in APP/PS1 mice. Nature *493*, 674-678.

Hernandez, J.C., Latz, E., and Urcuqui-Inchima, S. (2014). HIV-1 induces the first signal to activate the NLRP3 inflammasome in monocyte-derived macrophages. Intervirology *57*, 36-42.

Herold, S., Steinmueller, M., von Wulffen, W., Cakarova, L., Pinto, R., Pleschka, S., Mack, M., Kuziel, W.A., Corazza, N., Brunner, T., *et al.* (2008). Lung epithelial apoptosis in influenza virus pneumonia: the role of macrophage-expressed TNF-related apoptosis-inducing ligand. The Journal of Experimental Medicine *205*, 3065-3077.

Herold, S., von Wulffen, W., Steinmueller, M., Pleschka, S., Kuziel, W.A., Mack, M., Srivastava, M., Seeger, W., Maus, U.A., and Lohmeyer, J. (2006). Alveolar Epithelial Cells Direct Monocyte Transepithelial Migration upon Influenza Virus Infection: Impact of Chemokines and Adhesion Molecules. The Journal of Immunology *177*, 1817-1824.

Hett, E.C., Slater, L.H., Mark, K.G., Kawate, T., Monks, B.G., Stutz, A., Latz, E., and Hung, D.T. (2013). Chemical genetics reveals a kinase-independent role for protein kinase R in pyroptosis. Nat. Chem. Biol. *9*, 398.

Hien, T.T., Liem, N.T., Dung, N.T., San, L.T., Mai, P.P., Chau, N.v.V., Suu, P.T., Dong, V.C., Mai, L.T.Q., Thi, N.T., *et al.* (2004). Avian Influenza A (H5N1) in 10 Patients in Vietnam. N. Engl. J. Med. *350*, 1179-1188.

References

Hillegass, J.M., Miller, J.M., MacPherson, M.B., Westbom, C.M., Sayan, M., Thompson, J.K., Macura, S.L., Perkins, T.N., Beuschel, S.L., Alexeeva, V., *et al.* (2013). Asbestos and erionite prime and activate the NLRP3 inflammasome that stimulates autocrine cytokine release in human mesothelial cells. Part. Fibre Toxicol. *10*, 1-14.

Hink, M.A., Griep, R.A., Borst, J.W., van Hoek, A., Eppink, M.H.M., Schots, A., and Visser, A.J.W.G. (2000). Structural Dynamics of Green Fluorescent Protein Alone and Fused with a Single Chain Fv Protein. J. Biol. Chem. *275*, 17556-17560.

Hirano, S., Zhou, Q., Furuyama, A., and Kanno, S. (2017). Differential Regulation of IL-1β and IL-6 Release in Murine Macrophages. Inflammation *40*, 1933-1943.

Hirota, J.A., Hirota, S.A., Warner, S.M., Stefanowicz, D., Shaheen, F., Beck, P.L., MacDonald, J.A., Hackett, T.-L., Sin, D.D., Van Eeden, S., and Knight, D.A. (2012). The airway epithelium nucleotide-binding domain and leucine-rich repeat protein 3 inflammasome is activated by urban particulate matter. J. Allergy Clin. Immunol. *129*, 1116-1125.e1116.

Hoegen, T., Tremel, N., Klein, M., Angele, B., Wagner, H., Kirschning, C., Pfister, H.W., Fontana, A., Hammerschmidt, S., and Koedel, U. (2011). The NLRP3 inflammasome contributes to brain injury in pneumococcal meningitis and is activated through ATP-dependent lysosomal cathepsin B release. J. Immunol. *187*, 5440-5451.

Hoeve, M.A., Nash, A.A., Jackson, D., Randall, R.E., and Dransfield, I. (2012). Influenza Virus A Infection of Human Monocyte and Macrophage Subpopulations Reveals Increased Susceptibility Associated with Cell Differentiation. PLoS One *7*, e29443.

Hofer, C.C., Woods, P.S., and Davis, I.C. (2015). Infection of mice with influenza A/WSN/33 (H1N1) virus alters alveolar type II cell phenotype. Am. J. Physiol. Lung Cell Mol. Physiol. *308*, L628-638.

Hoffman, H.M., Mueller, J.L., Broide, D.H., Wanderer, A.A., and Kolodner, R.D. (2001). Mutation of a new gene encoding a putative pyrin-like protein causes familial cold autoinflammatory syndrome and Muckle-Wells syndrome. Nat. Genet. *29*, 301-305.

Hofmann, P., Sprenger, H., Kaufmann, A., Bender, A., Hasse, C., Nain, M., and Gemsa, D. (1997). Susceptibility of mononuclear phagocytes to influenza A virus infection and possible role in the antiviral response. J. Leukoc. Biol. *61*, 408-414.

Hogquist, K.A., Nett, M.A., Unanue, E.R., and Chaplin, D.D. (1991). Interleukin 1 is processed and released during apoptosis. Proc. Natl. Acad. Sci. U. S. A. *88*, 8485-8489.

Holmes, W.E., Lee, J., Kuang, W.J., Rice, G.C., and Wood, W.I. (1991). Structure and functional expression of a human interleukin-8 receptor. Science *253*, 1278-1280.

Honda, K., Takaoka, A., and Taniguchi, T. (2006). Type I Inteferon Gene Induction by the Interferon Regulatory Factor Family of Transcription Factors. Immunity *25*, 349-360.

References

Hoppstadter, J., Diesel, B., Zarbock, R., Breinig, T., Monz, D., Koch, M., Meyerhans, A., Gortner, L., Lehr, C.M., Huwer, H., and Kiemer, A.K. (2010). Differential cell reaction upon Toll-like receptor 4 and 9 activation in human alveolar and lung interstitial macrophages. Respir. Res. *11*, 124.

Hornung, V., Ablasser, A., Charrel-Dennis, M., Bauernfeind, F., Horvath, G., Caffrey, D.R., Latz, E., and Fitzgerald, K.A. (2009). AIM2 recognizes cytosolic dsDNA and forms a caspase-1-activating inflammasome with ASC. Nature *458*, 514-518.

Hornung, V., Bauernfeind, F., Halle, A., Samstad, E.O., Kono, H., Rock, K.L., Fitzgerald, K.A., and Latz, E. (2008). Silica crystals and aluminum salts activate the NALP3 inflammasome through phagosomal destabilization. Nat. Immunol. *9*, 847-856.

Hornung, V., Ellegast, J., Kim, S., Brzózka, K., Jung, A., Kato, H., Poeck, H., Akira, S., Conzelmann, K.-K., Schlee, M., *et al.* (2006). 5'-Triphosphate RNA Is the Ligand for RIG-I. Science *314*, 994-997.

Hoshino, K., Takeuchi, O., Kawai, T., Sanjo, H., Ogawa, T., Takeda, Y., Takeda, K., and Akira, S. (1999a). Cutting edge: Toll-like receptor 4 (TLR4)-deficient mice are hyporesponsive to lipopolysaccharide: evidence for TLR4 as the Lps gene product. J. Immunol. *162*, 3749-3752.

Hoshino, K., Tsutsui, H., Kawai, T., Takeda, K., Nakanishi, K., Takeda, Y., and Akira, S. (1999b). Cutting edge: generation of IL-18 receptor-deficient mice: evidence for IL-1 receptor-related protein as an essential IL-18 binding receptor. J. Immunol. *162*, 5041-5044.

Houser, K., and Subbarao, K. (2015). Influenza vaccines: challenges and solutions. Cell host & microbe *17*, 295-300.

Howard, A.D., Kostura, M.J., Thornberry, N., Ding, G.J.F., Limjuco, G., Weidner, J., Salley, J.P., Hogquist, K.A., Chaplin, D.D., Mumford, R.A., *et al.* (1991). IL-1-converting enzyme requires aspartic acid residues for processing of the IL-1β precursor at two distinct sites and does not cleave 31-kDa IL-1α. J. Immunol. *147*, 2964-2969.

Hu, Z., Zhou, Q., Zhang, C., Fan, S., Cheng, W., Zhao, Y., Shao, F., Wang, H.-W., Sui, S.-F., and Chai, J. (2015). Structural and biochemical basis for induced self-propagation of NLRC4. Science *350*, 399-404.

Huang, F.F., Barnes, P.F., Feng, Y., Donis, R., Chroneos, Z.C., Idell, S., Allen, T., Perez, D.R., Whitsett, J.A., Dunussi-Joannopoulos, K., and Shams, H. (2011). GM-CSF in the lung protects against lethal influenza infection. Am. J. Respir. Crit. Care Med. *184*, 259-268.

Huang, Z., Yu, M., Tong, S., Jia, K., Liu, R., Wang, H., Li, S., and Ning, Z. (2014). Tissue-specific expression of the NOD-like receptor protein 3 in BALB/c mice. J. Vet. Sci. *15*, 173-177.

Hufford, M.M., Richardson, G., Zhou, H., Manicassamy, B., Garcia-Sastre, A., Enelow, R.I., and Braciale, T.J. (2012). Influenza-infected neutrophils within the infected lungs act as antigen presenting cells for anti-viral CD8+ T cells. PLoS One *7*, e46581.

Hui, K.P.Y., Lee, S.M.Y., Cheung, C.-y., Ng, I.H.Y., Poon, L.L.M., Guan, Y., Ip, N.Y.Y., Lau, A.S.Y., and Peiris, J.S.M. (2009). Induction of Proinflammatory Cytokines in Primary Human

Macrophages by Influenza A Virus (H5N1) Is Selectively Regulated by IFN Regulatory Factor 3 and p38 MAPK. The Journal of Immunology *182*, 1088-1098.

Humke, E.W., Shriver, S.K., Starovasnik, M.A., Fairbrother, W.J., and Dixit, V.M. (2000). ICEBERG: A Novel Inhibitor of Interleukin-1β Generation. Cell *103*, 99-111.

Hussell, T., and Cavanagh, M.M. (2009). The innate immune rheostat: influence on lung inflammatory disease and secondary bacterial pneumonia. Biochem. Soc. Trans. *37*, 811-813.

Ichinohe, T., Lee, H.K., Ogura, Y., Flavell, R., and Iwasaki, A. (2009). Inflammasome recognition of influenza virus is essential for adaptive immune responses. J. Exp. Med. *206*, 79-87.

Ichinohe, T., Pang, I.K., and Iwasaki, A. (2010). Influenza virus activates inflammasomes via its intracellular M2 ion channel. Nat. Immunol. *11*, 404-410.

Ichinohe, T., Pang, I.K., Kumamoto, Y., Peaper, D.R., Ho, J.H., Murray, T.S., and Iwasaki, A. (2011). Microbiota regulates immune defense against respiratory tract influenza A virus infection. Proc. Natl. Acad. Sci. U. S. A. *108*, 5354-5359.

Ilyushina, N.A., Khalenkov, A.M., Seiler, J.P., Forrest, H.L., Bovin, N.V., Marjuki, H., Barman, S., Webster, R.G., and Webby, R.J. (2010). Adaptation of Pandemic H1N1 Influenza Viruses in Mice. J. Virol. *84*, 8607-8616.

Indalao, I.L., Sawabuchi, T., Takahashi, E., and Kido, H. (2017). IL-1β is a key cytokine that induces trypsin upregulation in the influenza virus-cytokine-trypsin cycle. Arch. Virol. *162*, 201-211.

Inohara, N., Ogura, Y., Chen, F.F., Muto, A., and Nuñez, G. (2001). Human Nod1 Confers Responsiveness to Bacterial Lipopolysaccharides. J. Biol. Chem. *276*, 2551-2554.

Ioannidis, I., Ye, F., McNally, B., Willette, M., and Flaño, E. (2013). Toll-like receptor expression and induction of type I and type III interferons in primary airway epithelial cells. J. Virol. *87*, 3261-3270.

Irving, A.T., Mimuro, H., Kufer, T.A., Lo, C., Wheeler, R., Turner, L.J., Thomas, B.J., Malosse, C., Gantier, M.P., Casillas, L.N., *et al.* (2014). The immune receptor NOD1 and kinase RIP2 interact with bacterial peptidoglycan on early endosomes to promote autophagy and inflammatory signaling. Cell host & microbe *15*, 623-635.

Isakov, E., Weisman-Shomer, P., and Benhar, M. (2014). Suppression of the pro-inflammatory NLRP3/interleukin-1β pathway in macrophages by the thioredoxin reductase inhibitor auranofin. Biochimica et Biophysica Acta (BBA) - General Subjects *1840*, 3153-3161.

Ismael, S., Nasoohi, S., and Ishrat, T. (2018). MCC950, the selective NLRP3 inflammasome inhibitor protects mice against traumatic brain injury. J. Neurotrauma.

Ito, M., Yanagi, Y., and Ichinohe, T. (2012). Encephalomyocarditis virus viroporin 2B activates NLRP3 inflammasome. PLoS Pathog. *8*, e1002857.

References

Itoh, Y., Shinya, K., Kiso, M., Watanabe, T., Sakoda, Y., Hatta, M., Muramoto, Y., Tamura, D., Sakai-Tagawa, Y., Noda, T., *et al.* (2009). In vitro and in vivo characterization of new swine-origin H1N1 influenza viruses. Nature *460*, 1021-1025.

Iyer, Shankar S., He, Q., Janczy, John R., Elliott, Eric I., Zhong, Z., Olivier, Alicia K., Sadler, Jeffrey J., Knepper-Adrian, V., Han, R., Qiao, L., *et al.* (2013). Mitochondrial Cardiolipin Is Required for Nlrp3 Inflammasome Activation. Immunity *39*, 311-323.

Jahnsen, F.L., Strickland, D.H., Thomas, J.A., Tobagus, I.T., Napoli, S., Zosky, G.R., Turner, D.J., Sly, P.D., Stumbles, P.A., and Holt, P.G. (2006). Accelerated antigen sampling and transport by airway mucosal dendritic cells following inhalation of a bacterial stimulus. J. Immunol. *177*, 5861-5867.

Jain, S., Benoit, S.R., Skarbinski, J., Bramley, A.M., and Finelli, L. (2012). Influenza-associated pneumonia among hospitalized patients with 2009 pandemic influenza A (H1N1) virus - United States, 2009. Clin. Infect. Dis. *54*, 1221-1229.

Jefferson, T., Rivetti, A., Di Pietrantonj, C., and Demicheli, V. (2018). Vaccines for preventing influenza in healthy children. Cochrane Database of Systematic Reviews.

Jeisy-Scott, V., Davis, W.G., Patel, J.R., Bowzard, J.B., Shieh, W.-J., Zaki, S.R., Katz, J.M., and Sambhara, S. (2011). Increased MDSC accumulation and Th2 biased response to influenza A virus infection in the absence of TLR7 in mice. PLoS One *6*, e25242.

Jeisy-Scott, V., Kim, J.H., Davis, W.G., Cao, W., Katz, J.M., and Sambhara, S. (2012). TLR7 Recognition is dispensable for influenza virus a infection but important for the induction of hemagglutinin-specific antibodies in response to the 2009 pandemic split vaccine in mice. J. Virol. *86*, 10988-10998.

Jessop, F., Hamilton, R.F., Jr., Rhoderick, J.F., Fletcher, P., and Holian, A. (2017). Phagolysosome acidification is required for silica and engineered nanoparticle-induced lysosome membrane permeabilization and resultant NLRP3 inflammasome activity. Toxicol. Appl. Pharmacol. *318*, 58-68.

Jewell, N.A., Cline, T., Mertz, S.E., Smirnov, S.V., Flaño, E., Schindler, C., Grieves, J.L., Durbin, R.K., Kotenko, S.V., and Durbin, J.E. (2010). Lambda interferon is the predominant interferon induced by influenza A virus infection in vivo. J. Virol. *84*, 11515-11522.

Jiang, J., Kang, T.B., Shim, D.W., Oh, N.H., Kim, T.J., and Lee, K.H. (2013). Indole-3-carbinol inhibits LPS-induced inflammatory response by blocking TRIF-dependent signaling pathway in macrophages. Food Chem. Toxicol. *57*, 256-261.

Jiang, Y., Wang, M., Huang, K., Zhang, Z., Shao, N., Zhang, Y., Wang, W., and Wang, S. (2012). Oxidized low-density lipoprotein induces secretion of interleukin-1β by macrophages via reactive oxygen species-dependent NLRP3 inflammasome activation. Biochem. Biophys. Res. Commun. *425*, 121-126.

References

Jimenez Fernandez, D., and Lamkanfi, M. (2015). Inflammatory caspases: key regulators of inflammation and cell death. Biol. Chem. *396*, 193-203.

Jin, M.S., Kim, S.E., Heo, J.Y., Lee, M.E., Kim, H.M., Paik, S.G., Lee, H., and Lee, J.O. (2007). Crystal structure of the TLR1-TLR2 heterodimer induced by binding of a tri-acylated lipopeptide. Cell *130*, 1071-1082.

Jin, T., Curry, J., Smith, P., Jiang, J., and Xiao, T.S. (2013a). Structure of the NLRP1 caspase recruitment domain suggests potential mechanisms for its association with procaspase-1. Proteins Struct. Funct. Bioinformatics *81*, 1266-1270.

Jin, T., Perry, A., Smith, P., Jiang, J., and Xiao, T.S. (2013b). Structure of the absent in melanoma 2 (AIM2) pyrin domain provides insights into the mechanisms of AIM2 autoinhibition and inflammasome assembly. J. Biol. Chem. *288*, 13225-13235.

Johansson, C., Wetzel, J.D., He, J., Mikacenic, C., Dermody, T.S., and Kelsall, B.L. (2007). Type I interferons produced by hematopoietic cells protect mice against lethal infection by mammalian reovirus. J. Exp. Med. *204*, 1349-1358.

Johnson, N.P., and Mueller, J. (2002). Updating the accounts: global mortality of the 1918-1920 "Spanish" influenza pandemic. Bull. Hist. Med. *76*, 105-115.

Juliana, C., Fernandes-Alnemri, T., Kang, S., Farias, A., Qin, F., and Alnemri, E.S. (2012). Non-transcriptional Priming and Deubiquitination Regulate NLRP3 Inflammasome Activation. J. Biol. Chem. *287*, 36617-36622.

Juliana, C., Fernandes-Alnemri, T., Wu, J., Datta, P., Solorzano, L., Yu, J.-W., Meng, R., Quong, A.A., Latz, E., Scott, C.P., and Alnemri, E.S. (2010). Anti-inflammatory Compounds Parthenolide and Bay 11-7082 Are Direct Inhibitors of the Inflammasome. J. Biol. Chem. *285*, 9792-9802.

Kahlenberg, J.M., Carmona-Rivera, C., Smith, C.K., and Kaplan, M.J. (2013). Neutrophil Extracellular Trap–Associated Protein Activation of the NLRP3 Inflammasome Is Enhanced in Lupus Macrophages. The Journal of Immunology *190*, 1217-1226.

Kahlenberg, J.M., and Dubyak, G.R. (2004). Mechanisms of caspase-1 activation by P2X7 receptor-mediated K+ release. Am. J. Physiol. Cell Physiol. *286*, C1100-C1108.

Kang, J.Y., Nan, X., Jin, M.S., Youn, S.J., Ryu, Y.H., Mah, S., Han, S.H., Lee, H., Paik, S.G., and Lee, J.O. (2009). Recognition of lipopeptide patterns by Toll-like receptor 2-Toll-like receptor 6 heterodimer. Immunity *31*, 873-884.

Kanneganti, T.-D., Ozoren, N., Body-Malapel, M., Amer, A., Park, J.-H., Franchi, L., Whitfield, J., Barchet, W., Colonna, M., Vandenabeele, P., *et al.* (2006a). Bacterial RNA and small antiviral compounds activate caspase-1 through cryopyrin/Nalp3. Nature *440*, 233-236.

Kanneganti, T.D., Body-Malapel, M., Amer, A., Park, J.H., Whitfield, J., Franchi, L., Taraporewala, Z.F., Miller, D., Patton, J.T., Inohara, N., and Nunez, G. (2006b). Critical role for Cryopyrin/Nalp3

in activation of caspase-1 in response to viral infection and double-stranded RNA. J. Biol. Chem. *281*, 36560-36568.

Karmakar, M., Katsnelson, M., Malak, H.A., Greene, N.G., Howell, S.J., Hise, A.G., Camilli, A., Kadioglu, A., Dubyak, G.R., and Pearlman, E. (2015). Neutrophil IL-1beta processing induced by pneumolysin is mediated by the NLRP3/ASC inflammasome and caspase-1 activation and is dependent on K+ efflux. J. Immunol. *194*, 1763-1775.

Kash, J.C., and Taubenberger, J.K. (2015). The Role of Viral, Host, and Secondary Bacterial Factors in Influenza Pathogenesis. The American Journal of Pathology *185*, 1528-1536.

Kash, J.C., Tumpey, T.M., Proll, S.C., Carter, V., Perwitasari, O., Thomas, M.J., Basler, C.F., Palese, P., Taubenberger, J.K., Garcia-Sastre, A., *et al.* (2006a). Genomic analysis of increased host immune and cell death responses induced by 1918 influenza virus. Nature *443*, 578-581.

Kash, J.C., Tumpey, T.M., Proll, S.C., Carter, V., Perwitasari, O., Thomas, M.J., Basler, C.F., Palese, P., Taubenberger, J.K., García-Sastre, A., *et al.* (2006b). Genomic analysis of increased host immune and cell death responses induced by 1918 influenza virus. Nature *443*, 578-581.

Kato, H., Takeuchi, O., Mikamo-Satoh, E., Hirai, R., Kawai, T., Matsushita, K., Hiiragi, A., Dermody, T.S., Fujita, T., and Akira, S. (2008). Length-dependent recognition of double-stranded ribonucleic acids by retinoic acid-inducible gene-I and melanoma differentiation-associated gene 5. J. Exp. Med. *205*, 1601-1610.

Kato, H., Takeuchi, O., Sato, S., Yoneyama, M., Yamamoto, M., Matsui, K., Uematsu, S., Jung, A., Kawai, T., Ishii, K.J., *et al.* (2006). Differential roles of MDA5 and RIG-I helicases in the recognition of RNA viruses. Nature *441*, 101-105.

Kato, K., Zemskova, M.A., Hanss, A.D., Kim, M.M., Summer, R., and Kim, K.C. (2017). Muc1 deficiency exacerbates pulmonary fibrosis in a mouse model of silicosis. Biochem. Biophys. Res. Commun. *493*, 1230-1235.

Katsnelson, M.A., Lozada-Soto, K.M., Russo, H.M., Miller, B.A., and Dubyak, G.R. (2016). NLRP3 inflammasome signaling is activated by low-level lysosome disruption but inhibited by extensive lysosome disruption: roles for K+ efflux and Ca2+ influx. Am. J. Physiol. Cell Physiol. *311*, C83-c100.

Katsura, H., Kobayashi, Y., Tata, P.R., and Hogan, B.L.M. (2019). IL-1 and TNFα Contribute to the Inflammatory Niche to Enhance Alveolar Regeneration. Stem Cell Reports *12*, 657-666.

Kayagaki, N., Stowe, I.B., Lee, B.L., O'Rourke, K., Anderson, K., Warming, S., Cuellar, T., Haley, B., Roose-Girma, M., Phung, Q.T., *et al.* (2015). Caspase-11 cleaves gasdermin D for non-canonical inflammasome signalling. Nature *526*, 666.

Kayagaki, N., Wong, M.T., Stowe, I.B., Ramani, S.R., Gonzalez, L.C., Akashi-Takamura, S., Miyake, K., Zhang, J., Lee, W.P., Muszynski, A., *et al.* (2013). Noncanonical inflammasome activation by intracellular LPS independent of TLR4. Science *341*, 1246-1249.

References

Kebaabetswe, L.P., Haick, A.K., and Miura, T.A. (2013). Differentiated phenotypes of primary murine alveolar epithelial cells and their susceptibility to infection by respiratory viruses. Virus Res. *175*, 110-119.

Kim, K.S., Jung, H., Shin, I.K., Choi, B.R., and Kim, D.H. (2015). Induction of interleukin-1 beta (IL-1β) is a critical component of lung inflammation during influenza A (H1N1) virus infection. J. Med. Virol. *87*, 1104-1112.

Kim, T.H., and Lee, H.K. (2014). Differential Roles of Lung Dendritic Cell Subsets Against Respiratory Virus Infection. Immune Netw. *14*, 128-137.

Kim, T.S., and Braciale, T.J. (2009). Respiratory dendritic cell subsets differ in their capacity to support the induction of virus-specific cytotoxic CD8+ T cell responses. PLoS One *4*, e4204.

Kim, T.S., Hufford, M.M., Sun, J., Fu, Y.X., and Braciale, T.J. (2010). Antigen persistence and the control of local T cell memory by migrant respiratory dendritic cells after acute virus infection. J. Exp. Med. *207*, 1161-1172.

Kitazawa, M., Hida, S., Fujii, C., Taniguchi, S.i., Ito, K., Matsumura, T., Okada, N., Sakaizawa, T., Kobayashi, A., Takeoka, M., and Miyagawa, S.-I. (2017). ASC Induces Apoptosis via Activation of Caspase-9 by Enhancing Gap Junction-Mediated Intercellular Communication. PLoS One *12*, e0169340-e0169340.

Kobasa, D., Jones, S.M., Shinya, K., Kash, J.C., Copps, J., Ebihara, H., Hatta, Y., Hyun Kim, J., Halfmann, P., Hatta, M., *et al.* (2007). Aberrant innate immune response in lethal infection of macaques with the 1918 influenza virus. Nature *445*, 319.

Kobasa, D., Takada, A., Shinya, K., Hatta, M., Halfmann, P., Theriault, S., Suzuki, H., Nishimura, H., Mitamura, K., Sugaya, N., *et al.* (2004). Enhanced virulence of influenza A viruses with the haemagglutinin of the 1918 pandemic virus. Nature *431*, 703.

Kofoed, E.M., and Vance, R.E. (2011). Innate immune recognition of bacterial ligands by NAIPs determines inflammasome specificity. Nature *477*, 592-595.

Kosteli, A., Sugaru, E., Haemmerle, G., Martin, J.F., Lei, J., Zechner, R., and Ferrante, A.W., Jr. (2010). Weight loss and lipolysis promote a dynamic immune response in murine adipose tissue. J. Clin. Invest. *120*, 3466-3479.

Kostura, M.J., Tocci, M.J., Limjuco, G., Chin, J., Cameron, P., Hillman, A.G., Chartrain, N.A., and Schmidt, J.A. (1989). Identification of a monocyte specific pre-interleukin 1 beta convertase activity. Proceedings of the National Academy of Sciences *86*, 5227-5231.

Kotenko, S.V., Gallagher, G., Baurin, V.V., Lewis-Antes, A., Shen, M., Shah, N.K., Langer, J.A., Sheikh, F., Dickensheets, H., and Donnelly, R.P. (2003). IFN-λs mediate antiviral protection through a distinct class II cytokine receptor complex. Nat. Immunol. *4*, 69-77.

Krishnan, S.M., Dowling, J.K., Ling, Y.H., Diep, H., Chan, C.T., Ferens, D., Kett, M.M., Pinar, A., Samuel, C.S., Vinh, A., *et al.* (2016). Inflammasome activity is essential for one

kidney/deoxycorticosterone acetate/salt-induced hypertension in mice. Br. J. Pharmacol. *173*, 752-765.

Kufer, T.A., Kremmer, E., Adam, A.C., Philpott, D.J., and Sansonetti, P.J. (2008). The pattern-recognition molecule Nod1 is localized at the plasma membrane at sites of bacterial interaction. Cell. Microbiol. *10*, 477-486.

Kumar, V., Abbas, A.K., and Aster, J.C. (2014). Chapter 3: inflammation and repair. In Robbins & Cotran Pathologic Basis of Disease (Philadelphia, UNITED STATES: Elsevier), pp. 69-111.

Kummer, J.A., Broekhuizen, R., Everett, H., Agostini, L., Kuijk, L., Martinon, F., Bruggen, R.v., and Tschopp, J. (2007). Inflammasome Components NALP 1 and 3 Show Distinct but Separate Expression Profiles in Human Tissues Suggesting a Site-specific Role in the Inflammatory Response. J. Histochem. Cytochem. *55*, 443-452.

Kuri, P., Schieber, N.L., Thumberger, T., Wittbrodt, J., Schwab, Y., and Leptin, M. (2017). Dynamics of in vivo ASC speck formation. The Journal of cell biology *216*, 2891-2909.

Kuwano, K., Kawashima, T., and Arai, S. (1993). Antiviral effect of TNF-alpha and IFN-gamma secreted from a CD8+ influenza virus-specific CTL clone. Viral Immunol. *6*, 1-11.

Laliberte, R.E., Perregaux, D.G., Hoth, L.R., Rosner, P.J., Jordan, C.K., Peese, K.M., Eggler, J.F., Dombroski, M.A., Geoghegan, K.F., and Gabel, C.A. (2003). Glutathione s-transferase omega 1-1 is a target of cytokine release inhibitory drugs and may be responsible for their effect on interleukin-1beta posttranslational processing. J. Biol. Chem. *278*, 16567-16578.

Lam, W.Y., Tang, J.W., Yeung, A.C.M., Chiu, L.C.M., Sung, J.J.Y., and Chan, P.K.S. (2008). Avian Influenza Virus A/HK/483/97(H5N1) NS1 Protein Induces Apoptosis in Human Airway Epithelial Cells. J. Virol. *82*, 2741-2751.

Lamkanfi, M., Denecker, G., Kalai, M., D'hondt, K., Meeus, A., Declercq, W., Saelens, X., and Vandenabeele, P. (2004). INCA, a Novel Human Caspase Recruitment Domain Protein That Inhibits Interleukin-1β Generation. J. Biol. Chem. *279*, 51729-51738.

Lamkanfi, M., Mueller, J.L., Vitari, A.C., Misaghi, S., Fedorova, A., Deshayes, K., Lee, W.P., Hoffman, H.M., and Dixit, V.M. (2009). Glyburide inhibits the Cryopyrin/Nalp3 inflammasome. The Journal of Cell Biology *187*, 61-70.

Lara-Tejero, M., Sutterwala, F.S., Ogura, Y., Grant, E.P., Bertin, J., Coyle, A.J., Flavell, R.A., and Galán, J.E. (2006). Role of the caspase-1 inflammasome in Salmonella typhimurium pathogenesis. The Journal of Experimental Medicine *203*, 1407-1412.

Larsen, C.M., Faulenbach, M., Vaag, A., Volund, A., Ehses, J.A., Seifert, B., Mandrup-Poulsen, T., and Donath, M.Y. (2007). Interleukin-1-receptor antagonist in type 2 diabetes mellitus. N. Engl. J. Med. *356*, 1517-1526.

References

Lattin, J.E., Schroder, K., Su, A.I., Walker, J.R., Zhang, J., Wiltshire, T., Saijo, K., Glass, C.K., Hume, D.A., Kellie, S., and Sweet, M.J. (2008). Expression analysis of G Protein-Coupled Receptors in mouse macrophages. Immunome Res. *4*, 5.

Lauwerys, B.R., Garot, N., Renauld, J.C., and Houssiau, F.A. (2000). Cytokine production and killer activity of NK/T-NK cells derived with IL-2, IL-15, or the combination of IL-12 and IL-18. J. Immunol. *165*, 1847-1853.

Lawrence, T.M., Hudacek, A.W., de Zoete, M.R., Flavell, R.A., and Schnell, M.J. (2013). Rabies virus is recognized by the NLRP3 inflammasome and activates interleukin-1beta release in murine dendritic cells. J. Virol. *87*, 5848-5857.

Le Goffic, R., Balloy, V., Lagranderie, M., Alexopoulou, L., Escriou, N., Flavell, R., Chignard, M., and Si-Tahar, M. (2006). Detrimental contribution of the Toll-like receptor (TLR)3 to influenza A virus-induced acute pneumonia. PLoS Pathog. *2*, 0526-0535.

Le Goffic, R., Pothlichet, J., Vitour, D., Fujita, T., Meurs, E., Chignard, M., and Si-Tahar, M. (2007). Cutting edge: Influenza A virus activates TLR3-dependent inflammatory and RIG-I-dependent antiviral responses in human lung epithelial cells. J. Immunol. *178*, 3368-3372.

Lee, H.M., Kim, J.J., Kim, H.J., Shong, M., Ku, B.J., and Jo, E.K. (2013). Upregulated NLRP3 inflammasome activation in patients with type 2 diabetes. Diabetes *62*, 194-204.

Lee, N., Chan, P.K., Wong, C.K., Wong, K.T., Choi, K.W., Joynt, G.M., Lam, P., Chan, M.C., Wong, B.C., Lui, G.C., *et al.* (2011a). Viral clearance and inflammatory response patterns in adults hospitalized for pandemic 2009 influenza A(H1N1) virus pneumonia. Antivir. Ther. *16*, 237-247.

Lee, N., Wong, C.K., Chan, P.K.S., Chan, M.C.W., Wong, R.Y.K., Lun, S.W.M., Ngai, K.L.K., Lui, G.C.Y., Wong, B.C.K., Lee, S.K.W., *et al.* (2011b). Cytokine Response Patterns in Severe Pandemic 2009 H1N1 and Seasonal Influenza among Hospitalized Adults. PLoS One *6*, e26050.

Lee, S.H., Stehlik, C., and Reed, J.C. (2001). COP, a Caspase Recruitment Domain-containing Protein and Inhibitor of Caspase-1 Activation Processing. J. Biol. Chem. *276*, 34495-34500.

Lemaitre, B., Nicolas, E., Michaut, L., Reichhart, J.-M., and Hoffmann, J.A. (1996). The Dorsoventral Regulatory Gene Cassette spätzle/Toll/cactus Controls the Potent Antifungal Response in Drosophila Adults. Cell *86*, 973-983.

LeMessurier, K.S., Lin, Y., McCullers, J.A., and Samarasinghe, A.E. (2016). Antimicrobial peptides alter early immune response to influenza A virus infection in C57BL/6 mice. Antiviral Res. *133*, 208-217.

Lewis, K.L., Caton, M.L., Bogunovic, M., Greter, M., Grajkowska, L.T., Ng, D., Klinakis, A., Charo, I.F., Jung, S., Gommerman, J.L., *et al.* (2011). Notch2 receptor signaling controls functional differentiation of dendritic cells in the spleen and intestine. Immunity *35*, 780-791.

References

Li, X., Thome, S., Ma, X., Amrute-Nayak, M., Finigan, A., Kitt, L., Masters, L., James, J.R., Shi, Y., Meng, G., and Mallat, Z. (2017). MARK4 regulates NLRP3 positioning and inflammasome activation through a microtubule-dependent mechanism. Nat. Commun. *8*, 15986-15986.

Li, X., Zhang, Y., Xia, M., Gulbins, E., Boini, K.M., and Li, P.L. (2014). Activation of Nlrp3 inflammasomes enhances macrophage lipid-deposition and migration: Implication of a novel role of inflammasome in atherogenesis. PLoS One *9*, e87552.

Liepinsh, E., Barbals, R., Dahl, E., Sharipo, A., Staub, E., and Otting, G. (2003). The Death-domain Fold of the ASC PYRIN Domain, Presenting a Basis for PYRIN/PYRIN Recognition. J. Mol. Biol. *332*, 1155-1163.

Lightfield, K.L., Persson, J., Trinidad, N.J., Brubaker, S.W., Kofoed, E.M., Sauer, J.D., Dunipace, E.A., Warren, S.E., Miao, E.A., and Vance, R.E. (2011). Differential requirements for NAIP5 in activation of the NLRC4 inflammasome. Infect. Immun. *79*, 1606-1614.

Lima-Junior, D.S., Costa, D.L., Carregaro, V., Cunha, L.D., Silva, A.L., Mineo, T.W., Gutierrez, F.R., Bellio, M., Bortoluci, K.R., Flavell, R.A., *et al.* (2013). Inflammasome-derived IL-1beta production induces nitric oxide-mediated resistance to Leishmania. Nat. Med. *19*, 909-915.

Lin, K.L., Suzuki, Y., Nakano, H., Ramsburg, E., and Gunn, M.D. (2008). CCR2+ monocyte-derived dendritic cells and exudate macrophages produce influenza-induced pulmonary immune pathology and mortality. J. Immunol. *180*, 2562-2572.

Liu, B., Mori, I., Hossain, M.J., Dong, L., Takeda, K., and Kimura, Y. (2004). Interleukin-18 improves the early defence system against influenza virus infection by augmenting natural killer cell-mediated cytotoxicity. J. Gen. Virol. *85*, 423-428.

Liu, K.-C., Fang, J.-M., Jan, J.-T., Cheng, T.-J.R., Wang, S.-Y., Yang, S.-T., Cheng, Y.-S.E., and Wong, C.-H. (2012a). Enhanced Anti-influenza Agents Conjugated with Anti-inflammatory Activity. J. Med. Chem. *55*, 8493-8501.

Liu, T., Zhang, L., Joo, D., and Sun, S.-C. (2017). NF-κB signaling in inflammation. Signal Transduction And Targeted Therapy *2*, 17023.

Liu, T., Zhou, Y., Li, P., Duan, J.-X., Liu, Y.-P., Sun, G.-Y., Wan, L., Dong, L., Fang, X., Jiang, J.-X., and Guan, C.-X. (2016a). Blocking triggering receptor expressed on myeloid cells-1 attenuates lipopolysaccharide-induced acute lung injury via inhibiting NLRP3 inflammasome activation. Sci. Rep. *6*, 39473-39473.

Liu, W., Yin, Y., Zhou, Z., He, M., and Dai, Y. (2014). OxLDL-induced IL-1beta secretion promoting foam cells formation was mainly via CD36 mediated ROS production leading to NLRP3 inflammasome activation. Inflamm. Res. *63*, 33-43.

Liu, X., Zhang, Z., Ruan, J., Pan, Y., Magupalli, V.G., Wu, H., and Lieberman, J. (2016b). Inflammasome-activated gasdermin D causes pyroptosis by forming membrane pores. Nature *535*, 153-158.

References

Liu, Y., Li, S., Zhang, G., Nie, G., Meng, Z., Mao, D., Chen, C., Chen, X., Zhou, B., and Zeng, G. (2013). Genetic variants in IL1A and IL1B contribute to the susceptibility to 2009 pandemic H1N1 influenza A virus. BMC Immunol. *14*, 37.

Liu, Y., Zheng, J., Liu, Y., Wen, L., Huang, L., Xiang, Z., Lam, K.T., Lv, A., Mao, H., Lau, Y.L., and Tu, W. (2018). Uncompromised NK cell activation is essential for virus-specific CTL activity during acute influenza virus infection. Cell. Mol. Immunol. *15*, 827-837.

Liu, Z., Zaki, M.H., Vogel, P., Gurung, P., Finlay, B.B., Deng, W., Lamkanfi, M., and Kanneganti, T.-D. (2012b). Role of Inflammasomes in Host Defense against Citrobacter rodentium Infection. J. Biol. Chem. *287*, 16955-16964.

Loh, L., Wang, Z., Sant, S., Koutsakos, M., Jegaskanda, S., Corbett, A.J., Liu, L., Fairlie, D.P., Crowe, J., Rossjohn, J., *et al.* (2016). Human mucosal-associated invariant T cells contribute to antiviral influenza immunity via IL-18–dependent activation. Proc. Natl. Acad. Sci. U. S. A. *113*, 10133-10138.

Lomedico, P.T., Gubler, U., Hellmann, C.P., Dukovich, M., Giri, J.G., Pan, Y.C., Collier, K., Semionow, R., Chua, A.O., and Mizel, S.B. (1984). Cloning and expression of murine interleukin-1 cDNA in Escherichia coli. Nature *312*, 458-462.

Lu, A., Li, Y., Schmidt, F.I., Yin, Q., Chen, S., Fu, T.-M., Tong, A.B., Ploegh, H.L., Mao, Y., and Wu, H. (2016). Molecular basis of caspase-1 polymerization and its inhibition by a new capping mechanism. Nat. Struct. Mol. Biol. *23*, 416-425.

Lu, A., Magupalli, Venkat G., Ruan, J., Yin, Q., Atianand, Maninjay K., Vos, M.R., Schröder, Gunnar F., Fitzgerald, Katherine A., Wu, H., and Egelman, Edward H. (2014). Unified Polymerization Mechanism for the Assembly of ASC-Dependent Inflammasomes. Cell *156*, 1193-1206.

Lu, X., Tumpey, T.M., Morken, T., Zaki, S.R., Cox, N.J., and Katz, J.M. (1999). A mouse model for the evaluation of pathogenesis and immunity to influenza A (H5N1) viruses isolated from humans. J. Virol. *73*, 5903-5911.

Lund, J.M., Alexopoulou, L., Sato, A., Karow, M., Adams, N.C., Gale, N.W., Iwasaki, A., and Flavell, R.A. (2004). Recognition of single-stranded RNA viruses by Toll-like receptor 7. Proc. Natl. Acad. Sci. U. S. A. *101*, 5598-5603.

Luo, M., Hu, L., Li, D., Wang, Y., He, Y., Zhu, L., and Ren, W. (2017). MD-2 regulates LPS-induced NLRP3 inflammasome activation and IL-1beta secretion by a MyD88/NF-κB-dependent pathway in alveolar macrophages cell line. Mol. Immunol. *90*, 1-10.

Mabbott, N.A., Baillie, J.K., Brown, H., Freeman, T.C., and Hume, D.A. (2013). An expression atlas of human primary cells: inference of gene function from coexpression networks. BMC Genomics *14*, 632.

Madera, R.F., and Libraty, D.H. (2013). The role of MyD88 signaling in heterosubtypic influenza A virus infections. Virus Res. *171*, 216-221.

References

Mantovani, A., Allavena, P., Sica, A., and Balkwill, F. (2008). Cancer-related inflammation. Nature *454*, 436-444.

Mariathasan, S., Hewton, K., Monack, D.M., Vucic, D., French, D.M., Lee, W.P., Roose-Girma, M., Erickson, S., and Dixit, V.M. (2004). Differential activation of the inflammasome by caspase-1 adaptors ASC and Ipaf. Nature *430*, 213-218.

Mariathasan, S., Weiss, D.S., Newton, K., McBride, J., O'Rourke, K., Roose-Girma, M., Lee, W.P., Weinrauch, Y., Monack, D.M., and Dixit, V.M. (2006). Cryopyrin activates the inflammasome in response to toxins and ATP. Nature *440*, 228-232.

Marina-García, N., Franchi, L., Kim, Y.-G., Miller, D., McDonald, C., Boons, G.-J., and Núñez, G. (2008). Pannexin-1-Mediated Intracellular Delivery of Muramyl Dipeptide Induces Caspase-1 Activation via Cryopyrin/NLRP3 Independently of Nod2. The Journal of Immunology *180*, 4050-4057.

Marsters, S.A., Pennica, D., Bach, E., Schreiber, R.D., and Ashkenazi, A. (1995). Interferon gamma signals via a high-affinity multisubunit receptor complex that contains two types of polypeptide chain. Proc. Natl. Acad. Sci. U. S. A. *92*, 5401-5405.

Martín-Sánchez, F., Compan, V., and Pelegrín, P. (2016). Measuring NLR Oligomerization III: Detection of NLRP3 Complex by Bioluminescence Resonance Energy Transfer. In NLR Proteins: Methods and Protocols, F. Di Virgilio, and P. Pelegrín, eds. (New York, NY: Springer New York), pp. 159-168.

Martin, B.N., Wang, C., Zhang, C.J., Kang, Z., Gulen, M.F., Zepp, J.A., Zhao, J., Bian, G., Do, J.S., Min, B., *et al.* (2016). T cell-intrinsic ASC critically promotes T(H)17-mediated experimental autoimmune encephalomyelitis. Nat. Immunol. *17*, 583-592.

Martin, C., Burdon, P.C., Bridger, G., Gutierrez-Ramos, J.C., Williams, T.J., and Rankin, S.M. (2003). Chemokines acting via CXCR2 and CXCR4 control the release of neutrophils from the bone marrow and their return following senescence. Immunity *19*, 583-593.

Martinon, F., Agostini, L., Meylan, E., and Tschopp, J. (2004). Identification of Bacterial Muramyl Dipeptide as Activator of the NALP3/Cryopyrin Inflammasome. Curr. Biol. *14*, 1929-1934.

Martinon, F., Burns, K., and Tschopp, J. (2002). The Inflammasome: A Molecular Platform Triggering Activation of Inflammatory Caspases and Processing of pro-ILβ. Molecular cell *10*, 417-426.

Martinon, F., Petrilli, V., Mayor, A., Tardivel, A., and Tschopp, J. (2006). Gout-associated uric acid crystals activate the NALP3 inflammasome. Nature *440*, 237-241.

Masters, S.L., Dunne, A., Subramanian, S.L., Hull, R.L., Tannahill, G.M., Sharp, F.A., Becker, C., Franchi, L., Yoshihara, E., Chen, Z., *et al.* (2010a). Activation of the NLRP3 inflammasome by islet amyloid polypeptide provides a mechanism for enhanced IL-1[beta] in type 2 diabetes. Nat. Immunol. *11*, 897-904.

Masters, S.L., Dunne, A., Subramanian, S.L., Hull, R.L., Tannahill, G.M., Sharp, F.A., Becker, C., Franchi, L., Yoshihara, E., Chen, Z., *et al.* (2010b). Activation of the NLRP3 inflammasome by islet amyloid polypeptide provides a mechanism for enhanced IL-1beta in type 2 diabetes. Nature immunology *11*, 897-904.

Masumoto, J., Taniguchi, S.i., Ayukawa, K., Sarvotham, H., Kishino, T., Niikawa, N., Hidaka, E., Katsuyama, T., Higuchi, T., and Sagara, J. (1999). ASC, a Novel 22-kDa Protein, Aggregates during Apoptosis of Human Promyelocytic Leukemia HL-60 Cells. J. Biol. Chem. *274*, 33835-33838.

Mathie, S.A., Dixon, K.L., Walker, S.A., Tyrrell, V., Mondhe, M., O'Donnell, V.B., Gregory, L.G., and Lloyd, C.M. (2015). Alveolar macrophages are sentinels of murine pulmonary homeostasis following inhaled antigen challenge. Allergy *70*, 80-89.

Matrosovich, M.N., Matrosovich, T.Y., Gray, T., Roberts, N.A., and Klenk, H.D. (2004). Human and avian influenza viruses target different cell types in cultures of human airway epithelium. Proc. Natl. Acad. Sci. U. S. A. *101*, 4620-4624.

Matsubayashi, T., Sugiura, H., Arai, T., Oh-Ishi, T., and Inamo, Y. (2006). Anakinra therapy for CINCA syndrome with a novel mutation in exon 4 of the CIAS1 gene. Acta Pædiatrica *95*, 246-249.

Matsui, T., and Amagai, M. (2015). Dissecting the formation, structure and barrier function of the stratum corneum. Int. Immunol. *27*, 269-280.

McAuley, J.L., Chipuk, J.E., Boyd, K.L., Van De Velde, N., Green, D.R., and McCullers, J.A. (2010). PB1-F2 proteins from H5N1 and 20th century pandemic influenza viruses cause immunopathology. PLoS Pathog. *6*, e1001014.

McAuley, J.L., Tate, M.D., MacKenzie-Kludas, C.J., Pinar, A., Zeng, W., Stutz, A., Latz, E., Brown, L.E., and Mansell, A. (2013). Activation of the NLRP3 inflammasome by IAV virulence protein PB1-F2 contributes to severe pathophysiology and disease. PLoS Pathog. *9*, e1003392.

McCoy, A.J., Koizumi, Y., Higa, N., and Suzuki, T. (2010). Differential regulation of caspase-1 activation via NLRP3/NLRC4 inflammasomes mediated by aerolysin and type III secretion system during Aeromonas veronii infection. J. Immunol. *185*, 7077-7084.

McGill, J., Heusel, J.W., and Legge, K.L. (2009). Innate immune control and regulation of influenza virus infections. J. Leukoc. Biol. *86*, 803-812.

Medzhitov, R., and Janeway, C. (2000). Innate Immunity. N. Engl. J. Med. *343*, 338-344.

Meixenberger, K., Pache, F., Eitel, J., Schmeck, B., Hippenstiel, S., Slevogt, H., N'Guessan, P., Witzenrath, M., Netea, M.G., Chakraborty, T., *et al.* (2010). Listeria monocytogenes-Infected Human Peripheral Blood Mononuclear Cells Produce IL-1β, Depending on Listeriolysin O and NLRP3. The Journal of Immunology *184*, 922-930.

Meunier, E., Dick, M.S., Dreier, R.F., Schürmann, N., Broz, D.K., Warming, S., Roose-Girma, M., Bumann, D., Kayagaki, N., Takeda, K., *et al.* (2014). Caspase-11 activation requires lysis of pathogen-containing vacuoles by IFN-induced GTPases. Nature *509*, 366-370.

References

Miao, E.A., Alpuche-Aranda, C.M., Dors, M., Clark, A.E., Bader, M.W., Miller, S.I., and Aderem, A. (2006). Cytoplasmic flagellin activates caspase-1 and secretion of interleukin 1beta via Ipaf. Nature immunology *7*, 569-575.

Micheau, O., and Tschopp, J. (2003). Induction of TNF receptor I-mediated apoptosis via two sequential signaling complexes. Cell *114*, 181-190.

Miller, D.K., Ayala, J.M., Egger, L.A., Raju, S.M., Yamin, T.T., Ding, G.J., Gaffney, E.P., Howard, A.D., Palyha, O.C., and Rolando, A.M. (1993). Purification and characterization of active human interleukin-1 beta-converting enzyme from THP.1 monocytic cells. J. Biol. Chem. *268*, 18062-18069.

Miller, L.S., Pietras, E.M., Uricchio, L.H., Hirano, K., Rao, S., Lin, H., O'Connell, R.M., Iwakura, Y., Cheung, A.L., Cheng, G., and Modlin, R.L. (2007). Inflammasome-mediated production of IL-1beta is required for neutrophil recruitment against Staphylococcus aureus in vivo. J. Immunol. *179*, 6933-6942.

Misawa, T., Takahama, M., Kozaki, T., Lee, H., Zou, J., Saitoh, T., and Akira, S. (2013). Microtubule-driven spatial arrangement of mitochondria promotes activation of the NLRP3 inflammasome. Nat. Immunol. *14*, 454-460.

Mishra, B.B., Moura-Alves, P., Sonawane, A., Hacohen, N., Griffiths, G., Moita, L.F., and Anes, E. (2010). Mycobacterium tuberculosis protein ESAT-6 is a potent activator of the NLRP3/ASC inflammasome. Cell. Microbiol. *12*, 1046-1063.

Moayeri, M., Crown, D., Newman, Z.L., Okugawa, S., Eckhaus, M., Cataisson, C., Liu, S., Sastalla, I., and Leppla, S.H. (2010). Inflammasome Sensor Nlrp1b-Dependent Resistance to Anthrax Is Mediated by Caspase-1, IL-1 Signaling and Neutrophil Recruitment. PLoS Pathog. *6*, e1001222.

Molineaux, S.M., Casano, F.J., Rolando, A.M., Peterson, E.P., Limjuco, G., Chin, J., Griffin, P.R., Calaycay, J.R., Ding, G.J.F., Yamin, T.T., *et al.* (1993). Interleukin 1β (IL-1β) processing in murine macrophages requires a structurally conserved homologue of human IL-1β converting enzyme. Proc. Natl. Acad. Sci. U. S. A. *90*, 1809-1813.

Monici, M., Pratesi, R., Bernabei, P.A., Caporale, R., Ferrini, P.R., Croce, A.C., Balzarini, P., and Bottiroli, G. (1995). Natural fluorescence of white blood cells: spectroscopic and imaging study. J. Photochem. Photobiol. B *30*, 29-37.

Morales-García, G., Falfán-Valencia, R., García-Ramírez, R.A., Camarena, Á., Ramirez-Venegas, A., Castillejos-López, M., Pérez-Rodríguez, M., González-Bonilla, C., Grajales-Muñíz, C., Borja-Aburto, V., and Mejía-Aranguré, J.M. (2012). Pandemic influenza A/H1N1 virus infection and TNF, LTA, IL1B, IL6, IL8, and CCL polymorphisms in Mexican population: a case–control study. BMC Infect. Dis. *12*, 299-299.

Mordstein, M., Kochs, G., Dumoutier, L., Renauld, J.-C., Paludan, S.R., Klucher, K., and Staeheli, P. (2008). Interferon-λ Contributes to Innate Immunity of Mice against Influenza A Virus but Not against Hepatotropic Viruses. PLoS Pathog. *4*, e1000151.

References

Moreira, A.P., and Hogaboam, C.M. (2011). Macrophages in allergic asthma: fine-tuning their pro- and anti-inflammatory actions for disease resolution. J. Interferon Cytokine Res. *31*, 485-491.

Morens, D.M., Taubenberger, J.K., and Fauci, A.S. (2008). Predominant role of bacterial pneumonia as a cause of death in pandemic influenza: implications for pandemic influenza preparedness. J. Infect. Dis. *198*, 962-970.

Mori, I., Komatsu, T., Takeuchi, K., Nakakuki, K., Sudo, M., and Kimura, Y. (1995). Viremia induced by influenza virus. Microb. Pathog. *19*, 237-244.

Moriyama, M., Chen, I.Y., Kawaguchi, A., Koshiba, T., Nagata, K., Takeyama, H., Hasegawa, H., and Ichinohe, T. (2016). The RNA- and TRIM25-binding domains of influenza virus NS1 protein are essential for suppression of NLRP3 inflammasome-mediated interleukin-1β secretion. J. Virol. *90*, 4105-4114.

Moser, B., Wolf, M., Walz, A., and Loetscher, P. (2004). Chemokines: multiple levels of leukocyte migration control. Trends Immunol. *25*, 75-84.

Motani, K., Kawase, K., Imamura, R., Kinoshita, T., Kushiyama, H., and Suda, T. (2010). Activation of ASC induces apoptosis or necrosis, depending on the cell type, and causes tumor eradication. Cancer Sci. *101*, 1822-1827.

Motshwene, P.G., Moncrieffe, M.C., Grossmann, J.G., Kao, C., Ayaluru, M., Sandercock, A.M., Robinson, C.V., Latz, E., and Gay, N.J. (2009). An Oligomeric Signaling Platform Formed by the Toll-like Receptor Signal Transducers MyD88 and IRAK-4. The Journal of Biological Chemistry *284*, 25404-25411.

Mulay, S.R., Kulkarni, O.P., Rupanagudi, K.V., Migliorini, A., Darisipudi, M.N., Vilaysane, A., Muruve, D., Shi, Y., Munro, F., Liapis, H., and Anders, H.-J. (2013). Calcium oxalate crystals induce renal inflammation by NLRP3-mediated IL-1β secretion. The Journal of clinical investigation *123*, 236-246.

Muñoz-Planillo, R., Franchi, L., Miller, L.S., and Núñez, G. (2009). A Critical Role for Hemolysins and Bacterial Lipoproteins in Staphylococcus aureus-Induced Activation of the Nlrp3 Inflammasome. The Journal of Immunology *183*, 3942-3948.

Muñoz-Planillo, R., Kuffa, P., Martínez-Colón, G., Smith, Brenna L., Rajendiran, Thekkelnaycke M., and Núñez, G. (2013). K+ Efflux Is the Common Trigger of NLRP3 Inflammasome Activation by Bacterial Toxins and Particulate Matter. Immunity *38*, 1142-1153.

Murphy, E.A., Davis, J.M., McClellan, J.L., Carmichael, M.D., Rooijen, N.V., and Gangemi, J.D. (2011). Susceptibility to infection and inflammatory response following influenza virus (H1N1, A/PR/8/34) challenge: role of macrophages. J. Interferon Cytokine Res. *31*, 501-508.

Murphy, P.M., and Tiffany, H.L. (1991). Cloning of complementary DNA encoding a functional human interleukin-8 receptor. Science *253*, 1280-1283.

References

Muzio, M., Natoli, G., Saccani, S., Levrero, M., and Mantovani, A. (1998). The human toll signaling pathway: divergence of nuclear factor kappaB and JNK/SAPK activation upstream of tumor necrosis factor receptor-associated factor 6 (TRAF6). J. Exp. Med. *187*, 2097-2101.

Muzio, M., Ni, J., Feng, P., and Dixit, V.M. (1997). IRAK (Pelle) family member IRAK-2 and MyD88 as proximal mediators of IL-1 signaling. Science *278*, 1612-1615.

Nagar, A., DeMarco, R.A., and Harton, J.A. (2019). Inflammasome and Caspase-1 Activity Characterization and Evaluation: An Imaging Flow Cytometer–Based Detection and Assessment of Inflammasome Specks and Caspase-1 Activation. The Journal of Immunology *202*, 1003-1015.

Nakahira, K., Haspel, J.A., Rathinam, V.A.K., Lee, S.J., Dolinay, T., Lam, H.C., Englert, J.A., Rabinovitch, M., Cernadas, M., Kim, H.P., *et al.* (2011). Autophagy proteins regulate innate immune responses by inhibiting the release of mitochondrial DNA mediated by the NALP3 inflammasome. Nat. Immunol. *12*, 222-230.

Nambayan, R.J.T., Sandin, S.I., Quint, D.A., Satyadi, D.M., and de Alba, E. (2018). The inflammasome adapter ASC assembles into filaments with integral participation of its two Death Domains, PYD and CARD. J. Biol. Chem. *In press*.

Narasaraju, T., Ng, H.H., Phoon, M.C., and Chow, V.T.K. (2010). MCP-1 antibody treatment enhances damage and impedes repair of the alveolar epithelium in influenza pneumonitis. Am. J. Respir. Cell Mol. Biol. *42*, 732-743.

Narasaraju, T., Sim, M.K., Ng, H.H., Phoon, M.C., Shanker, N., Lal, S.K., and Chow, V.T. (2009). Adaptation of human influenza H3N2 virus in a mouse pneumonitis model: insights into viral virulence, tissue tropism and host pathogenesis. Microbes Infect *11*, 2-11.

Narasaraju, T., Yang, E., Samy, R.P., Ng, H.H., Poh, W.P., Liew, A.-A., Phoon, M.C., van Rooijen, N., and Chow, V.T. (2011). Excessive Neutrophils and Neutrophil Extracellular Traps Contribute to Acute Lung Injury of Influenza Pneumonitis. The American Journal of Pathology *179*, 199-210.

Negash, A.A., Ramos, H.J., Crochet, N., Lau, D.T.Y., Doehle, B., Papic, N., Delker, D.A., Jo, J., Bertoletti, A., Hagedorn, C.H., and Gale, M. (2013). IL-1β Production through the NLRP3 Inflammasome by Hepatic Macrophages Links Hepatitis C Virus Infection with Liver Inflammation and Disease. PLoS Pathog. *9*, e1003330.

Netea, M.G., Balkwill, F., Chonchol, M., Cominelli, F., Donath, M.Y., Giamarellos-Bourboulis, E.J., Golenbock, D., Gresnigt, M.S., Heneka, M.T., Hoffman, H.M., *et al.* (2017). A guiding map for inflammation. Nat. Immunol. *18*, 826-831.

Newton, R.C. (1986). Human Monocyte Production of Interleukin-1: Parameters of the Induction of Interleukin-1 Secretion by Lipopolysaccharides. J. Leukoc. Biol. *39*, 299-311.

Nussenzweig, M.C., Steinman, R.M., Gutchinov, B., and Cohn, Z.A. (1980). Dendritic cells are accessory cells for the development of anti- trinitrophenyl cytotoxic T lymphocytes. The Journal of Experimental Medicine *152*, 1070-1084.

References

O'Neill, L.A., and Bowie, A.G. (2007). The family of five: TIR-domain-containing adaptors in Toll-like receptor signalling. Nat. Rev. Immunol. *7*, 353-364.

Ocaña-Macchi, M., Bel, M., Guzylack-Piriou, L., Ruggli, N., Liniger, M., McCullough, K.C., Sakoda, Y., Isoda, N., Matrosovich, M., and Summerfield, A. (2009). Hemagglutinin-dependent tropism of H5N1 avian influenza virus for human endothelial cells. J. Virol. *83*, 12947-12955.

Ohtsuka, T., Liu, X.F., Koga, Y., Kitajima, Y., Nakafusa, Y., Ha, C.W., Lee, S.W., and Miyazaki, K. (2006). Methylation-induced silencing of ASC and the effect of expressed ASC on p53-mediated chemosensitivity in colorectal cancer. Oncogene *25*, 1807-1811.

Okada, N., Fujii, C., Matsumura, T., Kitazawa, M., Okuyama, R., Taniguchi, S., and Hida, S. (2016). Novel role of ASC as a regulator of metastatic phenotype. Cancer medicine *5*, 2487-2500.

Okamura, H., Tsutsi, H., Komatsu, T., Yutsudo, M., Hakura, A., Tanimoto, T., Torigoe, K., Okura, T., Nukada, Y., Hattori, K., and et al. (1995). Cloning of a new cytokine that induces IFN-gamma production by T cells. Nature *378*, 88-91.

Okin, D., and Medzhitov, R. (2012). Evolution of Inflammatory Diseases. Curr. Biol. *22*, R733-R740.

Orlowski, G.M., Colbert, J.D., Sharma, S., Bogyo, M., Robertson, S.A., and Rock, K.L. (2015). Multiple Cathepsins Promote Pro-IL-1β Synthesis and NLRP3-Mediated IL-1β Activation. J. Immunol. *195*, 1685-1697.

Ormo, M., Cubitt, A.B., Kallio, K., Gross, L.A., Tsien, R.Y., and Remington, S.J. (1996). Crystal structure of the Aequorea victoria green fluorescent protein. Science *273*, 1392-1395.

Oroz, J., Barrera-Vilarmau, S., Alfonso, C., Rivas, G., and de Alba, E. (2016). Asc Pyrin Domain Self-Associates and Binds Nlrp3 Using Equivalent Binding Interfaces. J. Biol. Chem. *291*, 19487-19501.

Osterlund, P., Pirhonen, J., Ikonen, N., Ronkko, E., Strengell, M., Makela, S.M., Broman, M., Hamming, O.J., Hartmann, R., Ziegler, T., and Julkunen, I. (2010). Pandemic H1N1 2009 influenza A virus induces weak cytokine responses in human macrophages and dendritic cells and is highly sensitive to the antiviral actions of interferons. J. Virol. *84*, 1414-1422.

Pabst, D., Kuehn, J., Schuler-Luettmann, S., Wiebe, K., and Lebiedz, P. (2011). Acute Respiratory Distress Syndrome as a presenting manifestation in young patients infected with H1N1 influenza virus. Eur. J. Intern. Med. *22*, e119-124.

Palazon-Riquelme, P., Worboys, J.D., Green, J., Valera, A., Martin-Sanchez, F., Pellegrini, C., Brough, D., and Lopez-Castejon, G. (2018). USP7 and USP47 deubiquitinases regulate NLRP3 inflammasome activation. EMBO reports *19*, e44766.

Pang, I.K., Ichinohe, T., and Iwasaki, A. (2013a). IL-1R signaling in dendritic cells replaces pattern-recognition receptors in promoting $CD8^+$ T cell responses to influenza A virus. Nat. Immunol. *14*, 246-253.

Pang, I.K., Pillai, P.S., and Iwasaki, A. (2013b). Efficient influenza A virus replication in the respiratory tract requires signals from TLR7 and RIG-I. Proc. Natl. Acad. Sci. U. S. A. *110*, 13910-13915.

Pavillard, L.E., Canadas-Lozano, D., Alcocer-Gomez, E., Marin-Aguilar, F., Pereira, S., Robertson, A.A.B., Muntane, J., Ryffel, B., Cooper, M.A., Quiles, J.L., *et al.* (2017). NLRP3-inflammasome inhibition prevents high fat and high sugar diets-induced heart damage through autophagy induction. Oncotarget *8*, 99740-99756.

Peiró, T., Patel, D.F., Akthar, S., Gregory, L.G., Pyle, C.J., Harker, J.A., Birrell, M.A., Lloyd, C.M., and Snelgrove, R.J. (2017). Neutrophils drive alveolar macrophage IL-1β release during respiratory viral infection. Thorax *73*, 546-556.

Peisley, A., Wu, B., Xu, H., Chen, Z.J., and Hur, S. (2014). Structural basis for ubiquitin-mediated antiviral signal activation by RIG-I. Nature *509*, 110-114.

Peisley, A., Wu, B., Yao, H., Walz, T., and Hur, S. (2013). RIG-I forms signaling-competent filaments in an ATP-dependent, ubiquitin-independent manner. Mol. Cell *51*, 573-583.

Perregaux, D., Barberia, J., Lanzetti, A.J., Geoghegan, K.F., Carty, T.J., and Gabel, C.A. (1992). IL-1 beta maturation: evidence that mature cytokine formation can be induced specifically by nigericin. J. Immunol. *149*, 1294-1303.

Perregaux, D., and Gabel, C.A. (1994). Interleukin-1 beta maturation and release in response to ATP and nigericin. Evidence that potassium depletion mediated by these agents is a necessary and common feature of their activity. J. Biol. Chem. *269*, 15195-15203.

Perregaux, D.G., McNiff, P., Laliberte, R., Hawryluk, N., Peurano, H., Stam, E., Eggler, J., Griffiths, R., Dombroski, M.A., and Gabel, C.A. (2001). Identification and characterization of a novel class of interleukin-1 post-translational processing inhibitors. J. Pharmacol. Exp. Ther. *299*, 187-197.

Perrone, L.A., Plowden, J.K., Garcia-Sastre, A., Katz, J.M., and Tumpey, T.M. (2008). H5N1 and 1918 pandemic influenza virus infection results in early and excessive infiltration of macrophages and neutrophils in the lungs of mice. PLoS Pathog. *4*, e1000115.

Pestka, S., Krause, C.D., and Walter, M.R. (2004). Interferons, interferon-like cytokines, and their receptors. Immunol. Rev. *202*, 8-32.

Petrilli, V., Papin, S., Dostert, C., Mayor, A., Martinon, F., and Tschopp, J. (2007). Activation of the NALP3 inflammasome is triggered by low intracellular potassium concentration. Cell Death Differ. *14*, 1583-1589.

Pham, C.T. (2006). Neutrophil serine proteases: specific regulators of inflammation. Nat. Rev. Immunol. *6*, 541-550.

Phipps-Yonas, H., Seto, J., Sealfon, S.C., Moran, T.M., and Fernandez-Sesma, A. (2008). Interferon-beta pretreatment of conventional and plasmacytoid human dendritic cells enhances their activation by influenza virus. PLoS Pathog. *4*, e1000193.

References

Pichlmair, A., Schulz, O., Tan, C.P., Näslund, T.I., Liljeström, P., Weber, F., and Reis e Sousa, C. (2006). RIG-I-Mediated Antiviral Responses to Single-Stranded RNA Bearing 5'-Phosphates. Science *314*, 997-1001.

Pielak, R.M., and Chou, J.J. (2011). Influenza M2 proton channels. Biochim. Biophys. Acta *1808*, 522-529.

Pierini, R., Juruj, C., Perret, M., Jones, C.L., Mangeot, P., Weiss, D.S., and Henry, T. (2012). AIM2/ASC triggers caspase-8-dependent apoptosis in Francisella-infected caspase-1-deficient macrophages. Cell Death Differ. *19*, 1709-1721.

Pillay, J., den Braber, I., Vrisekoop, N., Kwast, L.M., de Boer, R.J., Borghans, J.A., Tesselaar, K., and Koenderman, L. (2010). In vivo labeling with 2H2O reveals a human neutrophil lifespan of 5.4 days. Blood *116*, 625-627.

Pinar, A., Dowling, J.K., Bitto, N.J., Robertson, A.A., Latz, E., Stewart, C.R., Drummond, G.R., Cooper, M.A., McAuley, J.L., Tate, M.D., and Mansell, A. (2017). PB1-F2 Peptide Derived from Avian Influenza A Virus H7N9 Induces Inflammation via Activation of the NLRP3 Inflammasome. J. Biol. Chem. *292*, 826-836.

Poltorak, A., He, X., Smirnova, I., Liu, M.Y., Van Huffel, C., Du, X., Birdwell, D., Alejos, E., Silva, M., Galanos, C., *et al.* (1998). Defective LPS signaling in C3H/HeJ and C57BL/10ScCr mice: mutations in Tlr4 gene. Science *282*, 2085-2088.

Pontillo, A., Silva, L.T., Oshiro, T.M., Finazzo, C., Crovella, S., and Duarte, A.J. (2012). HIV-1 induces NALP3-inflammasome expression and interleukin-1beta secretion in dendritic cells from healthy individuals but not from HIV-positive patients. AIDS *26*, 11-18.

Pothlichet, J., Meunier, I., Davis, B.K., Ting, J.P.Y., Skamene, E., von Messling, V., and Vidal, S.M. (2013). Type I IFN triggers RIG-I/TLR3/NLRP3-dependent inflammasome activation in influenza A virus infected cells. PLoS Pathog. *9*, e1003256.

Poyet, J.-L., Srinivasula, S.M., Tnani, M., Razmara, M., Fernandes-Alnemri, T., and Alnemri, E.S. (2001). Identification of Ipaf, a Human Caspase-1-activating Protein Related to Apaf-1. J. Biol. Chem. *276*, 28309-28313.

Primiano, M.J., Lefker, B.A., Bowman, M.R., Bree, A.G., Hubeau, C., Bonin, P.D., Mangan, M., Dower, K., Monks, B.G., Cushing, L., *et al.* (2016). Efficacy and Pharmacology of the NLRP3 Inflammasome Inhibitor CP-456,773 (CRID3) in Murine Models of Dermal and Pulmonary Inflammation. J. Immunol. *197*, 2421-2433.

Proell, M., Gerlic, M., Mace, Peter D., Reed, John C., and Riedl, Stefan J. (2013). The CARD plays a critical role in ASC foci formation and inflammasome signalling. Biochem. J. *449*, 613-621.

Purnama, C., Ng, S.L., Tetlak, P., Setiagani, Y.A., Kandasamy, M., Baalasubramanian, S., Karjalainen, K., and Ruedl, C. (2014). Transient ablation of alveolar macrophages leads to massive pathology of influenza infection without affecting cellular adaptive immunity. Eur. J. Immunol. *44*, 2003-2012.

References

Py, Bénédicte F., Kim, M.-S., Vakifahmetoglu-Norberg, H., and Yuan, J. (2013). Deubiquitination of NLRP3 by BRCC3 Critically Regulates Inflammasome Activity. Mol. Cell *49*, 331-338.

Qiu, F., Maniar, A., Diaz, M.Q., Chapoval, A.I., and Medvedev, A.E. (2011). Activation of cytokine-producing and antitumor activities of natural killer cells and macrophages by engagement of Toll-like and NOD-like receptors. Innate Immun. *17*, 375-387.

Rada, B.K., Geiszt, M., Kaldi, K., Timar, C., and Ligeti, E. (2004). Dual role of phagocytic NADPH oxidase in bacterial killing. Blood *104*, 2947-2953.

Ramani, V., and Awasthi, S. (2015). Toll-like receptor 4-interacting SPA4 peptide suppresses the NLRP3 inflammasome in response to LPS and ATP stimuli. J. Leukoc. Biol. *98*, 1037-1048.

Ramírez-Martínez, G., Cruz-Lagunas, A., Jiménez-Alvarez, L., Espinosa, E., Ortíz-Quintero, B., Santos-Mendoza, T., Herrera, M.T., Canché-Pool, E., Mendoza, C., Bañales, J.L., *et al.* (2013). Seasonal and pandemic influenza H1N1 viruses induce differential expression of SOCS-1 and RIG-I genes and cytokine/chemokine production in macrophages. Cytokine *62*, 151-159.

Ramos, E., Aróstegui, J.I., Campuzano, S., Rius, J., Bousoño, C., and Yagüe, J. (2005). Positive clinical and biochemical responses to anakinra in a 3-yr-old patient with cryopyrin-associated periodic syndrome (CAPS). Rheumatology *44*, 1072-1073.

Ramos, H.J., Lanteri, M.C., Blahnik, G., Negash, A., Suthar, M.S., Brassil, M.M., Sodhi, K., Treuting, P.M., Busch, M.P., Norris, P.J., and Gale, M., Jr. (2012). IL-1β signaling promotes CNS-intrinsic immune control of West Nile virus infection. PLoS Pathog. *8*, e1003039.

Ratsimandresy, R.A., Chu, L.H., Khare, S., de Almeida, L., Gangopadhyay, A., Indramohan, M., Misharin, A.V., Greaves, D.R., Perlman, H., Dorfleutner, A., and Stehlik, C. (2017). The PYRIN domain-only protein POP2 inhibits inflammasome priming and activation. Nat Commun *8*, 15556.

Ren, H., Kong, Y., Liu, Z., Zang, D., Yang, X., Wood, K., Li, M., and Liu, Q. (2018). Selective NLRP3 (Pyrin Domain-Containing Protein 3) Inflammasome Inhibitor Reduces Brain Injury After Intracerebral Hemorrhage. Stroke *49*, 184-192.

Ren, R., Wu, S., Cai, J., Yang, Y., Ren, X., Feng, Y., Chen, L., Qin, B., Xu, C., Yang, H., *et al.* (2017). The H7N9 influenza A virus infection results in lethal inflammation in the mammalian host via the NLRP3-caspase-1 inflammasome. Sci. Rep. *7*, 7625.

Richards, N., Schaner, P., Diaz, A., Stuckey, J., Shelden, E., Wadhwa, A., and Gumucio, D.L. (2001). Interaction between Pyrin and the Apoptotic Speck Protein (ASC) Modulates ASC-induced Apoptosis. J. Biol. Chem. *276*, 39320-39329.

Riera Romo, M., Perez-Martinez, D., and Castillo Ferrer, C. (2016). Innate immunity in vertebrates: an overview. Immunology *148*, 125-139.

Riteau, N., Baron, L., Villeret, B., Guillou, N., Savigny, F., Ryffel, B., Rassendren, F., Le Bert, M., Gombault, A., and Couillin, I. (2012). ATP release and purinergic signaling: A common pathway for particle-mediated inflammasome activation. Cell Death and Disease *11*, e403.

References

Riteau, N., Gasse, P., Fauconnier, L., Gombault, A., Couegnat, M., Fick, L., Kanellopoulos, J., Quesniaux, V.F.J., Marchand-Adam, S., Crestani, B., *et al.* (2010). Extracellular ATP is a danger signal activating P2X 7 receptor in lung inflammation and fibrosis. Am. J. Respir. Crit. Care Med. *182*, 774-783.

Roach, D.R., Bean, A.G., Demangel, C., France, M.P., Briscoe, H., and Britton, W.J. (2002). TNF regulates chemokine induction essential for cell recruitment, granuloma formation, and clearance of mycobacterial infection. J. Immunol. *168*, 4620-4627.

Roberts, T.L., Idris, A., Dunn, J.A., Kelly, G.M., Burnton, C.M., Hodgson, S., Hardy, L.L., Garceau, V., Sweet, M.J., Ross, I.L., *et al.* (2009). HIN-200 Proteins Regulate Caspase Activation in Response to Foreign Cytoplasmic DNA. Science *323*, 1057-1060.

Robertson, J.S., Nicolson, C., Harvey, R., Johnson, R., Major, D., Guilfoyle, K., Roseby, S., Newman, R., Collin, R., Wallis, C., *et al.* (2011). The development of vaccine viruses against pandemic A(H1N1) influenza. Vaccine *29*, 1836-1843.

Robinson, K.M., Ramanan, K., Clay, M.E., McHugh, K.J., Pilewski, M.J., Nickolich, K.L., Corey, C., Shiva, S., Wang, J., and Alcorn, J.F. (2018). The inflammasome potentiates influenza/Staphylococcus aureus superinfection in mice. JCI insight *3*, 97470.

Rock, F.L., Hardiman, G., Timans, J.C., Kastelein, R.A., and Bazan, J.F. (1998). A family of human receptors structurally related to Drosophila Toll. Proc. Natl. Acad. Sci. U. S. A. *95*, 588-593.

Rodgers, B.C., and Mims, C.A. (1982a). Influenza virus replication in human alveolar macrophages. J. Med. Virol. *9*, 177-184.

Rodgers, B.C., and Mims, C.A. (1982b). Role of macrophage activation and interferon in the resistance of alveolar macrophages from infected mice to influenza virus. Infect. Immun. *36*, 1154-1159.

Rollins, B.J. (1997). Chemokines. Blood *90*, 909-928.

Rorvig, S., Ostergaard, O., Heegaard, N.H., and Borregaard, N. (2013). Proteome profiling of human neutrophil granule subsets, secretory vesicles, and cell membrane: correlation with transcriptome profiling of neutrophil precursors. J. Leukoc. Biol. *94*, 711-721.

Rosenblum, M.D., Remedios, K.A., and Abbas, A.K. (2015). Mechanisms of human autoimmunity. The Journal of Clinical Investigation *125*, 2228-2233.

Rotta Detto Loria, J., Rohmann, K., Droemann, D., Kujath, P., Rupp, J., Goldmann, T., and Dalhoff, K. (2013). Nontypeable Haemophilus Influenzae Infection Upregulates the NLRP3 Inflammasome and Leads to Caspase-1-Dependent Secretion of Interleukin-1β - A Possible Pathway of Exacerbations in COPD. PLoS One *8*, e66818-e66818.

Ruhl, S., and Broz, P. (2015). Caspase-11 activates a canonical NLRP3 inflammasome by promoting K(+) efflux. Eur. J. Immunol. *45*, 2927-2936.

References

Sabatel, C., Radermecker, C., Fievez, L., Paulissen, G., Chakarov, S., Fernandes, C., Olivier, S., Toussaint, M., Pirottin, D., Xiao, X., *et al.* (2017). Exposure to Bacterial CpG DNA Protects from Airway Allergic Inflammation by Expanding Regulatory Lung Interstitial Macrophages. Immunity *46*, 457-473.

Sagoo, P., Garcia, Z., Breart, B., Lemaitre, F., Michonneau, D., Albert, M.L., Levy, Y., and Bousso, P. (2016). In vivo imaging of inflammasome activation reveals a subcapsular macrophage burst response that mobilizes innate and adaptive immunity. Nat. Med. *22*, 64-71.

Sakai, S., Kawamata, H., Mantani, N., Kogure, T., Shimada, Y., Terasawa, K., Sakai, T., Imanishi, N., and Ochiai, H. (2000). Therapeutic Effect of Anti-Macrophage Inflammatory Protein 2 Antibody on Influenza Virus-Induced Pneumonia in Mice. J. Virol. *74*, 2472-2476.

Samstad, E.O., Niyonzima, N., Nymo, S., Aune, M.H., Ryan, L., Bakke, S.S., Lappegård, K.T., Brekke, O.L., Lambris, J.D., Damås, J.K., *et al.* (2014). Cholesterol crystals induce complement-dependent inflammasome activation and cytokine release. J. Immunol. *192*, 2837-2845.

Sand, J., Haertel, E., Biedermann, T., Contassot, E., Reichmann, E., French, L.E., Werner, S., and Beer, H.-D. (2018). Expression of inflammasome proteins and inflammasome activation occurs in human, but not in murine keratinocytes. Cell Death Dis. *9*, 24.

Sanders, C.J., Vogel, P., McClaren, J.L., Bajracharya, R., Doherty, P.C., and Thomas, P.G. (2013). Compromised respiratory function in lethal influenza infection is characterized by the depletion of type I alveolar epithelial cells beyond threshold levels. Am. J. Physiol. Lung Cell Mol. Physiol. *304*, L481-488.

Sanders, M.G., Parsons, M.J., Howard, A.G., Liu, J., Fassio, S.R., Martinez, J.A., and Bouchier-Hayes, L. (2015). Single-cell imaging of inflammatory caspase dimerization reveals differential recruitment to inflammasomes. Cell Death Dis. *6*, e1813.

Sato, M., Hata, N., Asagiri, M., Nakaya, T., Taniguchi, T., and Tanaka, N. (1998). Positive feedback regulation of type I IFN genes by the IFN-inducible transcription factor IRF-7. FEBS Lett. *441*, 106-110.

Sato, S., Sugiyama, M., Yamamoto, M., Watanabe, Y., Kawai, T., Takeda, K., and Akira, S. (2003). Toll/IL-1 receptor domain-containing adaptor inducing IFN-β (TRIF) associates with TNF receptor-associated factor 6 and TANK-binding kinase 1, and activates two distinct transcription factors, NF-κB and IFN-regulatory factor-3, in the Toll-like receptor signaling. J. Immunol. *171*, 4304-4310.

Sborgi, L., Ravotti, F., Dandey, V.P., Dick, M.S., Mazur, A., Reckel, S., Chami, M., Scherer, S., Huber, M., Bockmann, A., *et al.* (2015). Structure and assembly of the mouse ASC inflammasome by combined NMR spectroscopy and cryo-electron microscopy. Proc. Natl. Acad. Sci. U. S. A. *112*, 13237-13242.

Schindelin, J., Arganda-Carreras, I., Frise, E., Kaynig, V., Longair, M., Pietzsch, T., Preibisch, S., Rueden, C., Saalfeld, S., Schmid, B., *et al.* (2012). Fiji: an open-source platform for biological-image analysis. Nature Methods *9*, 676.

References

Schmid-Burgk, J.L., Gaidt, M.M., Schmidt, T., Ebert, T.S., Bartok, E., and Hornung, V. (2015). Caspase-4 mediates non-canonical activation of the NLRP3 inflammasome in human myeloid cells. Eur. J. Immunol. *45*, 2911-2917.

Schmidt, F.I., Lu, A., Chen, J.W., Ruan, J., Tang, C., Wu, H., and Ploegh, H.L. (2016). A single domain antibody fragment that recognizes the adaptor ASC defines the role of ASC domains in inflammasome assembly. The Journal of Experimental Medicine *213*, 771-790.

Schmitz, N., Kurrer, M., Bachmann, M.F., and Kopf, M. (2005). Interleukin-1 is responsible for acute lung immunopathology but increases survival of respiratory influenza virus infection. J. Virol. *79*, 6441-6448.

Schneider, C., Nobs, S.P., Heer, A.K., Kurrer, M., Klinke, G., van Rooijen, N., Vogel, J., and Kopf, M. (2014). Alveolar Macrophages Are Essential for Protection from Respiratory Failure and Associated Morbidity following Influenza Virus Infection. PLoS Pathog. *10*, e1004053.

Schyns, J., Bureau, F., and Marichal, T. (2018). Lung Interstitial Macrophages: Past, Present, and Future. Journal of immunology research *2018*, 5160794-5160794.

Sebag, S.C., Koval, O.M., Paschke, J.D., Winters, C.J., Jaffer, O.A., Dworski, R., Sutterwala, F.S., Anderson, M.E., and Grumbach, I.M. (2017). Mitochondrial CaMKII inhibition in airway epithelium protects against allergic asthma. JCI insight *2*, e88297-e88297.

Serbina, N.V., Salazar-Mather, T.P., Biron, C.A., Kuziel, W.A., and Pamer, E.G. (2003). TNF/iNOS-producing dendritic cells mediate innate immune defense against bacterial infection. Immunity *19*, 59-70.

Sester, D.P., Thygesen, S.J., Sagulenko, V., Vajjhala, P.R., Cridland, J.A., Vitak, N., Chen, K.W., Osborne, G.W., Schroder, K., and Stacey, K.J. (2015). A novel flow cytometric method to assess inflammasome formation. J. Immunol. *194*, 455-462.

Sester, D.P., Zamoshnikova, A., Thygesen, S.J., Vajjhala, P.R., Cridland, S.O., Schroder, K., and Stacey, K.J. (2016). Assessment of Inflammasome Formation by Flow Cytometry. Curr. Protoc. Immunol. *114*, 14.40.11-14.40.29.

Sha, W., Mitoma, H., Hanabuchi, S., Bao, M., Weng, L., Sugimoto, N., Liu, Y., Zhang, Z., Zhong, J., Sun, B., and Liu, Y.-J. (2014). Human NLRP3 inflammasome senses multiple types of bacterial RNAs. Proceedings of the National Academy of Sciences *111*, 16059-16064.

Shalek, A.K., Satija, R., Shuga, J., Trombetta, J.J., Gennert, D., Lu, D., Chen, P., Gertner, R.S., Gaublomme, J.T., Yosef, N., *et al.* (2014). Single-cell RNA-seq reveals dynamic paracrine control of cellular variation. Nature *510*, 363-369.

Shaner, N.C., Campbell, R.E., Steinbach, P.A., Giepmans, B.N.G., Palmer, A.E., and Tsien, R.Y. (2004). Improved monomeric red, orange and yellow fluorescent proteins derived from Discosoma sp. red fluorescent protein. Nat. Biotechnol. *22*, 1567-1572.

References

Shao, W., Yeretssian, G., Doiron, K., Hussain, S.N., and Saleh, M. (2007). The caspase-1 digestome identifies the glycolysis pathway as a target during infection and septic shock. J. Biol. Chem. *282*, 36321-36329.

Shaughnessy, L.M., and Swanson, J.A. (2007). The role of the activated macrophage in clearing Listeria monocytogenes infection. Front. Biosci. *12*, 2683-2692.

Shaw, M.L., and Palese, P. (2013). Chapter 40: Orthomyxoviridae. In Fields VIrology, D.M. Knipe, and P.M. Howley, eds. (Philadelphia: Lippincott Williams & Wilkins).

Shaw, O.M., Steiger, S., Liu, X., Hamilton, J.A., and Harper, J.L. (2014). Brief report: Granulocyte-macrophage colony-stimulating factor drives monosodium urate monohydrate crystal-induced inflammatory macrophage differentiation and NLRP3 inflammasome up-regulation in an in vivo mouse model. Arthritis Rheumatol *66*, 2423-2428.

Shi, J., Zhao, Y., Wang, K., Shi, X., Wang, Y., Huang, H., Zhuang, Y., Cai, T., Wang, F., and Shao, F. (2015). Cleavage of GSDMD by inflammatory caspases determines pyroptotic cell death. Nature *526*, 660.

Shi, J., Zhao, Y., Wang, Y., Gao, W., Ding, J., Li, P., Hu, L., and Shao, F. (2014). Inflammatory caspases are innate immune receptors for intracellular LPS. Nature *514*, 187.

Shieh, W.J., Blau, D.M., Denison, A.M., Deleon-Carnes, M., Adem, P., Bhatnagar, J., Sumner, J., Liu, L., Patel, M., Batten, B., *et al.* (2010). 2009 pandemic influenza A (H1N1): pathology and pathogenesis of 100 fatal cases in the United States. Am. J. Pathol. *177*, 166-175.

Shimada, K., Crother, Timothy R., Karlin, J., Dagvadorj, J., Chiba, N., Chen, S., Ramanujan, V.K., Wolf, Andrea J., Vergnes, L., Ojcius, David M., *et al.* (2012). Oxidized Mitochondrial DNA Activates the NLRP3 Inflammasome during Apoptosis. Immunity *36*, 401-414.

Shimazu, R., Akashi, S., Ogata, H., Nagai, Y., Fukudome, K., Miyake, K., and Kimoto, M. (1999). MD-2, a Molecule that Confers Lipopolysaccharide Responsiveness on Toll-like Receptor 4. The Journal of Experimental Medicine *189*, 1777-1782.

Shimizu, T., Takizawa, N., Watanabe, K., Nagata, K., and Kobayashi, N. (2011). Crucial role of the influenza virus NS2 (NEP) C-terminal domain in M1 binding and nuclear export of vRNP. FEBS Lett. *585*, 41-46.

Shirey, K.A., Lai, W., Patel, M.C., Pletneva, L.M., Pang, C., Kurt-Jones, E., Lipsky, M., Roger, T., Calandra, T., Tracey, K.J., *et al.* (2016). Novel strategies for targeting innate immune responses to influenza. Mucosal Immunol. *9*, 1173-1182.

Short, K.R., Kroeze, E.J.B.V., Fouchier, R.A.M., and Kuiken, T. (2014). Pathogenesis of influenza-induced acute respiratory distress syndrome. Lancet Infect. Dis. *14*, 57-69.

Shrivastava, S., Mukherjee, A., Ray, R., and Ray, R.B. (2013). Hepatitis C Virus Induces Interleukin-1β (IL-1β)/IL-18 in Circulatory and Resident Liver Macrophages. J. Virol. *87*, 12284-12290.

References

Shurety, W., Merino-Trigo, A., Brown, D., Hume, D.A., and Stow, J.L. (2000). Localization and post-Golgi trafficking of tumor necrosis factor-alpha in macrophages. J. Interferon Cytokine Res. *20*, 427-438.

Sidwell, R.W., Huffman, J.H., Barnard, D.L., Bailey, K.W., Wong, M.H., Morrison, A., Syndergaard, T., and Kim, C.U. (1998). Inhibition of influenza virus infections in mice by GS4104, an orally effective influenza virus neuraminidase inhibitor. Antiviral Res. *37*, 107-120.

Siegal, F.P., Kadowaki, N., Shodell, M., Fitzgerald-Bocarsly, P.A., Shah, K., Ho, S., Antonenko, S., and Liu, Y.J. (1999). The nature of the principal type 1 interferon-producing cells in human blood. Science *284*, 1835-1837.

Sirén, J., Imaizumi, T., Sarkar, D., Pietilä, T., Noah, D.L., Lin, R., Hiscott, J., Krug, R.M., Fisher, P.B., Julkunen, I., and Matikainen, S. (2006). Retinoic acid inducible gene-I and mda-5 are involved in influenza A virus-induced expression of antiviral cytokines. Microbes and Infection *8*, 2013-2020.

Soderberg, M., Hellstrom, S., Lundgren, R., and Bergh, A. (1990). Bronchial epithelium in humans recently recovering from respiratory infections caused by influenza or mycoplasma. Eur. Respir. J. *3*, 1023-1028.

Sokolovska, A., Becker, C.E., Ip, W.K., Rathinam, V.A., Brudner, M., Paquette, N., Tanne, A., Vanaja, S.K., Moore, K.J., Fitzgerald, K.A., *et al.* (2013). Activation of caspase-1 by the NLRP3 inflammasome regulates the NADPH oxidase NOX2 to control phagosome function. Nat. Immunol. *14*, 543-553.

Song, H., Liu, B., Huai, W., Yu, Z., Wang, W., Zhao, J., Han, L., Jiang, G., Zhang, L., Gao, C., and Zhao, W. (2016). The E3 ubiquitin ligase TRIM31 attenuates NLRP3 inflammasome activation by promoting proteasomal degradation of NLRP3. Nat. Commun. *7*, 13727-13727.

Song, N., Liu, Z.S., Xue, W., Bai, Z.F., Wang, Q.Y., Dai, J., Liu, X., Huang, Y.J., Cai, H., Zhan, X.Y., *et al.* (2017). NLRP3 Phosphorylation Is an Essential Priming Event for Inflammasome Activation. Mol. Cell *68*, 185-197.e186.

Srivastava, B., Błażejewska, P., Heßmann, M., Bruder, D., Geffers, R., Mauel, S., Gruber, A.D., and Schughart, K. (2009). Host Genetic Background Strongly Influences the Response to Influenza A Virus Infections. PLoS One *4*, e4857.

Stark, G.R., Kerr, I.M., Williams, B.R., Silverman, R.H., and Schreiber, R.D. (1998). How cells respond to interferons. Annu. Rev. Biochem. *67*, 227-264.

Steinman, R.M., and Witmer, M.D. (1978). Lymphoid dendritic cells are potent stimulators of the primary mixed leukocyte reaction in mice. Proc. Natl. Acad. Sci. U. S. A. *75*, 5132-5136.

Stienstra, R., Joosten, L.A.B., Koenen, T., van Tits, B., van Diepen, J.A., van den Berg, S.A.A., Rensen, P.C.N., Voshol, P.J., Fantuzzi, G., Hijmans, A., *et al.* (2010). The Inflammasome-Mediated Caspase-1 Activation Controls Adipocyte Differentiation and Insulin Sensitivity. Cell Metab. *12*, 593-605.

References

Stienstra, R., van Diepen, J.A., Tack, C.J., Zaki, M.H., van de Veerdonk, F.L., Perera, D., Neale, G.A., Hooiveld, G.J., Hijmans, A., Vroegrijk, I., *et al.* (2011). Inflammasome is a central player in the induction of obesity and insulin resistance. Proceedings of the National Academy of Sciences *108*, 15324-15329.

Stout-Delgado, H.W., Vaughan, S.E., Shirali, A.C., Jaramillo, R.J., and Harrod, K.S. (2012). Impaired NLRP3 inflammasome function in elderly mice during influenza infection is rescued by treatment with nigericin. J. Immunol. *188*, 2815-2824.

Stutz, A., Horvath, G.L., Monks, B.G., and Latz, E. (2013). ASC Speck Formation as a Readout for Inflammasome Activation. In The Inflammasome: Methods and Protocols, C.M. De Nardo, and E. Latz, eds. (Totowa, NJ: Humana Press), pp. 91-101.

Stutz, A., Kolbe, C.C., Stahl, R., Horvath, G.L., Franklin, B.S., van Ray, O., Brinkschulte, R., Geyer, M., Meissner, F., and Latz, E. (2017). NLRP3 inflammasome assembly is regulated by phosphorylation of the pyrin domain. J. Exp. Med. *214*, 1725-1736.

Subramanian, N., Natarajan, K., Clatworthy, M.R., Wang, Z., and Germain, R.N. (2013). The adaptor MAVS promotes NLRP3 mitochondrial localization and inflammasome activation. Cell *153*, 348-361.

Sullivan, S.G., Chilver, M.B., Carville, K.S., Deng, Y.-M., Grant, K.A., Higgins, G., Komadina, N., Leung, V.K., Minney-Smith, C.A., Teng, D., *et al.* (2017). Low interim influenza vaccine effectiveness, Australia, 1 May to 24 September 2017. Eurosurveillance *22*, 17-00707.

Sun, G., Ota, C., Kitaoka, S., Chiba, Y., Takayanagi, M., Kitamura, T., Yamamoto, K., Fujie, H., Mikami, H., Uematsu, M., *et al.* (2015). Elevated serum levels of neutrophil elastase in patients with influenza virus-associated encephalopathy. J. Neurol. Sci. *349*, 190-195.

Sun, S., Xia, S., Ji, Y., Kersten, S., and Qi, L. (2012). The ATP-P2X 7 signaling axis is dispensable for obesity-associated inflammasome activation in adipose tissue. Diabetes *61*, 1471-1478.

Sundararajan, A., Huan, L., Richards, K.A., Marcelin, G., Alam, S., Joo, H., Yang, H., Webby, R.J., Topham, D.J., Sant, A.J., and Sangster, M.Y. (2012). Host differences in influenza-specific CD4 T cell and B cell responses are modulated by viral strain and route of immunization. PLoS One *7*, e34377.

Sung, S.S., Fu, S.M., Rose, C.E., Jr., Gaskin, F., Ju, S.T., and Beaty, S.R. (2006). A major lung CD103 (alphaE)-beta7 integrin-positive epithelial dendritic cell population expressing Langerin and tight junction proteins. J. Immunol. *176*, 2161-2172.

Sutterwala, F.S., Ogura, Y., Szczepanik, M., Lara-Tejero, M., Lichtenberger, G.S., Grant, E.P., Bertin, J., Coyle, A.J., Galán, J.E., Askenase, P.W., and Flavell, R.A. (2006). Critical Role for NALP3/CIAS1/Cryopyrin in Innate and Adaptive Immunity through Its Regulation of Caspase-1. Immunity *24*, 317-327.

References

Svetlikova, D., Kabat, P., Ohradanova, A., Pastorek, J., and Betakova, T. (2010). Influenza A virus replication is inhibited in IFN-λ2 and IFN-λ3 transfected or stimulated cells. Antiviral Res. *88*, 329-333.

Swirski, F.K., and Nahrendorf, M. (2013). Imaging macrophage development and fate in atherosclerosis and myocardial infarction. Immunol. Cell Biol. *91*, 297-303.

Szretter, K.J., Gangappa, S., Lu, X., Smith, C., Shieh, W.J., Zaki, S.R., Sambhara, S., Tumpey, T.M., and Katz, J.M. (2007). Role of host cytokine responses in the pathogenesis of avian H5N1 influenza viruses in mice. J. Virol. *81*, 2736-2744.

Takiyama, A., Wang, L., Tanino, M., Kimura, T., Kawagishi, N., Kunieda, Y., Katano, H., Nakajima, N., Hasegawa, H., Takagi, T., *et al.* (2010). Sudden death of a patient with pandemic influenza (A/H1N1pdm) virus infection by acute respiratory distress syndrome. Jpn. J. Infect. Dis. *63*, 72-74.

Tan, C.Z., and Arndt, J. (2001). Chapter 2 - The refractive index of silica glass and its dependence on pressure, temperature, and the wavelength of the incident light. In Silicon-Based Material and Devices, H.S. Nalwa, ed. (Burlington: Academic Press), pp. 51-91.

Tate, M.D., Brooks, A.G., and Reading, P.C. (2008). The role of neutrophils in the upper and lower respiratory tract during influenza virus infection of mice. Respir. Res. *9*, 57.

Tate, M.D., Brooks, A.G., and Reading, P.C. (2011a). Correlation between sialic acid expression and infection of murine macrophages by different strains of influenza virus. Microbes Infect *13*, 202-207.

Tate, M.D., Brooks, A.G., and Reading, P.C. (2011b). Inhibition of lectin-mediated innate host defences in vivo modulates disease severity during influenza virus infection. Immunol. Cell Biol. *89*, 482-491.

Tate, M.D., Brooks, A.G., Reading, P.C., and Mintern, J.D. (2012). Neutrophils sustain effective CD8+ T-cell responses in the respiratory tract following influenza infection. Immunol. Cell Biol. *90*, 197-205.

Tate, M.D., Deng, Y.M., Jones, J.E., Anderson, G.P., Brooks, A.G., and Reading, P.C. (2009). Neutrophils ameliorate lung injury and the development of severe disease during influenza infection. J. Immunol. *183*, 7441-7450.

Tate, M.D., Ioannidis, L.J., Croker, B., Brown, L.E., Brooks, A.G., and Reading, P.C. (2011c). The role of neutrophils during mild and severe influenza virus infections of mice. PLoS One *6*, e17618.

Tate, M.D., Ong, J.D., Dowling, J.K., McAuley, J.L., Robertson, A.B., Latz, E., Drummond, G.R., Cooper, M.A., Hertzog, P.J., and Mansell, A. (2016). Reassessing the role of the NLRP3 inflammasome during pathogenic influenza A virus infection via temporal inhibition. Sci. Rep. *6*, 27912.

Tate, M.D., Pickett, D.L., van Rooijen, N., Brooks, A.G., and Reading, P.C. (2010). Critical role of airway macrophages in modulating disease severity during influenza virus infection of mice. J. Virol. *84*, 7569-7580.

Tate, M.D., Schilter, H.C., Brooks, A.G., and Reading, P.C. (2011d). Responses of mouse airway epithelial cells and alveolar macrophages to virulent and avirulent strains of influenza A virus. Viral Immunol. *24*, 77-88.

Taylor, R.M. (1941). Experimental infection with influenza A virus in mice: the increase in intrapulmonary virus after inoculation and the influence of various factors thereon. J. Exp. Med. *73*, 43-55.

Teijaro, J.R., Walsh, K.B., Cahalan, S., Fremgen, D.M., Roberts, E., Scott, F., Martinborough, E., Peach, R., Oldstone, M.B., and Rosen, H. (2011). Endothelial cells are central orchestrators of cytokine amplification during influenza virus infection. Cell *146*, 980-991.

Teijaro, J.R., Walsh, K.B., Rice, S., Rosen, H., and Oldstone, M.B.A. (2014). Mapping the innate signaling cascade essential for cytokine storm during influenza virus infection. Proceedings of the National Academy of Sciences *111*, 3799-3804.

Terra, J.K., Cote, C.K., France, B., Jenkins, A.L., Bozue, J.A., Welkos, S.L., LeVine, S.M., and Bradley, K.A. (2010). Cutting Edge: Resistance to Bacillus anthracis Infection Mediated by a Lethal Toxin Sensitive Allele of Nalp1b/Nlrp1b. The Journal of Immunology *184*, 17-20.

Thiele, S., and Rosenkilde, M.M. (2014). Interaction of chemokines with their receptors--from initial chemokine binding to receptor activating steps. Curr. Med. Chem. *21*, 3594-3614.

Thomas, J.M., Pos, Z., Reinboth, J., Wang, R.Y., Wang, E., Frank, G.M., Lusso, P., Trinchieri, G., Alter, H.J., Marincola, F.M., and Thomas, E. (2014). Differential responses of plasmacytoid dendritic cells to influenza virus and distinct viral pathogens. J. Virol. *88*, 10758-10766.

Thomas, P.G., Dash, P., Aldridge Jr, J.R., Ellebedy, A.H., Reynolds, C., Funk, A.J., Martin, W.J., Lamkanfi, M., Webby, R.J., Boyd, K.L., *et al.* (2009). The intracellular sensor NLRP3 mediates key innate and healing responses to influenza A virus via the regulation of caspase-1. Immunity *30*, 566-575.

Thornberry, N.A., Bull, H.G., Calaycay, J.R., Chapman, K.T., Howard, A.D., Kostura, M.J., Miller, D.K., Molineaux, S.M., Weidner, J.R., Aunins, J., *et al.* (1992). A novel heterodimeric cysteine protease is required for interleukin-1[beta]processing in monocytes. Nature *356*, 768-774.

Ting, J.P.Y., Lovering, R.C., Alnemri, E.S., Bertin, J., Boss, J.M., Davis, B.K., Flavell, R.A., Girardin, S.E., Godzik, A., Harton, J.A., *et al.* (2008). The NLR Gene Family: A Standard Nomenclature. Immunity *28*, 285-287.

To, K.F., Chan, P.K., Chan, K.F., Lee, W.K., Lam, W.Y., Wong, K.F., Tang, N.L., Tsang, D.N., Sung, R.Y., Buckley, T.A., *et al.* (2001). Pathology of fatal human infection associated with avian influenza A H5N1 virus. J. Med. Virol. *63*, 242-246.

To, K.K.W., Hung, I.F.N., Li, I.W.S., Lee, K.-L., Koo, C.-K., Yan, W.-W., Liu, R., Ho, K.-Y., Chu, K.-H., Watt, C.-L., *et al.* (2010). Delayed Clearance of Viral Load and Marked Cytokine Activation in Severe Cases of Pandemic H1N1 2009 Influenza Virus Infection. Clin. Infect. Dis. *50*, 850-859.

References

Topham, D.J., Tripp, R.A., and Doherty, P.C. (1997). CD8+ T cells clear influenza virus by perforin or Fas-dependent processes. J. Immunol. *159*, 5197-5200.

Torigoe, K., Ushio, S., Okura, T., Kobayashi, S., Taniai, M., Kunikata, T., Murakami, T., Sanou, O., Kojima, H., Fujii, M., *et al.* (1997). Purification and characterization of the human interleukin-18 receptor. J. Biol. Chem. *272*, 25737-25742.

Trammell, R.A., Liberati, T.A., and Toth, L.A. (2012). Host genetic background and the innate inflammatory response of lung to influenza virus. Microbes and Infection *14*, 50-58.

Tran, H.B., Lewis, M.D., Tan, L.W., Lester, S.E., Baker, L.M., Ng, J., Hamilton-Bruce, M.A., Hill, C.L., Koblar, S.A., Rischmueller, M., *et al.* (2012). Immunolocalization of NLRP3 Inflammasome in Normal Murine Airway Epithelium and Changes following Induction of Ovalbumin-Induced Airway Inflammation. J. Allergy *2012*, 819176.

Triantafilou, K., Hughes, T.R., Triantafilou, M., and Morgan, B.P. (2013a). The complement membrane attack complex triggers intracellular Ca2+ fluxes leading to NLRP3 inflammasome activation. Journal of Cell Science *126*, 2903-2913.

Triantafilou, K., Kar, S., Vakakis, E., Kotecha, S., and Triantafilou, M. (2013b). Human respiratory syncytial virus viroporin SH: a viral recognition pathway used by the host to signal inflammasome activation. Thorax *68*, 66-75.

Trifonov, V., Racaniello, V., and Rabadan, R. (2009). The Contribution of the PB1-F2 Protein to the Fitness of Influenza A Viruses and its Recent Evolution in the 2009 Influenza A (H1N1) Pandemic Virus. PLoS Currents *1*, RRN1006.

Tripathi, S., Batra, J., Cao, W., Sharma, K., Patel, J.R., Ranjan, P., Kumar, A., Katz, J.M., Cox, N.J., Lal, R.B., *et al.* (2013). Influenza A virus nucleoprotein induces apoptosis in human airway epithelial cells: implications of a novel interaction between nucleoprotein and host protein Clusterin. Cell Death Dis. *4*, e562.

Tumpey, T.M., Basler, C.F., Aguilar, P.V., Zeng, H., Solorzano, A., Swayne, D.E., Cox, N.J., Katz, J.M., Taubenberger, J.K., Palese, P., and Garcia-Sastre, A. (2005). Characterization of the reconstructed 1918 Spanish influenza pandemic virus. Science *310*, 77-80.

Turvey, S.E., and Broide, D.H. (2010). Innate immunity. J. Allergy Clin. Immunol. *125*, S24-S32.

Tye, H., Kennedy, Catherine L., Najdovska, M., McLeod, L., McCormack, W., Hughes, N., Dev, A., Sievert, W., Ooi, Chia H., Ishikawa, T.-o., *et al.* (2012). STAT3-Driven Upregulation of TLR2 Promotes Gastric Tumorigenesis Independent of Tumor Inflammation. Cancer Cell *22*, 466-478.

Tzeng, T.-C., Schattgen, S., Monks, B., Wang, D., Cerny, A., Latz, E., Fitzgerald, K., and Golenbock, Douglas T. (2016). A Fluorescent Reporter Mouse for Inflammasome Assembly Demonstrates an Important Role for Cell-Bound and Free ASC Specks during In Vivo Infection. Cell Reports *16*, 571-582.

References

Uhlen, M., Fagerberg, L., Hallstrom, B.M., Lindskog, C., Oksvold, P., Mardinoglu, A., Sivertsson, A., Kampf, C., Sjostedt, E., Asplund, A., *et al.* (2015). Proteomics. Tissue-based map of the human proteome. Science *347*, 1260419.

Vajjhala, P.R., Lu, A., Brown, D.L., Pang, S.W., Sagulenko, V., Sester, D.P., Cridland, S.O., Hill, J.M., Schroder, K., Stow, J.L., *et al.* (2015). The Inflammasome Adaptor ASC Induces Procaspase-8 Death Effector Domain Filaments. J. Biol. Chem. *290*, 29217-29230.

Van de Craen, M., Vandenabeele, P., Declercq, W., Van den Brande, I., Van Loo, G., Molemans, F., Schotte, P., Van Criekinge, W., Beyaert, R., and Fiers, W. (1997). Characterization of seven murine caspase family members. FEBS Lett. *403*, 61-69.

van der Heijden, T., Kritikou, E., Venema, W., van Duijn, J., van Santbrink, P.J., Slutter, B., Foks, A.C., Bot, I., and Kuiper, J. (2017). NLRP3 Inflammasome Inhibition by MCC950 Reduces Atherosclerotic Lesion Development in Apolipoprotein E-Deficient Mice-Brief Report. Arterioscler. Thromb. Vasc. Biol. *37*, 1457-1461.

Van Der Sluijs, K.F., Van Elden, L.J.R., Arens, R., Nijhuis, M., Schuurman, R., Florquin, S., Kwakkel, J., Akira, S., Jansen, H.M., Lutter, R., and Van Der Polls, T. (2005). Enhanced viral clearance in interleukin-18 gene-deficient mice after pulmonary infection with influenza A virus. Immunology *114*, 112-120.

van der Velden, A.W., Velasquez, M., and Starnbach, M.N. (2003). Salmonella rapidly kill dendritic cells via a caspase-1-dependent mechanism. J. Immunol. *171*, 6742-6749.

van Riel, D., Leijten, L.M.E., van der Eerden, M., Hoogsteden, H.C., Boven, L.A., Lambrecht, B.N., Osterhaus, A.D.M.E., and Kuiken, T. (2011). Highly Pathogenic Avian Influenza Virus H5N1 Infects Alveolar Macrophages without Virus Production or Excessive TNF-Alpha Induction. PLoS Pathog. *7*, e1002099.

van Wilgenburg, B., Scherwitzl, I., Hutchinson, E.C., Leng, T., Kurioka, A., Kulicke, C., de Lara, C., Cole, S., Vasanawathana, S., Limpitikul, W., *et al.* (2016). MAIT cells are activated during human viral infections. Nat. Commun. *7*, 11653-11653.

Vandanmagsar, B., Youm, Y.-H., Ravussin, A., Galgani, J.E., Stadler, K., Mynatt, R.L., Ravussin, E., Stephens, J.M., and Dixit, V.D. (2011). The NLRP3 inflammasome instigates obesity-induced inflammation and insulin resistance. Nat. Med. *17*, 179-188.

VanoOsten Anderson, R., McGill, J., and Legge, K.L. (2010). Quantification of the frequency and multiplicity of infection of respiratory- and lymph node-resident dendritic cells during influenza virus infection. PLoS One *5*, e12902.

Vigano, E., Diamond, C.E., Spreafico, R., Balachander, A., Sobota, R.M., and Mortellaro, A. (2015). Human caspase-4 and caspase-5 regulate the one-step non-canonical inflammasome activation in monocytes. Nat Commun *6*, 8761.

Vijay, R., Fehr, A.R., Janowski, A.M., Athmer, J., Wheeler, D.L., Grunewald, M., Sompallae, R., Kurup, S.P., Meyerholz, D.K., Sutterwala, F.S., *et al.* (2017). Virus-induced inflammasome

activation is suppressed by prostaglandin D(2)/DP1 signaling. Proc. Natl. Acad. Sci. U. S. A. *114*, E5444-E5453.

Walev, I., Reske, K., Palmer, M., Valeva, A., and Bhakdi, S. (1995). Potassium-inhibited processing of IL-1 beta in human monocytes. The EMBO Journal *14*, 1607-1614.

Wang, J.-G., Williams, J.C., Davis, B.K., Jacobson, K., Doerschuk, C.M., Ting, J.P.-Y., and Mackman, N. (2011). Monocytic microparticles activate endothelial cells in an IL-1β–dependent manner. Blood *118*, 2366-2374.

Wang, J., Oberley-Deegan, R., Wang, S., Nikrad, M., Funk, C.J., Hartshorn, K.L., and Mason, R.J. (2009). Differentiated human alveolar type II cells secrete antiviral IL-29 (IFN-λ1) in response to influenza a infection. J. Immunol. *182*, 1296-1304.

Wang, J.P., Bowen, G.N., Padden, C., Cerny, A., Finberg, R.W., Newburger, P.E., and Kurt-Jones, E.A. (2008). Toll-like receptor-mediated activation of neutrophils by influenza A virus. Blood *112*, 2028-2034.

Wang, L., Qu, P., Zhao, J., and Chang, Y. (2014a). NLRP3 and downstream cytokine expression elevated in the monocytes of patients with coronary artery disease. Arch. Med. Sci. *10*, 791-800.

Wang, L., Schmidt, S., Larsen, P.P., Meyer, J.H., Roush, W.R., Latz, E., Holz, F.G., and Krohne, T.U. (2019). Efficacy of novel selective NLRP3 inhibitors in human and murine retinal pigment epithelial cells. J. Mol. Med. *97*, 523-532.

Wang, S.-M., Liao, Y.-T., Hu, Y.-S., Ho, T.-S., Shen, C.-F., Wang, J.-R., Lin, Y.-S., and Liu, C.-C. (2014b). Immunophenotype expressions and cytokine profiles of influenza A H1N1 virus infection in pediatric patients in 2009. Dis. Markers *2014*, 195453-195453.

Wang, S., Miura, M., Jung, Y.-k., Zhu, H., Gagliardini, V., Shi, L., Greenberg, A.H., and Yuan, J. (1996). Identification and Characterization of Ich-3, a Member of the Interleukin-1β Converting Enzyme (ICE)/Ced-3 Family and an Upstream Regulator of ICE. J. Biol. Chem. *271*, 20580-20587.

Wang, S., Miura, M., Jung, Y.-k., Zhu, H., Li, E., and Yuan, J. (1998). Murine Caspase-11, an ICE-Interacting Protease, Is Essential for the Activation of ICE. Cell *92*, 501-509.

Wang, X., Li, M., Zheng, H., Muster, T., Palese, P., Beg, A.A., and Garcia-Sastre, A. (2000). Influenza A virus NS1 protein prevents activation of NF-kappaB and induction of alpha/beta interferon. J. Virol. *74*, 11566-11573.

Wang, Z., Zhang, A., Wan, Y., Liu, X., Qiu, C., Xi, X., Ren, Y., Wang, J., Dong, Y., Bao, M., *et al.* (2014c). Early hypercytokinemia is associated with interferon-induced transmembrane protein-3 dysfunction and predictive of fatal H7N9 infection. Proc. Natl. Acad. Sci. U. S. A. *111*, 769-774.

Wareing, M.D., Lyon, A., Inglis, C., Giannoni, F., Charo, I., and Sarawar, S.R. (2007). Chemokine regulation of the inflammatory response to a low-dose influenza infection in CCR2-/- mice. J. Leukoc. Biol. *81*, 793-801.

References

Wei, X.Q., Leung, B.P., Niedbala, W., Piedrafita, D., Feng, G.J., Sweet, M., Dobbie, L., Smith, A.J., and Liew, F.Y. (1999). Altered immune responses and susceptibility to Leishmania major and Staphylococcus aureus infection in IL-18-deficient mice. J. Immunol. *163*, 2821-2828.

Wen, H., Gris, D., Lei, Y., Jha, S., Zhang, L., Huang, M.T.-H., Brickey, W.J., and Ting, J.P.Y. (2011). Fatty acid-induced NLRP3-ASC inflammasome activation interferes with insulin signaling. Nat. Immunol. *12*, 408-415.

Wilson, K.P., Black, J.-A.F., Thomson, J.A., Kim, E.E., Griffith, J.P., Navia, M.A., Murcko, M.A., Chambers, S.P., Aldape, R.A., Raybuck, S.A., and Livingston, D.J. (1994). Structure and mechanism of interleukin-1 beta converting enzyme. Nature *370*, 270-275.

Witzenrath, M., Pache, F., Lorenz, D., Koppe, U., Gutbier, B., Tabeling, C., Reppe, K., Meixenberger, K., Dorhoi, A., Ma, J., *et al.* (2011). The NLRP3 inflammasome is differentially activated by pneumolysin variants and contributes to host defense in pneumococcal pneumonia. J. Immunol. *187*, 434-440.

World Health Organisation (2018). Influenza at the human-animal interface: Summary and assessment, 26 January to 2 March 2018. In WHO Monthly Risk Assessment Summary: Influenza at the Human-Animal Interface (Geneva, World Health Organisation).

Wortzman, M.E., Lin, G.H.Y., and Watts, T.H. (2013). Intrinsic TNF/TNFR2 Interactions Fine-Tune the CD8 T Cell Response to Respiratory Influenza Virus Infection in Mice. PLoS One *8*, e68911.

Wu, J., Fernandes-Alnemri, T., and Alnemri, E.S. (2010). Involvement of the AIM2, NLRC4, and NLRP3 inflammasomes in caspase-1 activation by Listeria monocytogenes. J. Clin. Immunol. *30*, 693-702.

Wu, M.F., Chen, S.T., Yang, A.H., Lin, W.W., Lin, Y.L., Chen, N.J., Tsai, I.S., Li, L., and Hsieh, S.L. (2013). CLEC5A is critical for dengue virus-induced inflammasome activation in human macrophages. Blood *121*, 95-106.

Wu, W., Zhang, W., Duggan, E.S., Booth, J.L., Zou, M.H., and Metcalf, J.P. (2015). RIG-I and TLR3 are both required for maximum interferon induction by influenza virus in human lung alveolar epithelial cells. Virology *482*, 181-188.

Wynn, T.A., Chawla, A., and Pollard, J.W. (2013). Macrophage biology in development, homeostasis and disease. Nature *496*, 445-455.

Xiao, H., Killip, M.J., Staeheli, P., Randall, R.E., and Jackson, D. (2013a). The human interferon-induced MxA protein inhibits early stages of influenza A virus infection by retaining the incoming viral genome in the cytoplasm. J. Virol. *87*, 13053-13058.

Xiao, Y.L., Kash, J.C., Beres, S.B., Sheng, Z.M., Musser, J.M., and Taubenberger, J.K. (2013b). High-throughput RNA sequencing of a formalin-fixed, paraffin-embedded autopsy lung tissue sample from the 1918 influenza pandemic. The Journal of Pathology *229*, 535-545.

References

Xu, L., Bao, L., Li, F., Lv, Q., Ma, Y., Zhou, J., Xu, Y., Deng, W., Zhan, L., Zhu, H., *et al.* (2011). Adaption of Seasonal H1N1 Influenza Virus in Mice. PLoS One *6*, e28901.

Xue, Q., Lu, Y., Eisele, M.R., Sulistijo, E.S., Khan, N., Fan, R., and Miller-Jensen, K. (2015). Analysis of single-cell cytokine secretion reveals a role for paracrine signaling in coordinating macrophage responses to TLR4 stimulation. Science signaling *8*, ra59.

Yamamoto, M., Yaginuma, K., Tsutsui, H., Sagara, J., Guan, X., Seki, E., Yasuda, K., Yamamoto, M., Akira, S., Nakanishi, K., *et al.* (2004). ASC is essential for LPS-induced activation of procaspase-1 independently of TLR-associated signal adaptor molecules. Genes Cells *9*, 1055-1067.

Yamasaki, K., Muto, J., Taylor, K.R., Cogen, A.L., Audish, D., Bertin, J., Grant, E.P., Coyle, A.J., Misaghi, A., Hoffman, H.M., and Gallo, R.L. (2009). NLRP3/Cryopyrin Is Necessary for Interleukin-1β (IL-1β) Release in Response to Hyaluronan, an Endogenous Trigger of Inflammation in Response to Injury. J. Biol. Chem. *284*, 12762-12771.

Yan, Y., Jiang, W., Spinetti, T., Tardivel, A., Castillo, R., Bourquin, C., Guarda, G., Tian, Z., Tschopp, J., and Zhou, R. (2013). Omega-3 Fatty Acids Prevent Inflammation and Metabolic Disorder through Inhibition of NLRP3 Inflammasome Activation. Immunity *38*, 1154-1163.

Yang, J., Zhang, E., Liu, F., Zhang, Y., Zhong, M., Li, Y., Zhou, D., Chen, Y., Cao, Y., Xiao, Y., *et al.* (2014). Flagellins of salmonella typhi and nonpathogenic escherichia coli are differentially recognized through the NLRC4 pathway in macrophages. J. Innate Immun. *6*, 47-57.

Yang, Y., Guo, F., Zhao, W., Gu, Q., Huang, M., Cao, Q., Shi, Y., Li, J., Chen, J., Yan, J., *et al.* (2015). Novel avian-origin influenza A (H7N9) in critically ill patients in China. Critical care medicine *43*, 339-345.

Yang, Y., Wang, H., Kouadir, M., Song, H., and Shi, F. (2019). Recent advances in the mechanisms of NLRP3 inflammasome activation and its inhibitors. Cell Death Dis. *10*, 128-128.

Yaron, J.R., Gangaraju, S., Rao, M.Y., Kong, X., Zhang, L., Su, F., Tian, Y., Glenn, H.L., and Meldrum, D.R. (2015). K(+) regulates Ca(2+) to drive inflammasome signaling: dynamic visualization of ion flux in live cells. Cell Death Dis. *6*, e1954.

Yatmaz, S., Seow, H.J., Gualano, R.C., Wong, Z.X., Stambas, J., Selemidis, S., Crack, P.J., Bozinovski, S., Anderson, G.P., and Vlahos, R. (2013). Glutathione peroxidase-1 reduces influenza A virus-induced lung inflammation. Am. J. Respir. Cell Mol. Biol. *48*, 17-26.

Yona, S., Kim, K.W., Wolf, Y., Mildner, A., Varol, D., Breker, M., Strauss-Ayali, D., Viukov, S., Guilliams, M., Misharin, A., *et al.* (2013). Fate mapping reveals origins and dynamics of monocytes and tissue macrophages under homeostasis. Immunity *38*, 79-91.

Youm, Y.H., Adijiang, A., Vandanmagsar, B., Burk, D., Ravussin, A., and Dixit, V.D. (2011). Elimination of the NLRP3-ASC inflammasome protects against chronic obesity-induced pancreatic damage. Endocrinology *152*, 4039-4045.

References

Yu, H., Gao, Z., Feng, Z., Shu, Y., Xiang, N., Zhou, L., Huai, Y., Feng, L., Peng, Z., Li, Z., *et al.* (2008). Clinical Characteristics of 26 Human Cases of Highly Pathogenic Avian Influenza A (H5N1) Virus Infection in China. PLoS One *3*, e2985.

Yu, J., Nagasu, H., Murakami, T., Hoang, H., Broderick, L., Hoffman, H.M., and Horng, T. (2014). Inflammasome activation leads to Caspase-1-dependent mitochondrial damage and block of mitophagy. Proc. Natl. Acad. Sci. U. S. A. *111*, 15514-15519.

Yu, J.W., Wu, J., Zhang, Z., Datta, P., Ibrahimi, I., Taniguchi, S., Sagara, J., Fernandes-Alnemri, T., and Alnemri, E.S. (2006). Cryopyrin and pyrin activate caspase-1, but not NF-κB, via ASC oligomerization. Cell Death Differ. *13*, 236-249.

Zamarin, D., Garcia-Sastre, A., Xiao, X., Wang, R., and Palese, P. (2005). Influenza virus PB1-F2 protein induces cell death through mitochondrial ANT3 and VDAC1. PLoS Pathog. *1*, e4.

Zamora, A.E., Aguilar, E.G., Sungur, C.M., Khuat, L.T., Dunai, C., Lochhead, G.R., Du, J., Pomeroy, C., Blazar, B.R., Longo, D.L., *et al.* (2017). Licensing delineates helper and effector NK cell subsets during viral infection. JCI insight *2*, 87032.

Zanoni, I., Ostuni, R., Marek, L.R., Barresi, S., Barbalat, R., Barton, G.M., Granucci, F., and Kagan, J.C. (2011). CD14 controls the LPS-induced endocytosis of Toll-like Receptor 4. Cell *147*, 868-880.

Zeng, H., Pappas, C., Belser, J.A., Houser, K.V., Zhong, W., Wadford, D.A., Stevens, T., Balczon, R., Katz, J.M., and Tumpey, T.M. (2012). Human Pulmonary Microvascular Endothelial Cells Support Productive Replication of Highly Pathogenic Avian Influenza Viruses: Possible Involvement in the Pathogenesis of Human H5N1 Virus Infection. J. Virol. *86*, 667-678.

Zhai, Y., Meng, X., Ye, T., Xie, W., Sun, G., and Sun, X. (2018). Inhibiting the NLRP3 Inflammasome Activation with MCC950 Ameliorates Diabetic Encephalopathy in db/db Mice. Molecules *23*, E522.

Zhang, B., Wang, B., Cao, S., Wang, Y., and Wu, D. (2017a). Silybin attenuates LPS-induced lung injury in mice by inhibiting NF-κB signaling and NLRP3 activation. Int. J. Mol. Med. *39*, 1111-1118.

Zhang, L., Chen, S., Ruan, J., Wu, J., Tong, A.B., Yin, Q., Li, Y., David, L., Lu, A., Wang, W.L., *et al.* (2015). Cryo-EM structure of the activated NAIP2-NLRC4 inflammasome reveals nucleated polymerization. Science *350*, 404-409.

Zhang, W.H., Wang, X., Narayanan, M., Zhang, Y., Huo, C., Reed, J.C., and Friedlander, R.M. (2003). Fundamental role of the Rip2/caspase-1 pathway in hypoxia and ischemia-induced neuronal cell death. Proc. Natl. Acad. Sci. U. S. A. *100*, 16012-16017.

Zhang, Y., Li, X., Grailer, J.J., Wang, N., Wang, M., Yao, J., Zhong, R., Gao, G.F., Ward, P.A., Tan, D.-X., and Li, X. (2016). Melatonin alleviates acute lung injury through inhibiting the NLRP3 inflammasome. J. Pineal Res. *60*, 405-414.

References

Zhang, Y., Lv, X., Hu, Z., Ye, X., Zheng, X., Ding, Y., Xie, P., and Liu, Q. (2017b). Protection of Mcc950 against high-glucose-induced human retinal endothelial cell dysfunction. Cell Death Dis. *8*, e2941-e2941.

Zhang, Y., Wang, Y., Gilmore, X., Xu, K., and Mbawuike, I.N. (2001). Independent and synergistic effects of interleukin-18 and interleukin-12 in augmenting cytotoxic T lymphocyte responses and IFN-gamma production in aging. J. Interferon Cytokine Res. *21*, 843-850.

Zhao, C., Qi, X., Ding, M., Sun, X., Zhou, Z., Zhang, S., Zen, K., and Li, X. (2016). Pro-inflammatory cytokine dysregulation is associated with novel avian influenza A (H7N9) virus in primary human macrophages. J. Gen. Virol. *97*, 299-305.

Zhao, X., Pu, D., Zhao, Z., Zhu, H., Li, H., Shen, Y., Zhang, X., Zhang, R., Shen, J., Xiao, W., and Chen, W. (2017). Teuvincenone F Suppresses LPS-Induced Inflammation and NLRP3 Inflammasome Activation by Attenuating NEMO Ubiquitination. Front. Pharmacol. *8*, 565-565.

Zhao, Y., Yang, J., Shi, J., Gong, Y.N., Lu, Q., Xu, H., Liu, L., and Shao, F. (2011). The NLRC4 inflammasome receptors for bacterial flagellin and type III secretion apparatus. Nature *477*, 596-602.

Zheng, B.-J., Chan, K.-W., Lin, Y.-P., Zhao, G.-Y., Chan, C., Zhang, H.-J., Chen, H.-L., Wong, S.S.Y., Lau, S.K.P., Woo, P.C.Y., *et al.* (2008). Delayed antiviral plus immunomodulator treatment still reduces mortality in mice infected by high inoculum of influenza A/H5N1 virus. Proc. Natl. Acad. Sci. U. S. A. *105*, 8091-8096.

Zheng, S.C., Zhu, X.X., Xue, Y., Zhang, L.H., Zou, H.J., Qiu, J.H., and Liu, Q. (2015). Role of the NLRP3 inflammasome in the transient release of IL-1β induced by monosodium urate crystals in human fibroblast-like synoviocytes. Journal of Inflammation (United Kingdom) *12*, 30.

Zhou, G., Juang, S.W.W., and Kane, K.P. (2013). NK cells exacerbate the pathology of influenza virus infection in mice. Eur. J. Immunol. *43*, 929-938.

Zhou, R., Yazdi, A.S., Menu, P., and Tschopp, J. (2011). A role for mitochondria in NLRP3 inflammasome activation. Nature *469*, 221-225.